University of Bath

PHD

Automatic gain control in mobile radio receivers.

Burrows, D. F.

Award date:
1982

Awarding institution:
University of Bath

[Link to publication](#)

AUTOMATIC GAIN CONTROL IN MOBILE RADIO RECEIVERS

submitted by D.F. Burrows

for the degree of Ph.D.

of the University of Bath

1982

COPYRIGHT

ProQuest Number: U336537

All rights reserved

INFORMATION TO ALL USERS
The quality of this reproduction is dependent upon the quality of the copy submitted.

In the unlikely event that the author did not send a complete manuscript
and there are missing pages, these will be noted. Also, if material had to be removed,
a note will indicate the deletion.
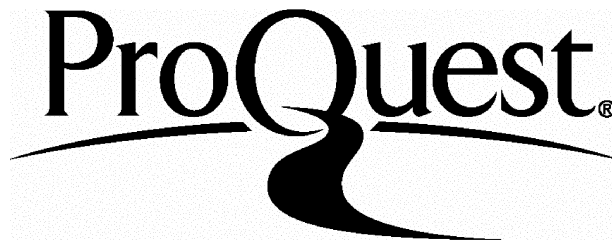
ProQuest U336537

Published by ProQuest LLC(2015). Copyright of the Dissertation is held by the Author.

TO MY PARENTS

ACKNOWLEDGEMENTS

SYNOPSIS

In the mobile multipath environment the received signal can be
adversely affected by unwanted, random envelope modulation. With AM-type
systems these envelope variations are impressed directly on to the
receiver's demodulated output. Automatic Gain Control (AGC) can be used
to reduce the unwanted envelope fading without distorting the required
modulation. This thesis begins by analysing mobile radio propagation
in some detail and develops worst-case deterministic test signals to study
the performance of AGC. The dynamic performance of a variety of AGC
systems is then described along with their application to mobile radio
receivers.

Initially, conventional feedback AGC systems are discussed. These
are shown to be capable of suppressing deep, unwanted fading only if it
occurs at rates well below that of the wanted envelope modulation.
The effects of time delay and the use of coherent envelope detectors are
analysed and shown to worsen the dynamic performance of feedback AGC.
Feedforward AGC systems, which can possess greatly improved dynamics,
are then introduced. A form of feedforward AGC is developed which can
achieve a specified dynamic performance with the narrowest of all control
bandwidths. Finally, the effects of signal-carrier decorrelation, noise
and interference are shown to limit the ultimate performance of all AGC
systems.

CONTENTS

APPENDICES

Large signal performance of feedback automatic gain
control systems.

Performance limits of feedforward automatic gain control
in mobile radio receivers.

ABBREVIATIONS

AFC	Automatic Frequency Control
AGC	Automatic Gain Control
AGCSIM	Automatic Gain Control Simulation Programme
AM	Amplitude Modulation
BFFAGC	Bandpass Filter Feedforward Automatic Gain Control
CDF	Cumulative Distribution Function
CMOS	Complementary Metal Oxide Semiconductor
CTD	Charge Transfer Device
D/A	Digital to Analogue Convertor
DIL	Dual in Line
DBM	Double Balanced Mixer
E	Electric
EIFBAGC	Exponential Integrator Feedback Automatic Gain Control
EMF	Electro Motive Force
FBAGC	Feedback Automatic Gain Control
FFAGC	Feedforward Automatic Gain Control
FFSR	Feedforward Signal Regeneration
FM	Frequency Modulation
IC	Integrated Circuit
IF	Intermediate Frequency
kHz	Kilohertz
LED	Light Emitting Diode
LFFAGC	Lowpass Filter Feedforward Automatic Gain Control
MHz	Megahertz
MOSFET	Metal Oxide Semiconductor Field Effect Transistor

MTDS	Multipath Time Delay Spread
OP-AMP	Operational Amplifier
PCB	Printed Circuit Board
PEP	Peak Envelope Power
PDF	Probability Distribution Function
PLL	Phase Locked Loop
PMR	Private Mobile Radio
PROM	Programmable Read Only Memory
PSD	Phase Sensitive Detector
RF	Radio Frequency
RMS,rms	Root Mean Square
SNR	Signal to Noise Ratio
SSB	Single Side Band
TIB	Tone in Band
TTIB	Transparent Tone in Band
UAP	UHF Audio Processor
UHF	Ultra High Frequency (300 MHz - 3,000 MHz)
VCOCXO	Voltage Controlled Oven Compensated Crystal Oscillator
VCO	Voltage Controlled Oscillator
VGA	Variable Gain Amplifier
VHF	Very High Frequency (30 MHz - 300 MHz)

SYMBOLS

A   dc integrator gain $\to \infty$; dc shift

A_n magnitude of nth harmonic

B   EIFBAGC exponentiator constant

BL   AGCSIM brickwall lowpass filter break frequency

B_p passband frequency limit

B_s stopband frequency limit

B_1 bandpass filter amplitude response at $(\omega_p - \omega_1)$

B_2 bandpass filter amplitude response at $(\omega_p + \omega_2)$

C   EIFBAGC exponentiator constant

CM   wanted tone compression

D   magnitude of sinusoid in $r_1(t)$

E   magnitude of signal

E'   magnitude of received signal at 1 metre

ER   AGCSIM measure of error

E_m modulation's magnitude

E_p pilot's magnitude

F   weighting function

$F_b(x)$ bandpass filtered version of x

FX   operation of EIFBAGC on input signal's envelope

F1   first order filtering function

F_1 filter in FBAGC

F_2 filter in FBAGC

G   average unwanted to wanted pilot power ratio

G_t transmitter antenna gain

G_r receiver antenna gain

G_1 combined antenna gains in appropriate directions

G_2	combined antenna gains in appropriate direction
H	height
H_r	receiver antenna height
H_t	transmitter antenna height
$H(s)$	transfer function in Laplace notation
$H(t)$	unit step function
Hz	Hertz
H_o	FBAGC circuit element gain
H_1	FBAGC circuit element gain
H_2	FBAGC circuit element gain
I	function of ω_N and D
I_N	bandpass filtered noise
J_{pi}	input peak
J_{po}	output peak
J_{ti}	input trough
J_{to}	output trough
K	complete elliptic integral of first kind
KI	AGCSIM input peak to trough ratio
KO	AGCSIM output peak to trough ratio
K_d	phase detector gain factor
K_i	peak to trough ratio at input
K_o	peak to trough ratio at output
K_o'	peak to trough ratio at output of matched time delay LFFAGC
K_o''	peak to trough ratio at output of matched time delay BFFAGC
L	amplitude response of filter
L'	approximate version of L
L_B	Butterworth filter amplitude response
L_ℓ	lower limit to passband amplitude ripple

L_s	upper limit to stopband amplitude ripple
L_u	upper limit to passband amplitude ripple
M	magnitude of reflection coefficient
N	integer
N_r	level crossing rate
P	B_2/B_1
PB	AGCSIM bottom path amplitude decorrelation factor
PS	phase shift
PT	AGCSIM top path amplitude decorrelation factor
P_F	relative amplitude decorrelation factor
P_r	received power
P_t	transmitted power
$P_{\frac{1}{2}}^{n}(x)$	associated Legendre function
Q	quality factor
R	signal or voltage ratio
RC	resistor capacitor product; AGCSIM first order filter
S	speed
S_A	aircraft speed
S_B	aircraft speed
S_E	power spectrum of E field component
S_E'	S_E with direct component
S_r	power spectrum of r(t)
SS1	scattering source 1
SS2	scattering source 2
T	specified value of time (delay)
TD	AGCSIM time delay
T_D	twin path relative time delay spread
T_c	EIFBAGC time constant

T_n	n^{th} value of T
$T_1 - T_5$	time delays
U	length
U'	length
V	volts
VT	AGCSIM threshold voltage
V_K	EIFBAGC reference voltage
V_O	peak amplitude of VCO output
V_T	threshold voltage
W	VGA gain in dB/V
X_2, X_2, X	distances on X-Y rectangular co-ordinates
Y_1, Y_2, Y	distances on X-Y rectangular co-ordinates
Z	real number greater than -1
a	lowpass filter gain at $2\omega_p$
b	mean received power
b_2	second moment of multipath signal
c	velocity of electromagnetic waves
c(t)	carrier or pilot reference
c'(t)	twin path version of c(t)
d	differentiation operator
d(t)	denominator voltage
$e_a(t)$	full carrier AM signal
$e_b(t)$	bandpass filter's output
$e_p(t)$	pilot at RF
$e_r(t)$	complete received signal
$e_{ra}(t)$	version of $e_r(t)$ translated down to audio frequencies
$e_s(t)$	pilot SSB signal

$e_1(t)$	received signal 1
$e_2(t)$	received signal 2
$f(t)$	real, bandpass signal
f_f	input fade frequency in Hz
g	relative pilot level
h	height
j	$\sqrt{-1}$
m	peak value of $m(t)$
$m(t)$	baseband modulation signal
mp	multiple path (subscript)
n	general variable
$n(t)$	numerator voltage
p	general variable
$p(r)$	probability density
r	specified value of $r(t)$
$r(t)$	signal envelope
$r(t)_{SLEW}$	slew rate of $r(t)$
r_ℓ	lower limit of envelope
$r_m(t)$	modulation's envelope
$r_p(t)$	pilot's envelope
r_u	specified level of unwanted pilot's envelope; upper limit of envelope
r_w	specified level of wanted pilot's evelope
$r_1(t)$	sinusoidal envelope fading
$r_2(t)$	two tone envelope fading
s	Laplace transform variable; seconds
t	time

t_p	twin path (subscript)
$u(t)$	phase of received signal
$u'(t)$	$u(t)$ referred to largest twin path signal
$v_a - v_e$	voltages around EIFBAGC loop
$v_g(t)$	gain control voltage
$v_i(t)$	input signal's envelope
$v_o(t)$	output signal's envelope
$v_{om}(t)$	modulation's envelope at output of BFFAGC circuit
$v_1(t)$	exponentiator input
$v_2(t)$	coherent EIFBAGC loop voltage
x	general variable
$x(t)$	required envelope variations
y	general variable
α	transmitter-receiver distance
β	phase of reflection coefficient
β_{pi}	position of input peak
β_{po}	position of output peak
β_{ti}	position of input trough
β_{to}	position of output trough
Γ	generalised factorial or gamma function
Δ	phase shift
$\Delta\omega$	pilot-modulation tone frequency difference
$\Delta\omega_{po}$	pull-out frequency
δ	angle; impulse function
δ'	angle
δ_1	angle
δ_2	angle

ε	dielectric constant of ground
ζ	damping factor of second order PLL
θ	phase response
θ'	approximate version of θ
θ_a	acceleration lag of type 2 PLL
θ_e	PLL phase error
θ_i	input signal's phase
θ_n	phase of nth Fourier series component
θ_o	phase of VCO
λ	wavelength
μ	arrival angle of direct component; micro
π	3.1416.....
ρ	normalised value of r
Σ	summation
σ	conductivity of ground
τ	differential time delay
τ_1	differential group delay of bandpass filter at $(\omega_p - \omega_1)$
τ_2	differential group delay of bandpass filter at $(\omega_p + \omega_2)$
ϕ	delay phase
ω	frequency
ω_a	convenient audio frequency
ω_c	carrier frequency
ω_d	maximum Doppler frequency
ω_f	fade rate
ω_h	highest frequency component of m(t)
ω_i	interfering tone frequency
ω_ℓ	lowest frequency component of m(t)
ω_m	frequency of maximum modulation enhancement

ω_N	frequency normalised to EIFBAGC bandwidth
ω_n	natural frequency of second order PLL
ω_o	bandpass filter centre frequency
ω_p	pilot or carrier frequency at BFFAGC input
ω_s	sinusoidal modulation frequency
ω_1	direct component frequency; upper twin path component frequency
ω_2	reflected component frequency; lower twin path component frequency
Ω	Ohm
∞	infinity

The following notes also apply to the main text unless otherwise stated:

1) Standard S.I. units used throughout text.

2) All angles are measured in radians (rad).

3) All frequency is measured in radians per second (rad.s^{-1}).

4) .....(dB) means: $20 \log_{10}$ (Voltage ratio) or

   $20 \log_{10}$ (Power ratio)

5) dBm. Decibels with respect to 1 milliwatt.

6) .....(t). Used to emphasise time dependence.

7) ln(x). Natural logarithm of x.

8) exp(x). Means exponentiate, raise e to power x.

9) $\underline{/x}$. Represents $\cos(\omega_c t + x)$.

10) $\hat{x}$. Means peak value of x.

11) Capital letters are also used as position markers.

CHAPTER 1

INTRODUCTION

1.1 Prologue

When information is transmitted across a radio frequency (RF) communications channel it is usually conveyed via envelope and/or phase variations of a carrier wave. The received signal will be degraded not only by thermal noise and interference but also by impairments introduced by the propagation characteristics of the medium. In particular, if the transmitter or receiver are mobile then random time varying envelope and phase variations can be impressed upon the received signal that affect wanted modulation. Automatic Gain Control (AGC) circuits are incorporated into some radio receivers to reduce the range of these unwanted envelope variations. If these unwanted envelope variations occur relatively slowly compared to wanted envelope modulation frequencies then the AGC circuitry has little difficulty in suppressing the former and passing the latter. Problems arise when the unwanted envelope variations occur at rates approaching wanted envelope modulation frequencies. A detailed knowledge of the performance of particular AGC systems is required to assess whether or not they are capable of satisfactorily coping with these envelope variations. This thesis presents a unified treatment of the dynamics of AGC circuits incorporated into modern land and air mobile receivers.

If a frequency modulated (FM) communication system is employed, then the use of limiters in the receiver renders the system largely insensitive to envelope variations. Thus FM receivers rarely use AGC. However, FM

transmissions tend to occupy larger bandwidths than equivalent amplitude modulation (AM) type signals that convey some or all of the transmitted information via envelope variations. With increasing numbers of users wanting to utilise fixed bandwidth allocations in the electromagnetic spectrum there is a move away from wideband FM systems to narrowband AM-type systems. This is most apparent in the UK private mobile radio (PMR) sector.

1.2 Mobile Radio

In 1976, excluding police and fire services, there were 195,000 mobile radio-telephones licensed for PMR use in the UK, with an estimated growth rate of 10% per year (1.1). In an attempt to relieve the increasing spectrum congestion, the Home Office (Directorate of Radio Technology) has been considering a change in modulation mode for PMR (1.2). The Home Office is evaluating the use of single sideband (SSB) in 5 kHz channel spacings compared to the more conventional FM and full carrier AM systems operated in 12.5 kHz channels at VHF and 25 kHz FM channels at UHF. Similar proposals are being investigated by the USA Federal Communications Commission (1.3). The reduced bandwidth requirement of SSB systems does not automatically mean they are spectrally more efficient as there are other considerations such as re-use distance. However, mathematical analysis has indicated that, in general, more efficient spectrum utilisation can be obtained by adopting SSB modulation (1.4). These results have been confirmed by practical trials and subjective comparisons of FM and SSB systems (1.5).

The other form of AM-type modulation that is to be briefly considered in this thesis is the use of full carrier AM by civil and military air-craft radio systems. Full carrier AM has been used for many years in

this application and much of the analysis relating to PMR systems will be shown to be directly applicable to aircraft communications.

1.3 Amplitude Modulation Systems

Full carrier AM and SSB are both members of the family of AM-type modulation systems that convey part or all of the baseband information via envelope modulation. The 2 members of this family of most interest are full carrier AM and a special form of SSB, referred to as pilot SSB. A mathematical definition of a full carrier AM signal, $e_a(t)$, is relatively straightforward, i.e.:

$$e_a(t) = E(1 + m(t))\cos \omega_c t \qquad (1.1)$$

where $m(t)$ is the baseband modulation signal, suitably processed so that $-1 < m(t) < +1$ and it occupies a baseband frequency range from ω_ℓ to ω_h. The transmitted carrier frequency is ω_c and E is a fixed magnitude. The various properties of this form of modulation are well known (1.6).

Less well known are the properties of pilot SSB modulation. This is the form of SSB modulation proposed for PMR use. The general mathematical definition of a pilot SSB signal, $e_s(t)$, can be written as:

$$e_s(t) = E \left[m(t) \Big|_{\omega \to \omega_c + \omega} + g \cos(\omega_c + \omega_p)t \right] \qquad (1.2)$$

where $m(t) \Big|_{\omega \to \omega_c + \omega}$ represents the upper sideband frequency translation process associated with conventional SSB (1.6). The second term in the brackets represents a pilot or tone transmitted at some specified level, g, below the peak transmitted signal at a frequency $(\omega_c + \omega_p)$. The pilot is used by the receiver as an amplitude and frequency reference, such a reference not being available with conventional SSB modulation. There

are a number of different proposed pilot SSB systems, differing mainly in the pilot's frequency. They are:

1) $\omega_p < 0$: Tone-below-band SSB. The pilot is transmitted at some frequency below the carrier (which is suppressed).

2) $\omega_p = 0$: Pilot carrier SSB.

3) $\omega_\ell < \omega_p < \omega_h$: Tone-in-band (TIB) SSB. The pilot is transmitted at some frequency within a notch in the modulation's spectrum.

4) $\omega_p > \omega_h$: Tone-above-band SSB. The pilot is transmitted at some frequency above the modulation's spectrum.

In the UK, pilot carrier SSB (1.7) and TIB SSB (1.8) have been proposed for PMR while tone-above-band using a frequency modulated tone is being considered in the USA by Lusignan (1.9).

1.4 Propagation Problems

The adoption of AM-type modulation such as pilot SSB results in improved spectrum efficiency at the expense of additional transmitter and receiver complexity. The main problem with AM-type systems is that if a fixed gain receiver is used, the envelope of the demodulated output signal is directly proportional to the RF input signal's envelope. Manual adjustment of an AM-type receiver's gain may be acceptable where the transmitter and receiver are stationary and the transmitted signal undergoes a constant propagation loss. Unfortunately, this situation does not exist in mobile radio communications where the received signal strength can vary rapidly over a wide range as the vehicle or aircraft moves. The variations arise as a result of the complicated signal propagation effects that characterise land and air mobile radio

communications. As a result, fixed gain receivers are rarely used in

AM-type radio systems. Instead, the receiver incorporates AGC circuitry.

1.5 Automatic Gain Control

The first practical AGC circuit was invented by H.A. Wheeler during

his Christmas vacation in 1925 (1.10). AGC circuits operate on the

envelope of the received signal and it is necessary to define "envelope"

before proceeding. The received signal is assumed to be real and of

the bandpass type so that it contains little energy outside a finite

frequency interval, centred approximately on ω_c. This signal, $e_r(t)$,

can always be expressed in the form:

$$e_r(t) \; = \; r(t) \; \cos(\omega_c t + u(t)); \; r(t) \; > \; 0 \qquad\qquad (1.3)$$

where $r(t)$ is the instantaneous length and $u(t)$ the instantaneous phase

of the phasor representing $e_r(t)$. The envelope of $e_r(t)$ is then given

by $r(t)$. A more rigorous definition may be found elsewhere (1.11) but

the aforementioned definition proves satisfactory for most purposes.

An alternative definition is to assume $e_r(t)$ to be converted to a very

high frequency SSB signal. Then the envelope, $r(t)$, is given by the

curve traced by the positive or negative peaks of the resulting signal

(1.12). For mathematical purposes the envelope will be assumed here to

be positive only, although some experimental results are made of plots

consisting of both $\pm r(t)$.

As stated in the prologue, the AGC circuits in the receiver face

the problem of distinguishing between wanted and unwanted envelope

variations of the received signal. The limitations of both conventional

and novel AGC circuits must be understood before the introduction of

new AM-type modulation systems such as pilot SSB. This thesis aims to discuss these limitations and the relevance of the results to mobile radio receivers.

1.6 Structure of Thesis

The thesis begins by discussing mobile radio propagation in some detail and proposes worst-case signals that can be used to test the various AGC systems. The performance and dynamic limitations of conventional AGC circuits are then analysed. Novel circuits that offer the promise of improved dynamics are introduced and the final part of the thesis discusses the ultimate limitations of AGC. Throughout the thesis the significance of the results for the various proposed pilot SSB systems is demonstrated. Feedback AGC systems are analysed with the use of feedforward mathematical models. These models give a unique conceptual understanding of the properties of conventional feedback AGC and allow direct comparisons to be made with other AGC systems.

CHAPTER 2

SINGLE AND TWIN PATH COMMUNICATIONS

The analysis and design of AGC systems requires a knowledge of the unwanted envelope variations they are required to suppress. In many mobile radio propagation situations the received signal's envelope can only be expressed by a set of non-deterministic statistics. Non-deterministic statistical analysis of an AGC system's response is greatly complicated by the non-linear nature of AGC. This work has concentrated on the analysis of the response of AGC systems to deterministic signals. The results are then used to make approximate predictions of AGC's response to non-deterministic inputs. It is therefore required to generate relevant deterministic signals that have properties similar to those encountered in the field.

This chapter considers some received signal variations that occur during mobile communications via single and twin path propagation. Both land and air communications are covered and the similarity between the two is demonstrated. Twin path models will be shown to accurately describe most aircraft communication situations while representing a worst-case land mobile one. Unless otherwise stated, both this and the next chapter considers communication to take place via the electric radiation field between 2 antennae using vertical polarisation, at a single frequency.

2.1 Large Scale Signal Variations

The signal variations considered in this section generally occur over travelled distances of many wavelengths. The variations are larger, but occur more slowly, than the local signal fluctuations described in later sections. Large scale variations of the received signal strength are often called "slow fading". The minimum requirement of the AGC circuitry in a mobile receiver is to satisfactorily suppress slow fading.

2.1.1 Free Space Propagation

Bullington (2.1) gives the general formula used for calculating the received power during single path free space propagation as:

$$P_r = P_t \left[\frac{\lambda}{4\pi\alpha}\right]^2 G_t G_r \tag{2.1}$$

where P_r is the received power, P_t is the transmitted power, λ the wavelength, α the distance from the transmitter to receiver, G_t the power gain of the transmitting antenna and G_r the power gain of the receiving antenna, both relative to an isotropic (non-directive) antenna. If the transmitter and receiver are spaced 1 wavelength apart the free space loss is 22 dB for isotropic antennae. If the receiver then moves directly away from the transmitter the direct received signal's strength falls by 6 dB for every doubling of the distance. However, single path free space propagation rarely occurs in mobile radio communications, and the next section considers a more realistic transmission situation.

2.1.2 Propagation Over a Plane Earth

In general, the presence of the ground causes the received power to vary more with distance than predicted by equation 2.1. Bullington (ibid) suggests that over a plane earth the received signal may be considered as the complex sum of the free space direct wave, a reflected wave, a "surface wave" and secondary effects. Section 2.4 on ground to air communications considers this mechanism in more detail. Here, the simplifications resulting from a low reflected signal grazing angle will be assumed, as occurs in VHF and UHF land mobile communications. Then, it can be shown that (2.2) the received power is given by:

$$P_r = P_t \left[\frac{H_t H_r}{\alpha^2} \right]^2 G_t G_r \qquad (2.2)$$

where H_t and H_r are the transmitter and receiver antenna heights respectively. If now the receiver moves directly away from the transmitter, the received signal strength falls by 12 dB for every doubling of the distance.

2.1.3 Effect of Obstructions

If the mobile suddenly goes behind an obstruction, the received signal strength does not change abruptly. Instead, it gradually reduces as some function of distance behind the obstruction. A general discussion on various obstruction shapes and the resulting diffraction effects is well covered elsewhere (2.1, 2.2, 2.3). However, it is noted here that once the mobile is not receiving line-of-sight transmission and positioned a few wavelengths behind the obstruction, the received signal

strength falls by at least 6 dB for every doubling of the distance from the edge. This effect is termed "shadowing".

2.1.4 Land Mobile Environment

Prediction of the absolute value of the mean received signal strength in the VHF and UHF urban land mobile environment is complicated (2.2, 2.4). However, most simple land mobile calculations assume a 12 dB loss for every doubling of the transmitter-receiver distance as derived in section 2.1.2. This variation with distance is somewhat less for very high base station antenna heights and somewhat more for distances above 15 km (2.2). Nevertheless, the problem remains to decide what large scale variations the AGC should have to suppress in the short term, caused, for example, by shadowing. As stated, the problem is ill-defined since in the very short term, over travelled distances of a fraction of a wavelength, the received signal's strength varies considerably. These very short term variations are commonly referred to as "fast fading" and are discussed in more detail in later sections.

The distinction between slow and fast fading is somewhat arbitrary. French (2.5) considers the slow fading to be suppressed by averaging the received signal over travelled distances of about 10 wavelengths. The slow fading is also found by French (ibid) to have an approximately log-normal envelope distribution in London at 462 MHz. The technique of averaging over 10 wavelengths to leave only fast fading has also been used successfully by Gladstone and McGeehan (2.6). Therefore, if the minimum requirement of a receiver's AGC system is to suppress slow fading it should average out the received signals envelope over

travelled distances of about 10 wavelengths.

2.1.5 Aircraft Environment

Prediction of the absolute value of the received signal strength in the VHF and UHF aircraft communications environment usually involves consideration of two main propagation paths. One path is the direct path (either base station to aircraft or aircraft to aircraft) and the other is the result of a reflection from the earth's surface. This particular situation is discussed in more detail in section 2.4.

However, on average, the large scale variation of the received signal strength follows a free space law, as described in section 2.1.1, up to the radio horizon (2.9). Reed and Russel (2.9) also state that beyond the radio horizon the received signal strength falls off exponentially between 0.4 and 1.5 dB per km, and over 50 km beyond it falls off by about 0.3 dB per km to distances of at least 650 km. It appears from their work that, neglecting twin path effects, large scale signal variations in the aircraft environment occur more slowly than in the land mobile environment. This section therefore concludes that an AGC system capable of suppressing the slow fading that occurs in the land mobile environment will adequately suppress the slow fading encountered in the aircraft environment.

2.2 Base to Land Mobile (One Direct, One Reflected Component)

There have been many attempts to model the phenomenon of fast fading in the land mobile radio environment. The one described here models suburban radio fading. It was first described by Ossana (2.7) in 1964,

but since then has been largely superseded by various "scattering" models, described in later sections. It is included here for 2 reasons. Firstly, it is a relatively simple model, partially substantiated by results from the field and secondly, Ossana (ibid) has considered the received signals envelope's power spectral density in more detail than some later authors. A full knowledge of the power spectral density is an important factor in the analysis and design of AGC systems.

Note that in this and subsequent propagation models the receiver is assumed to be mobile, operating from a fixed base station transmitter. Reciprocity will ensure that the same results are applicable to the signal arriving at the base station receiver from a mobile transmitter.

2.2.1 Model Description

The model assumes that over any short period of time the received signal is comprised of a direct component and an interfering component reflected, for example, from the side of a house. This is claimed by Ossana (ibid) to be the most likely propagation mechanism in some suburban residential areas where the buildings are well spaced out. Figure 2.1 shows the vehicle moving through the stationary standing wave pattern due to a direct and reflected component where δ' is the angle between the direction to the fixed base station and the direction to the reflector as seen from the mobile antenna, δ is the angle between the direction to the fixed base station and the direction of vehicle travel, U is the length of the reflector, U' is the length of the vehicle path in the reflected beam and S is the vehicle's speed. Diffraction

PLAN VIEW

Direction to base station   Direction to base station

← Assumed parallel →

Vertical plane
conducting
reflector
(side of
    building)

δ'

δ

Interference area
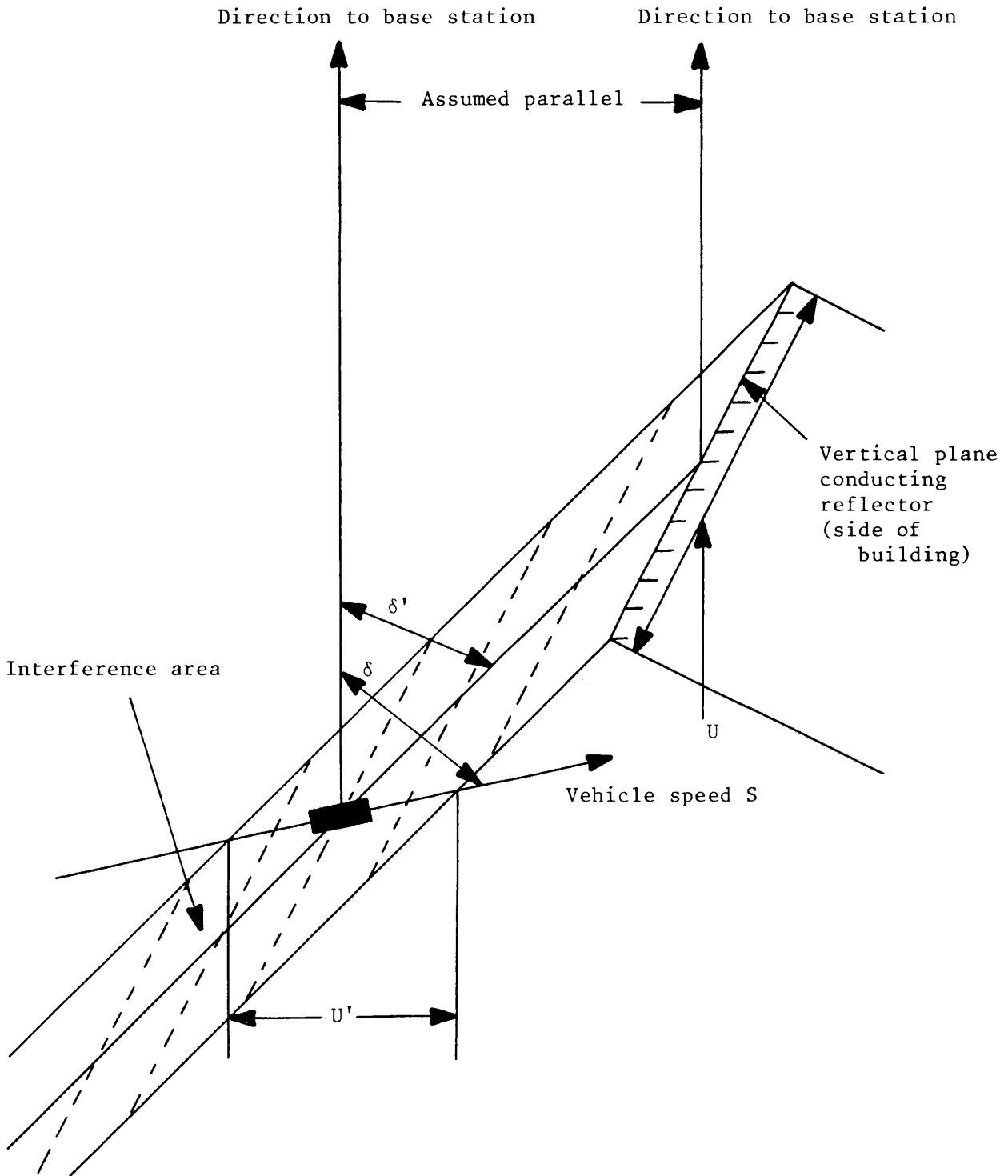
U

Vehicle speed S

U'

Figure 2.1   Vehicle moving through a standing wave pattern due to a
direct and reflected component.

effects are neglected and the model uses simple "ray" theory.

The model assumes that the direct and reflected components have the same amplitude, resulting in the received signal consisting of a series of peaks and trough nulls, with an envelope shape identical to that of a fullwave rectified sinewave. The trough nulls are shown in figure 2.1 by the dashed lines. The receiver is always assumed to receive a direct component, but only receives the reflected component when the vehicle travels through the interference area over the distance U'.

In order to analyse the received signal's properties over a reasonable length of time, it is necessary to consider the vehicle passing through a number of interference areas from separate buildings. It must be emphasised though that there is always assumed to be only 1 reflected component in any particular interference area and adjacent areas do not overlap.

2.2.2 Pre-detection Signal Characteristics

In the interference area, the pre-detection signal spectrum will consist of two equal components. If the maximum Doppler frequency is given by:

$$\omega_d = \frac{2\pi S}{\lambda} \qquad (2.3)$$

then the frequency of the direct component, ω_1, is:

$$\omega_1 = \omega_c + \omega_d \cos \delta \qquad (2.4)$$

where ω_c is the carrier frequency. N.B. all angular frequencies are in units of radians per second $(r.s^{-1})$. The frequency of the reflected

component, ω_2, is:

$$\omega_2 = \omega_c + \omega_d \cos(\delta - \delta') \qquad (2.5)$$

As the vehicle passes from 1 interference area to the next, ω_1 and ω_2 will change unless all the reflectors are orientated in the same direction and the base station is a large distance away. Ossana (ibid) analyses the effect of various reflector orientations and concludes that the received signal's spectrum prior to detection is most likely to contain 2 well spaced frequencies near ± maximum Doppler from the carrier.

2.2.3 Post-detection Envelope Characteristics

The only post-detection envelope characteristic considered by Ossana (ibid) and discussed here is the power spectrum. 2 cases are analysed. The first is where the angle to the base station is substantially constant but all reflector orientations are equally likely. The second case concerns the average of a large number of the first case where all angles to the base station are also equally likely.

The power spectrum in the first case is relatively flat up to a first peak of 5-10 dB at a frequency $\omega_d(1 - \cos \delta)$ then peaks again at $\omega_d(1 + \cos \delta)$. Above this frequency it falls rapidly by 15-25 dB, then the spectrum shape repeats itself in a harmonic fashion. These spectra were well substantiated by field trials in a suburban environment, where δ was known. The main discrepancy between theory and practice was a higher measured low frequency spectral content. This very slow fading was attributed to shadowing, "plane earth" signal variations, simultaneous reflections, non-random reflector orientations and other secondary effects.

The second main result was obtained by averaging a large number of these spectra with different δ angles. This revealed a power spectrum that is nearly flat to a frequency $2\omega_d$, then falls abruptly to a second harmonic shelf 16 dB lower.

The important point here is that in both cases Ossana (ibid) thought it necessary to consider the higher harmonics of the power spectrum, above $2\omega_d$. He did this by simply assigning a harmonic to each fundamental component weighted by the Fourier series of a full wave rectified sine wave. Although this technique appears very approximate, the results were born out well in practice. The significance of the higher frequency components is that they affect the received signal's envelope time waveform at the deepest part of the fade. It is near the bottom of a fade that an AGC system has to have the greatest rate of change of gain to suppress the fade. The importance of this will become apparent in chapter 5.

2.2.4 Limitations of the Model

The main limitation of Ossana's (ibid) model is its physical basis. It assumes that the received signal is always comprised of just 1 direct and 1 reflected component of equal amplitudes and fixed arrival angles in each interference area. Although this may be reasonable in the suburban environment with well spaced buildings and an elevated base station transmitter, in general this is not the case. In the urban environment especially, with buildings surrounding the vehicle and no line-of-sight transmission path, the received signal is more likely to be comprised of a number of scattered components of the original signal.

The scattering is caused not only by reflection but also by refraction and diffraction of the original signal due to nearby buildings and vehicles. The next section describes a simple scattering model with just 2 main received components. Scattering models with a large number of incoming components are described in chapter 3.

2.3 Base to Land Mobile (2 Scattered Components)

This section considers a simple scattering model where most of the received power has come from 2 points near the mobile. It is an extension of the suburban model to certain urban cases. The analysis considers the general case where the 2 received signals have different amplitudes and their arrival angles change with vehicle position. Once again, the analysis does not take into account the varying propagation characteristics of the channel described earlier (e.g. shadowing), and assumes the mean received power from each component remains constant over the distance travelled.

2.3.1 Model Description

Figure 2.2 shows a vehicle moving through the standing wave pattern due to 2 scattered signals. The components are assumed to originate from 2 nearby, fixed position, scattering sources. The zero time reference is chosen so that at t = 0, the positions of the 2 sources relative to the position and direction of the vehicles travel are X_1, Y_1 and X_2, Y_2, and δ_1 and δ_2 are the respective angles to the 2 sources. Let the received signal at the receiver's input from scattering source SS1 be E volts and the signal strength from scattering source SS2 be
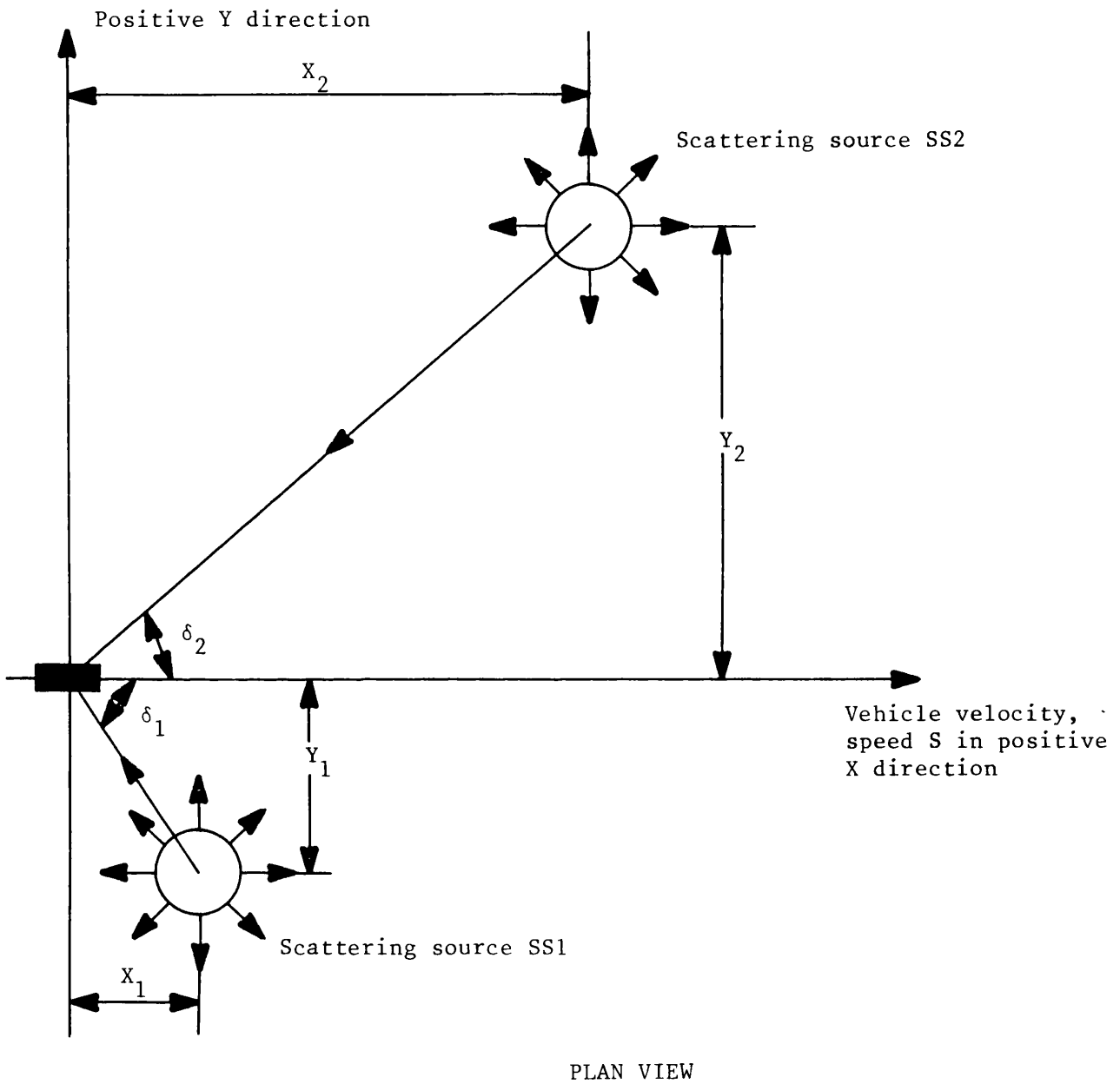
2.11

Positive Y direction

X_2

Scattering source SS2

Y_2

δ_2

δ_1

Vehicle velocity, speed S in positive X direction

Y_1

Scattering source SS1

X_1

PLAN VIEW

Figure 2.2 Vehicle moving through the standing wave pattern due to 2 scattering sources.

2.12

RE volts. Therefore, if, as before, the carrier frequency is ω_c and the maximum Doppler frequency is ω_d, defined by equation 2.3, then the received signal due to SS1, $e_1(t)$, is:

$$e_1(t) = E \cos(\omega_c t + \omega_d t \cos \delta_1) \qquad (2.6)$$

and the received signal due to source SS2, $e_2(t)$, is:

$$e_2(t) = RE \cos(\omega_c t + \omega_d t \cos \delta_2) \qquad (2.7)$$

Also, from simple geometry:

$$\cos \delta_1 = \frac{X_1 - St}{((X_1 - St)^2 + Y_1^2)^{\frac{1}{2}}} \qquad (2.8)$$

and

$$\cos \delta_2 = \frac{X_2 - St}{((X_2 - St)^2 + Y_2^2)^{\frac{1}{2}}} \qquad (2.9)$$

Note that the same received signal is obtained if the reflector has a positive or negative Y co-ordinate of the same amplitude. Therefore in this simple model it is immaterial whether the scattering sources are on the left, right or either side of the vehicle's path.

2.3.2 Pre-detection Signal Characteristics

The complete received signal, $e_r(t)$, resulting from the complex addition of $e_1(t)$ and $e_2(t)$ is:

$$e_r(t) = E(\cos(\omega_c t + \omega_d t \cos \delta_1) + R \cos(\omega_c t + \omega_d t \cos \delta_2)) \qquad (2.10)$$

The spectrum of $e_r(t)$ is formed by the 2 components that vary in "instantaneous" frequency as the vehicle approaches and passes the scattering sources. At $t = -\infty$ the spectrum consists of two super-imposed components at $(\omega_c + \omega_d)$. As the vehicle passes each source the associated shift from the carrier frequency goes to zero when directly adjacent to it, then tends to a value $-\omega_d$ at $t = +\infty$.

2.3.3 Post-detection Envelope Characteristics

The pre-detection signal $e_r(t)$ may also be written as:

$$e_r(t) = E(1 + R^2 + 2R \cos((\cos \delta_1 - \cos \delta_2)\omega_d t))^{\frac{1}{2}}$$

$$\left[\cos \omega_c t \pm \tan^{-1} \left[\frac{R \sin(\omega_d t \cos \delta_2) - \sin(\omega_d t \cos \delta_1)}{R \cos(\omega_d t \cos \delta_2) + \cos(\omega_d t \cos \delta_1)} \right] \right] \quad (2.11)$$

The signal's envelope, $r(t)$, is therefore given by:

$$r(t) = E(1 + R^2 + 2R \cos((\cos \delta_1 - \cos \delta_2)\omega_d t))^{\frac{1}{2}} \quad (2.12)$$

This envelope will now be analysed in some detail. A similar envelope function occurs in aircraft communications, and a detailed analysis will therefore cover this situation as well. Furthermore, the analysis will also allow comparison with the more general multiple path case in chapter 3.

The ratio of the maximum to minimum value of the fade, K_i, is given by:

$$K_i = \frac{1 + R}{1 - R} \quad (2.13)$$

Figure 2.3 shows r(t) for various values of K_i(dB). Notice that whereas the shallower fades appear to be sinusoidal, the deeper fades have a sharper trough. The waveform shape ultimately tends to that of a full wave rectified sinewave when R = 1 (K_i infinite).

The fade rate of r(t) is given by ω_f where:

$$\omega_f = (\cos \delta_1 - \cos \delta_2)\omega_d \qquad (2.14)$$

The fade rate varies as the vehicle passes the 2 sources, although the variation is a relatively slow process for scattering sources positioned some wavelengths from the vehicle. Appendix 1 discusses the general case, showing that the fade rate peaks twice somewhere near the 2 sources. If the magnitude of the Y co-ordinates are equal then the fade rate peaks just once, when the vehicle is equidistant from the sources. The maximum possible fade rate occurs when 1 source is directly in front and 1 source directly behind the vehicle: it is then twice maximum Doppler, $2\omega_d$.

In general, the receiver's AGC system is subjected to unwanted envelope variations of the form:

$$r(t) = E(1 + R^2 + 2R \cos \omega_f t)^{\frac{1}{2}} \qquad (2.15)$$

where $0 < R < 1$ and $0 < \omega_f < 2\omega_d$ in the twin scattering source model. Using equation (2.15) allows the analysis to continue without reference to any particular positioning of the scattering sources. The analysis concentrates on the properties of a single cycle of a fade, from peak to trough to peak, and assumes wherever necessary that ω_f is constant over this 1 cycle.
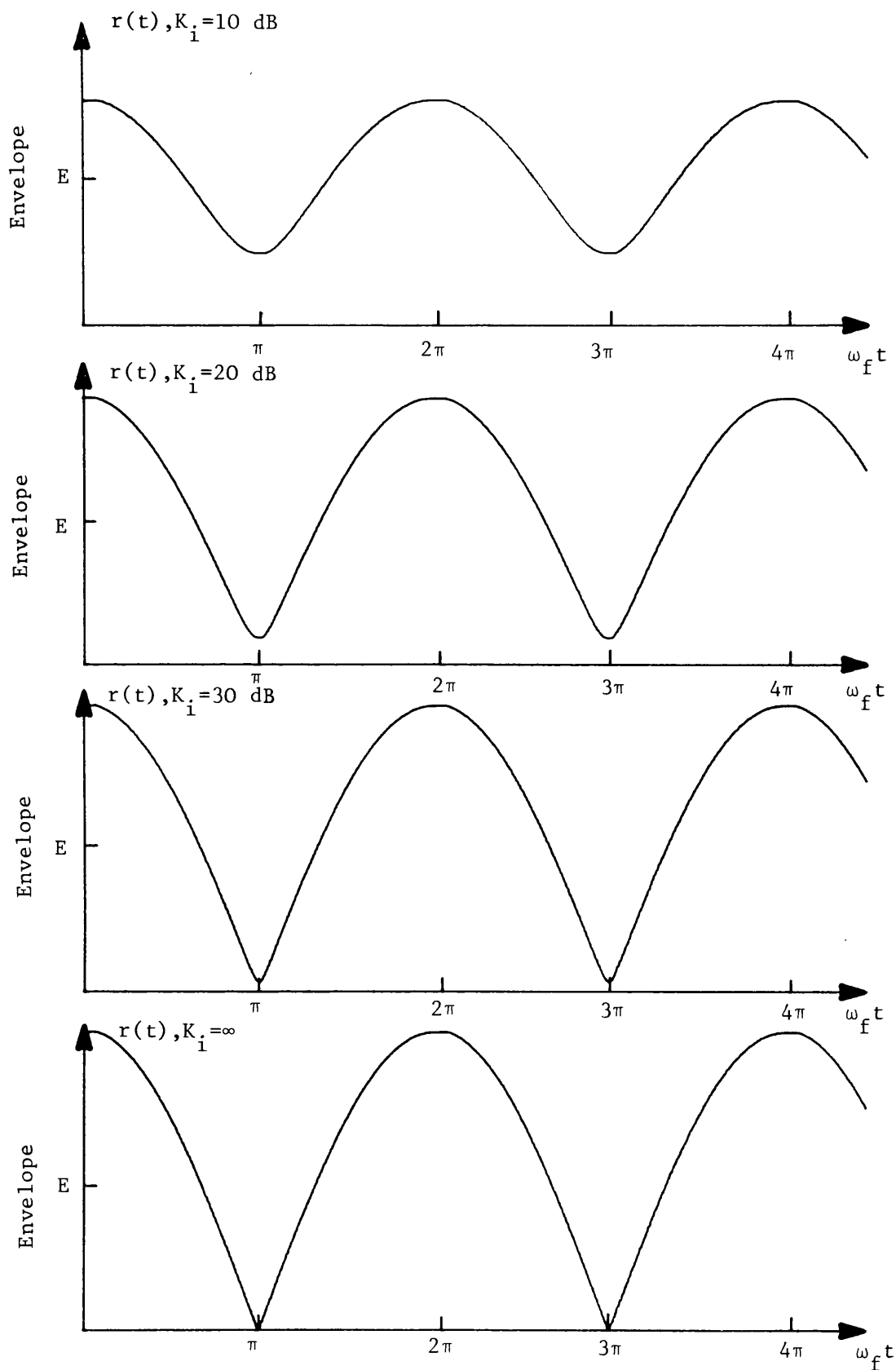
r(t),K_i=10 dB

Envelope

E

π 2π 3π 4π $\omega_f t$

r(t),K_i=20 dB

Envelope

E

π 2π 3π 4π $\omega_f t$

r(t),K_i=30 dB

Envelope

E

π 2π 3π 4π $\omega_f t$

r(t),K_i=∞

Envelope

E

π 2π 3π 4π $\omega_f t$

<u>Figure 2.3</u> Plots of the received signals envelope, r(t), for various
values of K_i (dB).

2.16

The first property of the envelope to be analysed assumes r(t) to be periodic in time, allowing it to be represented by a Fourier series. The Fourier series is, in practice, only valid over the range $0 \leqslant \omega_f t \leqslant 2\pi$. With this proviso, the series is obtained as follows:

r(t) consists of a dc component and a series of cosine components. That is, r(t) may be written as:

$$r(t) = \frac{A_o}{2} + \sum_{n=1}^{\infty} A_n \cos n\omega_f t \qquad (2.16)$$

where:

$$A_n = \frac{2E\omega_f}{\pi} \int_0^{\pi/\omega_f} (1 + R^2 + 2R \cos \omega_f t)^{\frac{1}{2}} \cos n\omega_f t \, dt \qquad (2.17)$$

The solution of this integral may be deduced from equation (1), page xxviii of Briggs and Lowan (2.8). After a simplification, n = 0 in the original equation (ibid), the equation is:

$$P_{\frac{1}{2}}^n(x) = \frac{\Gamma(n + 1.5)}{\pi \Gamma(1.5)} \int_0^{\pi} (x + \sqrt{(x^2 - 1)} \cos y)^{\frac{1}{2}} \cos ny \, dy \qquad (2.18)$$

where $P_{\frac{1}{2}}^n(x)$ is the associated Legendre function and Γ is the Gamma function. Substituting $x = \frac{1 + R^2}{1 - R^2}$ and rearranging equation 2.18 gives:

$$P_{\frac{1}{2}}^n \left[\frac{1 + R^2}{1 - R^2} \right] \frac{\Gamma(1.5)}{\Gamma(n + 1.5)} \sqrt{(1 - R^2)} = \frac{1}{\pi} \cdot \int_0^{\pi} (1 + R^2 + 2R \cos y)^{\frac{1}{2}} \cos ny \, dy$$
$$(2.19)$$

from which, by substituting $y = \omega_f t$, the required solution is obtained i.e.:

$$A_n = P_{\frac{1}{2}}^n \left[\frac{1 + R^2}{1 - R^2} \right] \frac{\Gamma(1.5)}{\Gamma(n + 1.5)} \, 2E \sqrt{(1 - R^2)} \qquad (2.20)$$

2.17

Equation 2.20 allows calculation of the magnitude of the various A_n

coefficients provided the associated Legendre function is known, for

example, from tables (2.8).

An alternative method for obtaining the various values of A_n, more

suited to computation, is to perform a discrete Fourier analysis of $r(t)$.

The formula for A_n may then be approximated (for example) by:

$$A_n = \frac{2E}{N} \sum_{p=0}^{N=1} \left[\left[1 + R^2 + 2R \cos \left[\frac{2\pi p}{N} \right] \right]^{\frac{1}{2}} \cos \left[\frac{2\pi pn}{N} \right] \right] \quad (2.21)$$

where N is an integer greater than $2(n + 1)$ for equation 2.21 to be

valid, larger values giving more accurate results. When R = 1 the

envelope, $r(t)$, is simply a fullwave rectified sinewave for which the

Fourier series is:

$$r(t) = \frac{4E}{\pi} \left[1 - \sum_{n=1}^{\infty} \frac{2 \cos n\pi \cos n\omega_f t}{(4n^2 - 1)} \right] \quad (2.22)$$

One interesting point concerns the difference between the rms and

the mean or dc value of $r(t)$. The rms value of $r(t)$ is given by:

$$r(t)_{rms} = \left[\frac{\omega_f}{2\pi} \int_0^{2\pi/\omega_f} (E^2(1 + R^2 + 2R \cos \omega_f t))dt \right]^{\frac{1}{2}} \quad (2.23)$$

which simplifies to:

$$r(t)_{rms} = E(1 + R^2)^{\frac{1}{2}} \quad (2.24)$$

The mean value is $A_0/2$. The difference between the rms and mean value

is largest when R = 1. Therefore, for any value of R:

$$1(0 \text{ dB}) < \frac{r(t)_{rms}}{r(t)_{mean}} < \frac{\pi}{2\sqrt{2}} (0.91 \text{ dB}) \quad (2.25)$$

Another relevant property of a single cycle of r(t) is its probability density function, calculated as follows. Let the value of r(t) for which the probability density is to be found be r where $E(1 - R) \leqslant r \leqslant E(1 + R)$. Then by definition:

$$p(r) = \frac{\omega_f}{\pi} \left[\frac{dt}{dr(t)} \text{ , with } r(t) \text{ replaced by } r \right] \qquad (2.26)$$

where p(r) is the probability density of r(t) at r. Since :

$$t = \frac{1}{\omega_f} \cos^{-1} \left[\frac{r(t)^2/E^2 - 1 - R^2}{2R} \right] \qquad (2.27)$$

and:

$$\frac{dt}{dr(t)} = \frac{-1}{\omega_f} \frac{1}{\left[1 - \left[\frac{r(t)^2/E^2 - 1 - R^2}{2R} \right]^2 \right]^{\frac{1}{2}}} \frac{r(t)}{RE^2} \qquad (2.28)$$

then:

$$p(r) = \frac{r}{\pi RE^2 \left[1 - \left[\frac{r^2/E^2 - 1 - R^2}{2R} \right]^2 \right]^{\frac{1}{2}}} \qquad (2.29)$$

The time duration below the level r of a single cycle of r(t) is also required. The envelope reaches the bottom part of the fade at a time π/ω_f seconds. The time taken to reach any other level, r, is given by equation 2.27. Therefore, the time spent below level r is twice the difference between the 2 aforementioned times per complete cycle of fade. If this time is represented by T then:

$$T = \frac{2}{\omega_f} \left[\pi - \cos^{-1} \left[\frac{r^2/E^2 - 1 - R^2}{2R} \right] \right] \qquad (2.30)$$

The final property of r(t) to be discussed here is its peak slew rate in decibels per second. This is analysed in Appendix 2 which shows that:

2.19

$$\hat{r}(t)_{slew} = \frac{20 \ \omega_f \ R \ \sin \left[\cos^{-1} \left[\frac{-2R}{1 + R^2} \right] \right]}{\ln(10) \left[1 + R^2 - \left[\frac{4R^2}{(1 + R^2)} \right] \right]} \qquad dB/s \qquad (2.31)$$

where $\hat{r}(t)_{slew}$ is the peak slew rate.

2.3.4 Limitations of the Model

Apart from the limitations discussed at the beginning of this

section, the main limitation with this particular model is that the

relative tone ratio, R, is fixed. This implies that the receiver will

always experience the same peak to trough ratio, K_1, as it moves along

through successive fades. This rarely happens in practice. The problem

would be overcome in a similar manner to Ossana's model (2.7) by

assuming that the vehicle moves abruptly out of the field from 2

particular sources and into the field of another 2. However, this

is obviously artificial and the model is best extended by increasing

the number of scattering sources instead. This approach is adopted

in Chapter 3.

It should be noted that the twin scattering model has provided some

very useful and analytically simple characteristics of the received

signal. It forms the basis of 1 of the deterministic signals used

to analyse and design AGC systems. Furthermore, it can be simulated

under laboratory conditions by simply summing together the outputs

of 2 signal generators of appropriate frequencies and amplitudes.

2.4 Aircraft Propagation

Signal propagation between a base station and an aircraft or between 2 aircraft can be described very accurately by the twin path model. The additional effects of the surface wave and other secondary effects as described by Bullington (ibid) can be neglected providing the antennae are several wavelengths above the ground. In this case Bullington (ibid) shows that the main components of the received signal are the "free space" direct wave and a ground reflected wave. This section considers the general aspects of the problem before analysing those parts relevant to AGC design. It will become apparent that the requirements of an avionic receiver's AGC system are very similar to those of a land mobile receiver's AGC system in the twin scattering source case.

2.4.1 Lobe Structure: General Considerations

The "lobe structure" is the 3-dimensional structure of contours of equal field strength around the transmitting antenna. The signal strength at a particular point is formed by the complex sum of the direct and ground reflected waves at that point, taking into account the magnitude and phase of the reflected component, the antenna's free space gain and the curvature of the earth. There are also slow time varying factors such as reflection and refraction by atmospheric turbulence, ducts and precipitation to be considered, although they mainly affect the weak signal strength region near and beyond the radio horizon. The general calculation of the exact shape of the lobe structure is adequately covered elsewhere (2.9). Here it is more relevant to consider the variations in the received signal strength encountered by an aircraft flying through the lobe structure . Of great importance in

2.21

this consideration is the magnitude and phase of the reflected component.

2.4.2 Reflection Coefficient

The reflection coefficient is a complex quantity relating the

magnitude, M, and the phase, β, of the ground reflected wave relative

to the incident wave. Vertical polarisation is the most commonly used

polarisation since it results in a lobe pattern with better coverage

and less deep nulls than horizontal polarisation. For this reason,

only vertical polarisation will be considered here although a more

general discussion can be found elsewhere (2.9). It will be assumed

here that the reflection occurs at a point on the ground, rather than,

as it does in practice, occurring over an area that usually includes

the first few Fresnel zones (2.3). Assuming the use of vertical polar-

isation and uniform reflection coefficient over the first few Fresnel

zones, the magnitude and phase of the reflected signal relative to the

incident signal is given by (2.1):

$$M \exp(j\beta) = \frac{\sin \delta - \frac{\sqrt{\varepsilon - j60\sigma\lambda - \cos^2 \delta}}{\varepsilon - j60\sigma\lambda}}{\sin \delta + \frac{\sqrt{\varepsilon - j60\sigma\lambda - \cos^2 \delta}}{\varepsilon - j60\sigma\lambda}} \tag{2.32}$$

where δ is the angle between the reflected ray and the ground, ε is

the dielectric constant of the ground, and σ is the ground's conductivity.

Normally, β is negative between 0 and $-\pi$, and M is some value between 0

and 1. Variations of M and β with δ at different frequencies for

different ground types can be found elsewhere (2.9). A general observation

is that as δ varies between zero and $\pi/2$, M decreases from unity to some

minimum value then rises, while β always increases from $-\pi$ to zero.

2.4.3 Constant Height Model

This simple propagation situation demonstrates the similarity between the equations describing twin path land mobile communications and aircraft communications. In this model propagation is assumed to take place via a direct and reflected path over a smooth plane earth either between a fixed transmitting base station and a receiver in an aircraft flying directly over the transmitter at a constant height or between 2 aircraft flying horizontal converging courses directly towards each other at different heights. This is shown in figure 2.4 where H_t and H_r are the transmitter and receiver antenna heights respectively, X is the horizontal distance between the transmitter and receiver at t = 0 and δ_1, δ_2, δ angles as indicated. The reflected component may be thought to originate from an image transmitter as shown. There is a striking similarity between this model and the twin scattering source analysis in section 2.3. The main differences are that with this model the mean received signal strength varies with time, as does the direct to reflected component ratio and the reflected components phase. The received signal's envelope may therefore be written down directly as:

$$r(t) \; = \; E(1 + R^2 + 2R \cos((\cos \delta_1 - \cos \delta_2)\omega_d t - \beta))^{\frac{1}{2}} \qquad (2.33)$$

where:

$$E \; = \; E' \; G_1((H_r - H_t)^2 + (X - St)^2)^{-\frac{1}{2}} \qquad (2.34)$$

E' is the received voltage at 1 metre, G_1 is the combined receiver/ transmitter antenna gains along the direct path, S is the closing speed (S = S_A + S_B) and the term in square roots represents the free space transmission loss.
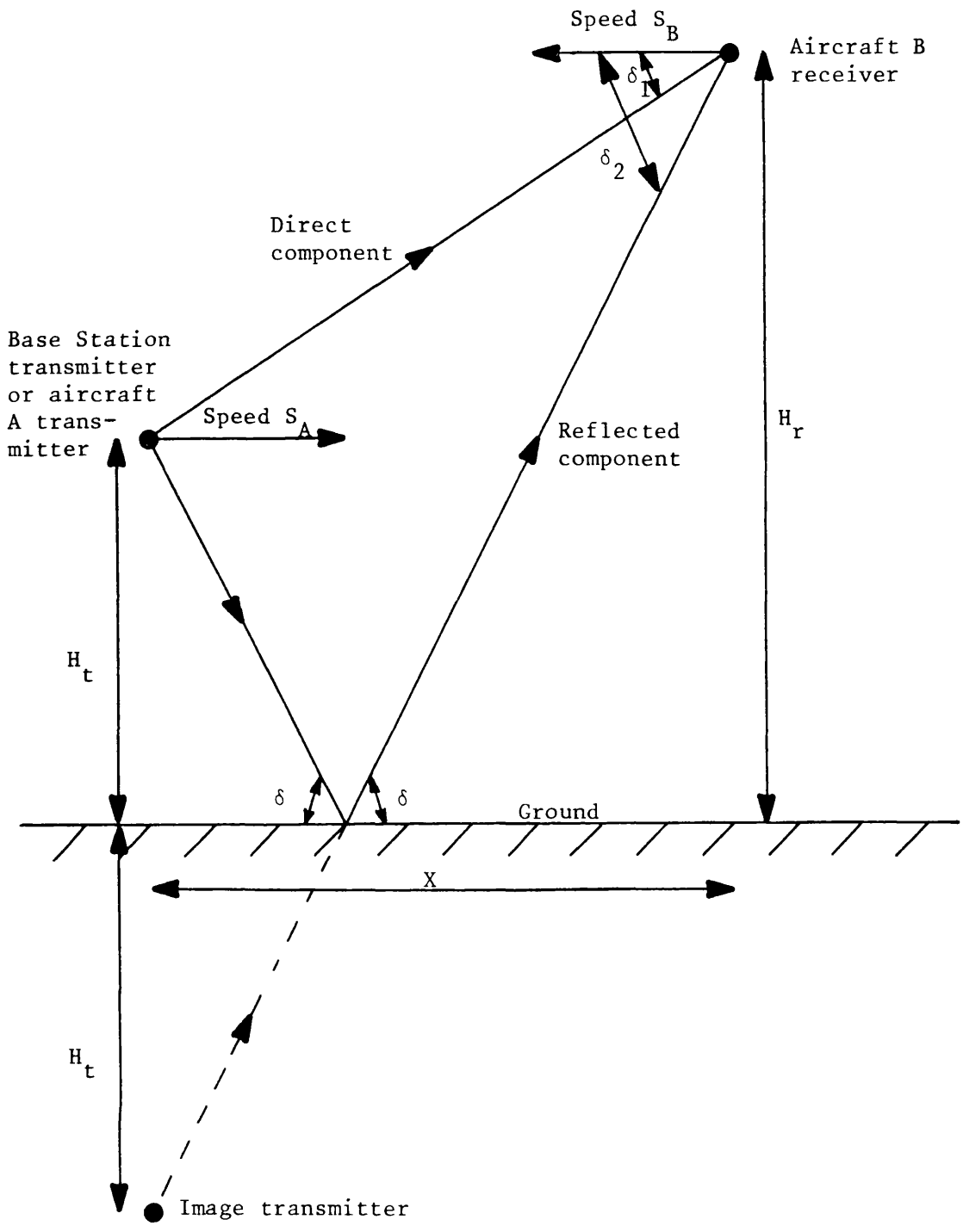
Figure 2.4 Illustration of the simple constant height model of aircraft propagation.

$$R = M \, G_2 \left[\frac{(H_r - H_t)^2 + (X - St)^2}{(H_r + H_t)^2 + (X - St)^2} \right]^{\frac{1}{2}} \qquad (2.35)$$

G_2 is the combined receiver/transmitter antenna gains along the reflected path and term in square roots is the ratio of the 2 path losses.

$$\cos \delta_1 = \frac{X - St}{((X - St)^2 + (H_r - H_t)^2)^{\frac{1}{2}}} \qquad (2.36)$$

(c.f. equation 2.8)

and:

$$\cos \delta_2 = \frac{X - St}{((X - St)^2 + (H_r + H_t)^2)^{\frac{1}{2}}} \qquad (2.37)$$

(c.f. equation 2.9)

Since β varies relatively slowly with time, the fade rate, ω_f, is given to good approximation by:

$$\omega_f \simeq (\cos \delta_1 - \cos \delta_2) \omega_d \qquad (2.38)$$

Unlike the land mobile twin scatterer model, $\cos \delta_1$ and $\cos \delta_2$ always have the same sign so the fade rate can never exceed ω_d, providing the aircraft are always flying at a constant height. However, the fade rates encountered in the aircraft situation can greatly exceed the land mobile situation due to the higher speeds involved. The maximum received fade rate may be calculated for a particular case using Appendix 1. In general, higher fade rates are encountered for inter-aircraft communications where the aircraft are at comparable heights than between a fixed base station and an aircraft.

The maximum fade rate occurs when the received signal strength is the highest. The fading has been described as causing a serious loss of intelligibility in normal amplitude modulated communication systems (2.9). An AGC system in the receiver capable of suppressing the fading could greatly improve the communications quality. Harris (2.10) has reported great difficulties in attempting both to mathematically model feedback AGC and suppress the fading using conventional feedback AGC techniques. Later in this thesis some simple mathematical models of feedback AGC systems are presented together with some unconventional AGC systems with greatly improved fast fading performance.

2.4.4 General Observations

Twin path models can still be used to analyse the received signal when the aircraft are flying more complicated courses. The main discrepancies between practical observations of r(t) and the theoretical predictions may be attributed to the earth's curvature and ground surface roughness. The magnitude of these effects and some practical results are discussed by Reed and Russell (2.9).

When flying over very rough ground it may be difficult to determine the exact time varying nature of the ground reflected signal. In this situation, practical measurements can give an estimate of the worst case (highest) values of fade rate and ground reflected component magnitude. Unfortunately, the obvious practical difficulties of obtaining the appropriate measurements and conducting AGC experiments with aircraft have prevented this topic from being pursued any further here. The remainder of this thesis therefore concentrates on land mobile communications. However, the models and analysis of AGC systems can be readily applied to the aircraft situation.

CHAPTER 3

MULTIPLE PATH COMMUNICATIONS

This chapter considers the more general VHF/UHF land mobile

communications environment where the received signal is the resultant

of many incoming components. The analysis concentrates on fast fading

effects assuming a fixed average received signal strength. The aim is

to derive some simple, relevant deterministic signals that can be used

to analyse and design AGC systems prior to operation in the field.

3.1 Land Mobile Environment

This section describes the physical basis of the various models used

to describe the phenomenon of fast fading in the urban land mobile

environment.

3.1.1 Physical Considerations - Scattering Model

The basic assumption behind most methods of modelling mobile radio

reception is that the received signal is comprised of many incoming components

arriving from all directions via the mechanism of scattering. Scattering

of the original transmitted signal is caused by reflection, refraction

and diffraction by buildings and vehicles in the immediate vicinity of the

mobile. The reception of an additional direct (line-of-sight) component is

usually treated as a special case. Scattering sets up a quasi-stationary

interference pattern of signal peaks and troughs over the required coverage

area. It is assumed here that the presence of the mobile itself does not

affect this pattern.

Without scattering, the received signal strength would be very low

in the absence of any direct component. The relatively large signal

strengths observed in practice in the field when the mobile is completely

surrounded by buildings etc. suggests that scattering, or some similar

mechanism, is present. Assuming this to be so, most models make no

further consideration of the exact physical radio frequency properties

of the environment surrounding the mobile. Instead, it is assumed after

Clarke (3.1) that at any point the received field is made up of a number

of generally horizontally travelling free-space plane waves whose azimuthal

angles of arrival occur at random for different positions of the receiver,

and whose phases are completely random such that the phase is rectangularly

distributed throughout 0 to 2π. This is the basis of the models to be

described in this chapter.

3.1.2 Statistical Method

The statistical method analyses the various statistical properties

of the received signal using mathematical techniques. Perhaps the most

widely quoted author using this method is Clarke (ibid). However, a

slightly more general analysis has been performed by Jakes (3.2). As

described above, both authors assume that a 2-dimensional model

(i.e. a plan view) of the urban environment is a sufficient description.

Recently, a 3-dimensional model has been proposed which also included

vertical propagation of the received signal (3.3). However, the slight

changes in the statistics of the received signal in this case have not

been substantiated by practical measurements. This chapter concentrates

on the well documented 2-dimensional model, as presented by Jakes

(ibid).

3.1.3 Computer Simulation

The other technique available for analysing the statistics of multipath models is that of computer simulation. A recent paper describes a new approach to the problem that not only takes into account fast fading but shadowing effects as well (2.6). Further reference to the paper gives details of the simulation whose results will be used here. A brief description follows.

The starting point of the simulation is a plan of the area under consideration. A number of rectangles are drawn representing buildings in the area on a statistical basis. The centre of each rectangle is regarded as a point scatterer in a similar manner to the twin scattering model described in chapter 2. A "mobile" moves with a fixed velocity, receiving waves from each scatterer, either directly or via a single reflection. If a rectangular block obstructs any wave at some point along the mobiles travel, the wave is abruptly eliminated from the computation of the resulting received signal's envelope. It is claimed that this eliminates waves from more distant scatterers and effectively simulates shadowing. The simulation also allows the addition of a direct component, and provides plots of the primary and secondary statistics of the resultant received signal's envelope.

3.2 Pre-detection Signal Characteristics

Jakes (ibid) concentrates on 1 main characteristic of the pre-detection signal. This is its power spectra as appearing across the input of mobile receiver from the antenna. A uniform horizontal distribution of received power with azimuthal angle is assumed and a vertical whip antenna with a gain of 1.5 is used to sense the vertically polarised electric (E) field.

3.2.1 Electric Field Spectra

Jakes (ibid) gives the power spectra of the E field, S_E, as:

$$S_E = \frac{3b}{\omega} \left[1 - \left[\frac{\omega - \omega_c}{\omega_d} \right] \right]^{-\frac{1}{2}} \qquad (3.1)$$

for $(\omega_c - \omega_d) < \omega < (\omega_c + \omega_d)$, zero otherwise, where b is the mean received power. This is a "U" shaped spectrum, centred on the nominal carrier frequency with a bandwidth of $2\omega_d$, twice maximum Doppler. S_E tends to infinity at $\omega = \omega_c \pm \omega_d$. Aulin (3.3), however, has shown that by considering a small but finite distribution of arrival angles in the vertical plane, different results are obtained. In general, the power spectrum is still "U" shaped but exhibits a finite valued "ledge" over a small region around $\omega = \omega_c \pm \omega_d$.

The pre-detection signal, $e_r(t)$, can be thought of as a randomly amplitude and phase modulated carrier so that:

$$e_r(t) = r(t) \cos(\omega_c t + u(t)) \qquad (3.2)$$

where r(t) and u(t) are infinitely wideband random processes that describe the envelope and phase modulation of the carrier respectively, as introduced by multipath fading. However, r(t) and u(t) are so related that resulting amplitude and phase modulated carrier's bandwidth never exceeds $2\omega_d$.

3.2.2 Direct Components

The effect of a direct component is usually allowed for in the analysis by assuming its angle of arrival does not change over the computation period. This results in the pre-detection power spectrum exhibiting a line or "delta" function at the incoming Doppler frequency. If the arrival angle

of the direct component is μ with respect to the mobile's velocity vector
and δ is the delta function then Jakes (ibid) shows the resultant electric
field spectral density can be written as:

$$S_E^1 = S_E + F\delta(\omega - \omega_c - \omega_d \cos \mu) \tag{3.3}$$

where F is a weighting function.

3.3 Post-detection Envelope Characteristics

This section is concerned with the statistical properties of the
received signal's envelope, $r(t)$, described in equation 3.2. These properties
will be described in some detail since $r(t)$ is the unwanted envelope
variation that AGC has to suppress in the multipath environment.

3.3.1 Probability Distribution

The probability distribution, $p(r)$, of $r(t)$ is given by the well known
Rayleigh density formula. Jakes (ibid) gives this as:

$$p(r) = \frac{r}{b} \exp(-r^2/2b) \quad \text{for} \quad r > 0 \tag{3.4}$$

or zero for $r < 0$, where r is the specified value of $r(t)$. The cumulative
distribution function (CDF) of $r(t)$ is defined by $p(r(t) < r)$ where:

$$p(r(t) < r) = 1 - \exp(-r^2/2b) \tag{3.5}$$

This distribution has an rms value of:

$$r(t)_{rms} = \sqrt{2b} \tag{3.6}$$

and a mean value of:

$$r(t)_{mean} = \sqrt{\frac{\pi b}{2}} \tag{3.7}$$

3.5

The difference between the rms and mean value of r(t) is 1.05 dB. The probability of finding the envelope at low values is very small. For example, it spends 99% of the time above one tenth of the rms value.

Reception of a direct component complicates the analysis of the envelope statistics. The general effect of a direct component is to smooth out the more extreme envelope variations. The probability density function has been evaluated by the work of Rice (3.4), from which it gets its name i.e. "Rician".

3.3.2 Power Spectrum

A full account of the analysis of the power spectrum of r(t) is given by Jakes (ibid). In this analysis, the power spectrum is only evaluated up to $2\omega_d$, twice maximum Doppler. Jakes (ibid) assumes that since 98.2% of the power lies in this band then this is sufficient. However, this means that the total power in the higher harmonics (above $2\omega_d$) is only 17.4 dB down with respect to this fundamental band. It will be shown later that knowledge of the higher harmonics of the detected envelope's spectrum is required for the analysis of AGC systems. Unfortunately, it has not been possible to evaluate the more general expanded integrals of the hypergeometric series to include the higher harmonics. The result presented here is that derived by Jakes (ibid). The power spectrum of r(t) is given by S_r where:

$$S_r = \frac{b}{4\omega_d} K\left[\left[1 - \left[\frac{\omega}{2\omega_d}\right]^2\right]^{\frac{1}{2}}\right] \qquad (3.8)$$

where K { } is the complete elliptic integral of the first kind and S_r is valid to $2\omega_d$. The true spectrum of r(t) extends to infinity.

3.3.3 Level Crossing Rates

The envelope r(t) falls to small values infrequently, shallower fades occuring more often. A useful indication of this phenomenon is the level crossing rate, N_r. This is the expected rate at which the envelope crosses a specified level, r, in the positive direction. If the normalised value, ρ, of r is defined by:

$$\rho = \frac{r}{r_{rms}} = \frac{r}{\sqrt{2b}} \qquad (3.9)$$

then the level crossing rate is given by Jakes (ibid) as:

$$N_r = \frac{\omega_d}{\sqrt{2\pi}} \, \rho \, \exp(-\rho^2) \qquad (3.10)$$

3.3.4 Duration of Fades

The average duration, T, of the time spent below the level ρ is given by Jakes (ibid) as:

$$T = \frac{\exp(\rho^2) - 1}{\rho \, \frac{\omega_d}{\sqrt{2\pi}}} \qquad (3.11)$$

The envelope spends a relatively small amount of time below the smaller levels.

3.3.5 Computer Simulation

3 sets of results have been presented for different plan layouts (2.6). Only 2 sets are discussed here since 1 set contains a direct wave. The analysis of the envelope was presented by 4 graphs. These are of the cumulative distribution, level crossing rates, fade duration and power spectrum. The following general observations are made of the relevant results:

i) They both had good fits to the Rayleigh CDF.

ii) In one case the level crossing rate was also a good fit to the "Rayleigh" predictions. In the other case there was a slight tendency to cross the deeper fades less frequently.

iii) In both cases, the duration of fades was a good fit to the "Rayleigh" prediction.

Perhaps the most interesting aspect of the simulation was the prediction of the power spectrum of r(t). A more full analysis has been made to include energy above twice maximum Doppler. The computer simulation showed marked deviations from the "Rayleigh" predictions. Practical results obtained from the field showed good agreement with the computer simulation predictions, even when the simulation plan was not completely identical to the field trial area.

The emphasis in this chapter is on the properties of a carrier wave at a single transmitted frequency as received by the mobile. There are several other important properties of the multipath environment not discussed so far. These include the effect of time delay spread and the statistical properties of the received signal's phase, u(t). These will be discussed later on at the relevant point in the thesis.

3.4 Comparison of Twin and Multiple Path Models

As mentioned earlier, this thesis concentrates on the analysis of the response of AGC systems to deterministic signals, as the exact analysis of AGC response to non-deterministic (e.g. multipath) signals is very complicated. This section presents a comparison of the general

properties of twin and multiple path signals. The aim is to show that
many properties of a twin path signal are likely to be more difficult
for an AGC system to cope with than a multiple path signal. This will
allow design of AGC systems that are to be operated in the multipath
environment to be based on more simple "worst case" analysis.

3.4.1 General Characteristics

The general shape of individual fades of the received signal's
envelope in twin and multiple path reception is similar. This can be
seen from plots shown in figure 3.1 comparing twin and multiple path
envelopes. The twin path envelope is computed from equation 2.15 while
the multiple path envelope is plotted from results taken in the field,
as described in the next chapter. The most obvious difference between
twin and multiple path reception is that with the former, successive
fades are (nearly) identical, whereas with the latter they are usually
different. Multiple path reception may be modelled by twin path reception
with time varying values of R and ω_f so that they change the shape of
each cycle of fade. However, this approach is not adopted here and twin
and multiple path reception are treated as 2 separate cases.

In the comparison to follow, the twin path received signal $e_r(t)$,
will be given by:

$$e_r(t) = E(\cos(\omega_c t - \omega_d t) + R \cos(\omega_c t + \omega_d t)) \qquad (3.12)$$

That is, the signal will be assumed to fade at the maximum expected
rate of twice ω_d. The general "Rayleigh" signal will be used to describe
the multiple path case. The comparison will be made between the "Rayleigh"
signal and 4 cases of the twin path signal. The twin path signals
have values of R of 1, 0.9387, 0.8182 and 0.5195 corresponding to peak

Multipath envelope, ω_d = 20 Hz

Twin path envelope, K_i = 10 dB

Twin path envelope, K_i = 20 dB

Twin path envelope, K_i = 30 dB

time
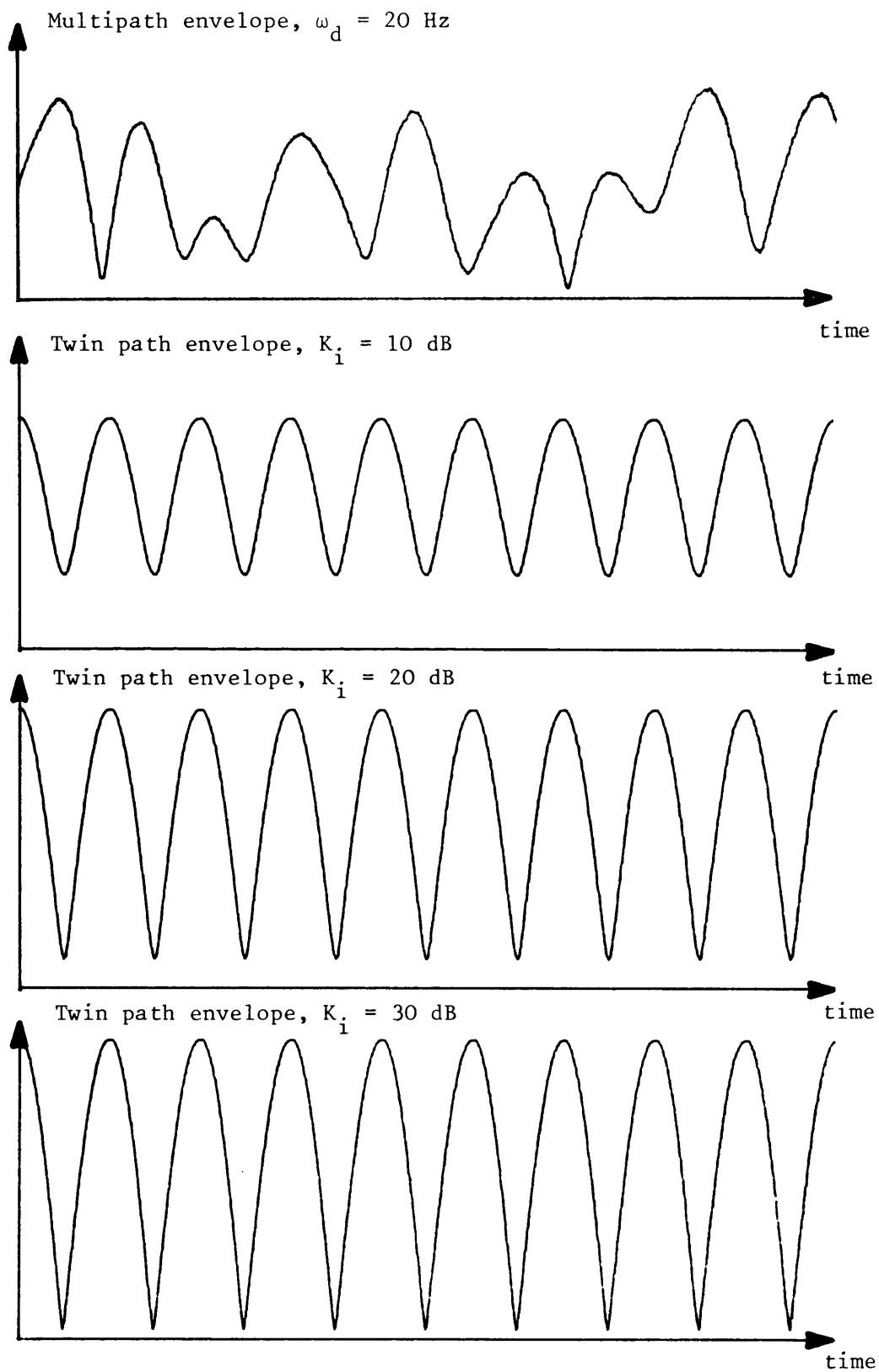
Figure 3.1   A comparison of the general shape of multiple path
and twin path envelope fading.

3.10

to trough fade ratios, K_i, of infinity, 30 dB, 20 dB and 10 dB

respectively.

3.4.2 Pre-detection Spectra

In order to distinguish between twin path and multiple path signals

the subscripts "tp" and "mp" will be used. The pre-detection power

spectrum of the twin path signal is given by S_{Etp} where:

$$S_{Etp} = \frac{E^2}{2} (\delta(\omega - (\omega_c - \omega_d)) + R^2\delta(\omega +(\omega_c+\omega_d))) \qquad (3.13)$$

The pre-detection power spectrum of the multipath signal, S_{Emp}, is given

by equation 3.1. Figure 3.2 compares the two spectra. Both S_{Etp} and

S_{Emp} are narrowband processes with zero energy outside $\omega_c \pm \omega_d$. However,

S_{Etp} is a discrete function while S_{Emp} is a smooth function with energy

distributed across the band.

3.4.3 Post-detection Statistical Comparison

This section compares the post-envelope detection properties of the

two cases as defined by sections 2.3.3 and 3.3.1-3.3.4. The axes of

the twin path graphs are labelled assuming E is unity while the axes of

the multiple path graphs are labelled assuming b is unity. The properties

that are compared are:

a) Probability Distribution. Equation 2.29 defines the probability

density of the twin path signal while equation 3.4 defines the probability

density of the multipath signal. Figure 3.3 shows the 2 equations

plotted on similar axes. The 2 plots are evidently very different. The

probability of finding the twin path envelope near its extremes is much

higher than with the multiple path envelope. The multiple path envelope

tails off slowly with increasing r compared to the twin path envelope.

3.11
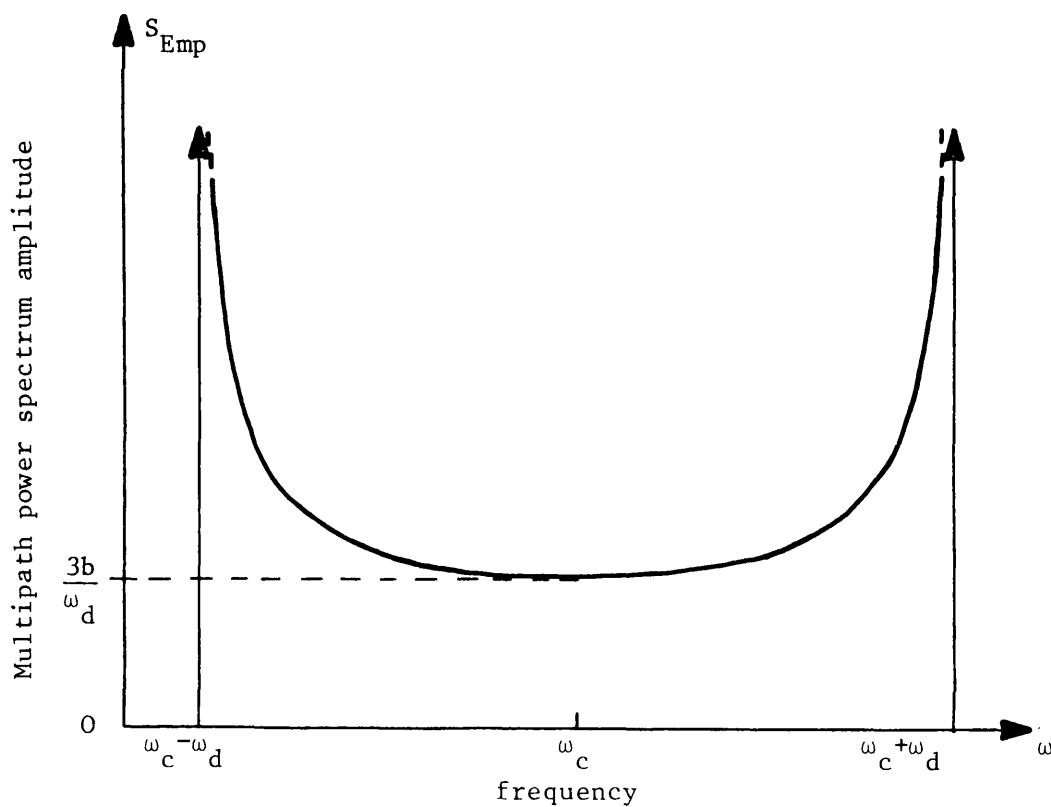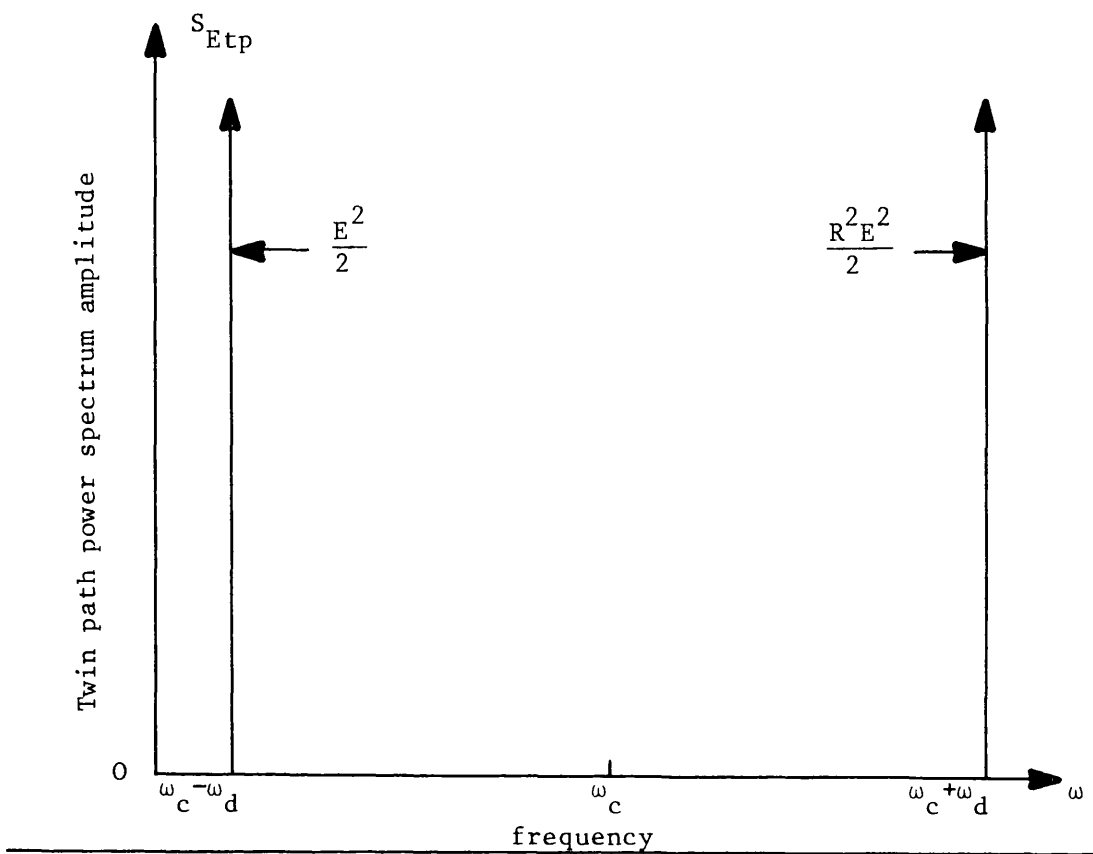
Figure 3.2   Comparison of the 2 pre-detection power spectra.
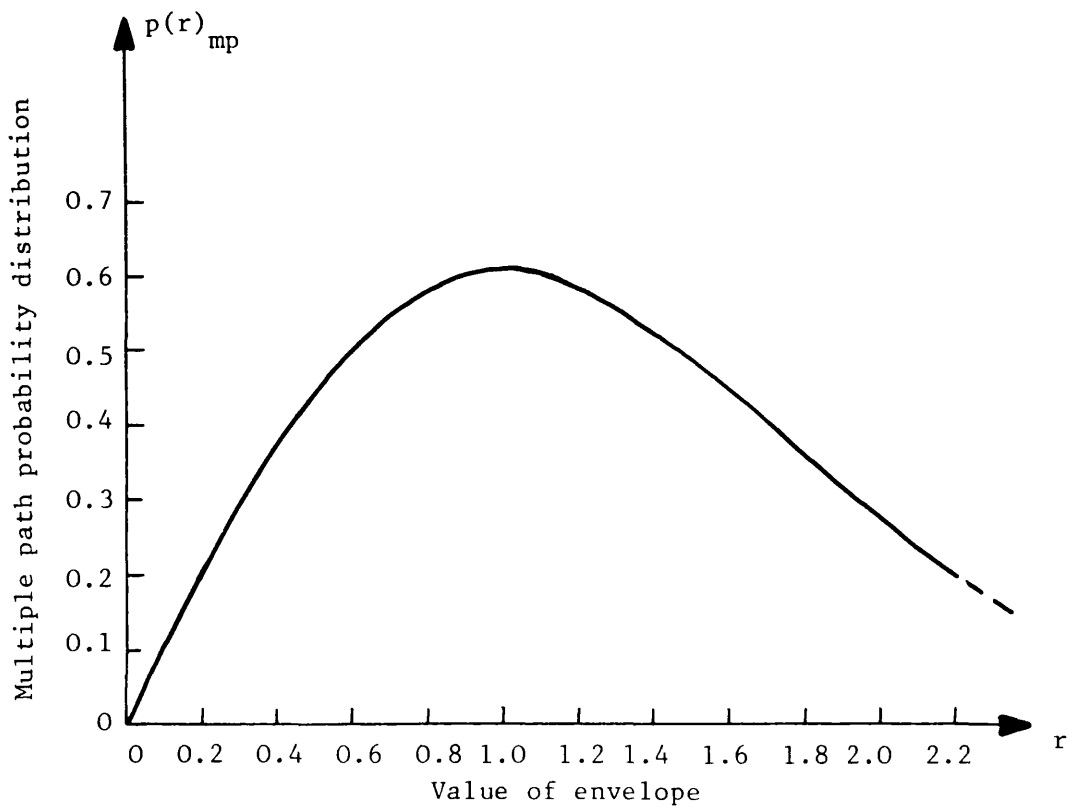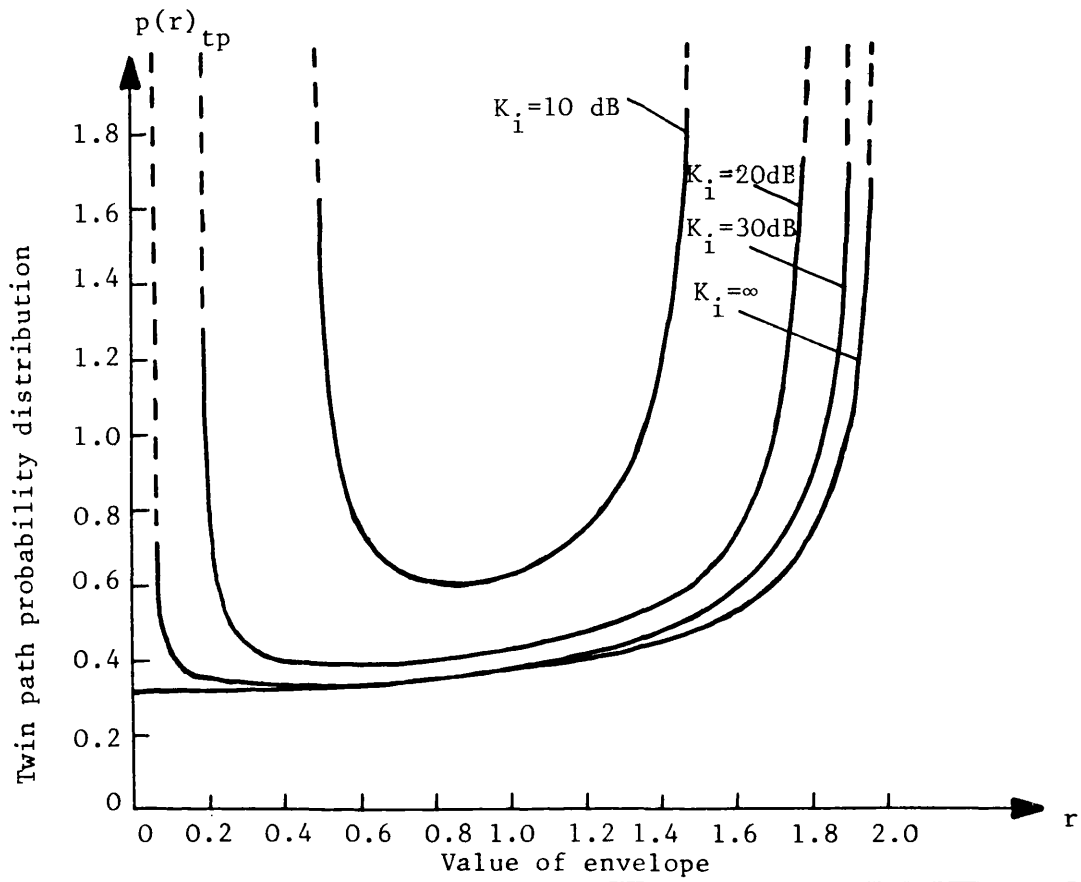
Figure 3.3   Comparison of the 2 post-detection probability distributions

b) Power Spectrum. Equation 2.21 with N = 64 was used to calculate the various harmonics of the twin path signal while equation 3.8 was used for the multipath spectrum. Figure 3.4 compares the 2 spectra. The comparison is not complete due to the lack of information on the multipath spectrum above twice maximum Doppler.

c) Level Crossing Rates. The level crossing rate of the twin path signal is evidently $2\omega_d$ for $(1 - R) \leqslant r \leqslant (1 + R)$, zero otherwise. This is plotted along with the multipath predictions from equation 3.10 in figure 3.5. The twin path signal has a much higher level crossing rate, over the range of levels it exists, than the multipath signal.

d) Duration of Fades. The duration of a twin path fade is available from equation 2.30 while equation 3.11 gives the same for the multipath case. Figure 3.6 compares the 2 equations. The duration of a twin path fade is seen to be much less than multiple path fades.

In general, an AGC system has more difficulty in suppressing fades the more rapid and the more deep they are. On this basis, the preceding graphs and analysis indicate that the twin path signal is a worst case signal for an AGC system to deal with compared to the multipath signal. This thesis will test the hypothesis experimentally that an AGC system capable of suppressing twin path fading of a certain peak to trough ratio at a fade rate of twice maximum Doppler will always perform better in the multipath environment to fades of the same peak to trough ratio.

3.5 AGC Test Signals

This section discusses the signals used in this work to analyse, design and characterise AGC systems for mobile radio receivers.
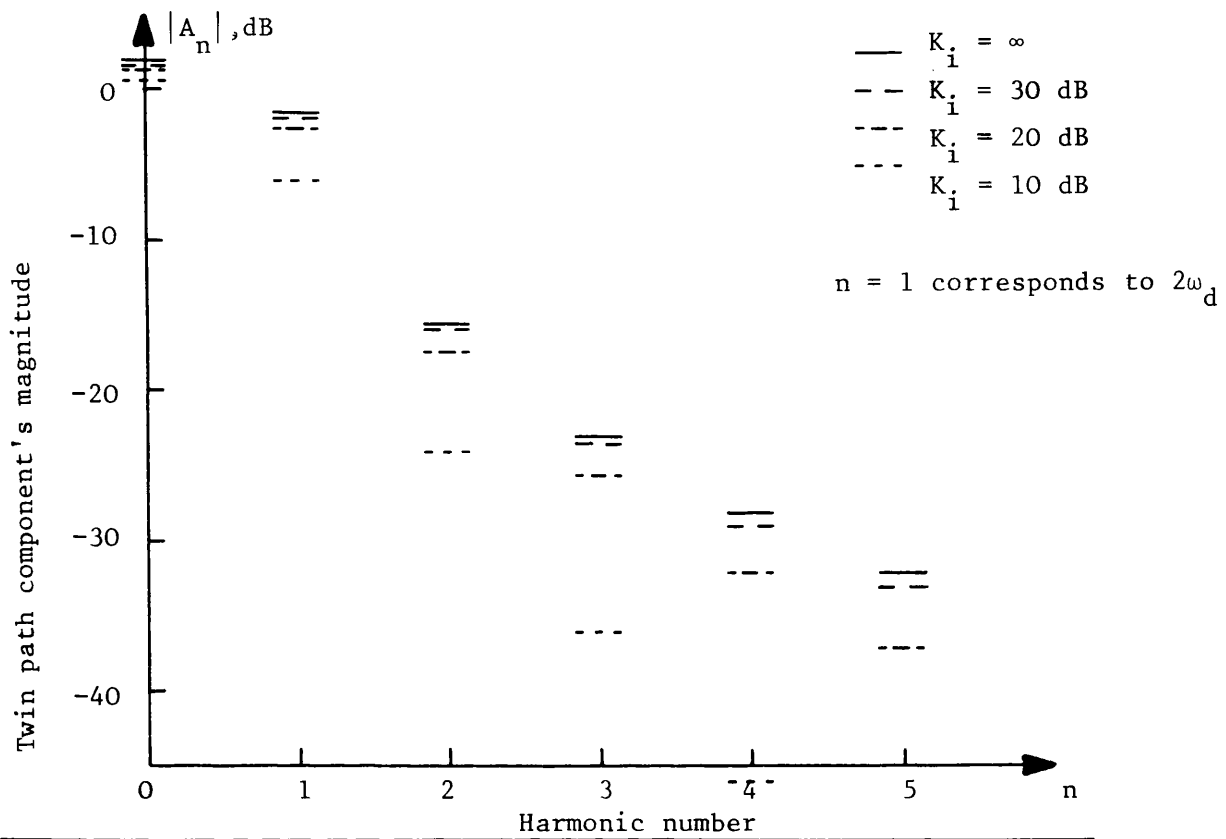
3.14
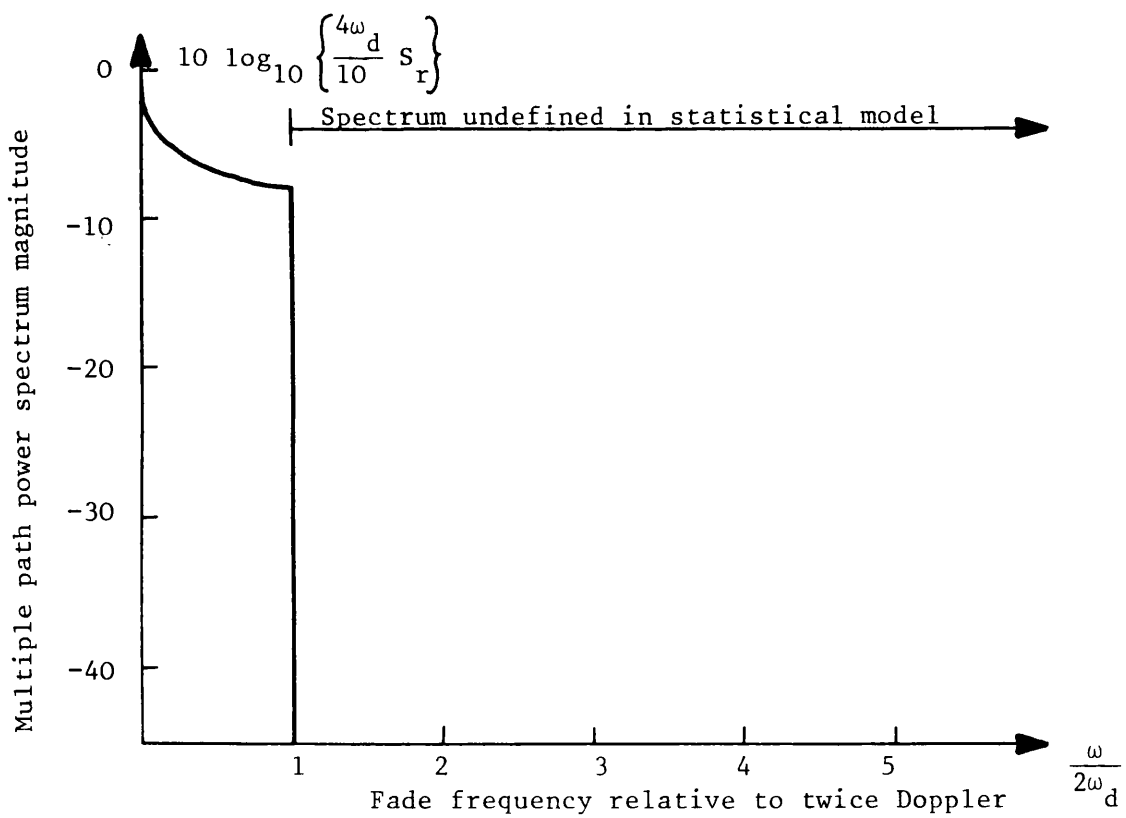
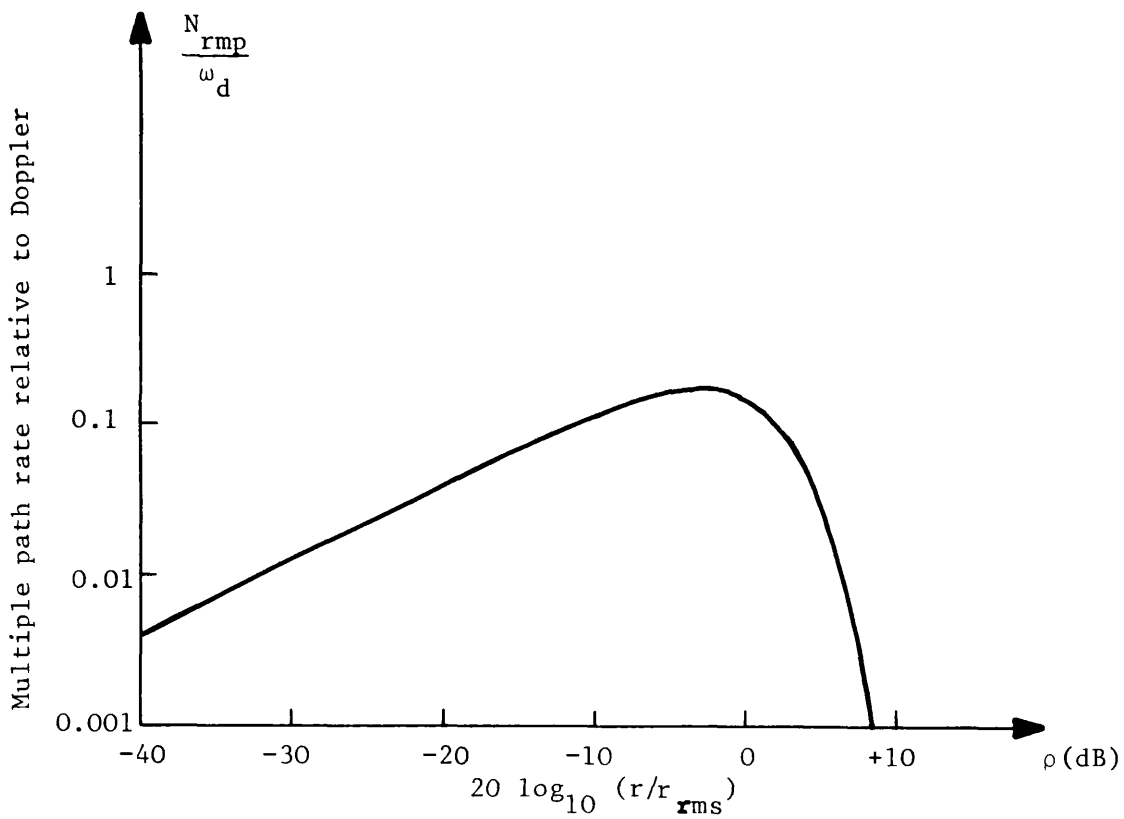Figure 3.4   Comparison of the 2 post-detection spectra
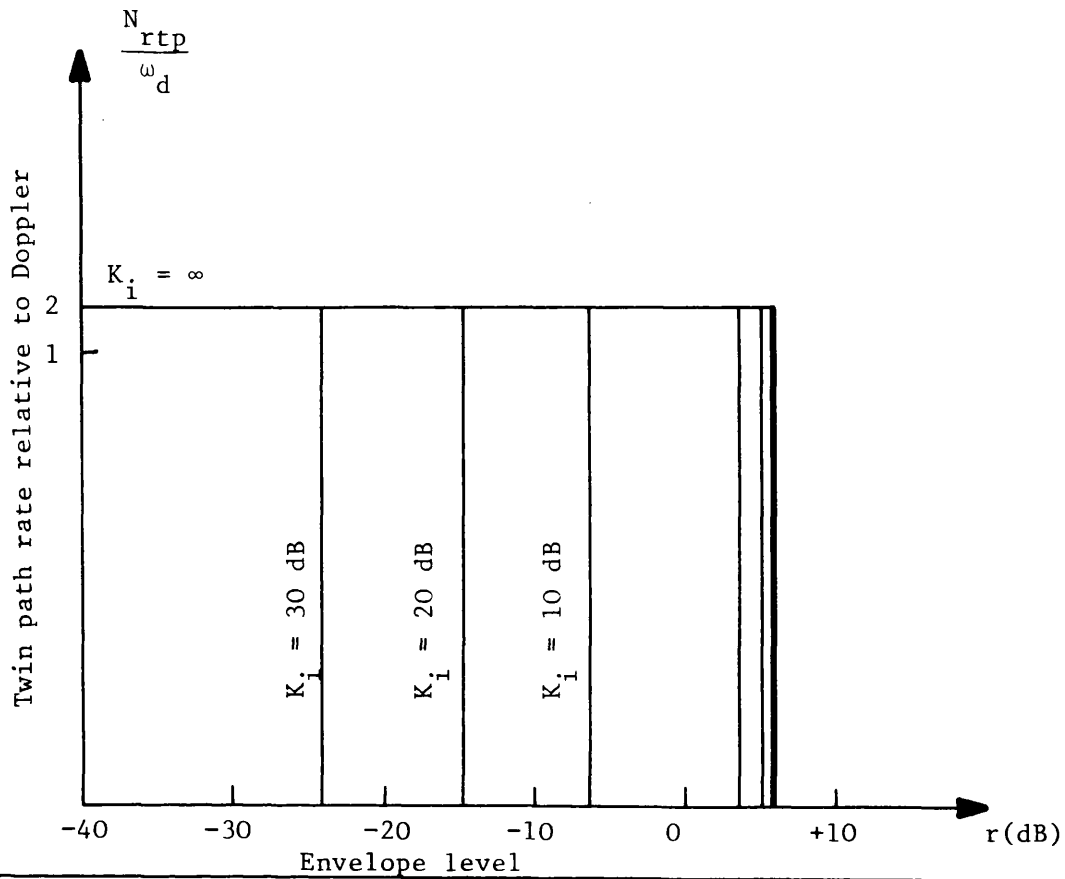
Figure 3.5   Comparison of the 2 post-detection envelope level
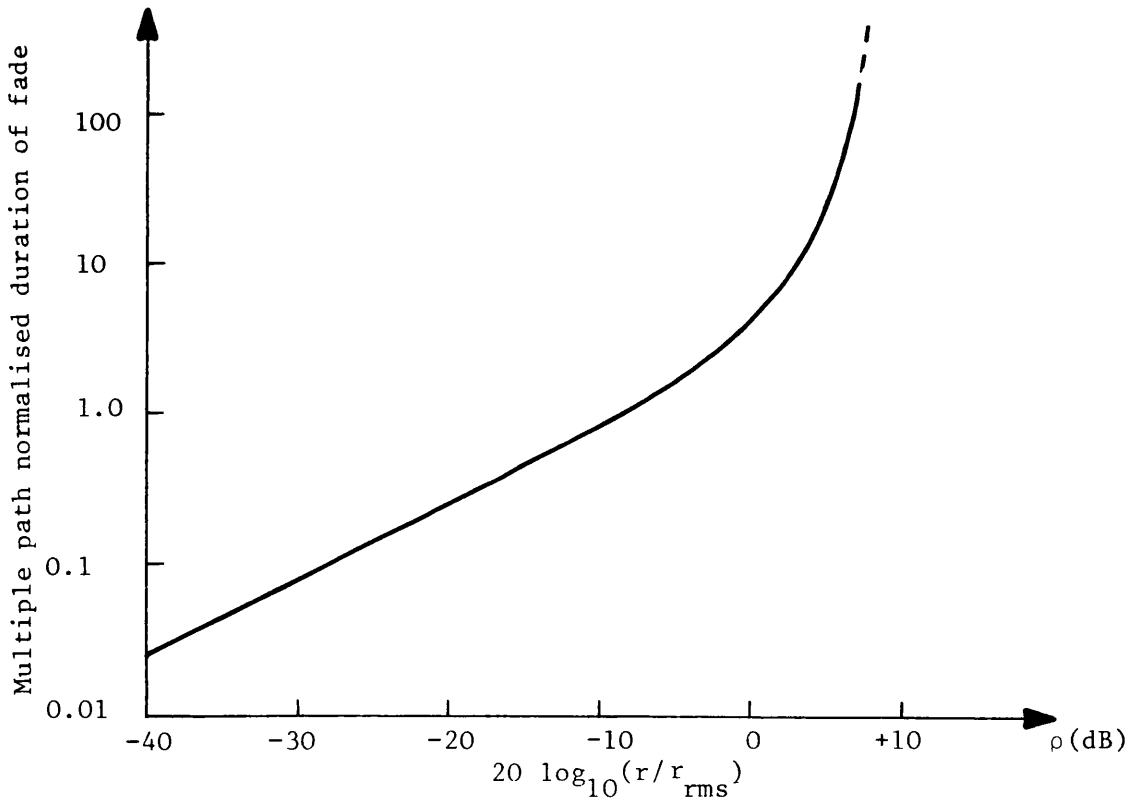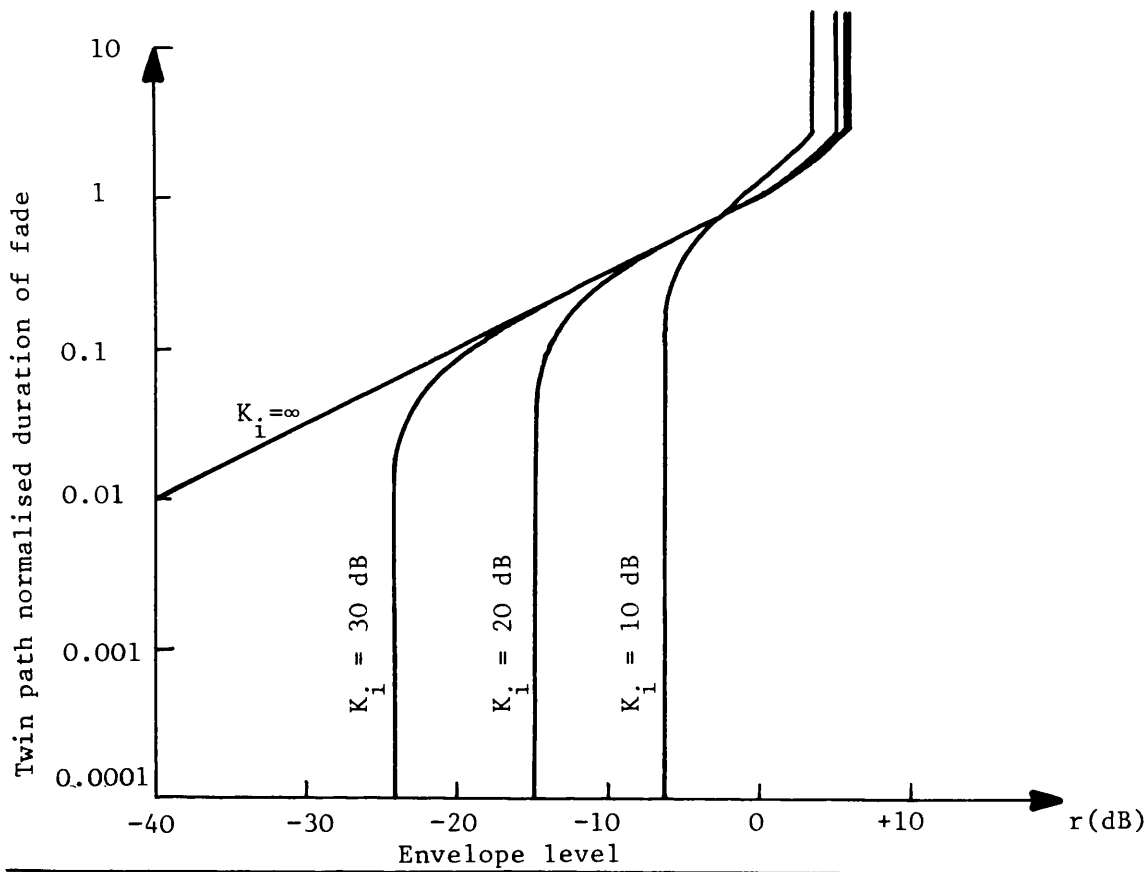   crossing rates

Figure 3.6 Comparison of the 2 post-detection envelope durations of fade.

3.5.1 Deterministic and Random Signals

2 deterministic and 1 source of random AGC test signals will
be used. The 2 deterministic signals will be used to show that the
response of an AGC system depends on the exact time varying nature of
the input envelope and not just on the peak to trough ratio and rate
of fading. The random AGC test signals will be obtained from recordings
of multipath fading from the field.

An AGC system should not only suppress unwanted envelope variations
but should not distort required envelope variations. The deterministic
AGC test signals are chosen so that they both fulfil a dual role. In
each case they can represent either a wanted or unwanted input envelope
variation. It will become apparent throughout the remainder of this
thesis that the main problem an AGC system faces is to distinguish
between the 2 sorts of envelope variations.

3.5.2 Deterministic AGC Test Signal One

One of the simplest tests of an AGC system's performance involves
sinusoidally modulating the input signal's envelope and observing the
response. The first deterministic AGC test signal is based on this and
comprises an envelope variation of the form:

$$r_1(t) = E(1 + D \sin \omega_s t) \tag{3.14}$$

where $0 < D < 1$ and ω_s is the modulation frequency in radians per second.
This signal has 2 main uses. First, it can represent some unwanted
signal variation, so the ability of an AGC system to suppress it is
required. Secondly, it can represent a wanted signal variation, so
the requirements for an AGC system to pass it undistorted are also
needed.

It has been suggested that it is possible to use $r_1(t)$ as a simple representation of multipath fast fading (8.4). However, it will become apparent later on that serious errors can arise through making this assumption if care is not taken. Nevertheless, the response of an AGC system to sinusoidal fading is revealing, and a full sinusoidal analysis will be made of the AGC systems under consideration.

3.5.3 Deterministic AGC Test Signal Two

The second deterministic AGC test signal is based on the twin path signal. It consists of 2 tones spaced ω_f apart in frequency, of relative level R, giving an envelope variation of the form:

$$r_2(t) = E(1 + R^2 + 2R \cos \omega_f t)^{\frac{1}{2}} \qquad (3.15)$$

The various properties of this signal have already been discussed. Once again, this signal has 2 main uses. Firstly, it can represent twin path fading so the ability of an AGC system to suppress it is required. Secondly, 1 tone can represent an interfering signal so the requirements for an AGC system not to respond to the interference are also needed.

3.5.4 Random AGC Test Signals

The final test of an AGC system for a mobile radio receiver is of its performance in the field, in the multipath fading environment. The ideal random AGC test signal is therefore obtained from multipath fast fading data. This could be obtained from fading simulators such as those described by Jakes (ibid). However, the approach adopted here is to obtain recordings of received signals in the field, and then play them back to various AGC systems in the laboratory. A problem is that

the multipath signals described so far consist of a randomly amplitude and phase modulated radio frequency (RF) signal. Receiving and demodulating this signal with a full carrier AM receiver will only provide information about envelope variations, while an FM receiver will only provide information about frequency variations. It is required to preserve the signal in its original form, i.e.:

$$e_r(t) = r(t) \cos(\omega_c t + u(t)) \qquad (3.16)$$

without independent demodulation of $r(t)$ and $u(t)$. The complete signal cannot be easily recorded at RF. The obvious solution is to use a frequency translating receiver to generate the signal $e_{ra}(t)$ from $e_r(t)$ where:

$$e_{ra}(t) = r(t) \cos(\omega_a t + u(t)) \qquad (3.17)$$

where ω_a is some convenient audio frequency. Frequency translation of this sort without amplitude or phase demodulation is automatically performed by a single sideband receiver. The operation of single side-band in the multipath environment is also of interest in its own right. The next chapter describes the design, construction and operation of a recording single sideband system used to provide the random AGC test signals.

3.20

CHAPTER 4

UHF SSB SYSTEM

This chapter describes the design and operation of an SSB system

operating at 456.925 MHz that is comprised of an audio processor,

transmitter and receiver. Although designed primarily to provide the

frequency translated carrier or pilot for test recording purposes, it

was also engineered to provide a speech communications channel.

4.1 Tone-in-band Modulation

This section describes the problem of simultaneous pilot and speech

transmission. Transmitting the pilot with the speech allows automatic

operation of the receiver gain and frequency control functions.

4.1.1 General Description

"Tone-in-band" (TIB) describes any narrowband SSB system that

transmits a low-level pilot in a notch situated at some point within

the baseband channel's spectrum. The UHF TIB SSB system described here

is based on the Wolfson VHF system. The Wolfson VHF system uses SSB

to transmit speech and data in 5 kHz channel spacings (1.8). The

Wolfson VHF system is aimed particularly at the civil land mobile radio

service and a great deal of the research has been conducted at "low

band", i.e. 86.2875 MHz. By transmitting a pilot together with the

speech it is possible to automatically tune (clarify) the local

oscillators in the receiver for satisfactory operation. Furthermore,

the pilot can be used by the AGC and squelch circuitry as an amplitude

reference. The pilot is notched out of the received signal prior to final audio amplification. The exact shape of the notch in the transmitted spectrum of the Wolfson VHF system is designed from PLL "speech pulling" considerations, described elsewhere (4.1).

The UHF system uses a wider, more rectangular notch in the transmitted signal than the VHF system. The UHF system also uses a slightly lower peak speech to pilot ratio of 10 dB, compared to the 15 dB ratio used in the VHF system. The UHF system's notch and pilot level were designed to minimise the speech interference around the pilot, baseband frequency 1.67 kHz, after it had passed through the bandpass filter described in chapter 9.

4.1.2 UHF Audio Processor (UAP)

The UAP processes the baseband speech signal prior to the input of the UHF SSB transmitter. The block diagram of the UAP is shown in figure 4.1, which shows it performing the following operations on the speech input:

i) The speech is first amplified and clipped by a commercially available Datong automatic RF speech processor, model ASP. This provides variable speech compression and defines the peak speech level. An output is available consisting of a 700 Hz tone at the peak speech level which is useful for calibrating the system.

ii) The output of the "Datong" is then applied to the notch circuit. The notch was formed by the parallel addition of a lowpass and bandpass (effectively highpass) filter as shown in figure 4.2. These filters were constructed using commercially available integrated circuit transversal
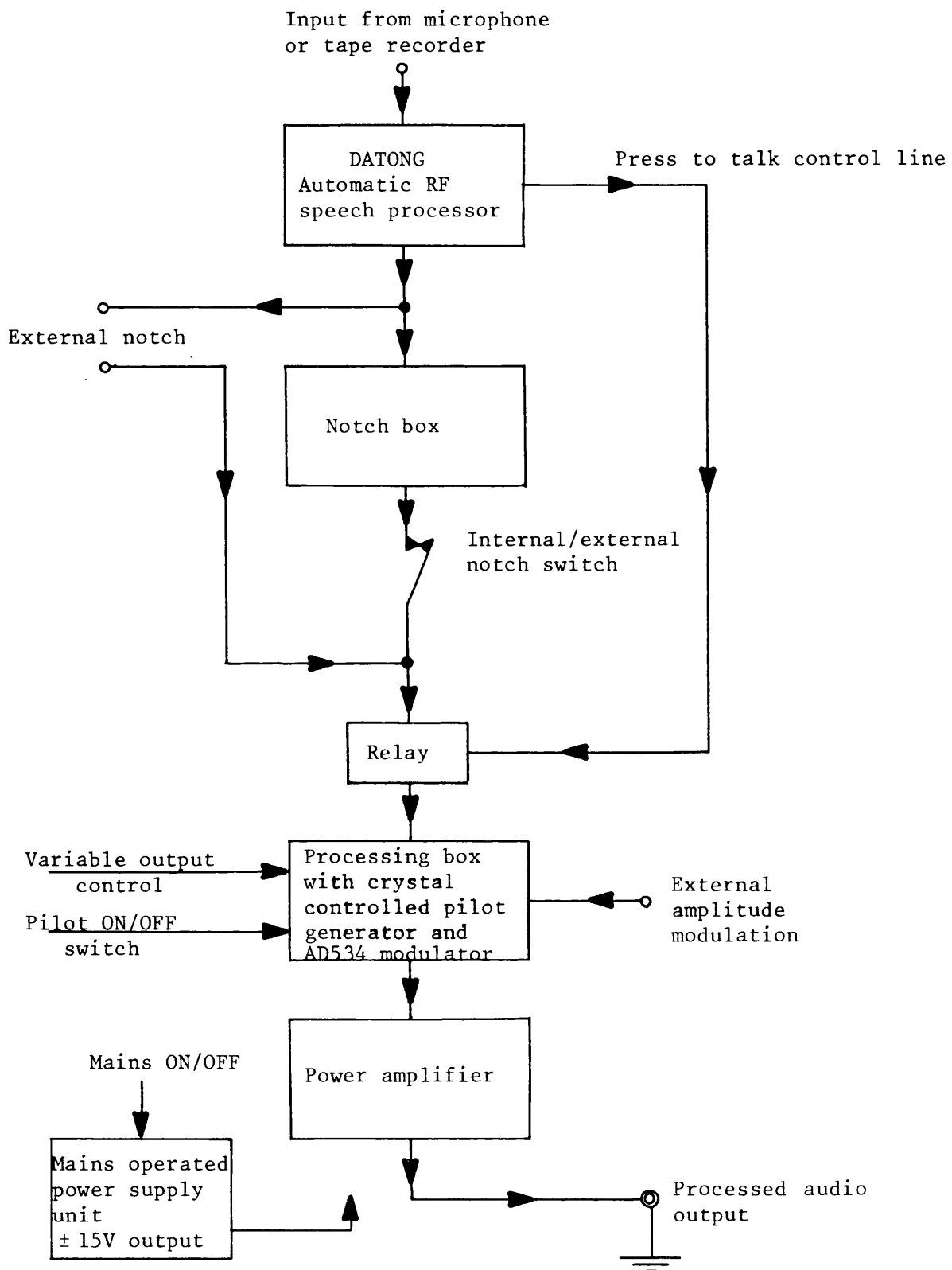
4.2

Input from microphone
or tape recorder

DATONG
Automatic RF
speech processor

Press to talk control line

External notch

Notch box

Internal/external
notch switch

Relay

Variable output
control

Pilot ON/OFF
switch

Processing box
with crystal
controlled pilot
generator and
AD534 modulator

External
amplitude
modulation

Mains ON/OFF

Power amplifier

Mains operated
power supply
unit
± 15V output

Processed audio
output

Figure 4.1 Block diagram of UHF audio processor

From DATONG → Variable gain pre-amplifier → 4th order lowpass Butterworth anti-aliasing filter -3 dB @ 4 kHz

Reticon R5602-1 transversal low-pass filter

44.902 kHz

Crystal controlled independently programmable clocks

43.947 kHz

Reticon R5602-4 transversal wide-bandpass filter

Summing amplifier

4th order lowpass Butterworth smoothing filter -3 dB @ 4 kHz → To relay
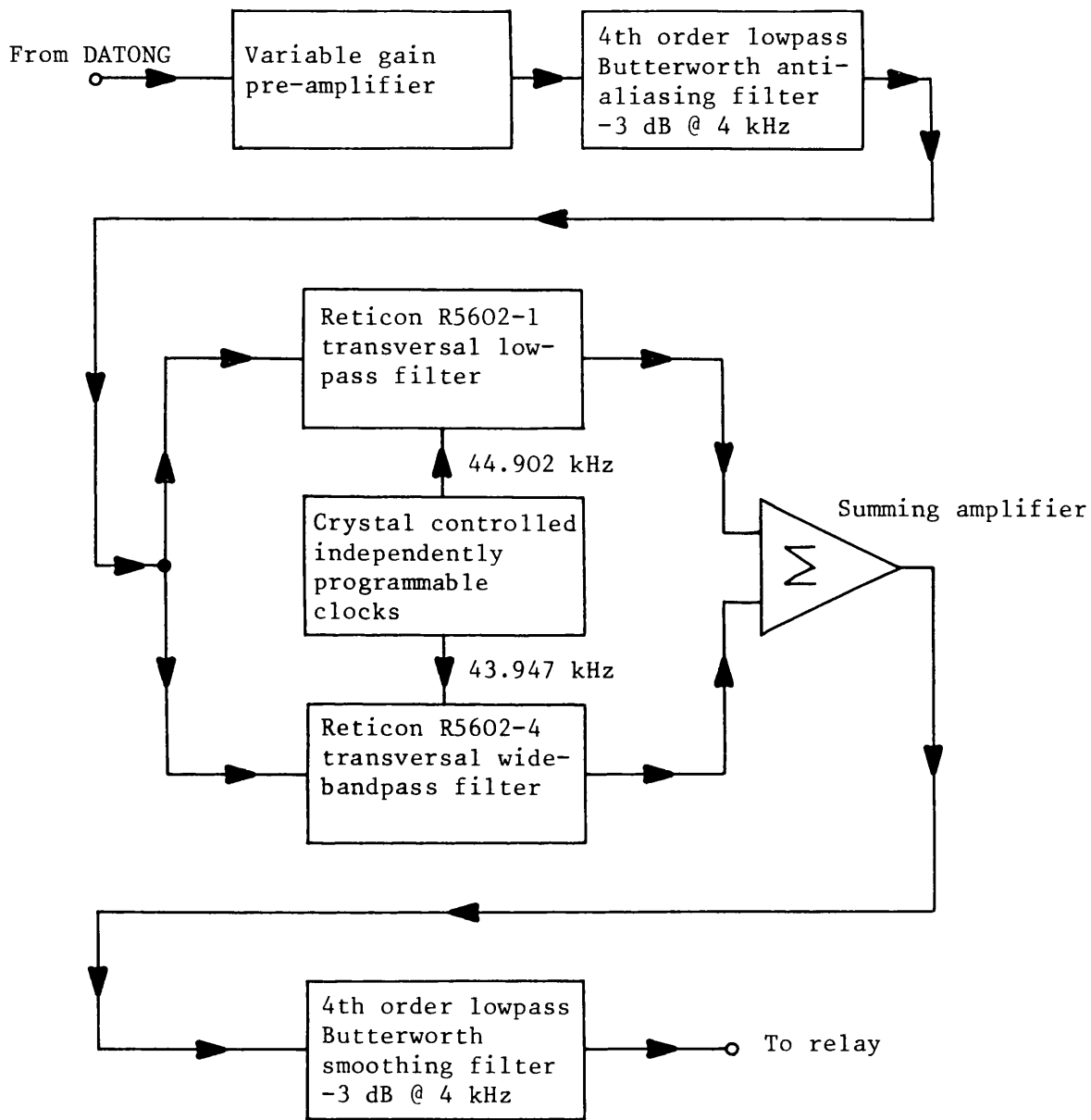
Figure 4.2   Block diagram of notch box

filters, the R5602-1 and R5602-4 (Reticon). The clocks required for both these devices were synthesised by independent frequency division of the output of a 4.131 MHz master crystal oscillator, with both filters sampling at one quarter of the applied clock frequency. 4th order Butterworth lowpass filters, -3 dB at 4 kHz, were used as input anti-aliasing and output clock smoothing filters. The resulting notch box frequency response is shown in figure 4.3.

iii) The output of the notch box, which can be by-passed if required, is then passed through a relay operated by a press-to-talk control line. The output of the relay is then passed into a general processing box. This adds a crystal controlled 1.67 kHz pilot tone to the incoming signal, -10 dB with respect to peak speech power. External amplitude modulation is possible using a linear modulator based on an AD534 (Analogue Devices) multiplier. The output level of this box is controlled by a user-accessible potentiometer, and a switch is incorporated to turn off the pilot if not required. The output is then passed into the final stage, an audio power amplifier capable of driving the 50 Ω input impedance of the low level UHF SSB generator.

The frequency response of the complete UAP from the input of the "Datong" to the power amplifier's output is shown in figure 4.4. The droop in the response, relative to the notch box alone, is caused by the "Datong". It is felt that the notch caused negligible distortion of the baseband speech signal's quality.
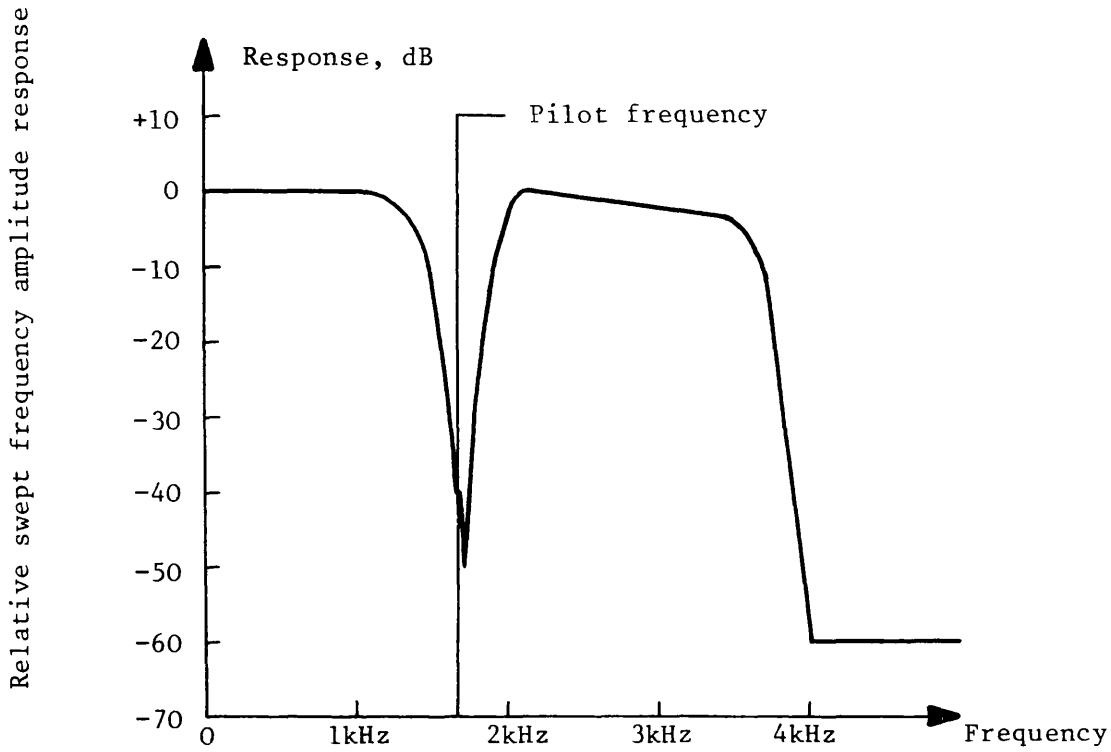
Figure 4.3 Frequency response of notch box
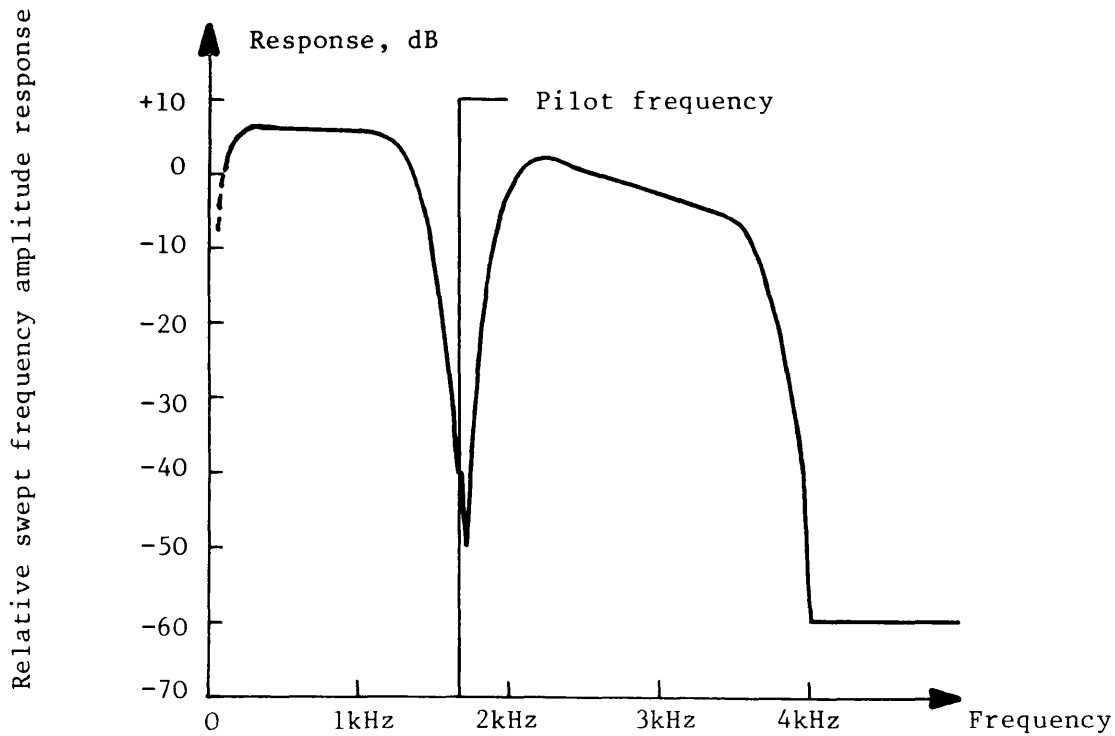
Figure 4.4 Frequency response of complete UHF audio processor

4.2 Transmitter

The transmitter generates the high power SSB signal in two main stages. Firstly, low level "on-channel" SSB is generated using the filter method (4.2). This is then followed by a linear amplifier to provide the required power.

4.2.1 Low Level UHF SSB Generator

This generates the on-channel SSB signal at low power levels, -15 dBm of pilot. Upper sideband modulation is used and the pilot is transmitted at 456.92667 MHz. The SSB is generated in 2 frequency conversion stages, shown by figure 4.5, as follows:

i) The incoming audio from the UAP is passed through an attenuator to the first double balanced mixer (DBM). In conjunction with a 10.7 MHz temperature compensated crystal oscillator, this unit generates a double sideband signal at 10.7 MHz. A crystal filter is used to select the upper sideband.

ii) The 10.7 MHz SSB signal is then passed through another attenuator to the input of a high frequency DBM. The local oscillator for this DBM, at 446.225 MHz, is derived from a voltage-controlled oven-compensated crystal oscillator (VCOCXO) operating at 27.8890625 MHz. The output of the high frequency DBM is bandpass filtered to give the required sideband prior to final amplification. The RF output provides -15 dBm of pilot at 456.92667 MHz when the audio input is driven by 1V peak-to-peak of pilot at 1.67 kHz.

456.925 MHz
SSB RF OUT

Aydin vector
MHD-152 RF amplifier

Mains ON/OFF

Mains operated
power supply
unit +10 Volt
DC output

External frequency control

Wainwright WBA-457-4AA1
Bandpass filter

446.225 MHz VCOCXO+drivers

N   is an attenuator
     pad, "N" is loss
     in dB

10.7 MHz SSB
Generator

Lorch FC-20IZ
double balanced mixer

10.7 MHz TCXO
and drivers

crystal filter

Audio in

MD113 double
balanced mixer

Figure 4.5   The low level UHF SSB generator

4.8

4.2.2 Power Amplifier

The power amplifier was obtained from SOTA Communication Systems.
It was designed to have a linear gain of 50 dB and provide a peak
envelope power (PEP) to the antenna feeder of 40 Watts. The antenna
was a 6 dB gain collinear mounted on the roof of the Wolfson Laboratory,
University of Bath. When in use, the pilot was transmitted at 2 Watts
with both forward and reflected power monitored on a throughline Watt-
meter. A photograph of the complete transmitter, comprising UAP, low
level UHF SSB generator and linear power amplifier is shown in figure 4.6.

4.2.3 Performance

The frequency response of the low level UHF SSB generator, defined
by the 10.7 MHz crystal filter, is shown in figure 4.7. When delivering
2 equal amplitude tones each at -10 dBm to the linear amplifier, the
third order intermodulation distortion products of the low level UHF SSB
generator are at -50 dBm and -60 dBm.

The linear power amplifier increased the distortion so that when
delivering 10 W_{rms} of 2 equal amplitude tones (40 W PEP) the third order
intermodulation distortion products were only -26 dB with respect to
either tone. In practice, with 2 Watts of pilot transmitted, the peak
transmitted envelope power was 17 Watts during speech modulation.

4.3 Receiver

The receiver is a phaselocked superhet with an intermediate frequency
(IF) of 10.7 MHz (4.3). Its construction was simplified by using the
appropriate circuit boards from the Wolfson VHF receiver wherever possible.
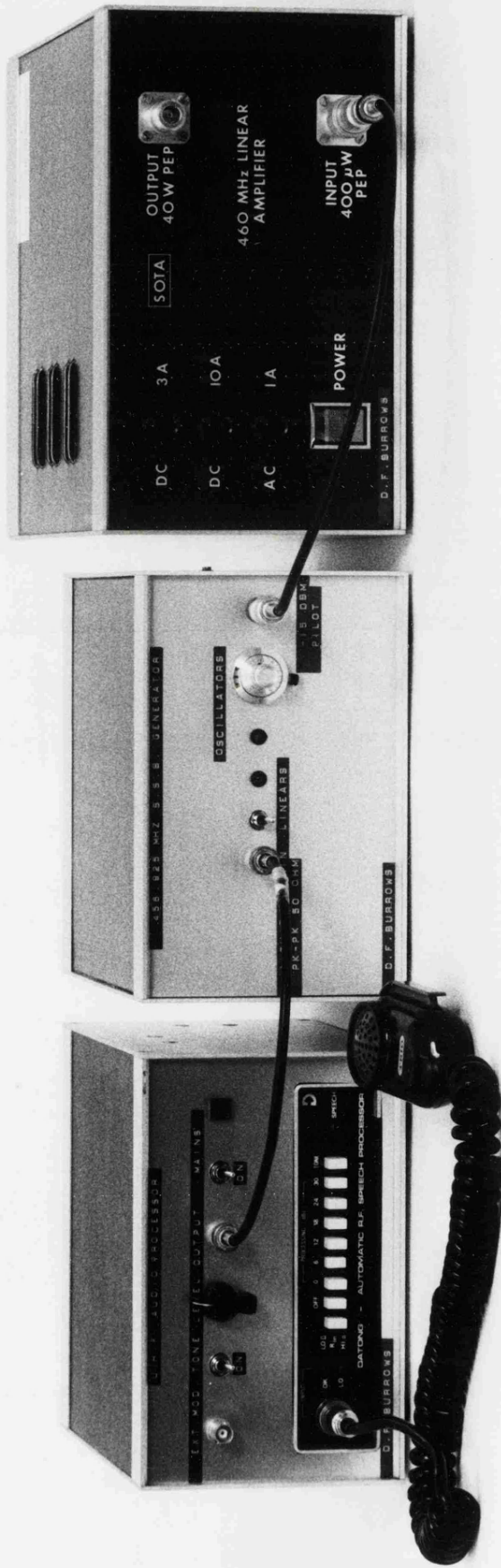
Figure 4.6   Photograph of complete UHF SSB transmitter

For this test, excitation applied at audio input (1V p-p)
and RF output power measured at 457 MHz. Relative frequency
refers either to audio output or output less carrier
frequency. Basic response is predominated by 10.7 MHz
crystal filter.

Relative response, dB

Relative Frequency
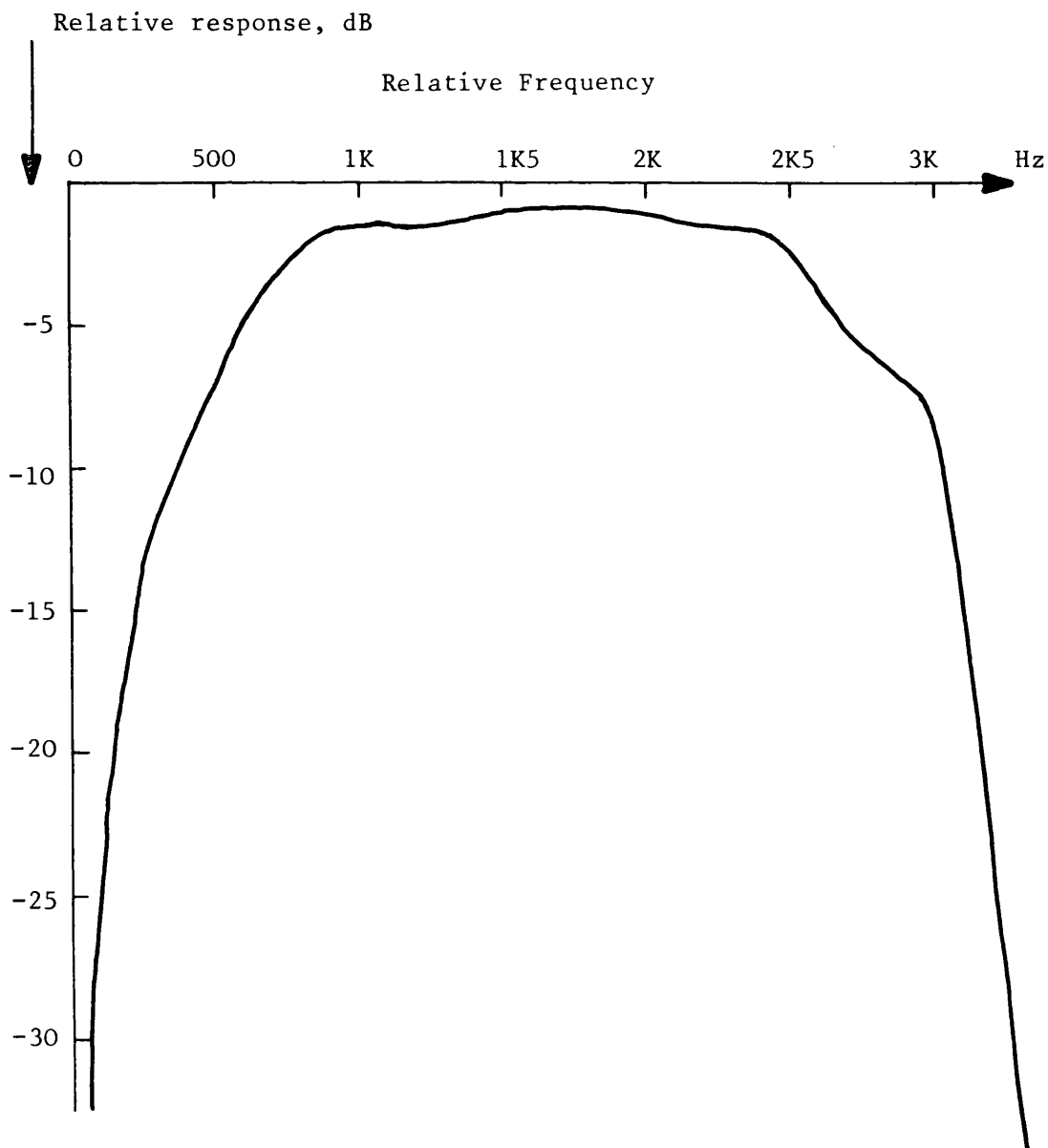
Figure 4.7 Frequency response of low level UHF SSB generator

4.3.1 General Description

Whereas the transmitter was designed as a fixed base station, the receiver was designed to be fully portable and independent of the vehicle power supply. To this end, it used an integral rechargeable power supply and had its own loudspeaker. It only required the addition of a suitable antenna for mobile operation.

The block diagram of the complete receiver is shown in figure 4.8. Its operation is described briefly as follows:

The incoming signal is first filtered and amplified at 457 MHz. It is then passed into a mixer and converted down to 10.7 MHz. The 10.7 MHz output is filteed by a crystal filter to give the required selectivity. After passing through a chain of IF amplifiers, it is demodulated by another mixer to audio. After preamplification, the pilot is removed from the composite signal by a notch prior to final audio amplification. The composite signal is available from a separate output for recording purposes. The next two sections discuss various aspects of the receiver in more detail.

4.3.2. RF and IF Circuitry

The front-end consists of a helical cavity tuned bipolar RF amplifier feeding a dual-gate MOSFET mixer. The high Q tuned circuits of the RF amplifier achieved an image rejection at 435.525 MHz of over 70 dB. The front-end conversion gain (RF in — IF out) was measured at 19 dB, with a noise figure of less than 14 dB (the overall receiver's noise figure). The IF output of the front-end is then fed into an upper sideband crystal filter. This has -3 dB points at 10.7 MHz and 10.70365 MHz, so it has little effect on the overall transmitter/receiver system frequency

4.12
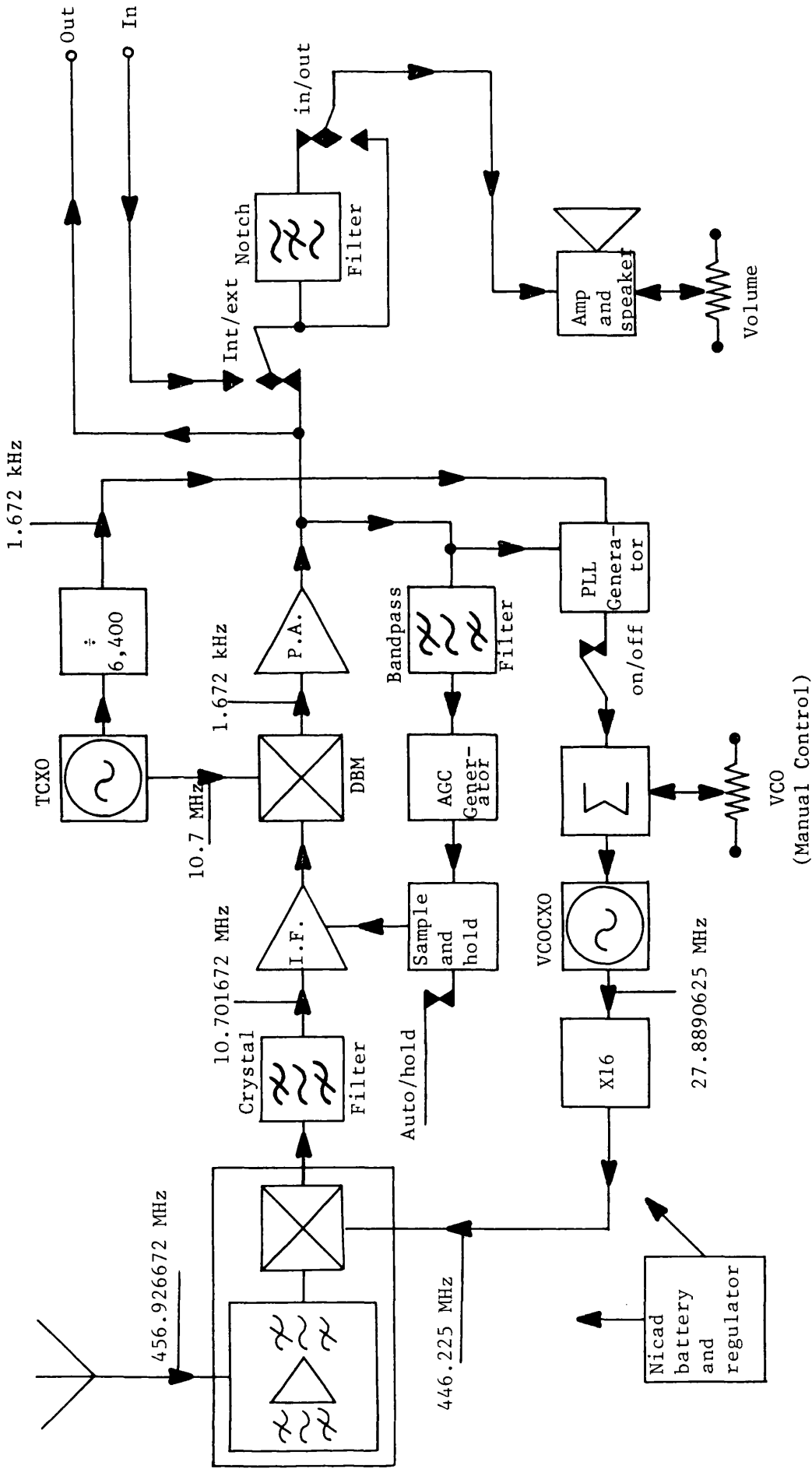
Figure 4.8   Block diagram of UHF SSB receiver

response, which is determined primarily by the transmitter.

The crystal filter is followed by the IF amplifiers consisting of three cascaded SL1612 (Plessey) low noise gain controlled amplifiers. These devices possessed a linear gain control characteristic when expressed as dB gain variation versus gain control voltage. This was measured at 97 dB per volt over the receiver's input range of 1 μV to 100 mV EMF. The IF stage delivered 1 mV rms of pilot to the final demodulator.

The front-end local oscillator and the final demodulator local oscillator are the same as those used in the transmitter. In the receiver, the frequency of the front-end local oscillator is voltage controlled and forms the PLL Voltage Controlled Oscillator (VCO). It possessed a gain control characteristic of 250 Hz per volt at 446.225 MHz.

4.3.3 Audio and Control Circuitry

A TL442 (Texas Instruments) is used as the 10.7 MHz demodulator (mixer), the output of which is pre-amplified at audio to give a pilot output at 1.672 kHz of 0.5V peak-to-peak. The following notch circuit uses an integrated circuit switch capacitor filter, the R5612 (Reticon). This has a -3 dB notch width of 550 Hz and a -50 dB notch width of 25 Hz, centred on 1.672 kHz. It is therefore narrower than the transmitter notch and does not significantly affect the overall system's frequency response. Provision was made to allow the use of additional external signal processing, as shown in figure 4.8. The final volume controlled power amplifier used a TDA2030 to drive a small loudspeaker fixed to the receiver's chassis.

The operation principles of the AGC loop around the IF amplifiers
are discussed in some detail in the following chapters. This receiver
derived its amplitude reference from the pilot at the output of a band-
pass filter. The overall AGC closed loop bandwidth was measured as
11 Hz. A sample-and-hold integrated circuit, the LF 398, is incorporated
as shown in figure 4.8 to allow disconnection of the AGC circuitry and
operation of the receiver at fixed gain.

The general principles of operation of the PLL incorporating
the front-end local oscillator are discussed in some detail in chapter 7.
The frequency reference is derived by division of the output of the
10.7 MHz local oscillator to 1.672 kHz (the 2 Hz offset with respect
to the original pilot frequency of 1.67 kHz is not significant). The
PLL control can be disabled and the receiver manually clarified. The
PLL was designed to be type 2 with critical damping and a natural
frequency of 3 Hz. The performance of similar PLL's in suppressing long
term frequency drifts is discussed in more detail in chapter 10.

All receiver circuits were powered from a Nickle-Cadmium battery
pack used to generate regulated +5V and +10V supply rails. The complete
receiver consumed approximately ½ amp which gave a battery life of
4 hours between charges of the 2 amp-hour battery. A photograph of
the complete receiver is shown in figure 4.9. Mounted on the top front
cover are seven user-accessible controls. From left to right they are:

i)   The main ON/OFF power switch and battery monitoring LEDS.

ii) The audio volume control.

iii) A PLL disable switch. When on "OFF" this disconnects the

     PLL control circuitry, allowing manual clarification with

     the:
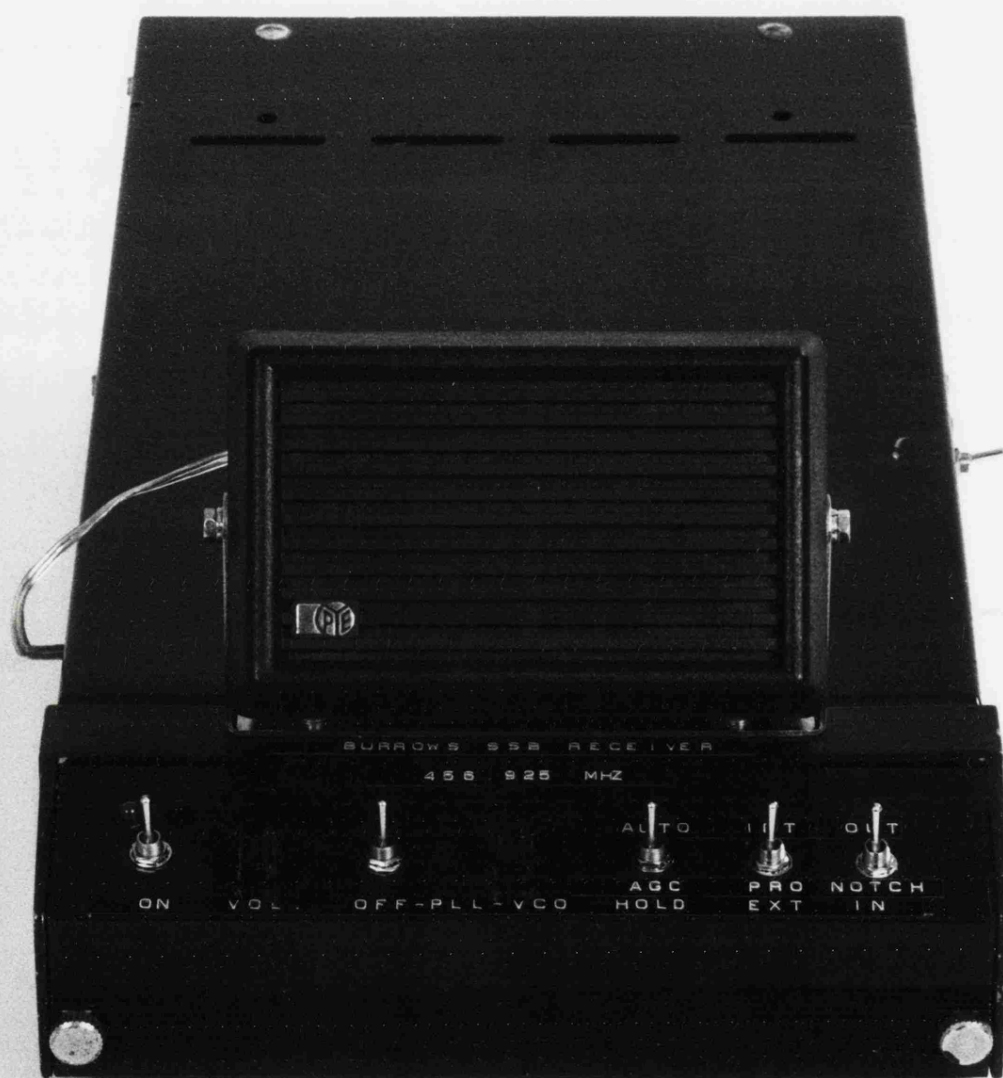
Figure 4.9 Photograph of complete UHF SSB receiver

iv) VCO bias control. This also assists frequency acquisition
of the PLL.

v) The AGC control switch. This switches between automatic
and fixed gain operation.

vi) Processing switch. This allows additional external processing
to be switched into the receivers operation.

vii) Notch switch. This allows operation with or without the
internal notch.

Underneath the top front cover are various input and output sockets,
and the rear of the receiver possesses additional battery isolation
switches and charging sockets.

Performance

Where relevant, the following performance figures refer to the
output of the pre-amplifier used for recording purposes.

i) Sensitivity: with 1 μV EMF of RF pilot applied to the antenna
input, the signal plus noise plus distortion to noise ratio was
measured at 12 dB and gave an overall receiver noise figure of about
14 dB.

ii) Spurious Responses: all measurable receiver spurious responses
were greater than 70 dB down. In particular, the image response was
-72 dB while the "spot" response at 451.575 MHz was -87 dB.

iii) Relative Receiver Drift: The VCOCXO was specified as having
a maximum frequency drift of 0.1 ppm over a 0° to 60°C temperature
range, giving a ± 0.05 ppm change at 456 MHz of ± 23 Hz. The 10.7 MHz

temperature compensated crystal oscillator was specified as having

a maximum frequency drift of 2 ppm over a -10° to +70°C range, giving a

± 1 ppm change at 10.7 MHz of ± 10.7 Hz. Therefore, the complete receiver

tuning drifts by about ± 34 Hz worst case over a 0° to 60°C temperature

range. Since the same oscillators were used in the transmitter, the

maximum relative receiver drift with a 60°C transmitter/receiver temperature

differential is 68 Hz. The receiver PLL can pull the VCOCXO over a

frequency range of greater than ± 1 kHz and no problems were encountered

with receiver phaselocking.

iv) AGC "Speech Modulation": the bandpass filter used to extract

the pilot from the composite signal for the AGC circuitry also allows

some speech energy through. The worst-case gain modulation using a peak

speech tone at 1.7 kHz was measured as less than 0.5 dB peak-to-peak.

v) PLL "Speech Modulation": in a similar test a peak speech tone

at 1 kHz caused the most modulation of the VCO control line. This

caused a peak-to-peak deviation of 62 Hz, or a modulation index on the

1.672 kHz pilot of 0.037.

4.4 Field Trial Data Collection

This section describes the field trials from which a collection

of tape recordings were made.

4.4.1 Equipment Description

As described earlier, the UHF SSB transmitter was situated in the

Wolfson Laboratory, University of Bath. As well as pilot only transmissions,

additional tones or speech recordings were also transmitted.

The mobile equipment is shown in the photograph of figure 4.10, before being mounted in a European Estate car used for the field trials. As well as the UHF SSB receiver, some additional equipment was also used. A Tandberg instrumentation tape recorder (series 115D) was used to record several tracks of information. The playback frequency response of the FM channels extended from dc to 5 kHz. The direct input channel was used to record a running commentary of the field trial and a series of marker blips.

The small box shown right of centre in the photograph of figure 4.10 was used to control some additional signal processing equipment described in more detail in chapter 9. The other small box with the meter monitors the receiver's AGC control line. This gives an approximate indication of the received signal strength to within ± 5 dB.

The antenna used on the car was similar to that used by the transmitter, i.e. a 6 dB gain collinear. A lowband VHF AM talk back link was also used to communicate with the laboratory during field trials.

4.4.2 Field Trial Routes

The field trials were conducted in and around the University and the City of Bath. The area and some routes used during the medium/high signal strength trials are shown in figure 4.11. This also shows the approximate signal strength measured at various points along the route while moving. The rapid drop in signal strength near Rainbow Wood Farm (approximately in the centre right of the map) was apparently caused by the loss of the line-of-sight path from the University. Other field trial routes used included Great Pulteney Street described elsewhere (2.6).
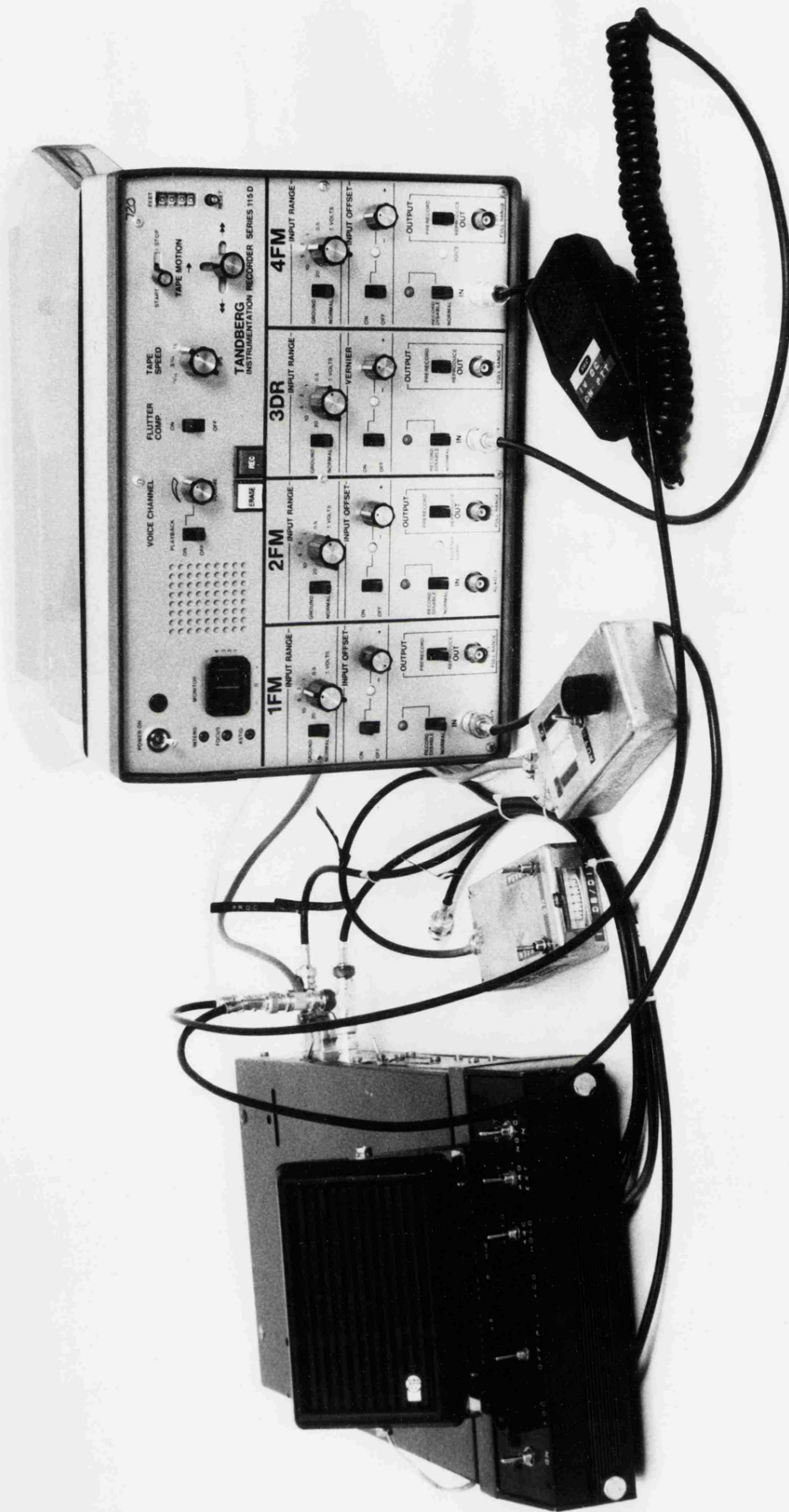
Figure 4.10 Photograph of field trial equipment

Signal strength shown in decibels above 1 µV(dBµV) for 2 Watts of transmitted
pilot
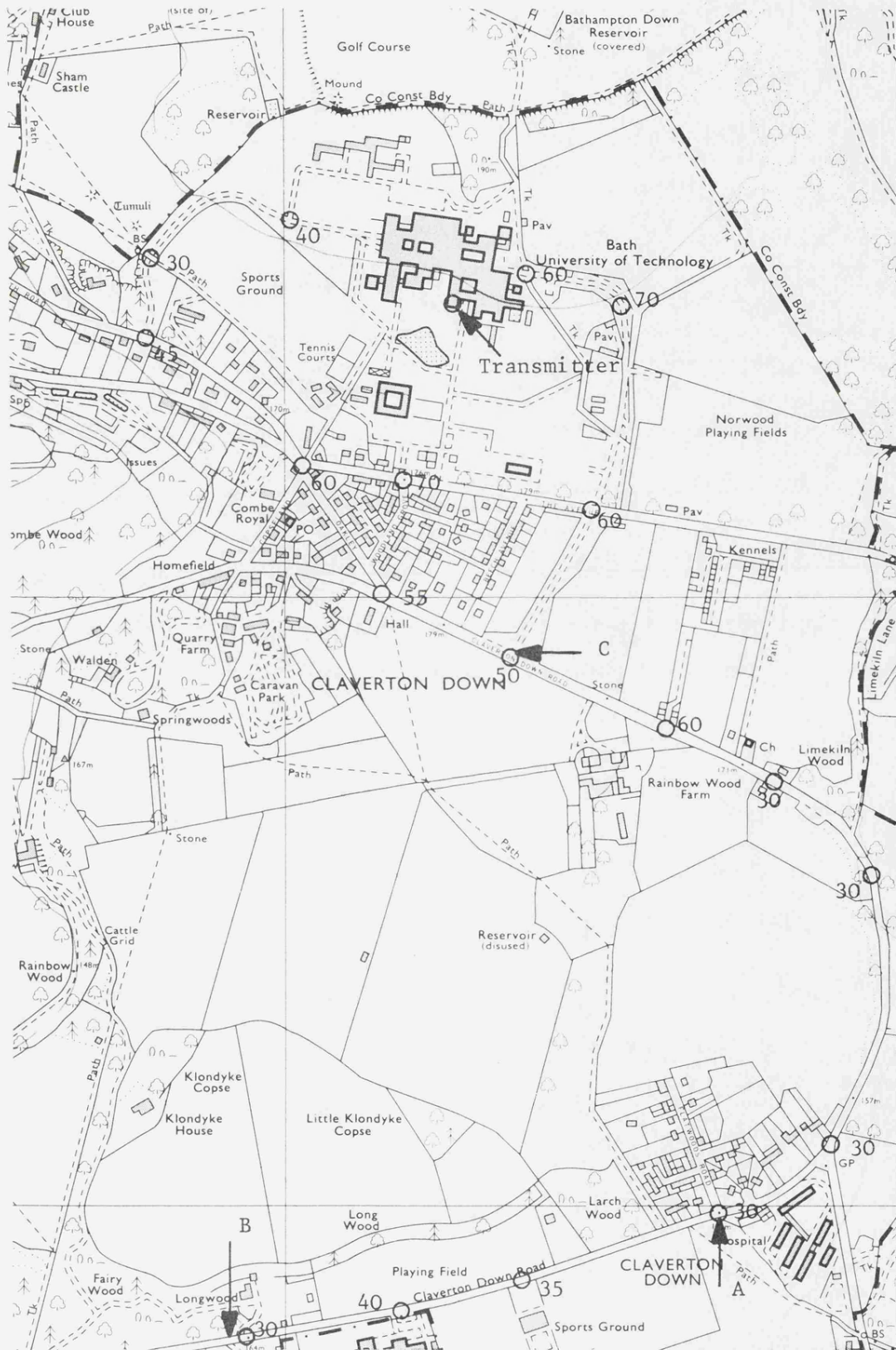
Figure 4.11   The field trial route used in most of the tests.
Reproduced from the 1973 Ordnance Survey 1:10,000 map
with the permission of the Controller of Her Majesty's
Stationary Office, Crown copyright reserved.

CHAPTER 5

FEEDBACK AGC

This chapter considers the analysis, design and characterisation

of ideal feedback AGC (FBAGC) systems in the absence of noise. The

response of FBAGC to those signals described in chapter 3 will be

calculated and compared with experimental results.

5.1 Fundamental Requirements

This section outlines the basic operational requirements of an FBAGC

system for use in mobile radio receivers.

5.1.1 Basic Operation on Input Envelope

Most FBAGC circuits used in mobile radio receivers can be represented

by the simple block diagram of figure 5.1. At some point(s) in the

receiver, the incoming signal, whose envelope is represented by $v_i(t)$,

is passed through a variable gain amplifier(s) (VGA) giving an output

signal whose envelope is represented by $v_o(t)$. The gain control generator

monitors the output and feeds back a signal, $v_g(t)$, that varies the gain

of the VGA in such a way so as to suppress the unwanted envelope variations

of the input. Before proceeding further, consider the exact nature of

the operation that FBAGC is required to perform on the input signal's

envelope.

$v_i(t)$ can be represented by an unwanted envelope variation, $r(t)$,

superimposed on the required envelope variation, $x(t)$, so that:

5.1

Input signal's
envelope   Input   Output   Output signal's
                                                                     envelope

$v_i(t)$○──────────►──── Variable ────────────►───────────●──►──○ $v_o(t)$
                         gain
                         amplifier
                         (VGA)
                                    $v_g(t)$

              ──────►
                                    $v_g(t)$

Gain control line
                         Gain control
                    ──◄── generator ──◄──
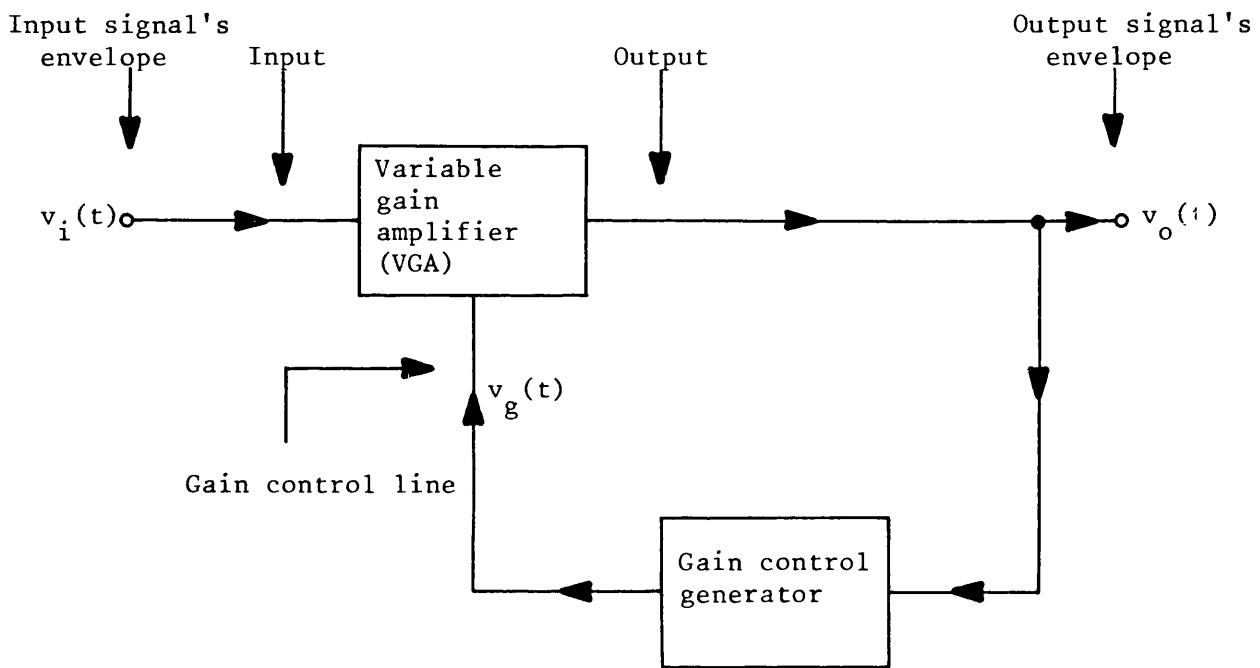
Figure 5.1   General block diagram of feedback AGC

5.2

$$v_i(t) \;=\; r(t)\,x(t) \qquad\qquad\qquad (5.1)$$

where by definition, $v_i(t)$, $r(t)$ and $x(t)$ are all $\geqslant 0$. The only simple

mathematical operation that can be performed by FBAGC on $v_i(t)$ to give

$x(t)$ is to divide $v_i(t)$ by $r(t)$. Any circuit that suppresses unwanted

envelope variations by the operation of division is an AGC circuit.

However, some AGC circuits only approximate the division process, resulting

in finite output variations by $r(t)$ even if the remainder of the circuit

is perfect. This is undesirable, therefore the first requirement of a

FBAGC system for a mobile radio receiver is :

Requirement 1: The FBAGC system is to perform the operation of envelope

division exactly.

5.1.2 Input-Level-Invariant Dynamics

The operation of envelope division cannot be a wideband process

and filtering is required in the loop. Since the unwanted envelope

variations extend in frequency from dc upwards, the dynamics of FBAGC

are determined by a lowpass filter. The filter should have a bandwidth

as large as possible to suppress unwanted envelope fast fading. However,

in full carrier AM systems the filter's bandwidth is limited to prevent

suppression of required envelope variations, such as speech modulation.

In pilot tone SSB systems the filter's bandwidth is limited to prevent

loop instability: this is discussed in more detail in chapter 6.

Whatever the closed loop -3 dB bandwidth is chosen to be, it should

be under the control of the circuit designer. Unfortunately, a major

problem with some FBAGC systems is that they possess a closed loop -3 dB

bandwidth that is not only a function of various circuit elements, but

also the mean level of the input signal (5.1, 5.2, 5.3, 5.4). They are

referred to as having input-level-variant dynamics and this undesirable

property prevents optimisation of the AGC system's performance over a

wide range of input levels. The second requirement of a FBAGC system

for a mobile radio receiver is therefore:

Requirement 2: The closed loop -3 dB bandwidth is to be independent of

the input so that the FBAGC system possesses input-level-invariant dynamics.

5.1.3 Unconditional Suppression

Obviously, a mobile radio receiver's FBAGC system should not enhance,

i.e. increase and worsen, unwanted envelope fading. Initially, this

requirement seems to be met by definition of the nature of FBAGC. In

fact, the next chapter shows that it is very difficult to ensure that

a FBAGC system will not enhance some types of unwanted envelope variations.

The ideal requirement is for an FBAGC system that will always suppress

unwanted envelope variations. This is defined as "unconditional

suppression". The third requirement of an FBAGC system for a mobile

receiver is therefore:

Requirement 3: The FBAGC system is to possess the property of unconditional

suppression.

5.1.4 Large Signal Model

The FBAGC system in a mobile radio receiver will be subject to large

input variations over a typical operating range of 130 dB (5.5). It is

therefore important to be able to analytically describe the FBAGC system's

large signal performance. However, considerable difficulty has been

experienced in the past by several authors with analysing the exact large

signal performance of FBAGC systems.

Oliver's analysis (5.1) only considers input variations so small or at such a high frequency that only a small variation in the VGA gain occurs. Banta (5.2) also places limits on the input variations so that only small variations in the VGA gain occurs for part of his analysis to hold. Gill and Leong (5.3) perform only an approximate analysis for large input variations, while Simpson and Tranter (5.4) had some difficulty in analysing the response of FBAGC to a simple step change in input envelope, only presenting experimental results for small variations. Victor and Brockman (5.6) only consider the response of FBAGC to input variations of 3 dB or less. Moskowitz (5.7) also only considers the response of FBAGC to input variations that are much less than the mean level of the input. Hughes (5.8) restricts the analysis of the loop rise time to input variations consisting of ± 2 dB steps. Finally, Plotkin's (5.9) analysis assumes only relatively small limiting swings over the nonlinear characteristic of his AGC circuitry.

The fourth requirement of an FBAGC system for a mobile radio receiver is:

Requirement 4: It should be possible to analyse the large signal performance of the FBAGC system.

5.1.5 Practicability

The 4 requirements described so far are concerned only with the theoretical performance of FBAGC. However, a very important requirement of any FBAGC system is that it should be easy to implement. In particular, its circuitry should be as simple as possible. Operation in the mobile radio environment places stringent requirements on circuit size, power consumption and reliability. On these grounds, a highly complicated

FBAGC system with very desirable properties will be rejected by receiver designers in favour of a more basic circuit. Fortunately, such a compromise is not necessary and this chapter will present an FBAGC system that satisfies the theoretical requirements with a minimum of circuit complexity. The fifth and final requirement of an FBAGC system for a mobile radio receiver is therefore:

Requirement 5: The FBAGC system shall be as simple as possible.

In the following text, the 5 requirements will be referred to as follows:

Requirement 1 (division)

Requirement 2 (input-level-invariance)

Requirement 3 (unconditional suppression)

Requirement 4 (large signal model)

Requirement 5 (simplicity)

5.2 An FBAGC System for Mobile Radio

This section considers the various FBAGC systems used by previous workers and derives an FBAGC system for mobile radio use. Although other FBAGC systems which meet the requirements of section 5.1 may exist, the FBAGC system proposed here is believed to be one of the simplest and most well understood.

The remainder of this chapter assumes the use of full carrier AM signals. The use of other AM-type modulation systems requires additional elements within the FBAGC loop for correct operation and are discussed in chapters 6 and 7.

5.2.1 Basic Loop Configuration

Most published FBAGC circuits can be represented by some variation of the general circuit shown in figure 5.2, usually with one or more elements omitted (5.1-5.6, 5.8-5.14, 5.17, 5.20). The VGA in figure 5.1 is represented by 3 elements in figure 5.2: H_1, the multiplier and H_0. The output signal is envelope detected and filtered by F_2 before being operated on by H_2. The output of H_2 is then compared to a fixed dc reference; the difference signal being filtered by F_1. The output of F_1 controls the gain of the VGA, completing the loop and suppressing envelope variations of $v_i(t)$. For convenience, $v_g(t)$ is shown as the control voltage of the unity gain multiplier and not as the input to H_1.

In the past, there has been some confusion as to the "best" FBAGC configuration. Several workers used either linear amplifiers for both H_1 and H_2 (5.2, 5.3, 5.4, 5.10) or nonlinear elements for both (5.6, 5.11) or both linear and nonlinear elements (5.1, 5.5, 5.8, 5.9, 5.12, 5.13, 5.14, 5.20). A similar variation in the type and position of the loop filter(s) exists, although most systems are designed to have a first order response. Furthermore, the envelope detector employed varies from a synchronous (i.e. coherent) detector to incoherent rectifier type and square law detectors. This confused situation can be clarified by the elimination of FBAGC systems that do not meet any of the 5 requirements of section 5.1.

It is therefore possible to immediately eliminate any of the aforementioned FBAGC systems that use linear amplifiers for both H_1 and H_2 since they have input-level-variant dynamics (5.20). It has been suggested that the use of a logarithmic element for H_2 and an exponential
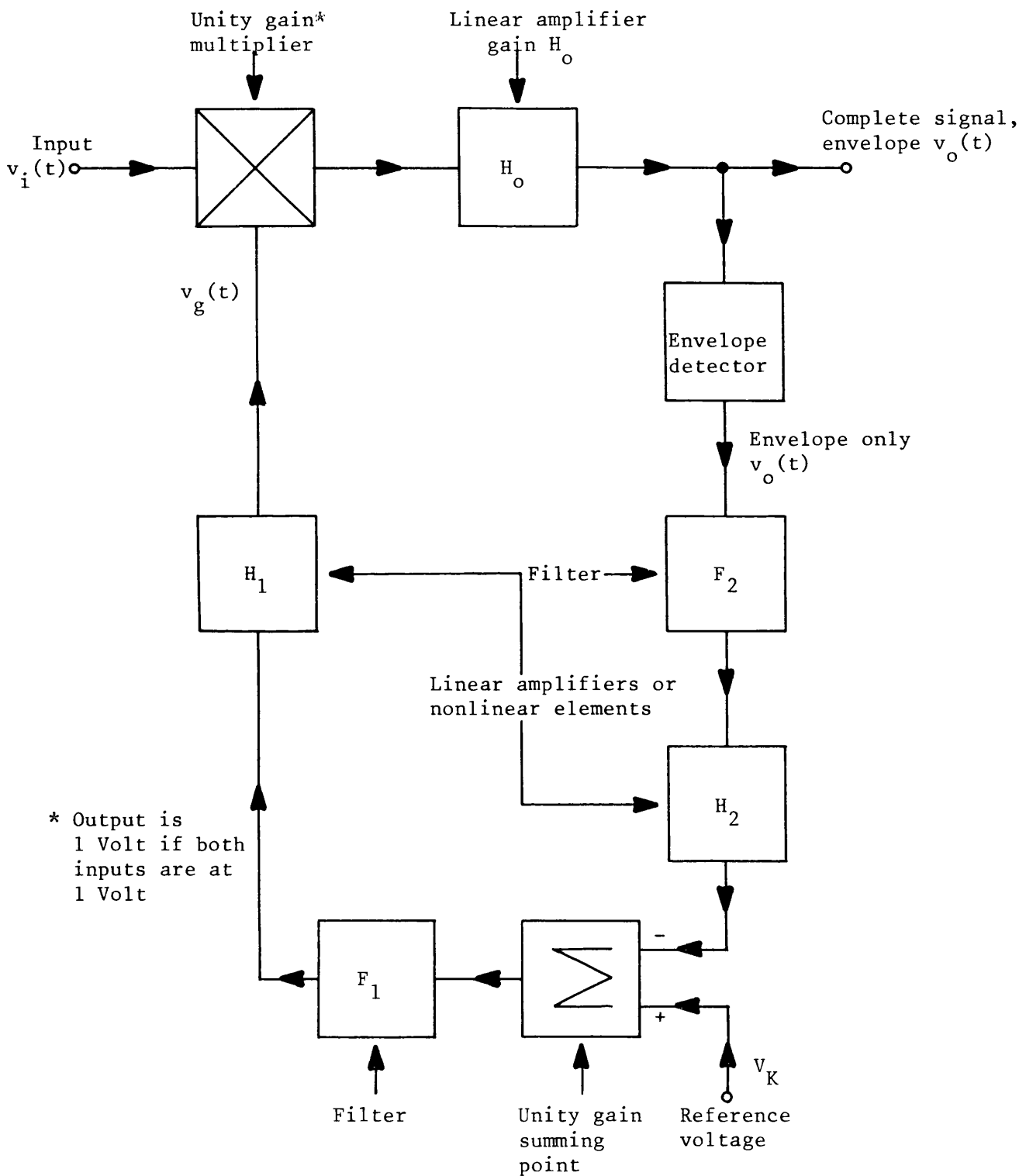
Figure 5.2 Block diagram of feedback AGC incorporating most reported circuit elements

element for H_1 will give input-level-invariant dynamics (5.6, 5.11).

However, these circuits can also be eliminated for mobile radio use

since a simpler technique is known. Williams (5.13) claims that the use

of an exponential element alone for H_1 will give input-level-invariant

dynamics. However, he also suggests the use of a type zero control loop

(5.15) which always results in finite output variations. This does not

meet requirement 1 (division).

The envelope detector lowpass filter, F_2, is not usually required

since the loop itself exhibits low pass characteristics due to F_1.

Indeed, chapter 6 shows that the inclusion of the filter F_2 can degrade

the loop's dynamic performance. The envelope detector should be of the

"precision-rectifier" or "absolute value" type, which is incoherent

(5.19). A nominally "coherent" envelope detector will translate any

phase variations of the incoming signal into additional unwanted envelope

variations (5.14). Chapter 7 discusses the use of coherent (PLL) envelope

detectors in more detail.

Based on these considerations, the FBAGC system shown in figure 5.3

is the one used throughout the rest of this thesis. It is similar to

the circuit used by Ohlson (5.12) with some signs changed and an extra

input omitted. It will be referred to as "Exponential-Integrator" FBAGC

or EIFBAGC.

5.2.2 Analysis of EIFBAGC Operation

This analysis is only concerned with the input and output signals'

envelopes. EIFBAGC has no effect on the phase of the input signal. The

envelope detector is assumed to be unity gain to $v_0(t)$ and the harmonics

of the detection process not to affect the circuit's operation.

5.9
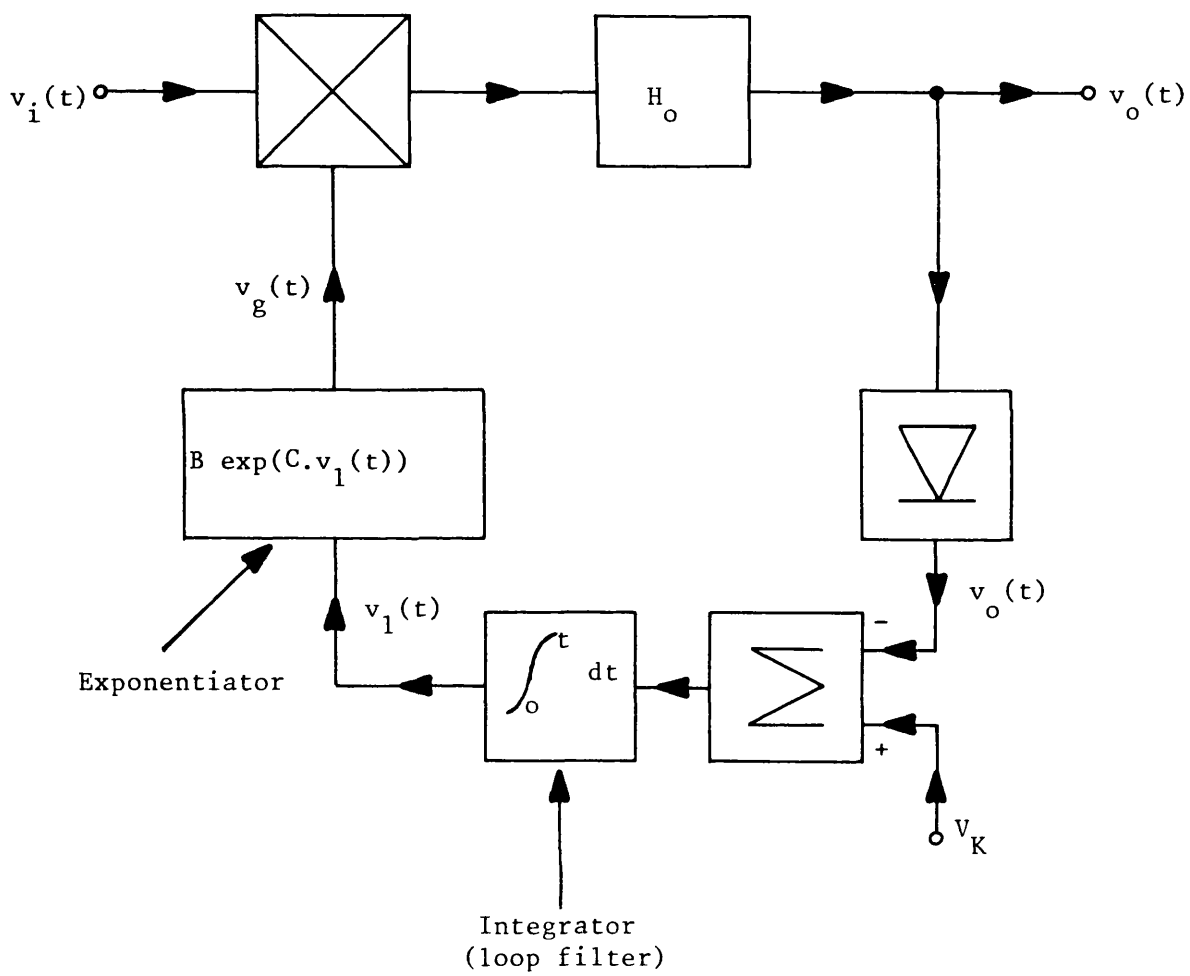
Figure 5.3 Block diagram of EIFBAGC circuit

Consider first the "static" equations of the loop, assuming a fixed input envelope, after any transients have died down. The output signal is given by:

$$v_o = v_i v_g H_o \qquad (5.2)$$

but: $v_g = B \exp(AC(V_K - v_o)) \qquad (5.3)$

where A is the gain of the integrator at dc $(A \to \infty)$.
From equations 5.2 and 5.3 then:

$$v_o = \frac{\ln(v_i)}{AC} + \frac{\ln(H_o)}{AC} + \frac{\ln(B)}{AC} - \frac{\ln(v_o)}{AC} + V_K \qquad (5.4)$$

so that, providing v_i, H_o, B or $v_o \neq$ zero, then as $A \to \infty$:

$$v_o = V_K \qquad (5.5)$$

therefore, from equation 5.2

$$v_g = \frac{V_K}{H_o v_i} \qquad (5.6)$$

That is, the static action of EIFBAGC is to maintain the output at a fixed value V_K by dividing the input by itself. This fulfils requirement 1 (division).

The dynamic operation of EIFBAGC can now be calculated. The differential equation of the input to the integrator is:

$$\frac{d}{dt} \left[\frac{(\ln(v_g(t)/B))}{C} \right] = V_K - v_o(t) \qquad (5.7)$$

but $v_o(t) = v_i(t) \, v_g(t) \, H_o \qquad (5.8)$

which gives the main loop equation:

$$v_i(t)v_g(t)H_o + \frac{d}{dt}\left[\frac{(\ln(v_g(t)/B))}{C}\right] - V_K = 0 \qquad (5.9)$$

The dynamic operation of EIFBAGC is now analysed via equation 5.9 using a method of analysis based on a generalisation of the "describing function" (5.16). The input is excited sinusoidally as described by equation (3.14) so that:

$$v_i(t) = E(1 + D \sin \omega_s t) \qquad (5.10)$$

Equation 5.6 suggests that the circuits response at $v_g(t)$ is linearly related to the inverse of $v_i(t)$. However, to preserve generality it must be assumed that some filtering operation has occurred due to the integrator. Therefore, it seems reasonable to write the steady state response at $v_g(t)$ as:

$$v_g(t) = \frac{V_K}{H_o E(1 + LD \sin(\omega_s t - \theta))} \qquad (5.11)$$

where L and θ are the amplitude and phase responses of the effective loop filtering operation at $v_g(t)$. Substituting $v_i(t)$ and $v_g(t)$ from equations 5.10 and 5.11 into 5.9 and simplifying gives:

$$\frac{V_K(1 + D \sin \omega_s t)}{(1 + LD \sin(\omega_s t - \theta))} - \frac{LD \omega_s \cos(\omega_s t - \theta)}{C(1 + LD \sin(\omega_s t - \theta))} - V_K = 0 \qquad (5.12)$$

This equation is solved in appendix 3 to give:

$$L = \frac{1}{(1 + \omega_N^2)^{\frac{1}{2}}} \qquad (5.13)$$

$$\theta = \tan^{-1}\omega_N \qquad (5.14)$$

5.12

where $\omega_N = \dfrac{\omega_s}{CV_K}$ (5.15)

and L and θ are the amplitude and phase equations of a first order lowpass filter with a -3 dB bandwidth of CV_K rs^{-1} or a time constant T_c of $1/CV_K$ seconds. In other words, the voltage $v_g(t)$ is a filtered and inverted version of the input, $v_i(t)$. The complicated feedback circuit shown in figure 5.3 can therefore be represented by the equivalent feedforward circuit model shown in figure 5.4. The feedforward model describes the response of EIFBAGC to envelope variations exactly. This result has been confirmed by Ohlson (5.12) using a different approach to the analysis. Note that in figure 5.4 the numerator, $n(t)$, equals the input, $v_i(t)$, while the denominator, $d(t)$, equals $V_K/(H_o v_g(t))$.

5.2.3 Properties of EIFBAGC

The previous section showed that EIFBAGC operates on the incoming signal's envelope by dividing it by a first order lowpass filtered version of itself. In addition to this, the circuit also possesses the following properties:

1) The output of the forward path amplifier, H_o, is inversely proportional to the gain of the envelope detector. However, the output of the envelope detector is independent of its gain and held at the mean level V_K.

2) The closed loop bandwidth, CV_K, is independent of the mean input signal's level, providing the input is within the designed operating range. This meets requirement 2 (input-level-invariance).

5.13
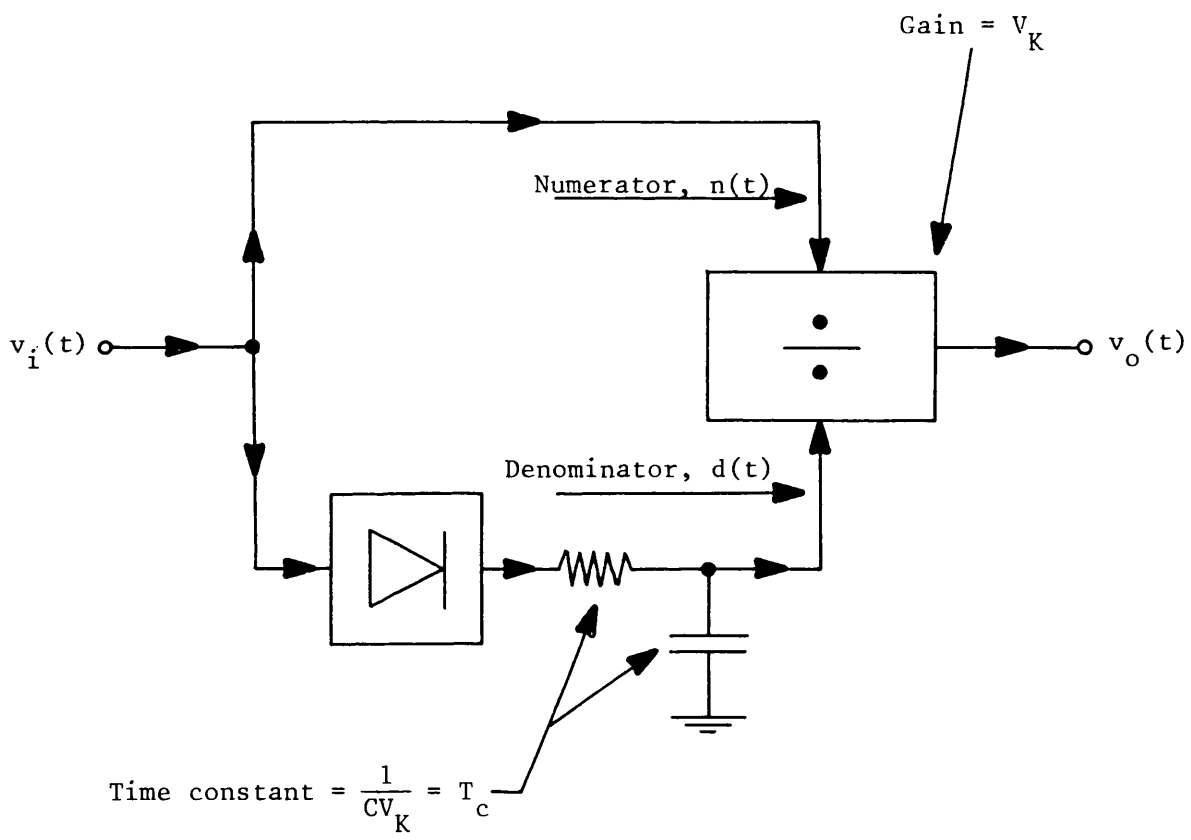
Figure 5.4 Feedforward model of EIFBAGC

The figure contains the following labels:

Gain = V_K

Numerator, n(t)

$v_i(t)$

$v_o(t)$

Denominator, d(t)

Time constant = $\dfrac{1}{CV_K}$ = T_c

3) The closed loop bandwidth is also independent of H_o, the forward path gain and B, an exponentiator constant.

4) The closed loop bandwidth is directly proportional to any gain of the summing junction or integrator. The circuit designer is often presented with a fixed decibel per volt gain control characteristic on the VGA and a fixed value of V_K based on requirements to deliver a certain signal level to subsequent stages. In this situation, the closed loop bandwidth is then usually varied by the integrator time constant to give the required value of closed loop bandwidth.

5) If the VGA has a negative C (i.e. an increasing loss with positive increasing $v_1(t)$) then this can be accommodated by reversing the signs on the inputs of the summing junction.

6) As stated earlier, the VGA gain control law is often presented in the form "dB gain variation per applied control volt". Assume that the variation of gain with $v_1(t)$ is W dB/volt then:

$$C = \frac{W}{20 \log_{10} e} \qquad (5.16)$$

or

$$C = 0.1151W \qquad (5.17)$$

5.2.4 Meeting the FBAGC Requirements

Requirement 1 (division) and requirement 2 (input-level-invariance) have already been shown to be properties of EIFBAGC. However, due to the non-linear nature of the circuit, it is difficult to prove that it meets requirement 3 (unconditional suppression) for a completely general input variation. EIFBAGC will be shown later in this chapter to meet

5.15

requirement 3 when subject to the sinusoidal and 2 tone test signals. Here it is revealing to calculate its response to a step change in input level:

Let $v_i(t) = E(1 + ZH(t))$ (5.18)

where $H(t)$ represents the unit step function and Z is a number greater than -1. The output of the feedforward model's lowpass filter, $d(t)$, is given by:

$$d(t) = E(1 + Z(1 - \exp(-t/T_c))) \quad (5.19)$$

The output of the circuit is therefore:

$$v_o(t) = \frac{V_K(1 + ZH(t))}{(1 + Z(1 - \exp(-t/T_c)))} \quad (5.20)$$

Figure 5.5 shows the response of EIFBAGC to both positive and negative input steps, where $V_K = E = 1$ to allow an input/output comparison. Note that the relative change of the input in decibel form is:

$$K_i(dB) = 20 \log_{10}(1 + Z) \quad (5.21)$$

while the relative change of the output in decibel form is:

$$K_o(dB) = 20 \log_{10}\left[\frac{1 + Z}{1 + Z(1 - \exp(-t/T_c))}\right] \quad (5.22)$$

the peak value of this, $\hat{K}_o(dB)$, occurrs at $t = 0$ and is:

$$\hat{K}_o(dB) = 20 \log_{10}(1 + Z) \quad (5.23)$$
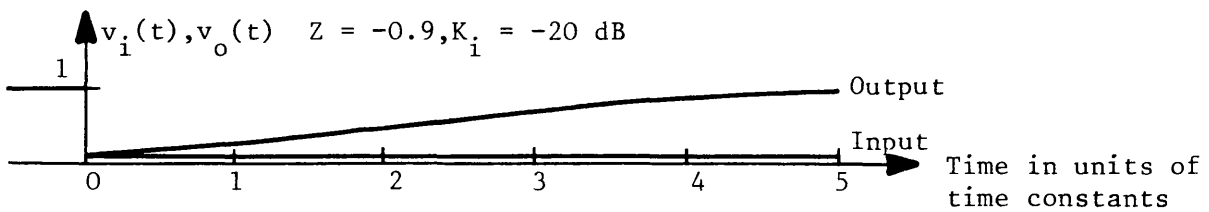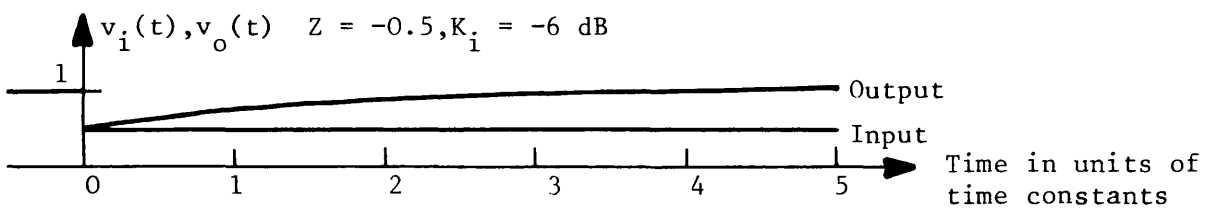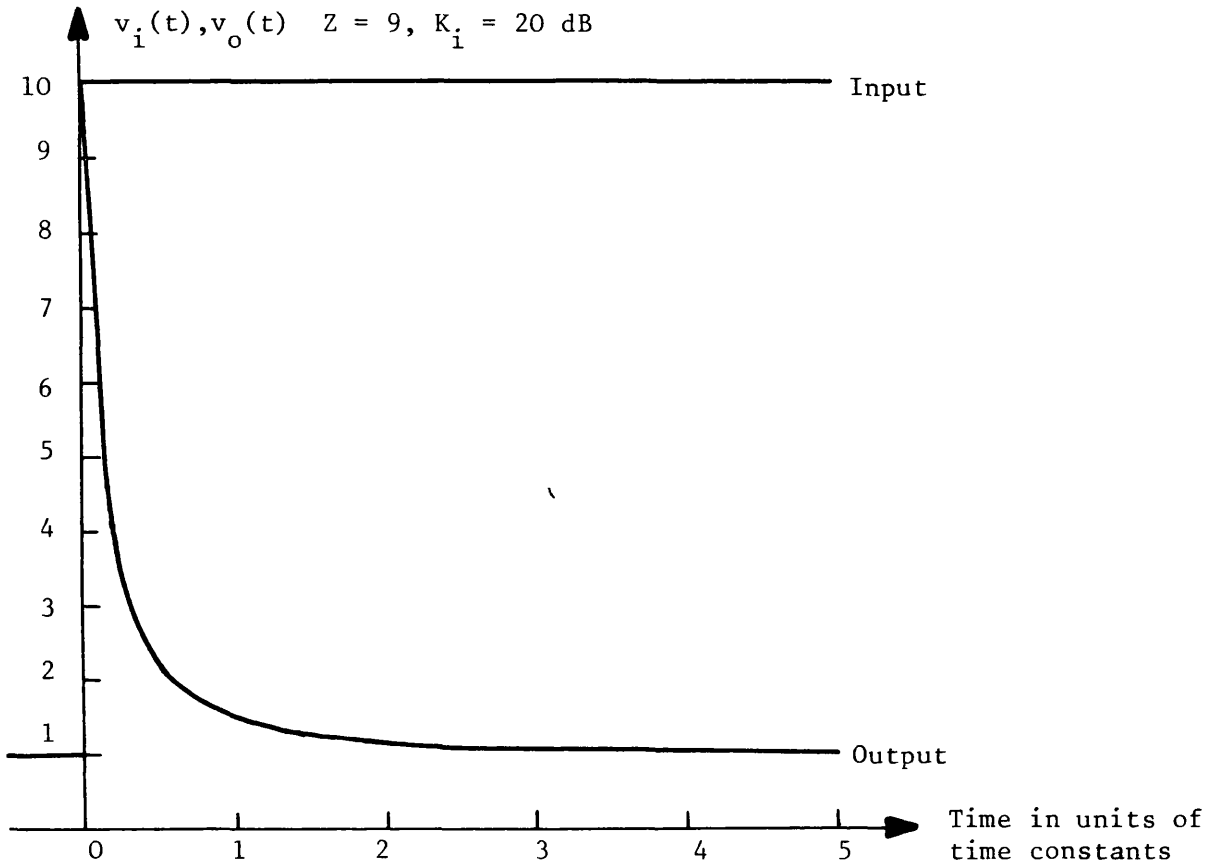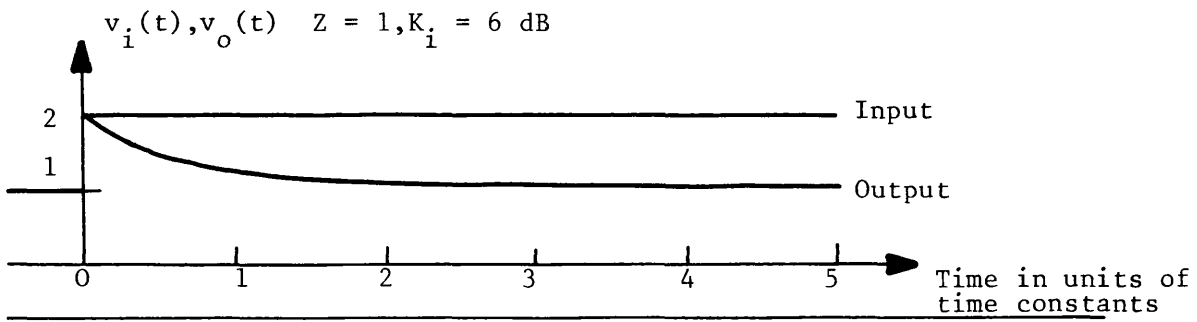
Figure 5.5   Response of EIFBAGC to step changes in input envelope

For a step change on the input, EIFBAGC always decreases the variation at the output with the output maximum occurring at t = 0 and not exceeding the input. It has not been possible to find an input envelope variation that an ideal EIFBAGC circuit will increase rather than suppress. Therefore, it is suggested that EIFBAGC meets requirement 3 (unconditional suppression).

Requirement 4 (large signal model) is met since the feedforward model is valid for all input variations providing $d(t) > 0$. However, it should be noted that the analysis of the response of the feedforward model is complicated by the division process. This is made apparent in the next main section when calculating the circuit's response to simple sinusoidal modulation results in some quite lengthy calculations. Requirement 5 (simplicity) is met since there is no known way to simplify the circuit without failing to meet any of the other requirements.

5.2.5 Practical Considerations

Any practical realisation of EIFBAGC in a radio receiver will use circuitry that depends on the receiver's specification, available technology and economics. It may be decided to deliberately degrade some aspect of an ideal EIFBAGC circuit's performance - for example, to have some variation of the loop bandwidth with input signal level. Alternatively, it may not be possible to accurately realise all of the circuit elements. However, it will be assumed in this section that it is required to realise EIFBAGC as accurately as possible, as, for example, in the work of Ball and Holmes (5.5) and McGeehan et al (1.8)

In most radio receivers, the total RF input to audio output gain is distributed between RF stages, mixers, filters, IF stages and audio

amplifiers. If any of these stages are gain controlled, then irrespective of their position in the radio receiver, the overall gain control characteristic of the receiver as seen by the output of the integrator should be exponential. Variations in the slope of the gain control characteristic, W, cause a corresponding variation in the EIFBAGC loop bandwidth. This is a problem especially when attempting to achieve maximum signal to noise performance from the receiver. This usually involves keeping the gain of the RF amplifiers at their maximum for input signal levels up to, say, 1 millivolt, while maintaining the receivers output at a fixed level by controlling the gain of other stages such as the IF amplifiers (5.17). For input levels greater than, say, 1 millivolt, the RF amplifiers may be included in the EIFBAGC control loop, reducing their gain to prevent subsequent stages from overloading (5.18). Care needs to be taken when abruptly including an additional gain control stage into the loop since this will cause the bandwidth to increase unless additional measures are taken to compensate for this. The effect of noise on the performance of FBAGC is discussed in chapter 10.

In practice, the receiver's gain cannot be increased above some maximum value due to noise considerations, and it can be limited by circuitry around the integrator. If a "hard" limiting action is incorporated and care taken that the integrator does not saturate, then the limiting action can be incorporated in the feedforward model as shown in figure 5.6. The threshold element has an output that follows the input variation unless it is below the threshold voltage, V_T, when it is clamped at the voltage V_T. When this has occurred variations on $v_i(t)$ are followed by variations on $v_o(t)$, thus losing AGC action. The simple resistor and diode circuit shown in figure 5.6 has the properties of the threshold element.
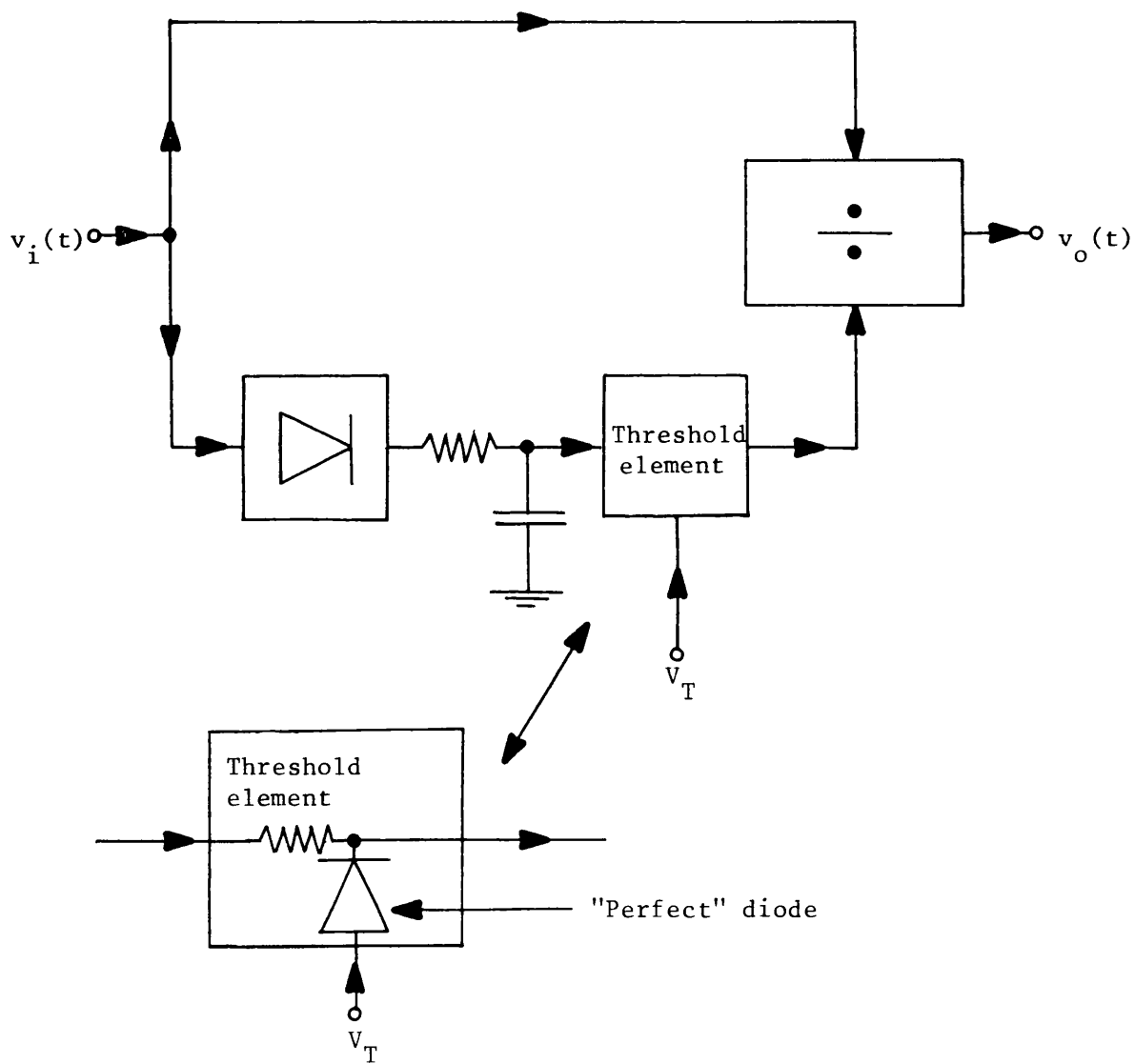
Figure 5.6   Feedforward model of EIFBAGC incorporating a
"hard" gain limiter

5.2.6 Precision EIFBAGC Circuit

A precision EIFBAGC circuit was built to check the aforementioned predictions. It was designed to operate both on signals generated in the laboratory and on recordings of the fading pilot tone. The circuit operates on carriers from dc to about 10 kHz. A "dc" carrier consists of a dc voltage (positive with this circuit) on to which modulation is superimposed. An ac carrier consists of a sinewave on to which modulation is superimposed.

The block diagram of the circuit is shown in figure 5.7. It is very similar to the block diagram of figure 5.3, and its operation follows that described in section 5.2.1. The closed loop bandwidth could be selected between 7 values: 1 Hz, 3 Hz, 10 Hz, 30 Hz, 100 Hz, 300 Hz and 1 kHz. The accuracy of the closed loop bandwidth selected was within 10%. The closed loop bandwidth varied by less than 2% when used in the ac mode over the input operating range 10V peak to peak to 0.2V peak to peak, demonstrating the level invariance of the closed loop bandwidth. When operated in the dc carrier mode, the precision rectifier is bypassed and the output of the circuit connected directly to the negative input of the summing junction. In the dc mode, the closed loop bandwidth varied by 6.5% over a 30 dB input range. The mean level of the output was 0.2V peak to peak when operated in the ac mode or 0.1V dc when operated in the dc mode. During dynamic testing the circuit performed as predicted theoretically, giving the results described in the rest of this chapter.
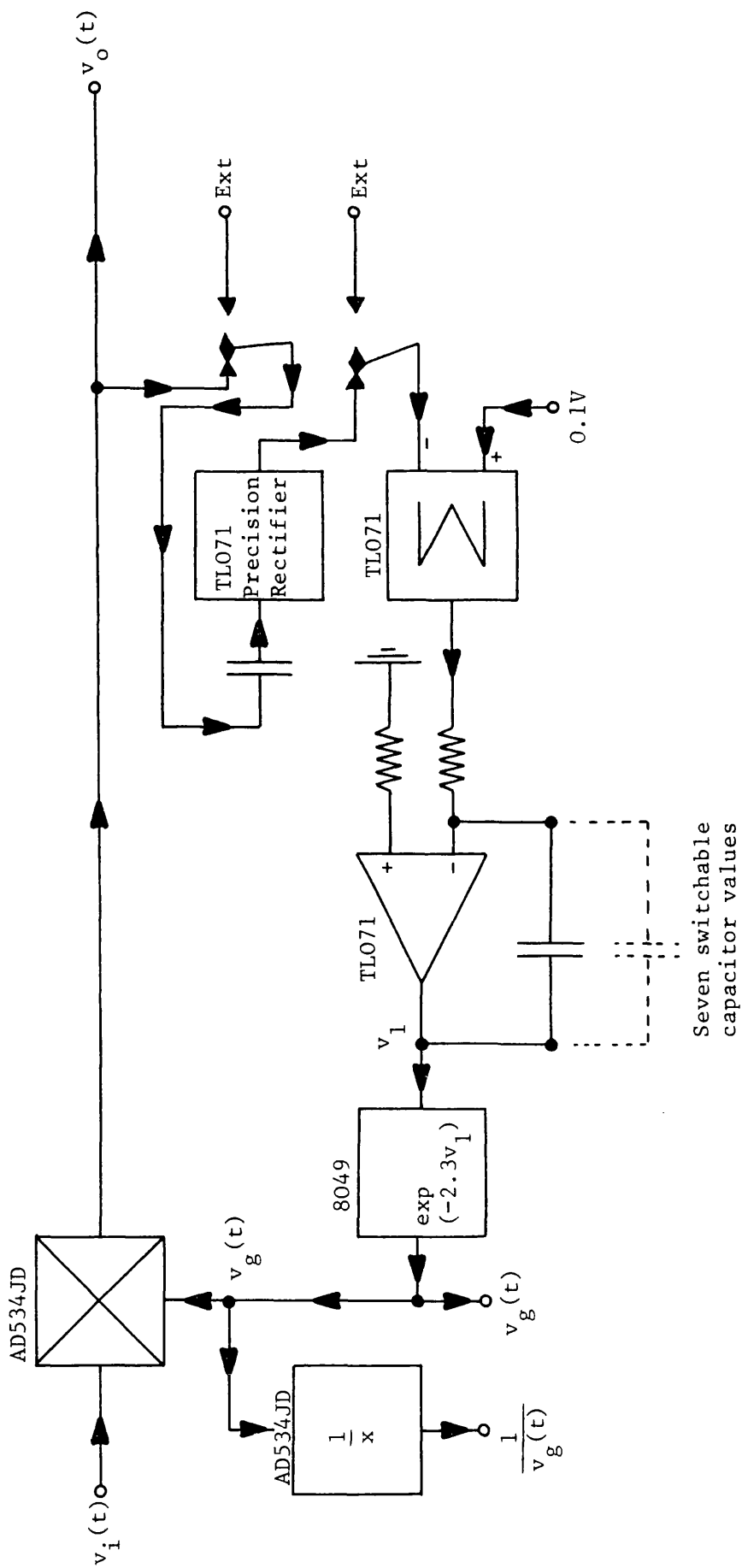
Figure 5.7   The precision EIFBAGC circuit block diagram

5.3 Response to Sinusoidal Modulation

This section discusses the response of EIFBAGC to sinusoidal input

modulation, i.e. deterministic AGC test signal 1. It will become

apparent that calculation of the response is complicated by the inherent

division process. Nevertheless, a full analysis has been performed and

the results checked by practical experiments wherever possible.

5.3.1 Requirements of the Analysis

The input to the circuit is $r_1(t)$ where:

$$r_1(t) = E(1 + D \sin \omega_N t) \qquad (5.24)$$

where $0 < D < 1$ and ω_N is the normalised frequency. The steady state

output of the circuit is given by equations 5.8 and 5.11 as:

$$v_o(t) = V_K \left[\frac{1 + D \sin \omega_N t}{1 + LD \sin(\omega_N t - \theta)} \right] \qquad (5.25)$$

As mentioned in section 3.5.2, there are 2 main areas of interest here.

The first is when $r_1(t)$ represents some unwanted signal variation, so

the ability of EIFBAGC to suppress it is required. The second area of

interest is when $r_1(t)$ represents some required signal variation, so the

distortion introduced by the EIFBAGC system is also required. EIFBAGC will,

in general, only adequately suppress unwanted input variations that occur

well inside the closed loop bandwidth while it will only pass relatively

undistorted, wanted input variations that occur well outside the closed

loop bandwidth. This can be shown by analysing 3 properties of equation

5.25. These are shown in figure 5.8 which also defines a number of the

variables used in the following work. The particular properties of the

output waveform that require analysing are:

5.23
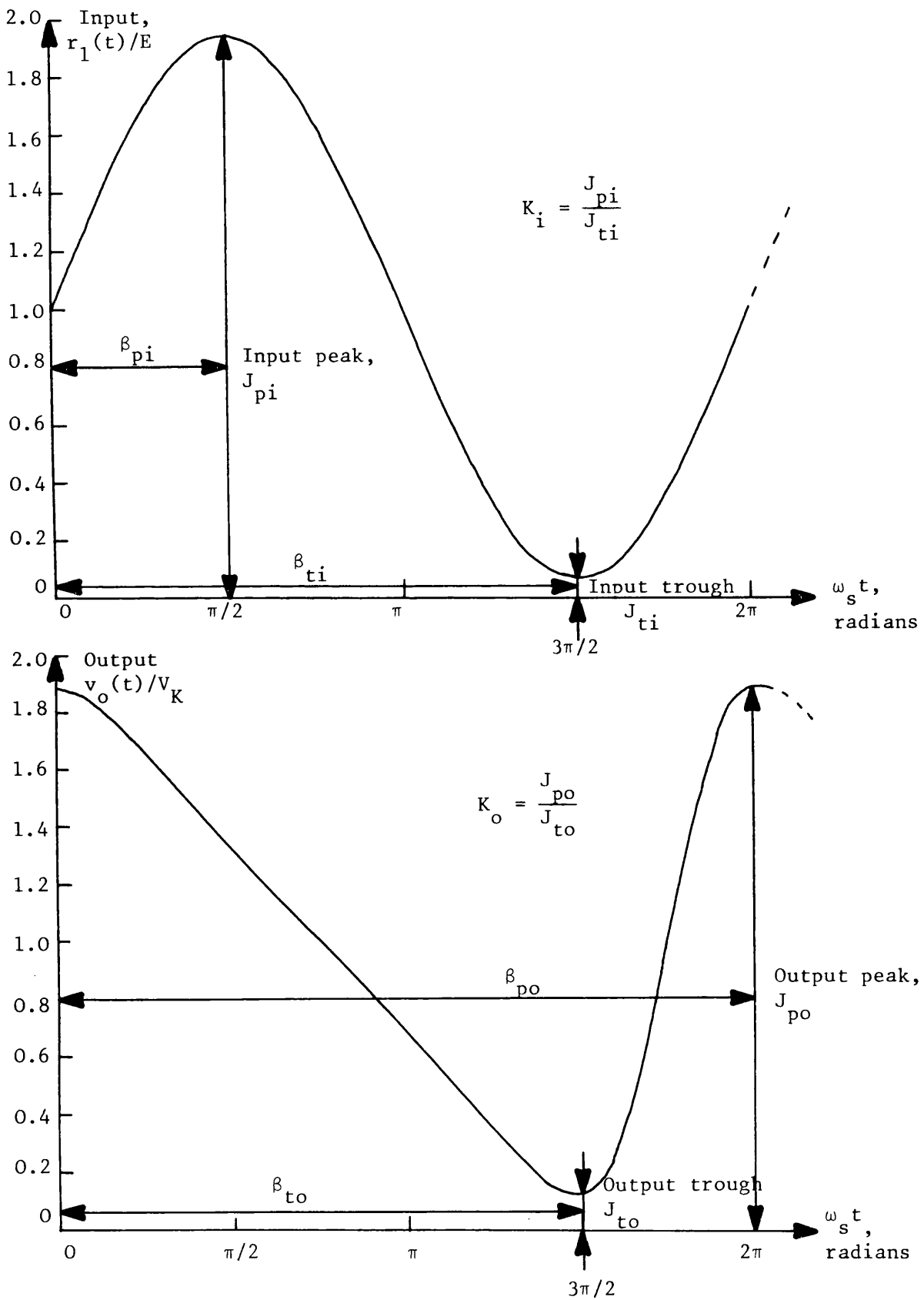
Figure 5.8   Illustration of input and output waveform properties
            of EIFBAGC during 30 dB sinusoidal envelope fade at $\omega_N = 1$

1) The positions of the peak and trough, β_{po} and β_{to}. In general, they do not occur at the same point in time as the input waveform's peak and trough, β_{pi} and β_i.

2) The ratio of the peak, J_{po}, to trough, J_{to}, called K_o. This may be calculated by substituting β_{po} and β_{to} into equation 5.25. However, a simpler solution is presented that gives the ratio directly. The residual output modulation, described by K_o, is sometimes referred to as the output ripple.

3) The harmonic content. The output waveform is evidently non-sinusoidal, exhibiting a characteristic fast-up, slow-down shape.

Note: unless otherwise stated, describing a variation as "x decibels" refers to the peak to trough ratio.

5.3.2 Peak and Trough Position

The position of the peak and trough of the output waveform are solved in appendix 4 to give:

$$\beta_{po} = \tan^{-1}\left[\frac{1}{\omega_N}\right] - \sin^{-1}\left[\frac{D}{(1 + \omega^2)^{\frac{1}{2}}_N}\right] + 2\pi \qquad (5.26)$$

$$\beta_{to} = \tan^{-1}\left[\frac{1}{\omega_N}\right] + \sin^{-1}\left[\frac{D}{(1 - \omega^2)^{\frac{1}{2}}_N}\right] + \pi \qquad (5.27)$$

For example, the peak and trough positions of the 30 dB fade at $\omega_N = 1$ shown in figure 5.8 occur at $\beta_{po} = 6.343$ radians (363°) and $\beta_{to} = 4.653$ radians (267°).

As stated earlier, equations 5.26 and 5.27 could be substituted into equation 5.25 to give the magnitude of the peak and troughs respectively. Dividing the peak by the trough would give K_O. However, a more elegant solution is given in the next section that generates K_O directly.

5.3.3 Peak to Trough Ratio

The peak to trough ratio of equation 5.25 has been solved elsewhere (5.20), (this paper is also included in the published paper section). The paper solves equation 5.25 for both the general case where L and θ can be any values, and also the particular case of EIFBAGC. The particular solution is relevant here and is given by:

$$K_O = \frac{1 + D \cdot \sqrt{\dfrac{\omega_N^2}{\omega_N^2 + 1 - D^2}}}{1 - D \cdot \sqrt{\dfrac{\omega_N^2}{\omega_N^2 + 1 - D^2}}} \qquad (5.28)$$

A plot of this equation for several values of D corresponding to K_i (dB) of 10, 20, 30, 40 and 50 dB is shown in figure 5.9. It is apparent that deep sinusoidal input variations are only well suppressed ($K_O < 3$ dB, say) if they occur at frequencies much below $\omega_N = 1$. This is a very important observation regarding the performance of EIFBAGC. In general, deep unwanted input envelope variations are only well suppressed by EIFBAGC if its bandwidth is much greater than the bandwidth of the input signal's envelope variations, typically by a factor of at least 10. For example, a 30 dB sinusoidal input envelope variation is reduced to less than 3 dB of output variation only below $\omega_N = 0.064$. That is, the bandwidth of the EIFBAGC circuit needs to be greater than 15.6 times the input fade
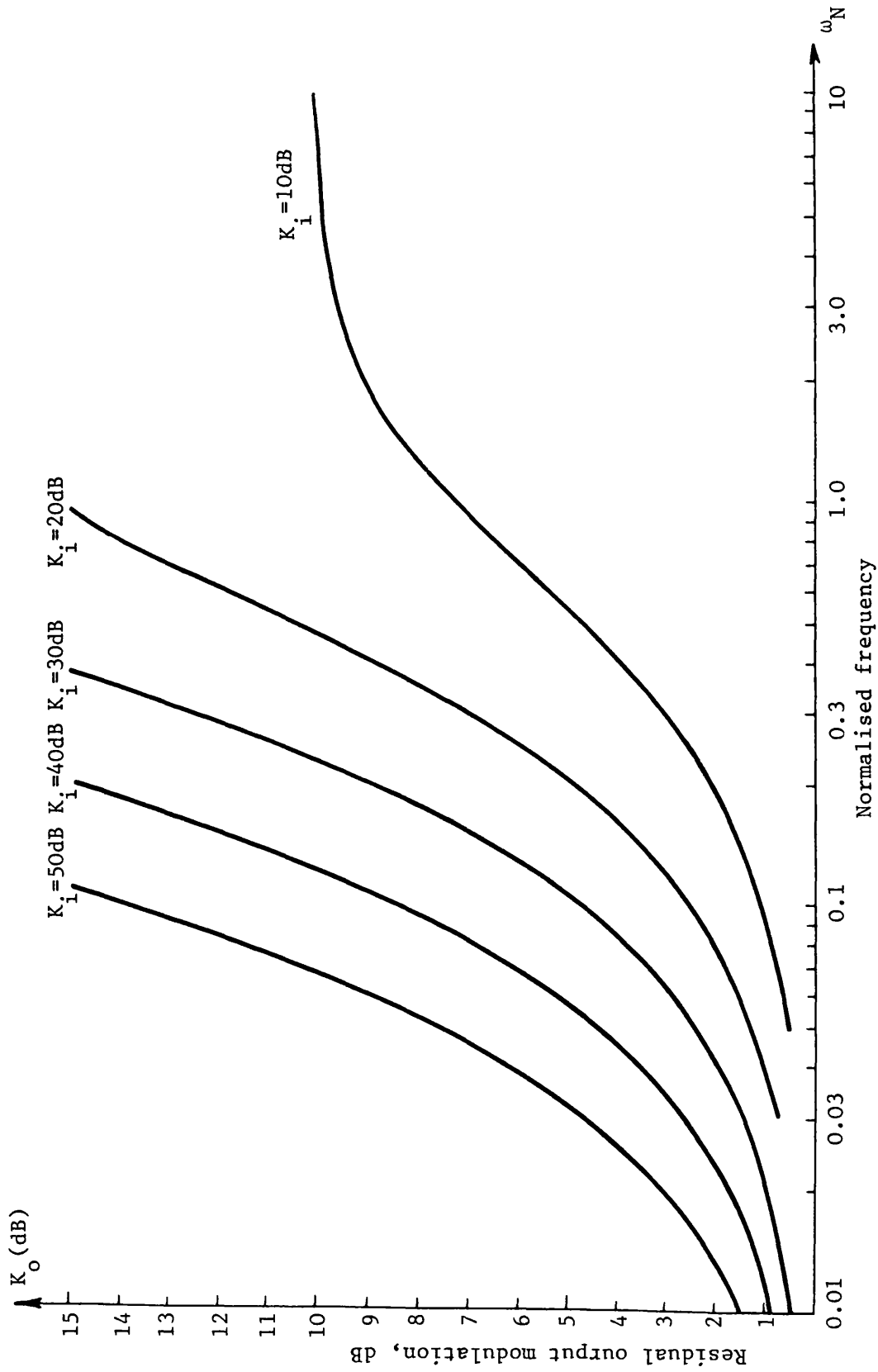
Figure 5.9 Residual output modulation, K_o(dB), for several values of K_i(dB), as a function of frequency for EIFBAGC

5.27

frequency, ω_s.

It will now be shown that EIFBAGC possesses the property of unconditional suppression for real sinusoidal input variations. That is, it is required to show that for any ω_N, $K_o < K_i$. The input variation peak to trough is:

$$K_i = \frac{1 + D}{1 - D} \qquad (5.29)$$

The output variation peak to trough is:

$$K_o = \frac{1 + ID}{1 - ID} \qquad (5.30)$$

$$\text{where} \quad I = \sqrt{\frac{\omega_N^2}{\omega_N^2 + 1 - D^2}} \qquad (5.31)$$

By inspection, K_o is only less than K_i if $I < 1$. From equation 5.31 I is always less than 1 if:

$$1 - D^2 > 0 \qquad (5.32)$$

$$\text{i.e.} \quad D^2 < 1 \qquad (5.33)$$

is the condition to be met so that EIFBAGC possesses the property of unconditional suppression. This condition is always met for any real envelope variation, therefore an ideal EIFBAGC system possesses the property of unconditional suppression for sinusoidal input variations.

5.3.4 Harmonic Content

For an EIFBAGC circuit, equation 5.25 can be rewritten as:

$$v_o(t) = V_K(1 + \sum_{n=1}^{\infty} A_n \cos(n\omega_N t + \theta_n)) \qquad (5.34)$$

The dc component can be immediately written down as V_K due to the nature of EIFBAGC, that is, it maintains the mean (dc) level of the output fixed at V_K. This result was confirmed during both theoretical and practical observations of $v_o(t)$.

The harmonics of equation 5.34 have been analysed using a 64 point discrete Fourier transform. The results of the analysis are plotted in figure 5.10 for D = 1. An approximate fit to A_n is solved in appendix 5. It is valid for $\omega_N > 1$ and most accurate for small D. The (worst case) fit for D = 1 is shown in figure 5.10. The approximate solution for A_n is:

$$A_n \simeq (D)^n (0.5L)^{n-1} \qquad (5.35)$$

The harmonics are required to estimate the degree of distortion EIFBAGC will introduce into a wanted signal variation in a full carrier AM system. The most distortion is introduced into the deepest and lowest frequency envelope variation. For example, in a speech transmission this may be a 100% modulation at 300 Hz. In order to pass this relatively undistorted, the bandwidth of the EIFBAGC circuit should be much less than the bandwidth of the 300 Hz signal, typically by a factor of 10. For example, the 300 Hz signal will have a second harmonic 26 dB down and a third harmonic 52 dB down relative to the fundamental component if transmitted through an EIFBAGC circuit with a bandwidth of 30 Hz. The predominant harmonic distortion is second harmonic for which the approximate solution is:
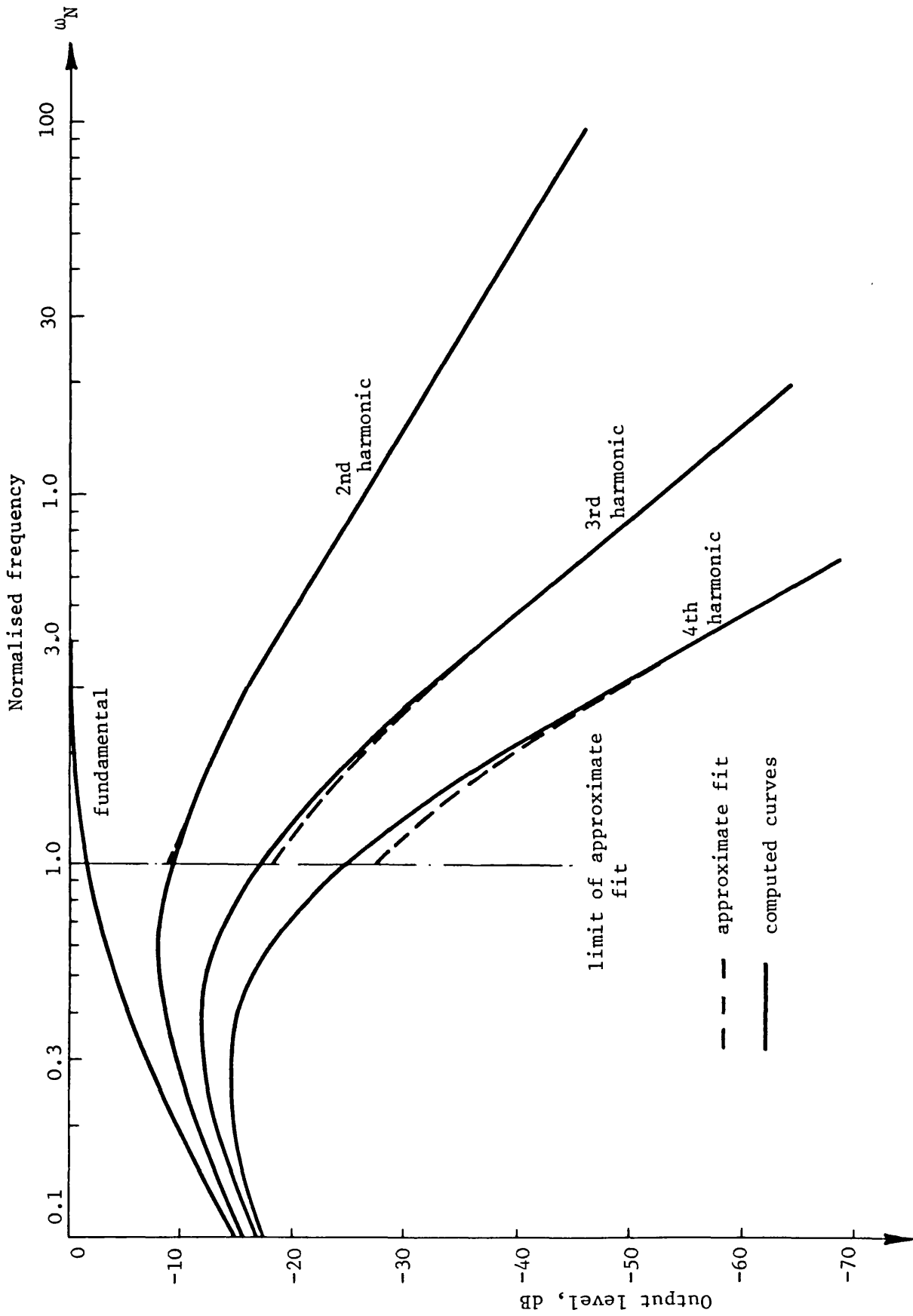
Figure 5.10 Harmonics of equation 5.34 for D = 1

$$A_2 = D^2 \; 0.5L \qquad\qquad\qquad (5.36)$$

from equation 5.35.

The results of both this and the previous section show that EIFBAGC possesses a large frequency transition region between those envelope fading frequencies it will satisfactorily suppress and those envelope modulation frequencies it will pass relatively undistorted. This transition region commences from about 0.1 of the closed loop bandwidth (30 dB of input fade modulation suppressed to 4.6 dB of output ripple) to about 10 times the closed loop bandwidth, (5% of second harmonic distortion for 100% input modulation). Over the transition region, deep envelope variations will be partially suppressed and grossly distorted.

5.3.5 Verification of Analysis

A practical verification of the analysis has been performed using the precision EIFBAGC circuit, the UHF SSB receiver described in chapter 4 and the IF stages of a full carrier AM receiver. In all cases, the experiments were performed as follows:

a) A carrier wave (RF, IF or audio/dc) was applied to the circuit and amplitude modulated by a sinusoid.

b) For various depths, the frequency of the sinusoidal amplitude modulation was varied and for each value the output ripple (K_o) was recorded. The peak and trough input and output values were measured on an oscilloscope. The precision EIFBAGC circuit was operated in dc carrier mode to obtain the output ripple results. When performing

deep modulation experiments care was taken to prevent modulation feed-through.

c) The harmonics of the output waveform were analysed using a spectrum analyser. The precision EIFBAGC circuit was operated in the ac mode for this part of the experiment using a 2 kHz carrier.

The results of these experiments are shown in figure 5.11. Figure 5.11(a) shows the measured output ripple as a function of frequency while figure 5.11(b) shows the measured output harmonic distortion as a function of frequency. In both cases good agreement has been observed between theory and practice.

A more full description of the experiments may be found elsewhere (5.20). As a result of these experiments, this section concludes that the feedforward model of EIFBAGC has been verified and shown to be able to allow prediction of the response of EIFBAGC to large input envelope variations.

5.4 Response to Two Tones

This section discusses the response of EIFBAGC to two tones, i.e. deterministic AGC test signal 2. Once again, the analysis relies on using the feedforward model and the results are checked by practical experiments wherever possible.

5.4.1 Requirements of the Analysis

The input to the circuit consists of 2 tones, relative level R, whose envelope is given by:
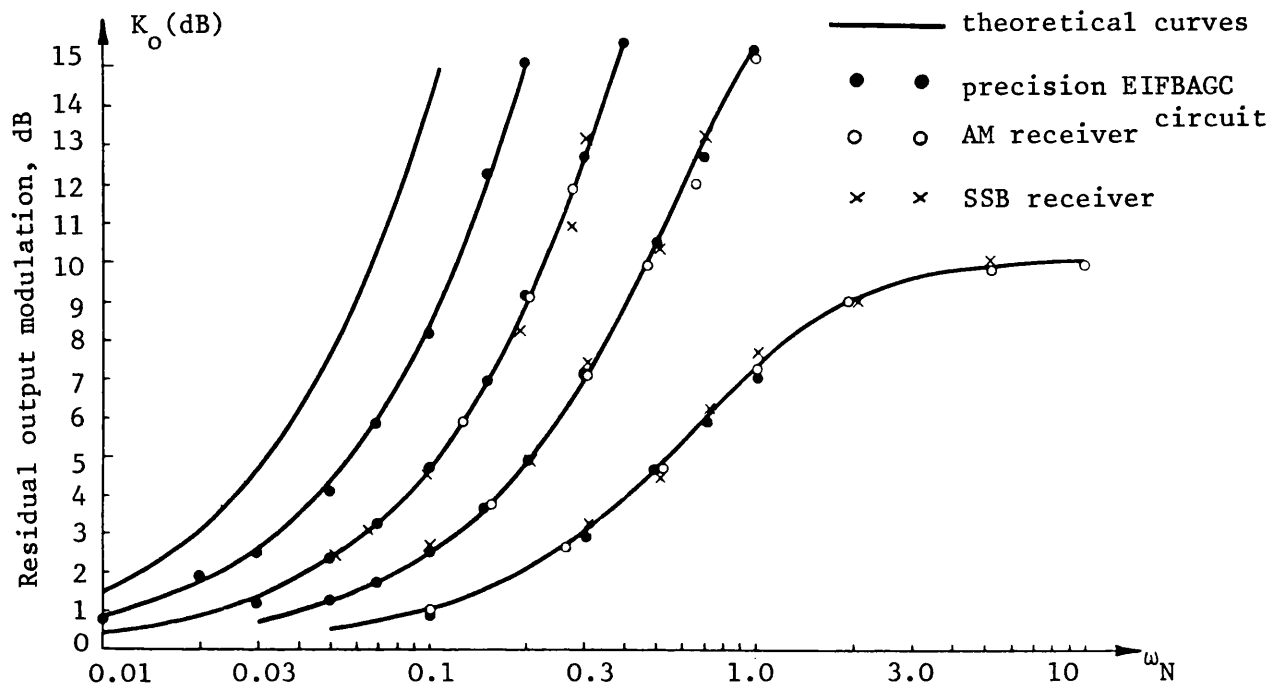
Figure 5.11(a)   Measured output ripple
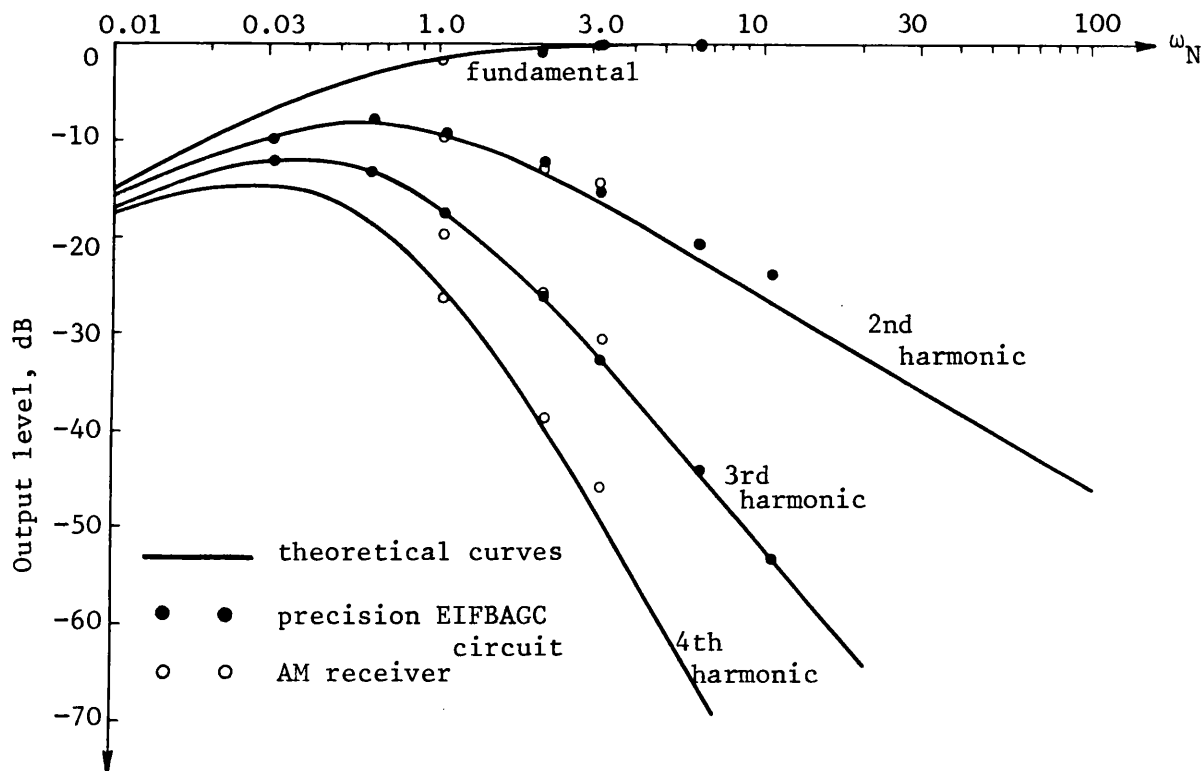
Figure 5.11(b)   Measured output harmonic level

$$r_2(t) = E(1 + R^2 + 2R \cos \omega_N t)^{\frac{1}{2}} \qquad (5.37)$$

where ω_N is the tone separation frequency normalised to the EIFBAGC
bandwidth. The steady state envelope variations of the output of the
circut are given by the feedforward model shown in figure 5.4 as:

$$v_0(t) = \frac{V_K(1 + R^2 + 2R \cos \omega_N t)^{\frac{1}{2}}}{F1((1 + R^2 + 2R \cos \omega_N t)^{\frac{1}{2}})} \qquad (5.38)$$

where F1 represents the first order filtering function, -3 dB at $\omega_N = 1$.

As mentioned in section 3.5.3, there are 2 main areas of interest
here. The first is when $r_1(t)$ represents twin path fading, so the
ability of an EIFBAGC system to suppress it is required. Alternatively
1 tone can represent an interfering signal and the other tone the AGC
reference so the requirements for the EIFBAGC system not to respond to
the interference are also required. With this second case, the analysis
is more applicable to pilot reference SSB systems than full carrier AM
systems.

As with sinusoidal input variations, EIFBAGC will only adequately
suppress 2 tone envelope variations that occur well inside the closed
loop bandwidth. Once again, this will be shown by analysing the peak
to trough ratio of equation 5.38 for various values of R and ω_N. In this
case, it has been necessary to use numerical techniques to perform the
analysis on a computer.

For the interfering tone case, there are 2 main steady state
effects. The first is an overall dc compression of the receivers gain,
resulting in a reduced level of the required tone. This dc compression
is independent of ω_N. The second effect is that the receivers gain is

5.34

modulated at the difference frequency between the 2 tones. These

effects are discussed in subsequent sections.

5.4.2 Peak to Trough Ratio

The equation of the output envelope, 5.38, has been analysed using

numerical techniques on a computer. The programme, called AGCSIM, is

described in detail in appendix 6. It was used to calculate the peak

to trough ratio of $v_o(t)$ for various values of R and ω_N . A 64 point

discrete Fourier transform was used for these runs which gave a worst

case peak to trough programme accuracy of better than 0.23 dB. The

results are shown plotted in figure 5.12. Some of the input and output

envelopes obtained during these runs are shown in figure 5.13.

Figure 5.12 shows that EIFBAGC requires a bandwidth considerably

greater than the fade rate to suppress deep twin path induced envelope

fades. The bandwidth required to suppress this fading is greater than

the bandwidth required to suppress equivalent sinusodal fading. For example,

suppression of a 30 dB fade to better than 3 dB of output ripple requires

ω_N to be less than ω_N = 0.022. That is, the bandwidth of the EIFBAGC

circuit needs to be greater than 45 times the input fade rate. This

compares to a bandwidth requirement of 15.6 in the equivalent sinusoidal

input modulation case.

Figure 5.12 allows the receiver designer to estimate the bandwidth

requirements of an EIFBAGC circuit to suppress twin path fading. The

receiver designer need only know the maximum fade rate and input

variation to design the EIFBAGC bandwidth to meet an output ripple

specification. For example, consider the UHF SSB system described in

chapter 4. When driving at 112 km/hr (70 mph) the fade rate can be as
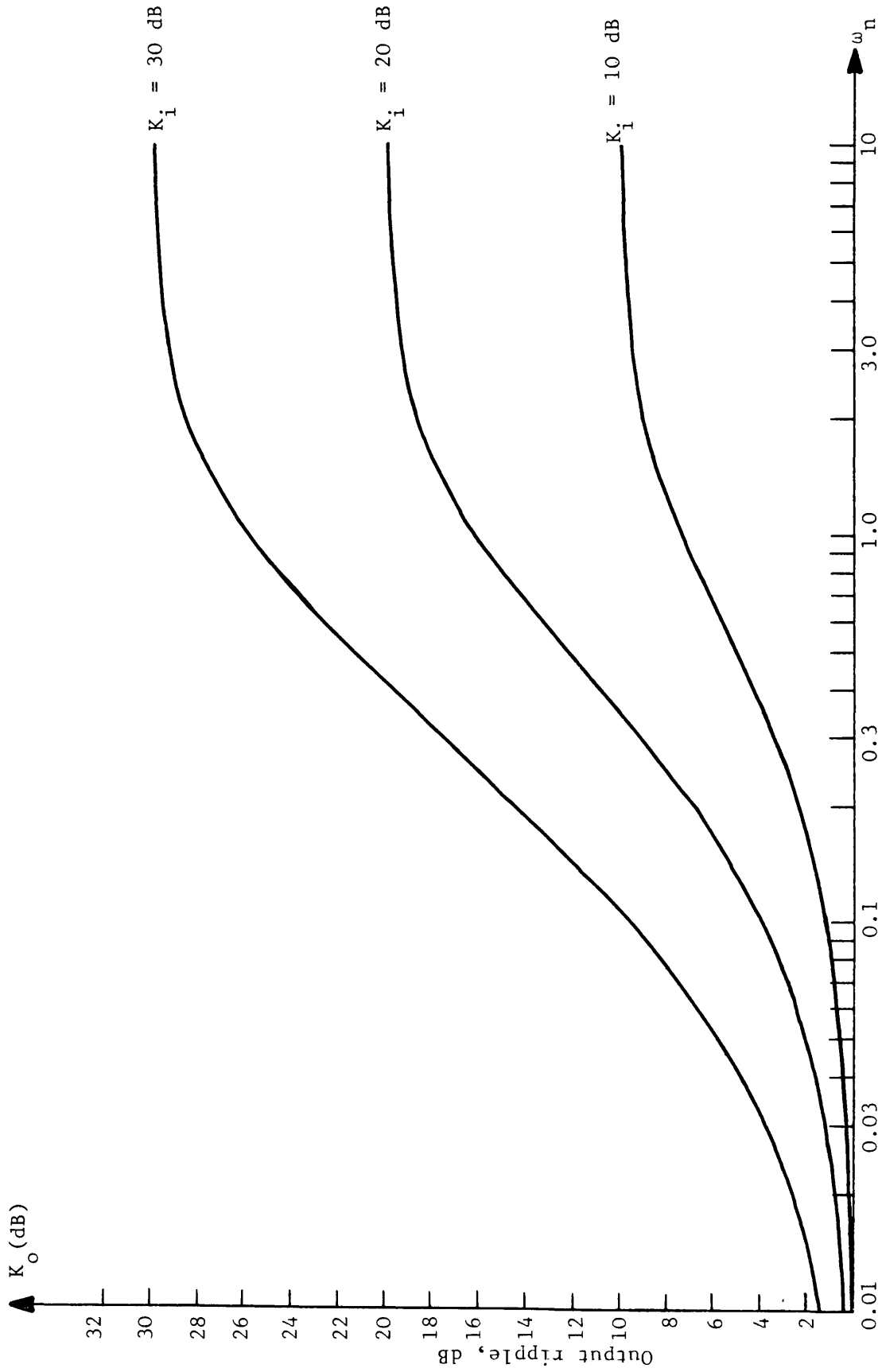
Figure 5.12   Theoretical output ripple of EIFBAGC in response to 2 tones
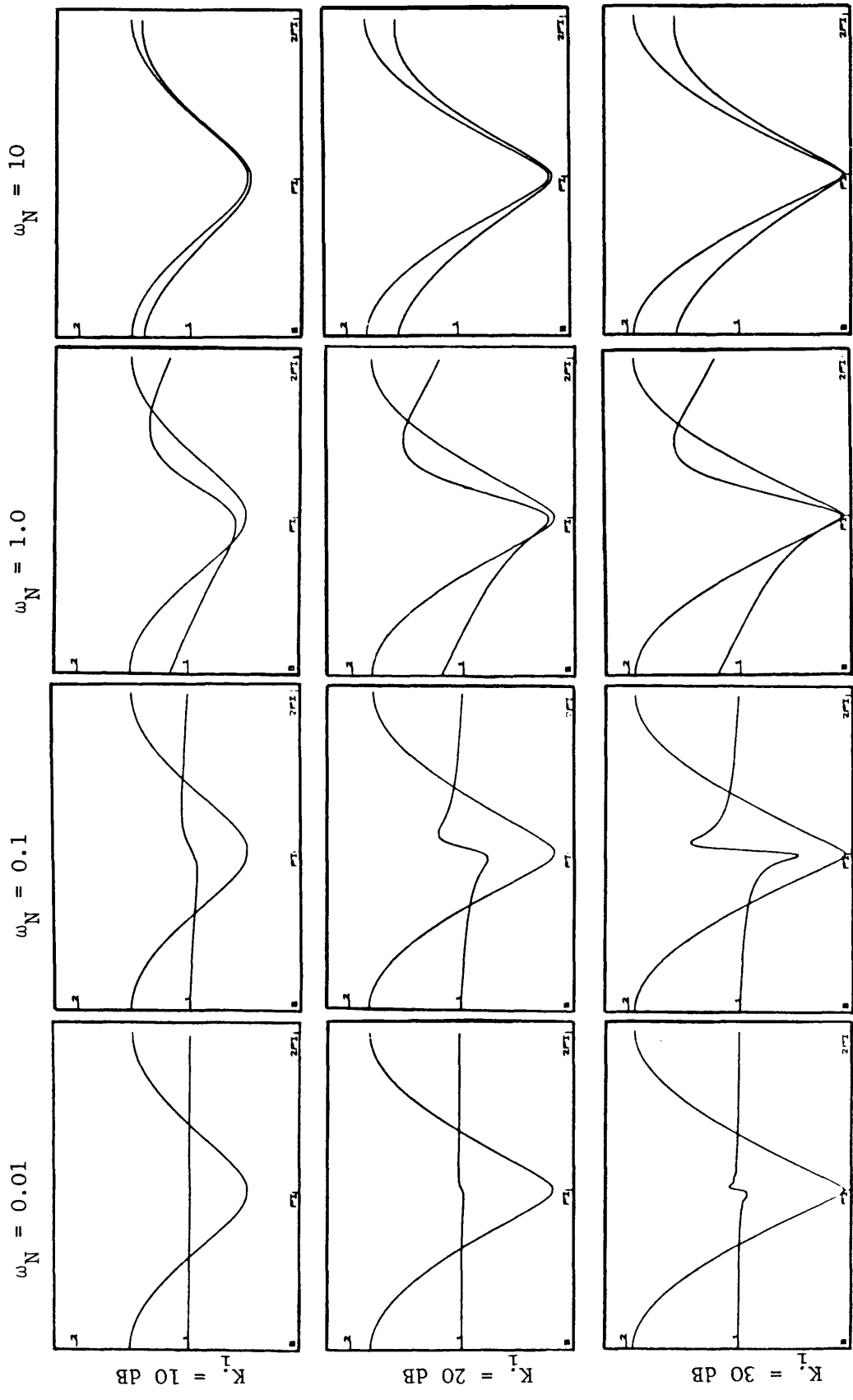
Figure 5.13 Some of the input and output envelope variations obtained from AGCSIM for the plot of figure 5.12

5.37

high as twice maximum Doppler, 95 Hz. What is the EIFBAGC bandwidth required to suppress a twin path fade 20 dB peak to trough to better than 3 dB of output ripple? Figure 5.12 shows that this suppression occurs at ω_N < 0.07. Therefore, the EIFBAGC circuit would require a bandwidth of 1.36 kHz. This would be unrealisable in practice for reasons that are discussed in the next chapter, i.e. stability. UHF inter-aircraft communications would also require the use of unrealisably high EIFBAGC bandwidths. In this case, speech distortion considerations prevent the use of the high bandwidths required to suppress the signal fading.

In Chapter 2 it was shown that during land or air mobile twin path communications both R and ω_f varied slowly over several cycles of input fading. The steady state 2 tone AGC test signal is only a convenient representation of the real situation. However, as indicated above the EIFBAGC bandwidth required to suppress the 2 tone test signal is very high relative to ω_f. The circuit's response will be negligibly affected by variations in R and ω_f that occur over several cycles of input fading. If a complete fade is defined from peak to trough to peak then the results obtained so far will allow accurate prediction of the response of EIFBAGC on a fade-by-fade basis.

5.4.3 Interfering Tone Compression and Modulation

Consider an EIFBAGC circuit operating on a steady single tone reference. If an additional tone is introduced to the input, and this interfering tone slowly increased in amplitude, then the reference tone will be decreased at the output of the circuit. This is because EIFBAGC maintains the average level of the overall output signal's

envelope at a constant level, and has no means of distinguishing between the 2 tones. This means level compression of the reference tone is dependent only on the relative levels of the 2 tones at the input of the envelope detector.

Calculation of the reference tone compression is a relatively simple matter. The dc value of the 2 tone signal's envelope is calculated and compared to the dc value of the single reference tone's envelope. The ratio of the 2 values is the mean level compression of the reference tone. If the reference tone is represented by $E \cos \omega_c t$ it has an envelope value E. If the reference and interfering tone are represented by the sum of $E \cos \omega_c t$ and $RE \cos \omega_i t$ where ω_i is the interfering tone frequency, the average (dc) value of the resulting signal's envelope has already been calculated in chapter 2, section 2.3.3. Using the discrete Fourier analysis described in that section, the dc component may be approximated by:

$$A_o = \frac{E}{N} \sum_{p=0}^{N-1} \left[1 + R^2 + 2R \cos \left[\frac{2\pi p}{N} \right] \right]^{\frac{1}{2}} \qquad (5.39)$$

The compression of the wanted tone, CM, is given by:

$$CM = 20 \log_{10} \left[\frac{A_o}{E} \right] \quad dB \qquad (5.40)$$

A plot of the compression, CM, versus interfering tone level is shown in figure 5.14. The value $N = 16$ was used to evaluate equation 5.39. The predicted dc value of $A_o = 1.2691$ for $R = 1$ differs from the theoretical value of $4/\pi$ by less than 2%.
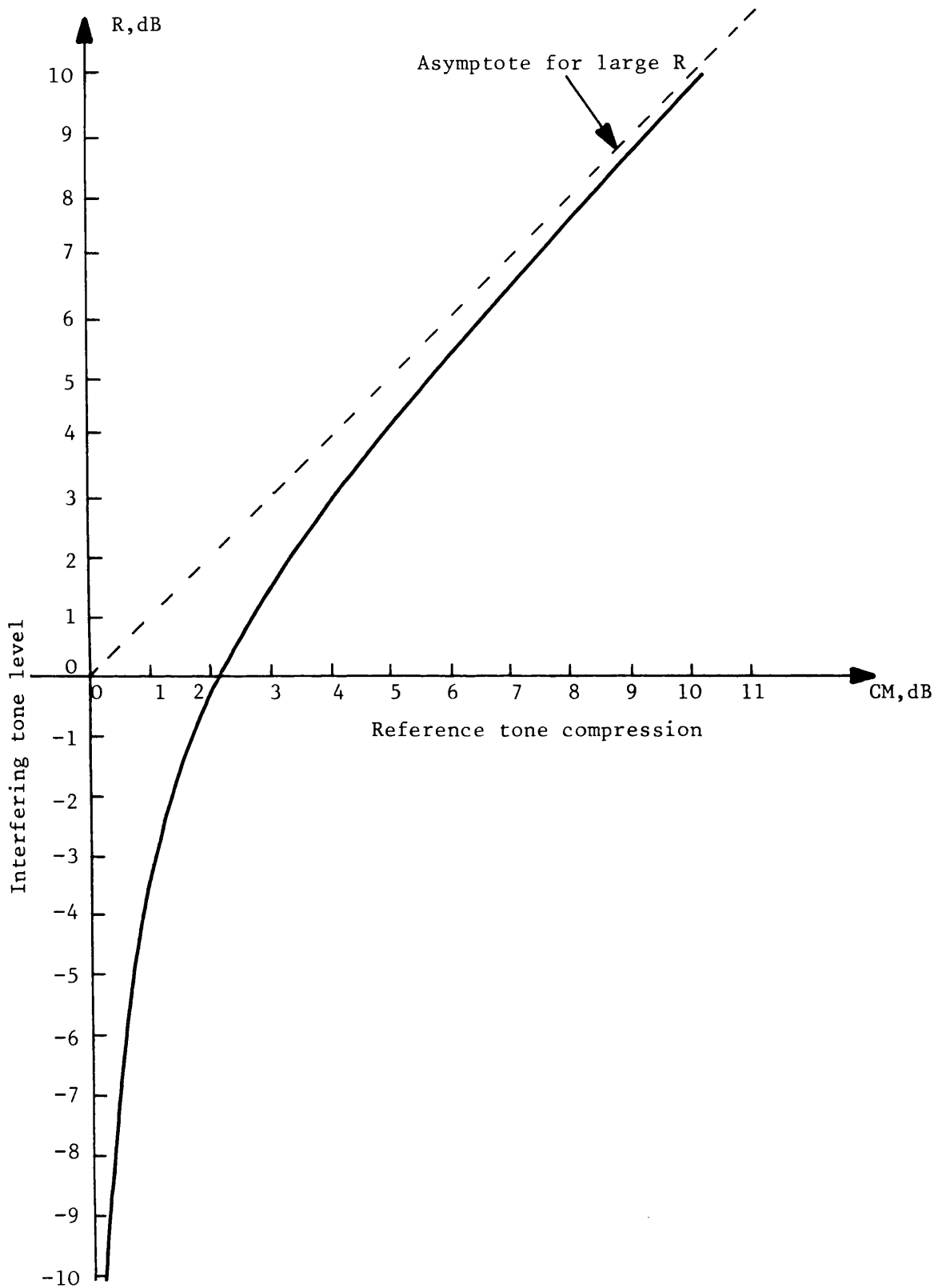
Figure 5.14 Graph of reference tone compression, CM, versus level of interfering tone, R

The other effect of a single interfering tone is that it will

cause the gain of the EIFBAGC circuit, and hence the reference tone, to

be nonlinearly amplitude modulated at the difference frequency between

the reference and interfering tones. If the interfering tone is well

separated in frequency from the reference tone, relative to the EIFBAGC

bandwidth, the effect will be negligibly small. If the interfering

tone to reference tone frequency difference is smaller than the EIFBAGC

bandwidth, the gain modulation will be large. The worst case peak to

trough gain modulation occurs for equal amplitude tones very close

together in frequency. The peak to trough ratio of the gain variation

is the same as the peak to trough ratio of the denominator of $v_o(t)$,

called $d(t)$ where:

$$d(t) = Fl((1 + R^2 + 2R \cos \omega_N t)^{\frac{1}{2}}) \tag{5.41}$$

where Fl represents the first order filtering function -3 dB at $\omega_N = 1$,

R is the relative level of the interfering tone to reference tone and

ω_N is the separation between the frequency of the 2 tones relative to

the EIFBAGC bandwidth. The computer programme, AGCSIM, described in

appendix 6 can be used to analyse the effect by setting the input

variable PT to zero. It will then plot the inverted gain control

voltage, $1/d(t)$, and calculate its peak to trough value. If the tone

separation, ω_N, is much less than unity then the peak to trough gain

variation is given by K_i where:

$$K_i = \frac{1 + R}{1 - R} \tag{5.42}$$

The effects of interfering tones on other aspects of FBAGC performance

are discussed further elsewhere (5.3). However, a general observation

regarding the gain modulation is that it is usually less of a problem

than the dc compression. This is due to the use, in general, of

relatively narrow EIFBAGC bandwidths where the problem of dc compression

predominates.

5.4.4 Practical Results

Practical experiments have been performed using the precision EIFBAGC

circuit described in section 5.2.6 to check the peak to trough ratio (K_0)

and dc compression predictions. The peak to trough ratio, K_0, was

measured as follows:

The input to the circuit was comprised of 2 tones, nominally at

2 kHz, spaced 30 Hz apart. Their relative levels were adjusted for

values of K_i of 10, 20 and 30 dB. The closed loop bandwidth was varied

to give a relative variation in ω_N. A sampling digital oscilloscope

gave a numerical reading of the peak and trough values of the input and

output signal's envelope. The results are shown plotted along with the

theoretical predictions from AGCSIM in figure 5.15. Evidently there is

good agreement between the 2.

The measurement of the dc compression was performed in a similar

manner but this time the output was observed on a spectrum analyser.

The tone separation used was 100 Hz with an EIFBAGC bandwidth of 10 Hz.

The results are shown plotted on figure 5.16. Once again, there is good

agreement between theoretical predictions and practical measurements.

5.5 Response to Field Trial Data

This section describes the response of the precision EIFBAGC circuit

to multipath fast fading, comparing the results with twin path predictions

and testing the worst case hypothesis.
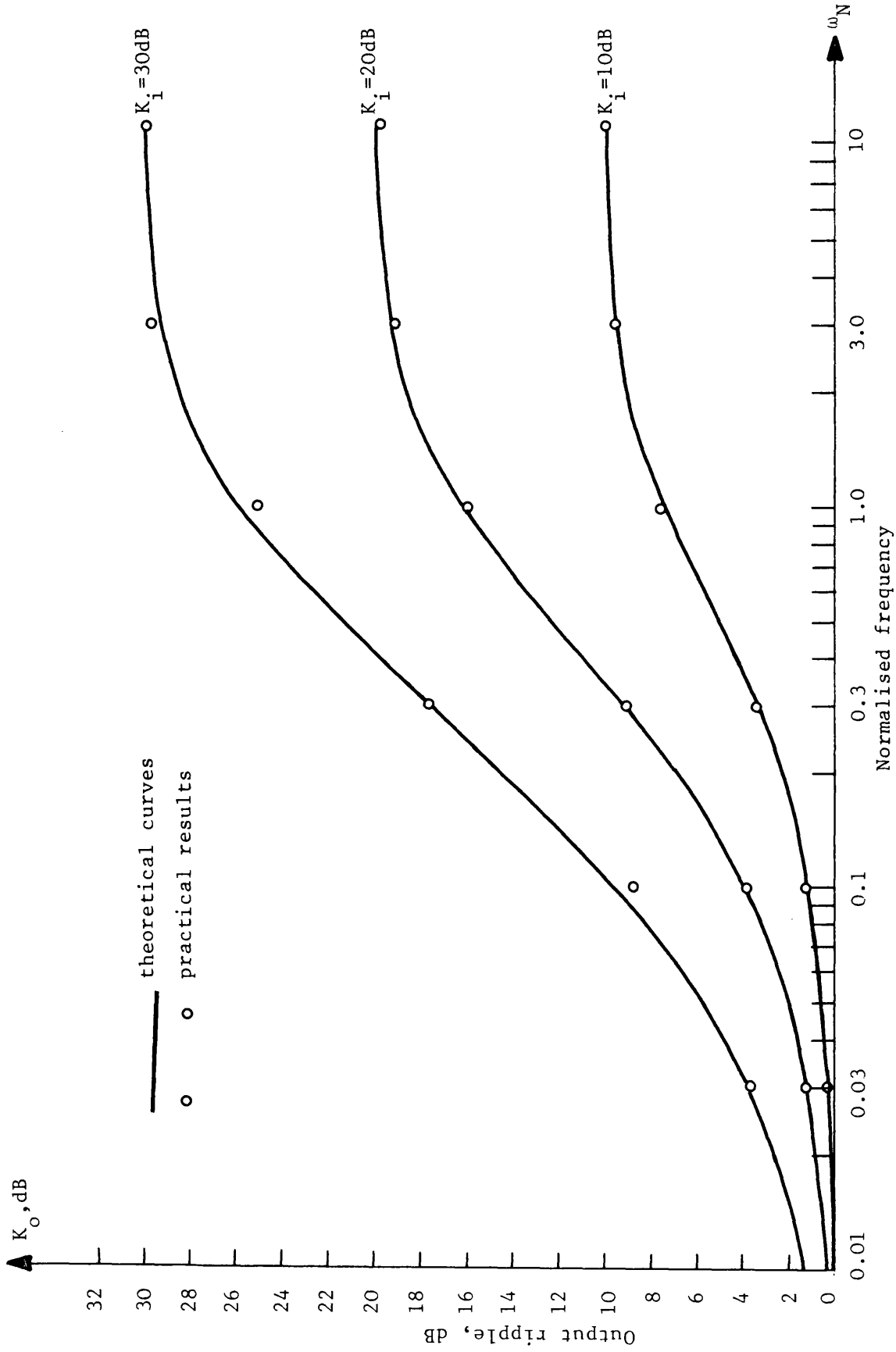
Figure 5.15 Practical measurements of output ripple of precision EIFBAGC circuit in response to 2 input tones
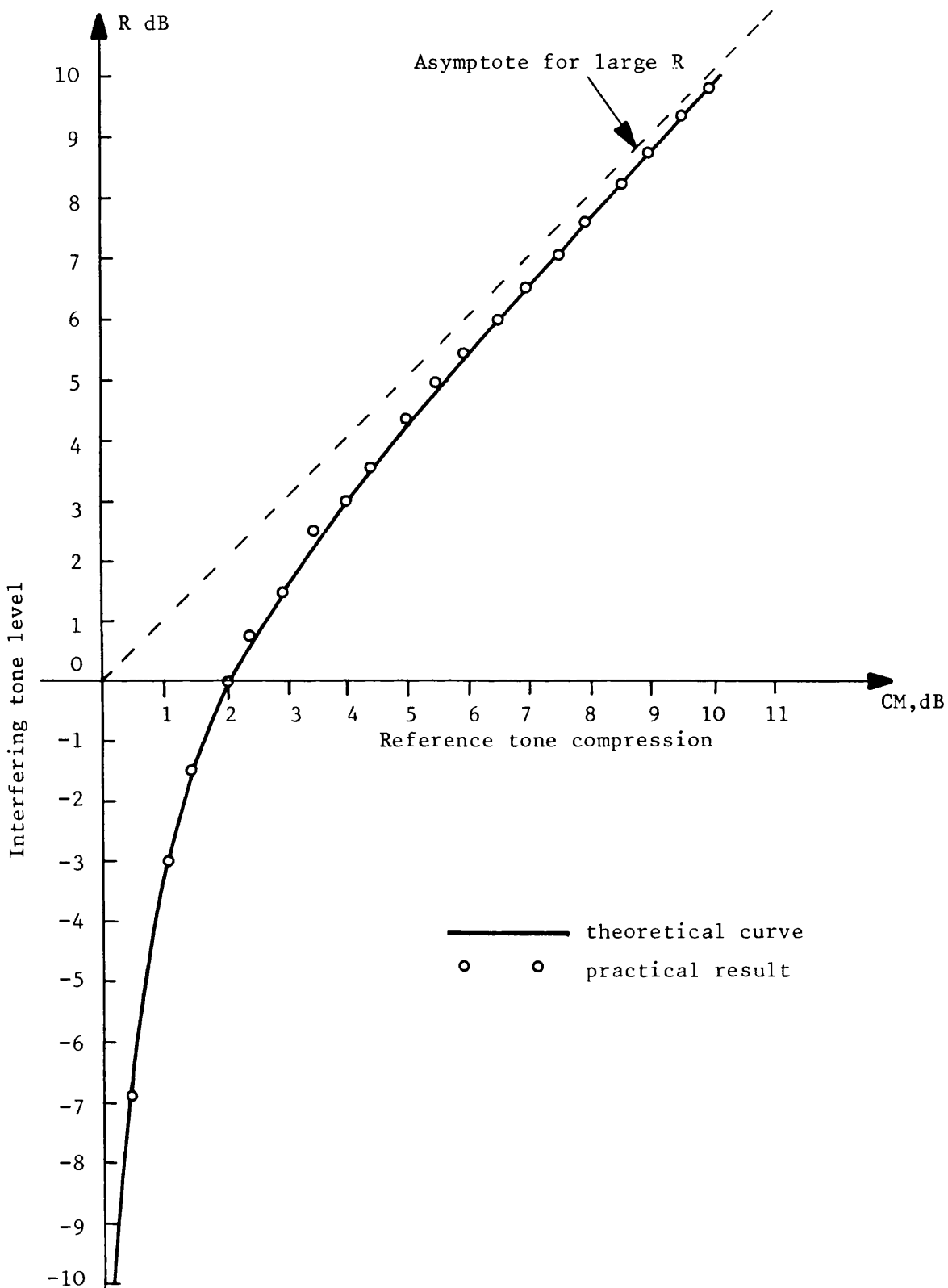
Figure 5.16   Graph of reference tone compression, CM, versus level of
interfering tone, R(dB), showing precision EIFBAGC circuit
results

5.5.1 Input Signal

For the tests, the input signal consisted of the 1.672 kHz pilot, recorded as described in chapter 4. The car was travelling in a suburban area near Bath University, position A on figure 4.11, for the particular segment of recording being described. The speed was about 50 km/hr (30 mph), giving a maximum fade rate $2\omega_d$ of 42 Hz. The mean received signal strength was 30 dB above 1 μV. Figure 5.17 is an 819 mS plot of the fading pilot's envelope, along with a series of position markers on each peak or trough. Table 5.1 gives the time of each marker from the reference point, a recording blip on the original tape used for triggering purposes. Also shown in Table 5.1 are the relative changes in envelope in between each marker, to the nearest dB, as calculated from readings taken from a digital recording oscilloscope. During this run, the receiver's EIFBAGC system was on "hold", preventing it from affecting the received pilot's envelope.

5.5.2 Precision EIFBAGC Circuit Response

The same recording of pilot just described was played back through the precision EIFBAGC circuit with various closed loop bandwidths. Plots of the output signal's envelope are shown in figures 5.18 to 5.24 inclusive, for increasing closed loop bandwidths. The same vertical scale has been used for all these plots to allow relative comparison (0.8V top to bottom).

The following general observations have been made regarding these plots:
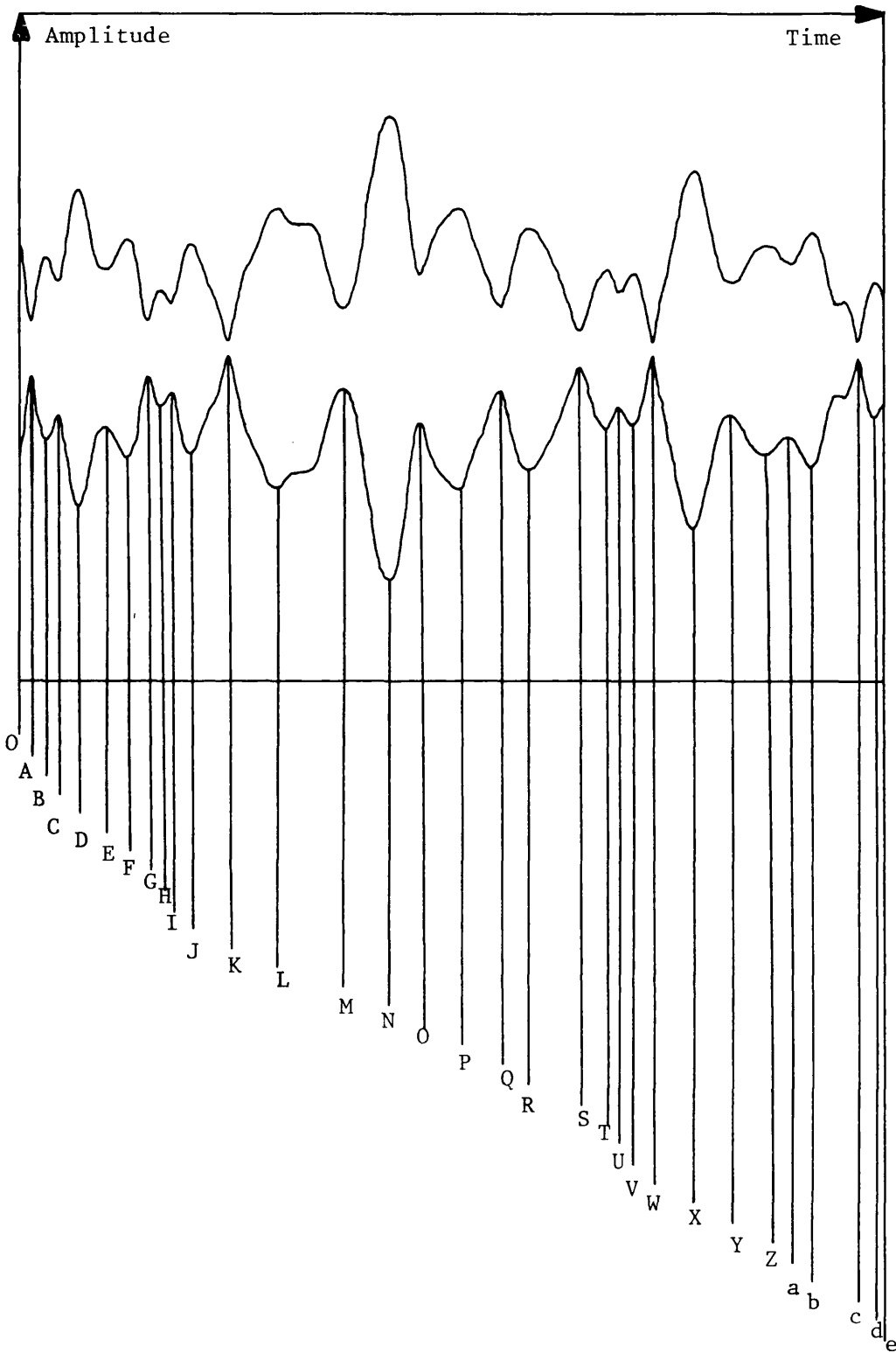
Figure 5.17   Input signal's envelope on the 819 millisecond run,
illustrating the position markers

Table 5.1   Data for figure 5.17

Position Marker	Time from start, mS	Change between markers, dB
0	0	
A	13	+ 14
B	27	− 3
C	39	+ 8
D	59	− 6
E	85	+ 3
F	104	− 13
G	124	+ 8
H	134	− 3
I	147	+ 8
J	164	− 29
K	200	+ 31
L	245	− 11
M	307	+ 16
N	353	− 10
O	382	+ 6
P	419	− 11
Q	458	+ 10
R	485	− 18
S	533	+ 14
T	557	− 3
U	570	+ 3
V	583	− 30
W	602	+ 37

Table 5.1 continued

X	640	− 9
Y	676	+ 4
Z	708	− 2
a	731	+ 3
b	752	− 24
c	796	+ 23
d	811	
e	819	

1)   The 1 Hz EIFBAGC circuit has had a negligible effect on the fast fading envelope, and figure 5.18 may be used as a normalised plot for comparison with the others.

2)   The 3 Hz EIFBAGC circuit has had a small but noticeable effect on the large envelope peak. Otherwise, figure 5.19 shows that it passes the fast fading almost without modification.

3)   The 10 Hz EIFBAGC circuit's output shown in figure 5.20 is seen to be introducing noticeable distortion to the envelope, of the characteristic "fast-up, slow-down" type which is even more noticeable in the faster circuits. However, there is still only a small suppression of the fast fading, the reduction of the relatively slow peaks being most apparent.

4)   The 30 Hz EIFBAGC circuit's output shown in figure 5.21 begins to demonstrate a noticeable reduction in the peak to trough ratio. For example, the 31 dB rise on the input from position markers K to L is reduced to 20 dB.

5)   The 100 Hz and 300 Hz EIFBAGC circuit's outputs shown in figures 5.22 and 5.23 exhibit much more fast fading suppression, albeit at the expense of reducing the deeper fades to relatively more rapid output spikes. The largest peak to trough output variation for the 300 Hz circuit is 10 dB, corresponding to the 37 dB input variation from W to X.

6)   Finally, what may be regarded as good AGC performance is demonstrated by the output of the 1 kHz EIFBAGC circuit shown in figure 5.24. The largest input peak to trough variation has been reduced to less than 4.5 dB of output ripple.
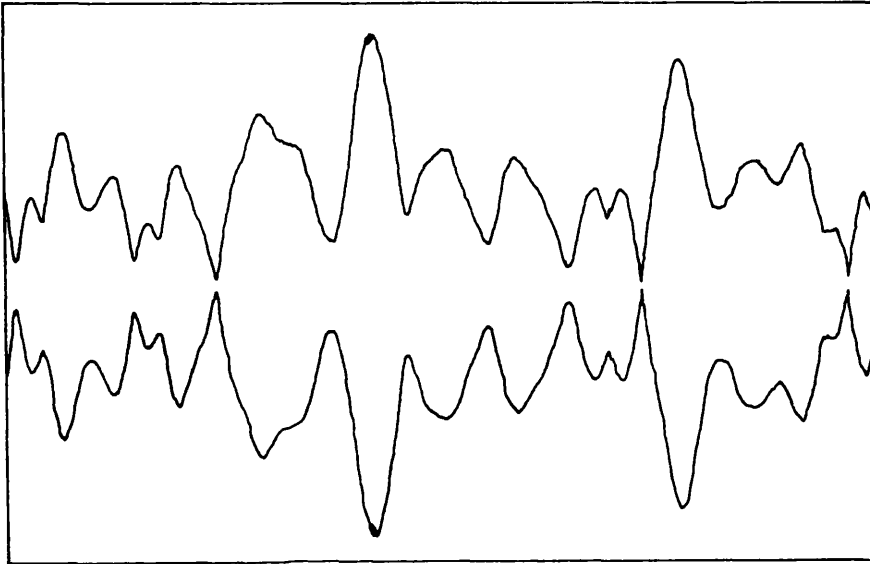
Figure 5.18 1 Hz precision EIFBAGC circuit output
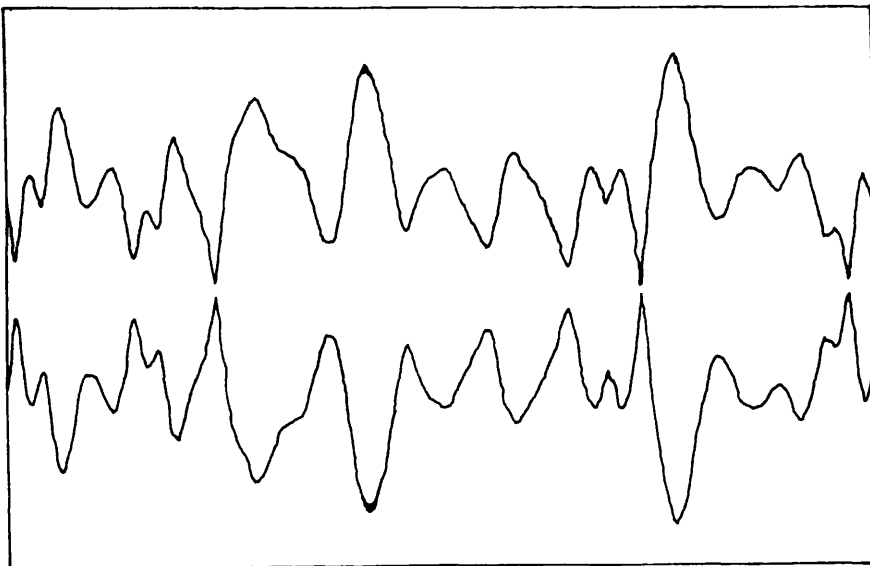
Figure 5.19 3 Hz precision EIFBAGC circuit output
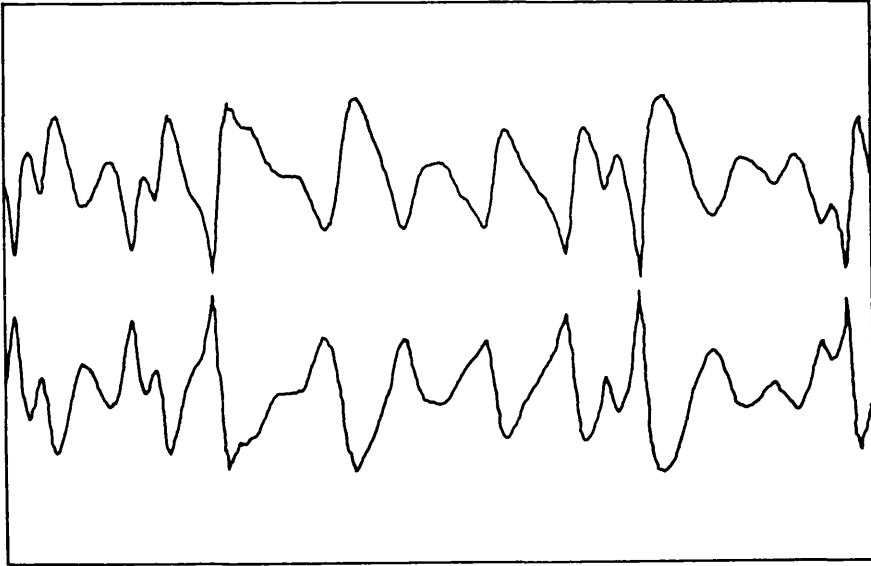
Figure 5.20   10 Hz precision EIFBAGC circuit output
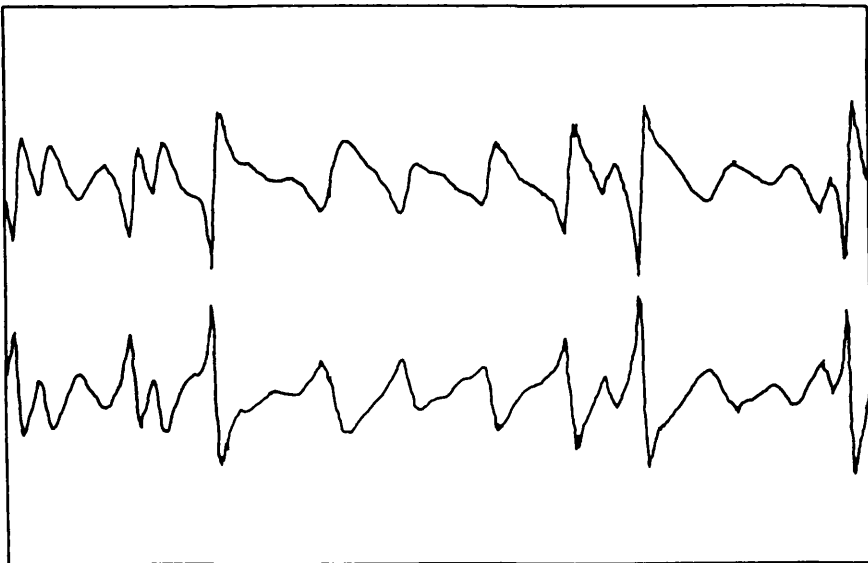
Figure 5.21   30 Hz precision EIFBAGC circuit output

5.51
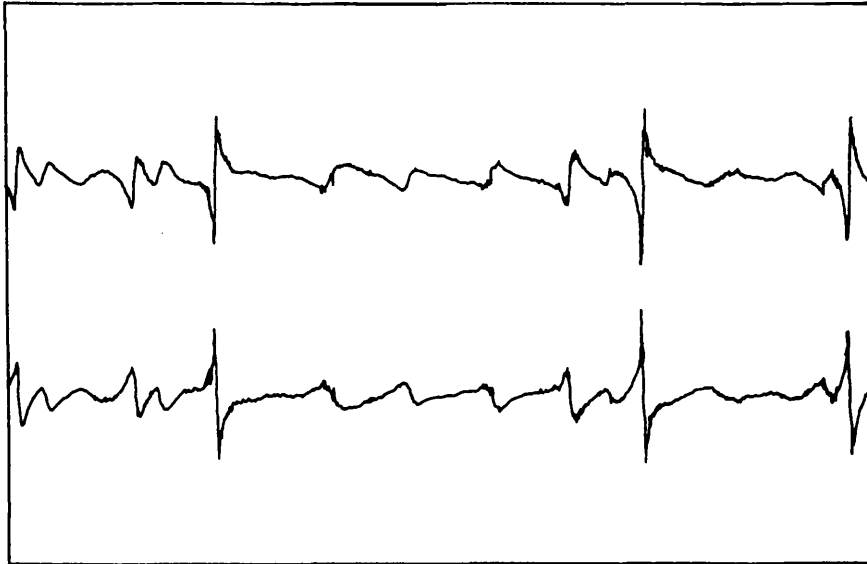
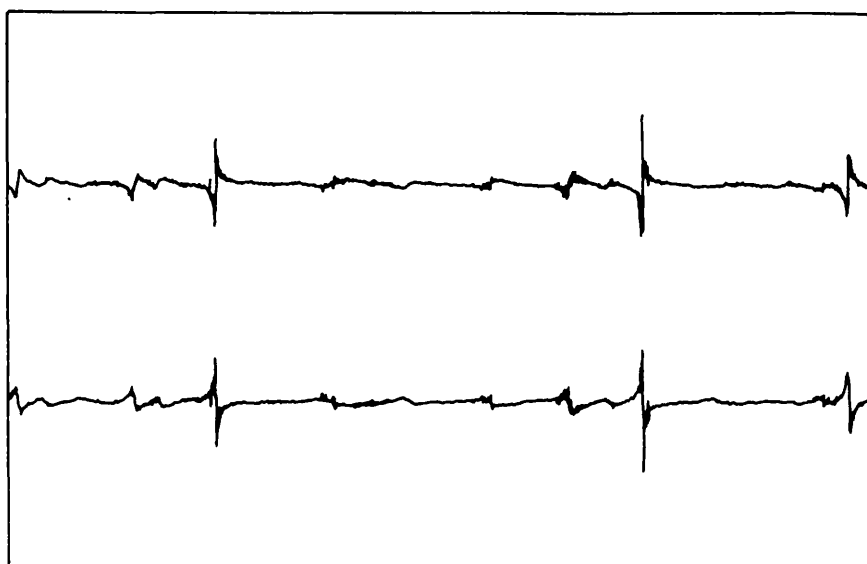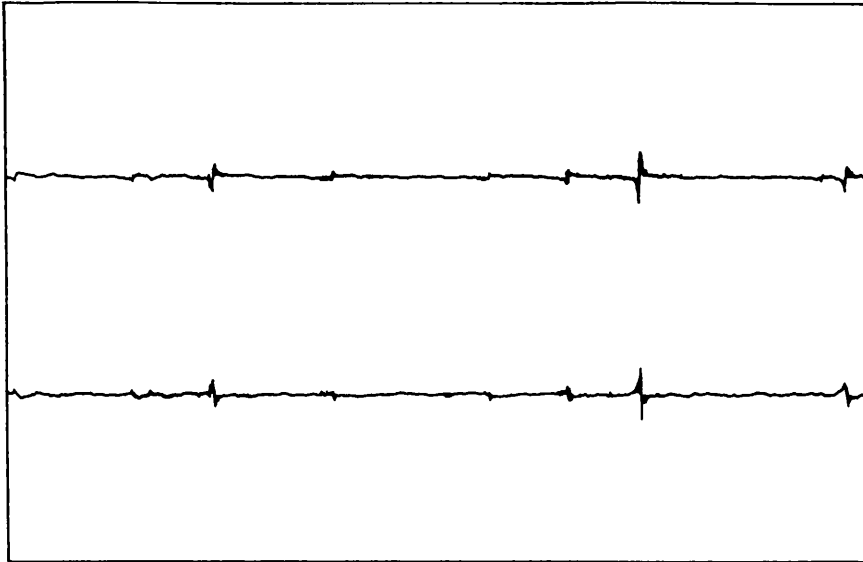Figure 5.22   100 Hz precision EIFBAGC circuit output

---

Figure 5.23   300 Hz precision EIFBAGC circuit output

Figure 5.24 1 kHz precision EIFBAGC circuit output

5.5.3 Comparison with Twin Path Predictions

Section 3.4.3 proposed that an AGC system will suppress multipath fading more than the equivalent worst-case twin path fade at $2\omega_d$ with the same peak to trough ratio. This hypothesis can be simply tested for the aforementioned test run. The largest input variation is from position markers W to X and is 37 dB. The worst case prediction can be extrapolated from the curves of figure 5.12, assuming a twin path fade rate of 42 Hz. The results are shown in table 5.2.

Table 5.2   Worst-case twin path prediction of output ripple, fade VWX

EIFBAGC bandwidth (Hz)	Worst-case twin path output ripple prediction (dB)	Measured output ripple (dB)
10	37	30
30	31	25
100	27	18
300	17	10
1K	8	4.5

As expected, in all cases the twin path signal at $2\omega_d$ predicts more output ripple than was measured with the multipath field trial data.

One general observation of the input waveform in figure 5.17 is that while there are envelope variations occurring at rates up to $2\omega_d$ (e.g. position markers T to U correspond to a fade rate of 38.5 Hz), the deeper fades occur more slowly. It is interesting to compare the output ripple predictions of a best fit twin path fade to the multipath case. This has been performed for fade JKL. The best fit twin path fade is assumed to be 30 dB peak to trough at 12.3 Hz (the same peak

5.54

to peak time as the multipath fade). The results are shown in Table 5.3.

Table 5.3   Best-fit twin path prediction of output
ripple fade JKL

EIFBAGC bandwidth (Hz)	Best-fit twin path output ripple prediction (dB)	Measured output ripple (dB)
10	27	25
30	20	20
100	11	12
300	5	7.5
1K	1.8	2.2

The best-fit twin path output ripple prediction is seen to give a good estimate of the measured output ripple.

5.5.4   Implications for System Design

Consideration of the EIFBAGC circuit's response to the aforementioned and other field trial data has resulted in the following system design implications:

1)   The bandwidth of the EIFBAGC circuit should be much greater than $2\omega_d$ for good fade suppression, the exact bandwidth required depending on the system specification.

2)   The twin path (2 tone) deterministic AGC test signal 2, fading at a rate $2\omega_d$, allows worst-case estimation of the EIFBAGC circuit's response for various depths of input fade.

3) The best-fit twin path signal allows estimation of the EIFBAGC system's response to particular multipath fades.

4) In a 457 MHz land mobile full carrier AM system, the EIFBAGC bandwidth required to give good fade suppression (300-1 kHz) is far in excess of the maximum bandwidth that can be allowed for reasons of speech distortion (typically 30 Hz).

The first question that arises is since it has been shown that fast fading at 457 MHz cannot be suppressed by EIFBAGC systems with reasonable bandwidths, what bandwidth should the system designer use? A lower bound on the bandwidth can be inferred by reference to section 2.1.4. It was stated there that the minimum requirement of a receiver's AGC system capable of suppressing slow fading is that it should average out the received signal's envelope over travelled distances of about 10 wavelengths. Certainly, the normalising process is automatically performed by the division action inherent in the EIFBAGC system. It will be assumed here that the maximum time constant of the EIFBAGC system should be less than the time taken to travel 10 wavelengths to approximate the averaging operation. This gives:

$$T_c \leqslant \frac{10 \lambda_c}{S} \qquad\qquad 5.43$$

where T_c is the closed loop EIFBAGC time constant, λ_c is the carrier wavelength and S is the maximum mobile's speed. For example, at 112 km/hr (70 mph) at 457 MHz, $T_c \leqslant 0.21$ second, i.e. the EIFBAGC bandwidth should be greater than 0.75 Hz. Such an EIFBAGC system should, ideally, only leave the fast fading superimposed on the output.

5.56

CHAPTER 6

FEEDBACK AGC WITH TIME DELAY

This chapter is concerned with the effect of pure, distributed time delay on the dynamics of EIFBAGC in the absence of noise. It deals primarily with the deterioration in the ability of EIFBAGC to suppress unwanted envelope variations. The previous chapter presented an exact feedforward model of EIFBAGC that was independent of input variations. This chapter presents an approximate feedforward model of EIFBAGC with time delay whose parameters are a function of the input variation.

6.1 Causes of Time Delay

In this section the common sources of time delay in receiver FBAGC systems are discussed. The elements actually affecting the dynamics of FBAGC are filter poles and zeros. The filters will later be shown to be adequately approximated by pure time delay, which results in considerable mathematical simplification.

6.1.1 Forward Path Filtering

In any radio receiver it takes a finite time for the signal information to pass along the forward path from antenna input to demodulated output. The time delay is primarily caused by the most selective filter in the forward path, such as the channel IF filter in a conventional superhet receiver (4.3) or the lowpass filter in a direct conversion receiver (6.1). The selective filter usually has a non-linear time delay (group delay) and amplitude response with frequency. However, this filter is invariably

followed by some variable gain amplifiers (VGA). If the receiver's EIFBAGC

system is designed so that the VGA following the most selective filter

predominates the overall gain control law, then the selective filter will

have a negligible effect on the closed loop dynamics. Nevertheless, the

analysis presented later in this chapter takes into account any time

delay introduced by forward path filtering.

6.1.2 Control Path Smoothing Filters

It has been suggested that a FBAGC circuit should incorporate a low

pass "smoothing" filter directly after the envelope detector, in addition

to the main loop filter (5.1, 5.4, 5.5, 5.7, 5.11, 5.14). Typically, a

first order filter is used for smoothing. A pure time delay representation

of a first order lowpass filter is valid up to about half its -3 dB bandwidth.

At this frequency its phase response is -0.46 radians and its amplitude

response -0.96 dB. An equivalent amount of pure time delay (equal to the

reciprocal of the lowpass filter's -3 dB bandwidth) would have a phase

response of -0.5 radians and be 0 dB down at half the lowpass filters

-3 dB bandwidth. Therefore, providing the envelope detector smoothing

filter's bandwidth is greater than about twice the theoretical EIFBAGC

bandwidth, the pure time delay approximation is good below $\omega_N = 1$.

The previous section showed that the receiver's EIFBAGC configuration

can be designed so that forward path filters do not introduce time delay

into the circuit. Smoothing filters (if required) can be designed to

have a very high relative bandwidth. Because of this, full carrier AM

receivers can be operated with an EIFBAGC system that is almost unaffected

by time delay effects. The previous chapter therefore adequately covers

the performance of the EIFBAGC circuitry used in full carrier AM receivers.

It will now be shown that, unfortunately, this is not the case for pilot

SSB systems which will generally always suffer from time delay problems.

6.1.3 Pilot Extraction in SSB Receivers

As mentioned in chapter 1, there are 4 basic pilot SSB systems,

differing only by the position of the pilot in the audio band. The

problem with these systems is that the pilot is transmitted some

7-20 dB below peak speech power. Therefore, unlike a full carrier AM

system, it is necessary to enhance the level of the pilot with respect

to the modulation prior to envelope detection. Alternatively, coherent

detection can be used. This is discussed in the next chapter. Here,

a simpler method of extracting the pilot's envelope is discussed, i.e.

bandpass filtering followed by precision rectification (1.8, 5.5).

The design of the bandpass filter is a compromise between 2

conflicting requirements. If its bandwidth is too wide, excessive

speech energy will be let through resulting in excessive compression

and modulation, as described in section 5.4.3. If it is too narrow, it

will possess a large group delay resulting in poor EIFBAGC dynamics.

Another question arises; is it better to use high order, but wide

bandpass filters or lower order, but narrower bandpass filters to

achieve the same speech rejection? Gardner's (4.3) comments on IF

filters in PLL receivers appear to apply here where he suggests it is

better to use as low an order filter as is possible to minimise the

group delay. This approach has been adopted by pilot SSB designers

(1.8, 5.5) who use a single complex-conjugate-pole-pair (first order)

bandpass filter.

The transfer function of this first order bandpass filter and the associated magnitude, phase and group delay equations have been conveniently analysed elsewhere (6.2). For a reasonably high Q (> 5 say) bandpass filter, the group delay at the centre is approximately twice the inverse of the bandwidth in radians per second. The group delay is approximately half this value at the band edges (6.3).

6.1.4 Other Causes of Time Delay

Other causes of time delay are usually negligible compared to the effects of pilot extraction in SSB receivers. However, they can affect the closed loop dynamics if care is not taken. Some of the other causes are:

1) Additional RC filtering. Some receiver FBAGC control lines possess 1 or more additional RC filters as well as the main loop filter and (possibly) envelope detector output smoothing filters. There is usually no reason to incorporate these unless they are used to greatly increase the response time of a VGA gain control line, allowing another VGA to control the FBAGC dynamics.

2) Higher order loops. As stated earlier, the problem with EIFBAGC is its large transition region. There is a temptation to deliberately increase the order of the loop, say to second order, in an attempt to reduce the width of the transition region (2.10). However, this may result in a degradation rather than improvement in the loop dynamics. This is because increasing the loop's order is very similar to the effect of adding pure time delay. Other workers have indicated that the first order loop is the optimum FBAGC loop. Victor and Brockman (5.6)

use Weiner optimisation methods to show that the closed-loop transfer function that minimises the noise induced gain jitter while holding the transient error to a specified value is first order. Banta (5.2) has analysed some unbounded transients that can arise as a result of using second order loops and concludes that a first order loop allows best FBAGC action. Finally, Oliver (5.1) has suggested that only first order loops do not suffer from "modulation enhancement" i.e. only first order loops possess the property of unconditional suppression.

3) Processing delays. Most of the work reported in this thesis uses conventional analogue techniques to implement the various circuit elements around an EIFBAGC control loop. However, with the increasing use of digital signal processing devices, it is only a matter of time before some elements such as the envelope detector, summing junction, integrator etc. are implemented in software. Care will need to be taken to prevent the inherent additional processing time delays from affecting the closed loop dynamics.

6.2   Effect of Loop Dynamics

This section discusses the effects of time delay on the dynamics of EIFBAGC systems (6.4).

6.2.1   General Loop Equation

The block diagram of the circuit to be analysed is shown in figure 6.1. This shows an EIFBAGC circuit with pure time delay elements inserted in between each element to represent any of the effects mentioned in section 6.1. Working counter-clockwise around the loop from $v_g(t)$ gives:

6.5
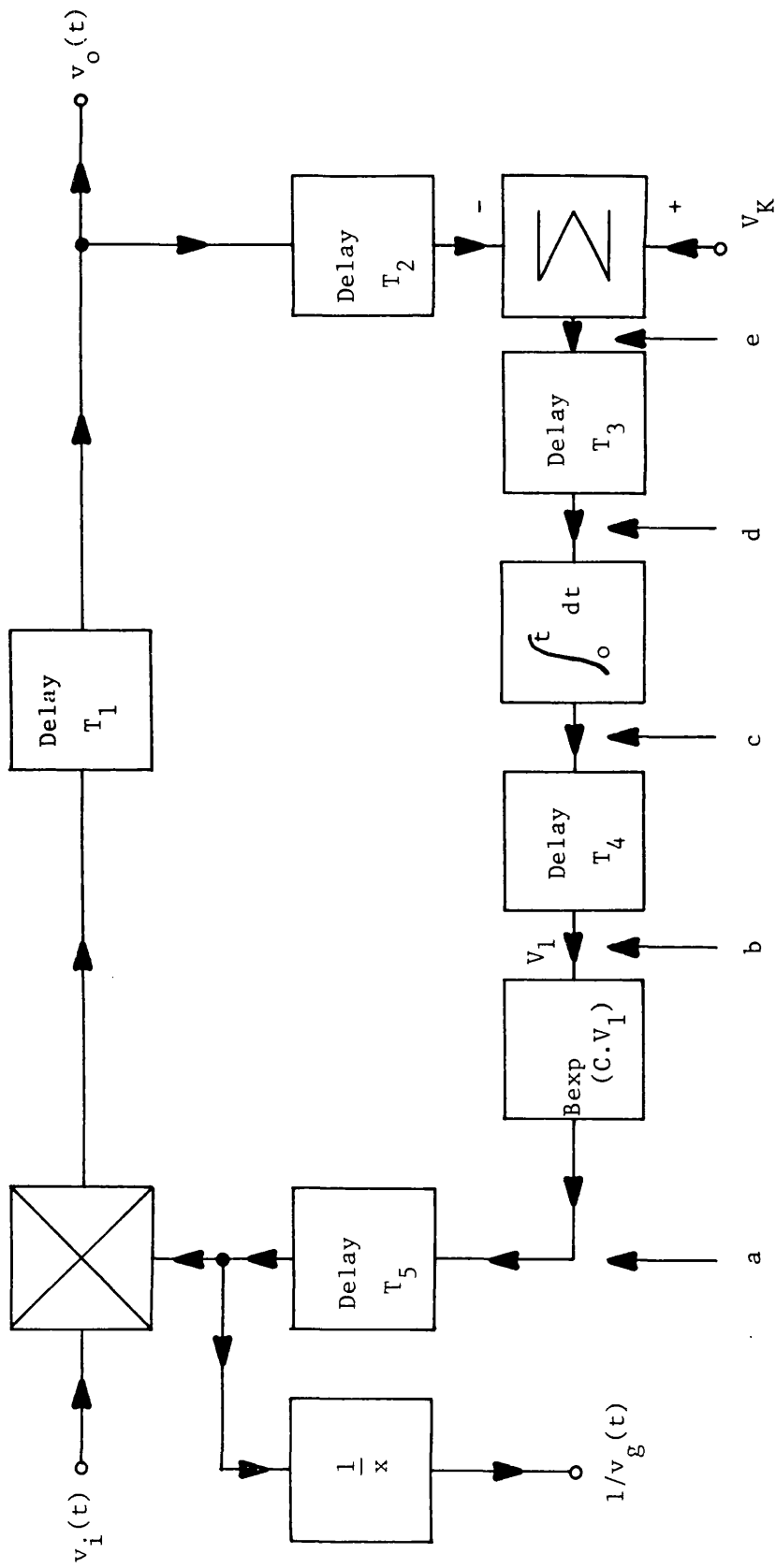
Figure 6.1 Exponential-integrator FBAGC incorporating distributed time delay

$$v_a = [v_g(t)]t \to t + T_5 \qquad (6.1)$$

$$v_b = \{\ln\{[v_g(t)]t \to t + T_5/B\}\}/C \qquad (6.2)$$

$$v_c = [\{\ln\{v_g(t)/B\}\}/C]t \to t + T_4 + T_5 \qquad (6.3)$$

$$v_d = \frac{d}{dt}\{[\{\ln\{v_g(t)/B\}\}/C]t \to t + T_4 + T_5\} \qquad (6.4)$$

$$\text{and} \quad v_e = \left[\frac{d}{dt}\{\ln\{v_g(t)/B\}\}/C\right]t \to t + T_3 + T_4 + T_5 \qquad (6.5)$$

Working clockwise from the output of the multiplier:

$$v_o(t) = [v_i(t)\, v_g(t)]t \to t - T_1 \qquad (6.6)$$

$$\text{and} \quad v_e = V_K - [v_i(t)\, v_g(t)]t \to t - T_1 - T_2 \qquad (6.7)$$

Equating equations 6.5 and 6.7 and simplifying results in the general loop equation:

$$\frac{d}{dt}\{\{\ln\{v_g(t)/B\}\}/C\} - V_K + [v_i(t)\, v_g(t)]t \to t - T = 0 \qquad (6.8)$$

$$\text{where} \quad T = \sum_{n=1}^{5} T_n \qquad (6.9)$$

Equation 6.8 is the general non-linear delay differential equation describing the dynamics. Note that the effect of any time delay is independent of its position around the loop.

6.2.2 DC and Fundamental Solution

Chapter 5 solved equation 6.8 exactly for T = 0. It showed that although the voltages around an EIFBAGC loop are non-linearly related to the input, $1/v_g(t)$ is simply a first order lowpass filtered version of $v_i(t)$. However, with time delay present $1/v_g(t)$ is no longer linearly

related to the input over all frequencies. A sinusoidal variation of $v_i(t)$ has been found experimentally to result in $1/v_g(t)$ consisting of:

i)   A lowpass filtered version of $v_i(t)$, the amplitude and phase of which are not first order and are predominantly a function of loop gain, time delay and frequency.

ii) Harmonics of $v_i(t)$, whose amplitudes are mainly functions of loop gain, time delay, input modulation depth and frequency.

iii) A dc shift that varies with loop gain, time delay, input modulation depth and frequency.

iv) Under certain conditions, subharmonics of the input.

In general, the fundamental component and dc shift predominate at $1/v_g(t)$. The harmonics and subharmonics are significant only when there is both a relatively large time delay and large input variation. The solution to equation 6.8 presented here uses a forced solution to $1/v_g(t)$ consisting simply of a filtered version of the input with an additional dc shift. This situation is represented by the feedforward model shown in figure 6.2. However, unlike the solution without time delay present, the model is only valid for sinusoidal input modulation. Nevertheless, it provides a valuable insight into the operation of EIFBAGC with time delay and helps explain the experimentally observed phenomena described later.

The input to the circuit is assumed to be of the standard form for AGC test signal 1:
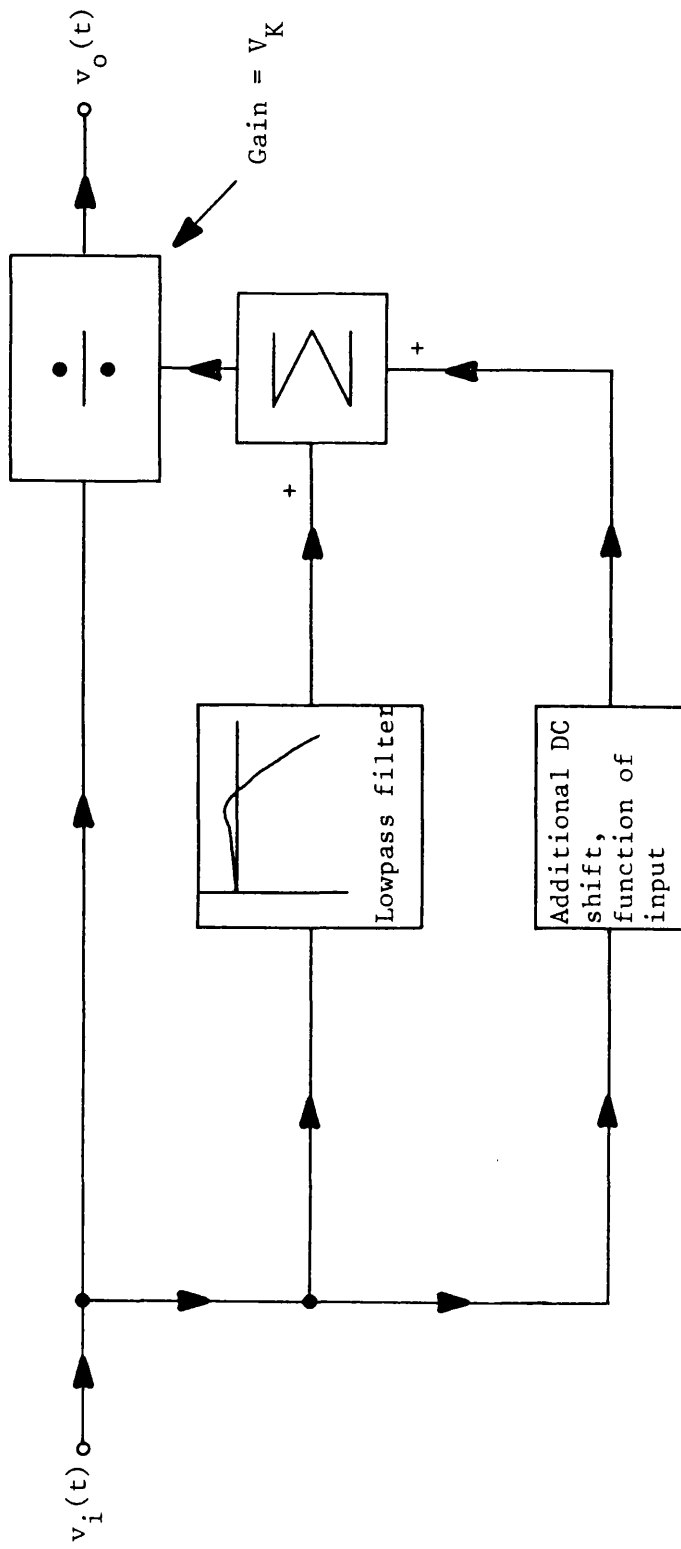
Figure 6.2   Feedforward approximate representation of EIFBAGC with time delay

6.9

$$v_i(t) = E(1 + D \sin \omega_s t) \qquad (6.10)$$

In response to this input, the approximate solution assumes a steady state voltage at $v_g(t)$ of:

$$v_g(t) = \frac{V_K}{E(A + LD \sin(\omega_s t - \theta))} \qquad (6.11)$$

where L is the loops amplitude response at ω_s, θ its phase response and A its dc shift. Note that A represents the total dc shift, so the dc shift path shown in the bottom of the feedforward model is (A-1).

Substitution of $v_i(t)$ and $v_g(t)$ from equations 6.10 and 6.11 into 6.8 and simplifying gives:

$$- \frac{LD \, \omega_s \cos(\omega_s t - \theta)}{C(A + LD \sin(\omega_s t - \theta))} - V_K + \frac{V_K(1 + D \sin(\omega_s t - \omega_s T))}{(A + LD \sin(\omega_s t - \omega_s T - \theta))} \approx 0$$

$$(6.12)$$

The solution of the fundamental and dc terms of equation 6.12 is lengthy and described in Appendix 7. The appendix presents the results as three simultaneous equations:

$$L = \frac{1}{(1 + \omega_N^2 + ((A-1) \div A)^2 - 2\omega_N \sin(\phi\omega_N) + 2((A-1) \div A) \cos(\phi\omega_N))^{\frac{1}{2}}} \qquad (6.13)$$

$$\theta = \tan^{-1} \left[\frac{\omega_N \cos(\phi\omega_N) + ((A-1) \div A)\sin(\phi\omega_N)}{1 - \omega_N \sin(\phi\omega_N) + ((A-1) \div A)\cos(\phi\omega_N)} \right] + N\pi \qquad (6.14)$$

$$A = 0.5 + 0.5\sqrt{1 + 2(L^2 D^2 \, \omega_N \sin(\phi\omega_N) - L^2 D^2 \cos(\phi\omega_N) + LD^2 \cos(\theta - \phi\omega_N)}$$

$$(6.15)$$

where

$$\phi = CV_K T \quad \text{radians} \qquad (6.16)$$

$$\omega_N = \frac{\omega_s}{CV_K} \qquad (6.17)$$

where N is an integer required for the correct solution of θ when the principal value of $\tan^{-1}$ is used. It should be noted that ϕ is the product of loop gain (i.e. loop bandwidth without time delay) and time delay. This is effectively a normalised phase shift due to time delay and will be called the loops "delay phase". Similarly, ω_N is a normalised frequency as in EIFBAGC without time delay.

Equations 6.13, 6.14 and 6.15 are unusable as they stand since they are all interrelated. Specifically, they indicate that not only is A, but L and θ are functions of the input. However, experimental observations have shown that the dependence of L and θ on A, and hence the input, is weak. For a good approximation and considerable simplification, A = 1 can be substituted into equations 6.13 and 6.14. This gives:

$$L' = \frac{1}{(1 + \omega_N^2 - 2\omega_N \sin(\phi\omega_N))^{\frac{1}{2}}} \qquad (6.18)$$

and

$$\theta' = \tan^{-1}\left[\frac{\omega_N \cos(\phi\omega_N)}{1 - \omega_N \sin(\phi\omega_N)}\right] + N\pi \qquad (6.19)$$

The value of A from equation 6.15, L' from equation 6.18 and θ' from equation 6.19 will be used throughout the rest of this chapter to describe the feedforward model.

6.2.3 Feedforward Model Characteristics

In practice, an EIFBAGC circuit with a delay phase equal to or greater than $\pi/2$ is found to be unstable. A delay phase of $\pi/2$ results in the lowpass filter's amplitude response in the feedforward model being infinite at $\omega_N = 1$. However, sub-harmonic generation has been observed for delay phases as low as $\pi/4$. Since this effect is not taken into

6.11

account by the feedforward model, the feedforward model's use will be restricted to values of delay phase where $\phi < \pi/4$.

The lowpass filter's amplitude frequency response has been plotted from equation 6.18 for 4 values of delay phase in figure 6.3. The general effect of time delay is to cause the amplitude response to exceed the delayless case over most frequencies. It is interesting to calculate the value of delay phase that causes the amplitude response to just exceed unity at some frequency. From equation 6.18

$$1 = \frac{1}{1 + \omega_N^2 - 2\omega_N \sin(\phi\omega_N)} \tag{6.20}$$

therefore:

$$\omega_N = 2 \sin(\phi\omega_N) \tag{6.21}$$

The value $\omega_N = 0$ and any value of ϕ is 1 solution to this equation. However, consider the case where $\omega_N \ll 1$ but not zero so that $\sin \phi\omega_N \simeq \omega_N$ then:

$$\omega_N = 2\phi\omega_N \tag{6.22}$$

so that $\phi = 0.5$. It is found also from plotting L' that for values of delay phase above 0.5, the amplitude response will exceed unity over some range of frequencies.

The lowpass filter's phase frequency response has been plotted from equation 6.19 for 4 values of delay phase in figure 6.4. When the phase is π (180°), the EIFBAGC circuit is dividing by the peak when the input is at its trough and vice-versa. In other words, the circuit is increasing the peak to trough ratio and not suppressing the fading.
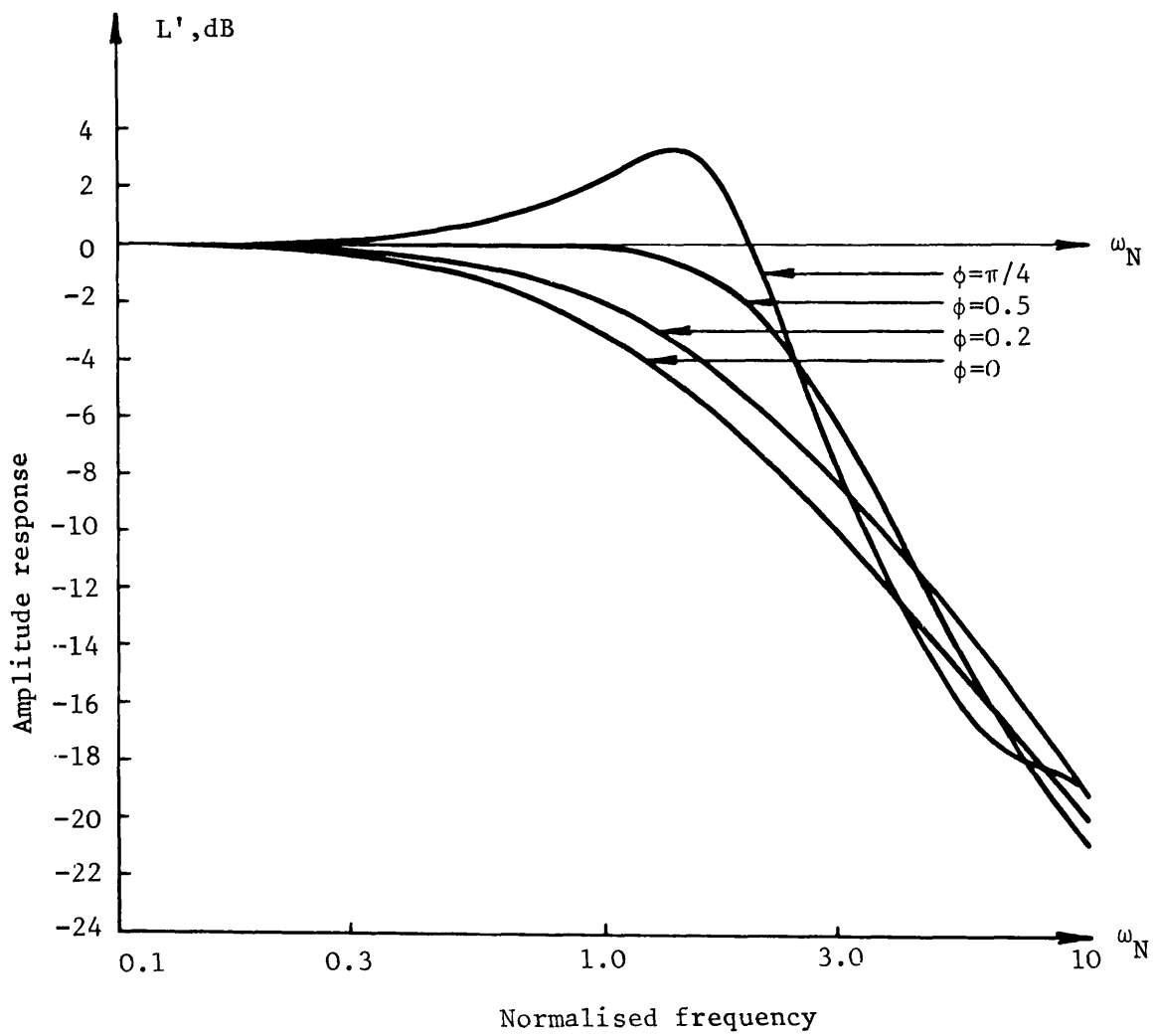
Figure 6.3   Amplitude response of EIFBAGC with time delay when
dc shift, A, equals unity
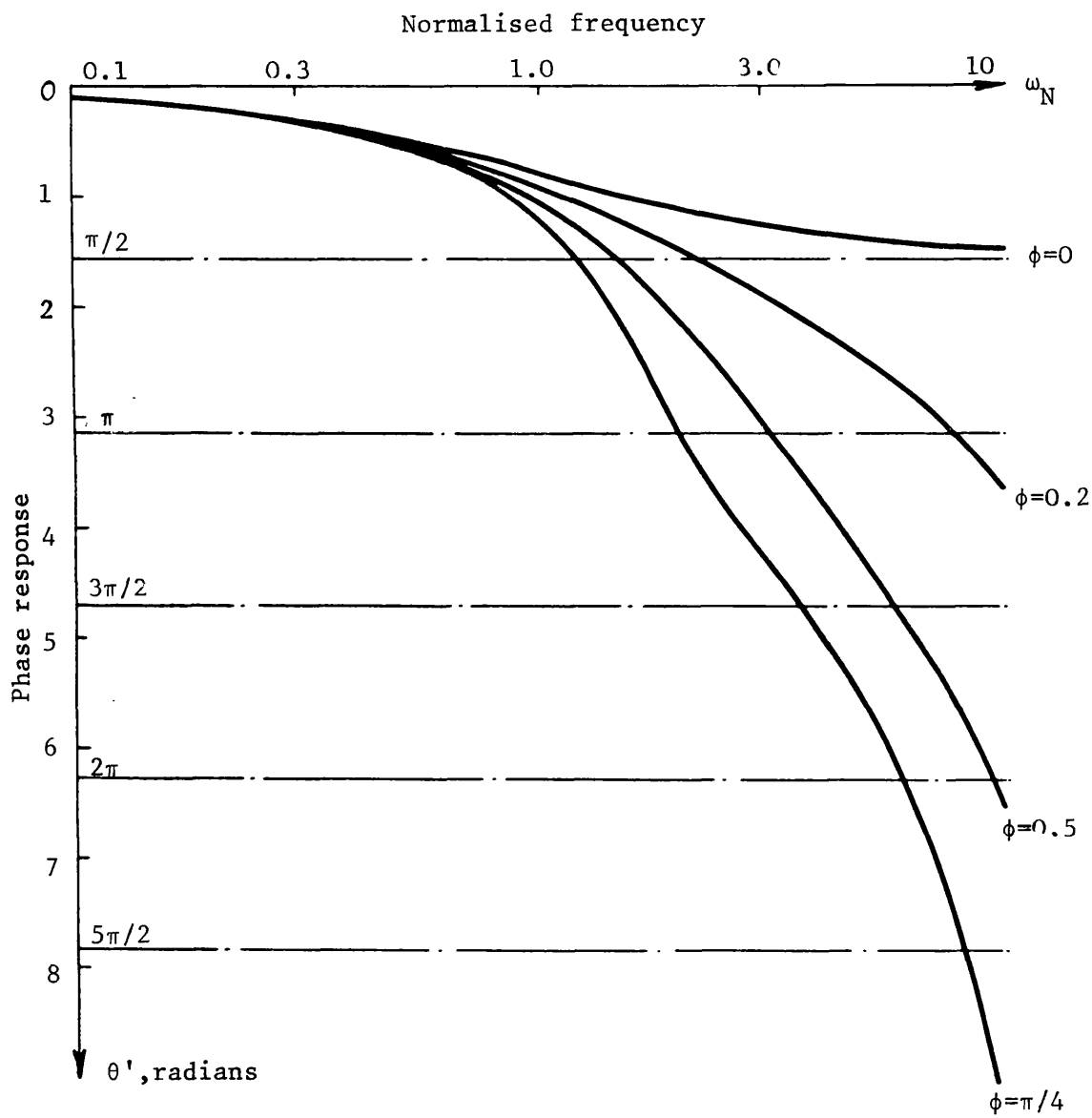
Figure 6.4 Phase response of EIFBAGC with time delay when dc shift, A, equals unity

6.14

When the phase is 2π (360°) the circuit's gain control voltage is exactly 1 cycle behind the input variation.

The dc shift, A, is plotted in figure 6.5 from equation 6.15 for D = 1. The dc shift, although relatively small, is a very significant factor when predicting output variations. For example, consider the significance of $\phi > 0.5$ so that the amplitude response exceeds unity over some range of frequencies. Without time delay, an EIFBAGC circuit will attempt to divide by zero and overload if:

$$LD > 1 \qquad\qquad (6.23)$$

which obviously never occurs for D < 1. However, according to equations 6.18 and 6.23 this will occur for some D < 1 if $\phi > 0.5$ so that the product LD is greater than 1. Nevertheless, the dc shift acts so as to prevent division by zero and EIFBAGC with time delay will not overload provided that:

$$\frac{L'D}{A} < 1 \qquad\qquad (6.24)$$

For real input envelope variations where D < 1, the ratio L'/A is always observed to be less than 1 and the loop does not overload if $\phi > 0.5$.

This may be considered using a different approach. If the circuit did overload and (in theory) divide by zero, the average value of the output envelope would be infinite. However, one experimental observation is that EIFBAGC always maintains the average value of the output signal's envelope at the value V_K, up to and including the point where the circuit is just unstable and oscillating. Since this is the case, the circuit does not divide by zero. In other words, as well as preventing overloading

6.15
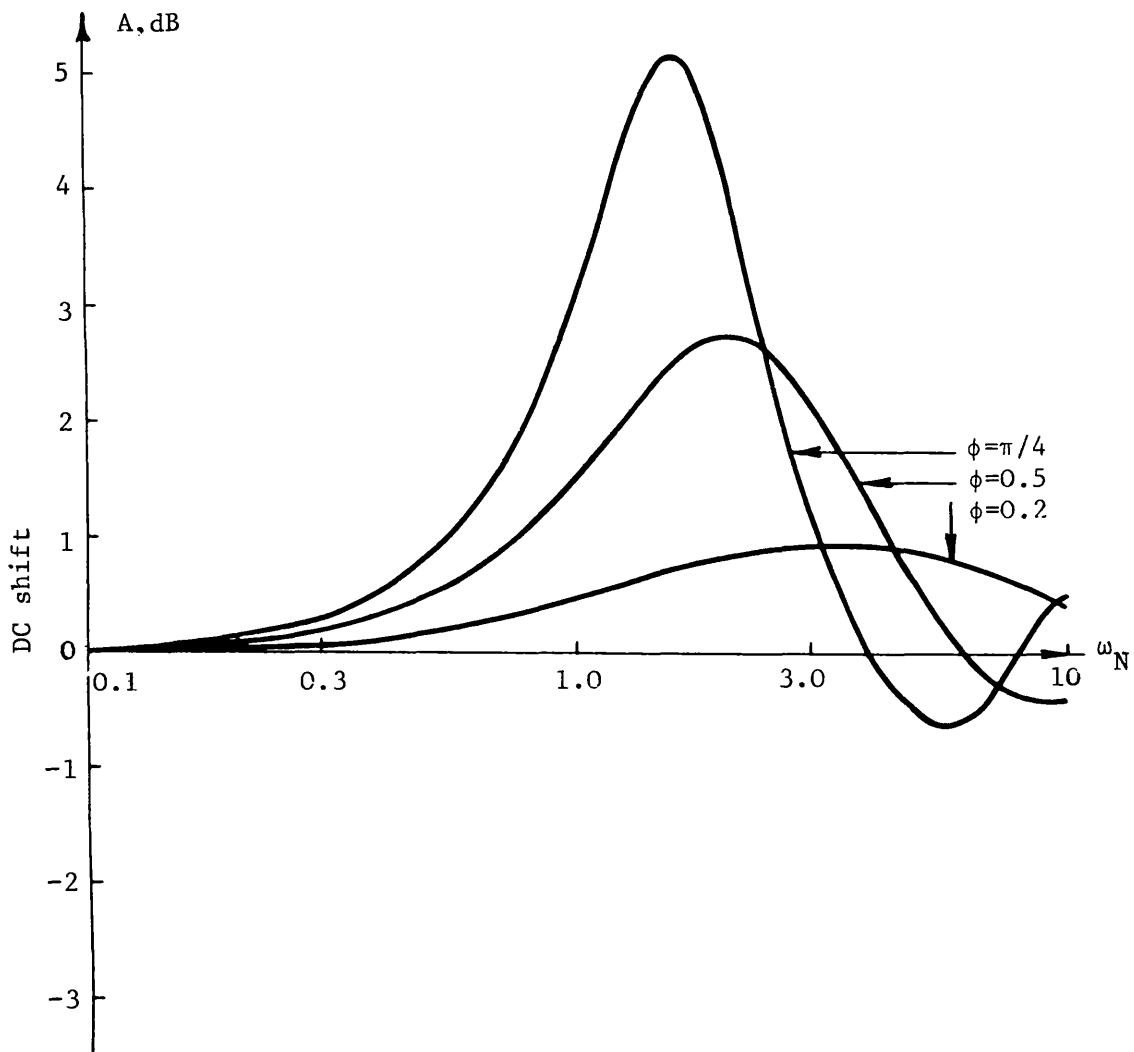
Figure 6.5   Variation of dc shift of EIFBAGC with time delay
for 100% input modulation

the dc shift maintains the average value of the output envelope constant.

It is evident from the preceding discussion that due to the excessive phase shift of the control voltage, EIFBAGC with time delay suffers from modulation enhancement. That is, for some values of D and ω_N it will increase rather than suppress envelope variations. In other words, time delay results in EIFBAGC failing to meet requirement 3 (unconditional suppression). This is discussed in more detail in the next section.

6.3 Response to Sinusoidal Modulation

This section discusses the response of EIFBAGC with time delay to sinusoidal input modulation, i.e. deterministic AGC test signal 1. It concentrates on the case where sinusoidal modulation represents some unwanted input signal variation and analyses the deterioration of the ability of EIFBAGC with time delay to suppress it.

6.3.1 Output Ripple

The input to the circuit is $r_1(t)$ where:

$$r_1(t) = E(1 + D \sin \omega_N t) \qquad (6.25)$$

where $0 < D < 1$ and ω_N is the normalised frequency. The steady state output of the circuit is given from the feedforward model by:

$$v_0(t) = V_K \left[\frac{1 + D \sin \omega_N t}{A + L'D \sin(\omega_N t - \theta')} \right] \qquad (6.26)$$

This equation is rewritten as:

$$v_0(t) = V_K/A \left[\frac{1 + D \sin \omega_N t}{1 + (L'/A)D \sin(\omega_N t - \theta')} \right] \qquad (6.27)$$

6.17

This equation is very similar to equation 5.25. The peak to trough ratio of equation 6.27 can be written down directly by substituting (L'/A) for L in the general solution for K_0 (5.20). This gives:

$$K_0 = \frac{1 - \left(\frac{L'}{A}\right) D^2 \cos\theta + D\sqrt{\left(\frac{L'}{A}\right)^2 D^2 \cos^2\theta + \left(\frac{L'}{A}\right)^2 + 1 - 2\left(\frac{L'}{A}\right)\cos\theta - \left(\frac{L'}{A}\right)^2 D^2}}{1 - \left(\frac{L'}{A}\right) D^2 \cos\theta - D\sqrt{\left(\frac{L'}{A}\right)^2 D^2 \cos^2\theta + \left(\frac{L'}{A}\right)^2 + 1 - 2\left(\frac{L'}{A}\right)\cos\theta - \left(\frac{L'}{A}\right)^2 D^2}}$$

$$(6.28)$$

Figure 6.6 is a plot of K_0 (dB) for various values of ϕ, ω_N and D. This graph confirms the most important characteristic of the effect of time delay on the performance of EIFBAGC with time delay. It shows that there exists a range of frequency over which the circuit increases the input variation rather than suppressing it. It is very interesting to analyse the relationship between the amplitude, phase and dc shift that causes this modulation enhancement.

The requirement for unconditional suppression (discussed in section 5.1.3) to exist in a feedforward model when subject to sinusoidal input variations, $r_1(t)$, may be written mathematically as:

$$K_0 < \frac{1 + D}{1 - D} \qquad (6.29)$$

Equation 6.28 for K_0 can be seen to be of the form:

$$K_0 = \frac{x + Dy}{x - Dy} \qquad (6.30)$$

where x and y may be obtained by inspection of equation 6.28. K_0 can therefore be rewritten as:

$$K_0 = \frac{1 + D\left(\frac{x}{y}\right)}{1 - D\left(\frac{y}{x}\right)} \qquad (6.31)$$

6.18
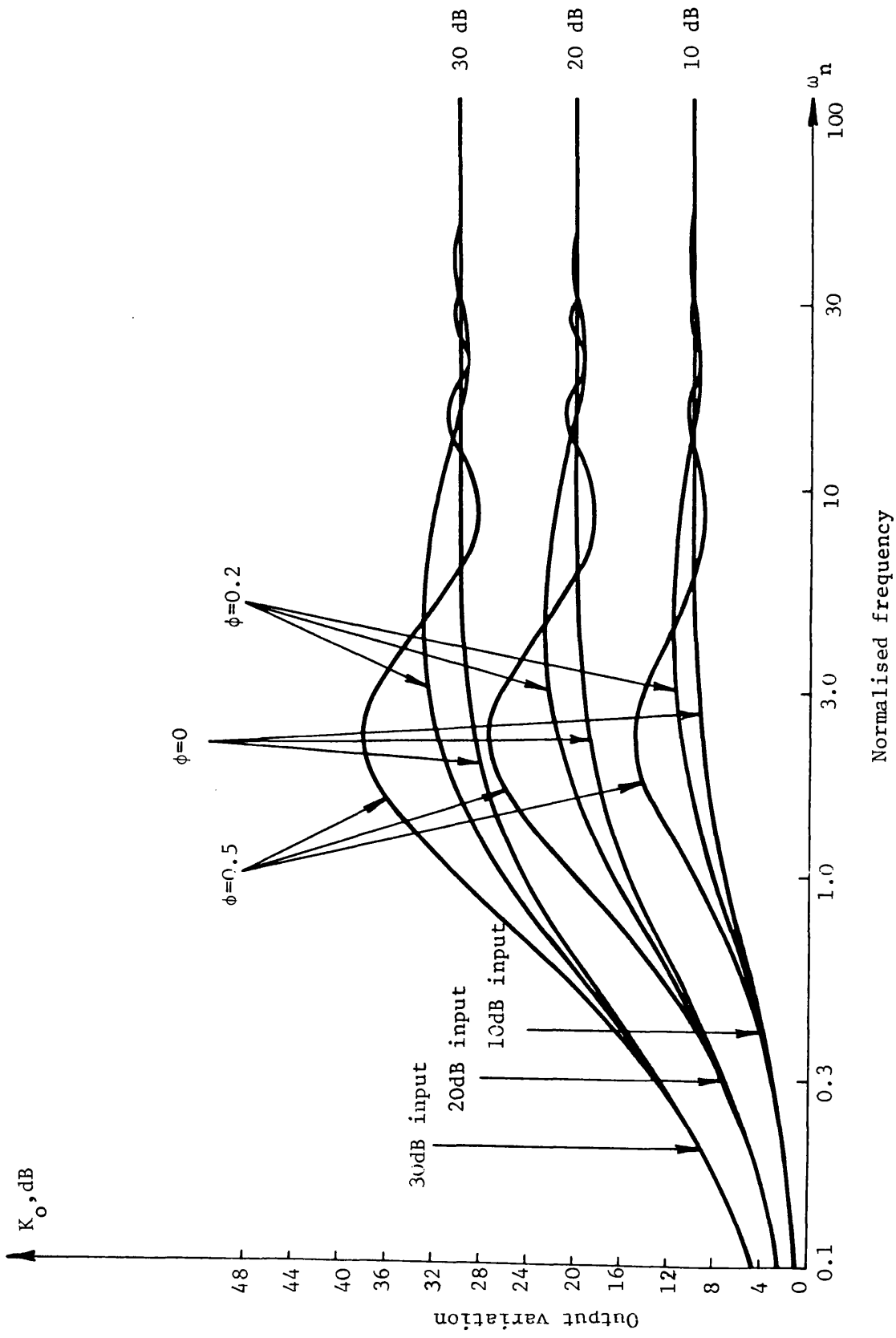
Figure 6.6 Output variation of EIFBAGC with time delay

The requirement for unconditional suppression may be written from equations 6.29 and 6.31 as:

$$\frac{1 + D \left(\frac{y}{x}\right)}{1 - D \left(\frac{y}{x}\right)} < \frac{1 + D}{1 - D} \qquad (6.32)$$

The requirement for unconditional suppression is therefore inferred to be:

$$\frac{y}{x} < 1 \qquad (6.33)$$

Equation 6.33 is analysed in Appendix 8. This shows that the requirement for unconditional suppression is:

$$\frac{L'}{A} < \frac{2 \cos \theta'}{1 + D^2 \cos^2 \theta'} \qquad (6.34)$$

The left hand side of this equation is always positive. However, the right hand side can be negative and unconditional suppression therefore does not occur for some values of $\theta > \pi/2$. Unconditional suppression only occurs in systems where the phase response never exceeds $\pi/2$. This is why second and higher order EIFBAGC systems should not be used if possible. For example, an EIFBAGC system with a deliberately designed second order response will have a phase response that tends to π for $\omega_N \gg 1$. Furthermore, the phase response of EIFBAGC with time delay exceeds $\pi/2$ for a high enough ω_N however small the time delay is. Therefore, modulation enhancement will occur in any EIFBAGC system with time delay over some range of frequencies. However, these effects can be made insignificant if care is taken, as the next section shows.

Here this analysis finishes by calculating what is the exact amplitude and phase characteristic for modulation enhancement to just not occur. This can be analysed by putting the maximum value of D into

equation 6.34 that equation 6.24 allows for overload to not occur. This
is analysed in Appendix 8 and gives the relationship as:

$$\frac{L'}{A} \leqslant \cos \theta' \qquad (6.35)$$

The amplitude and phase of a first order lowpass filter are related by:

$$L = \cos \theta \qquad (6.36)$$

From this it can be concluded that unconditional suppression only occurs
in first order systems for sinusoidal input modulation.

6.3.2 Modulation Enhancement Peaks

This section is concerned with the magnitude and frequency of the
worst modulation enhancement peak in figure 6.6. For a fixed delay phase
the frequency of maximum modulation enhancement, called ω_m, varies only
slightly with D. For example, with a delay phase of 0.5 radians the
frequency varies from $\omega_N = 2.28$ for 10 dB input variations to $\omega_N = 2.26$
for 30 dB input variations. Figure 6.7 is a plot of ω_N versus delay
phase for 30 dB input variations. ω_m is approximately the inverse of the
delay phase, therefore the non-normalised frequency of maximum modulation
enhancement occurs approximately at the inverse of the time delay. For
example 1 krs^{-1} with T = 1 ms.

The overshoot at ω_m, termed "excess K_0" is defined by:

"excess K_0" $= \{K_0(dB) - K_i(dB)\}$ at ω_m $\qquad (6.37)$

This is illustrated in figure 6.8 for various amounts of delay phase and
input modulation. The overshoot is not proportional to the input
modulation depth and tends to a constant value for larger input
modulations.
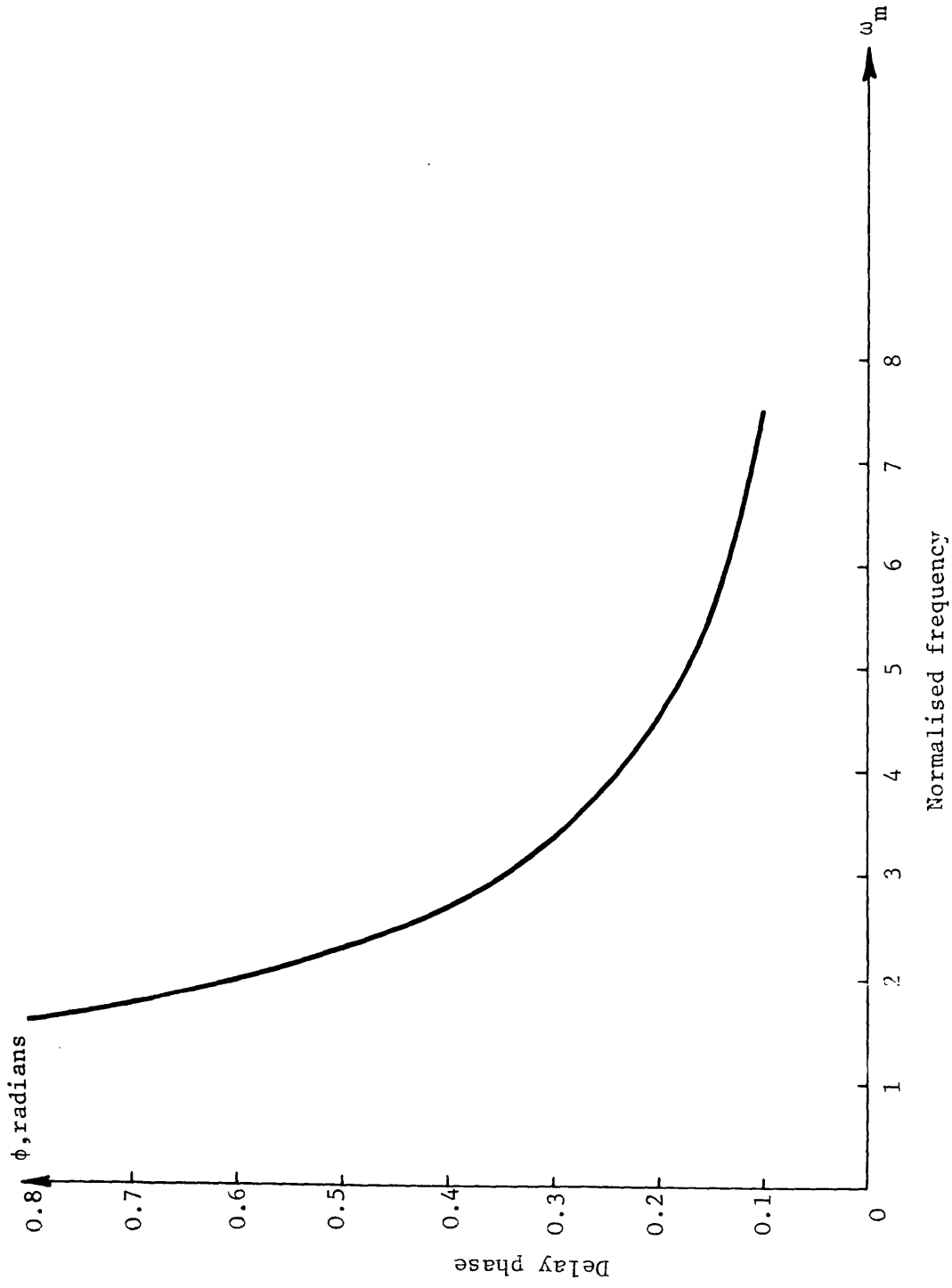
Figure 6.7 Frequency of maximum modulation enhancement versus delay phase

6.22
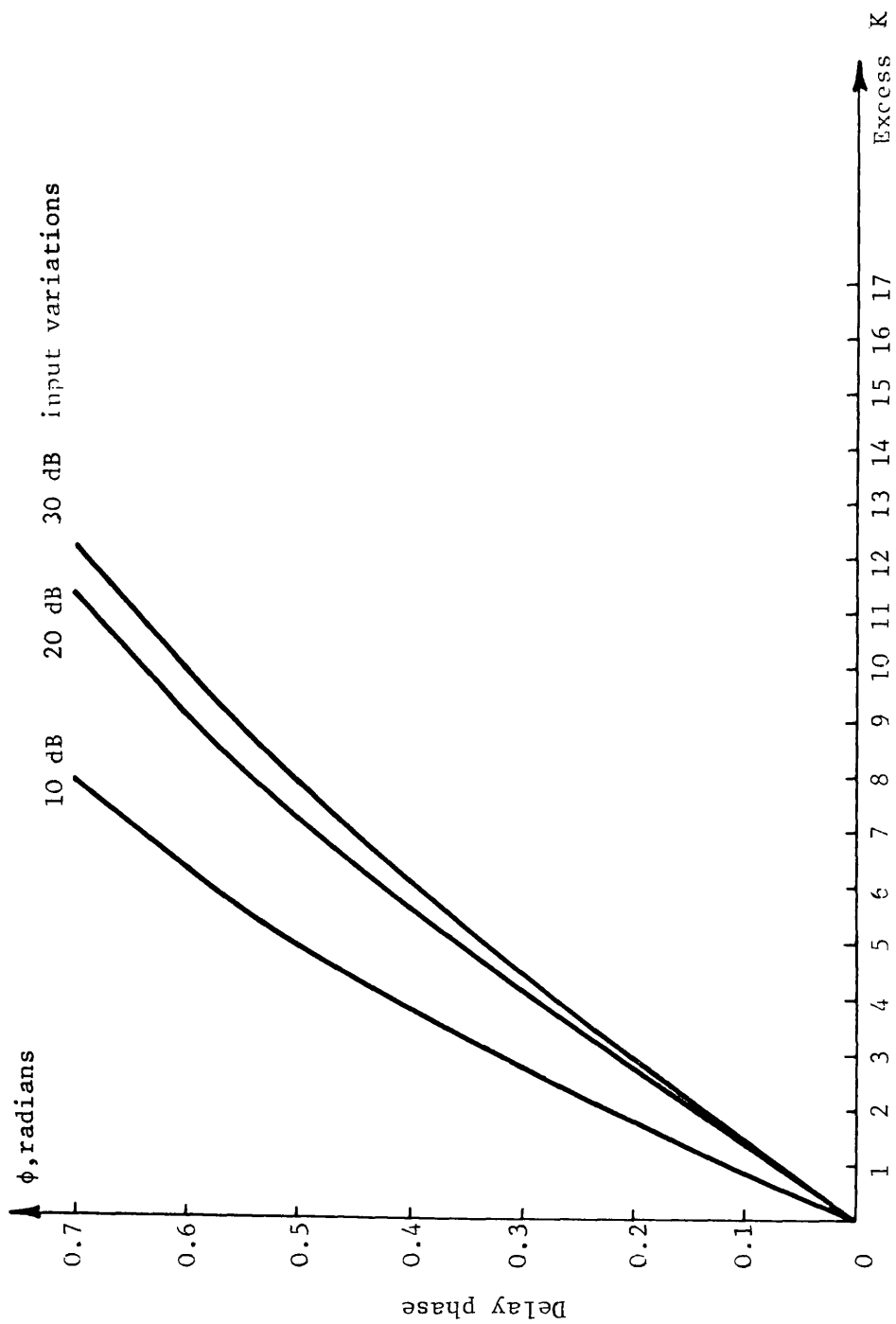
Figure 6.8 Excess K at ω_m versus delay phase

6.3.3 Experimental Observations

The experiments used the precision EIFBAGC circuit described in section 5.2.6 and a time delay unit inserted where T_2 is shown in figure 6.1. The time delay unit was based around a CCD delay line, the SAD512D. The time delay through this device is given by:

Time Delay = 512 ÷ Applied Clock Frequency

A 4.096 MHz master crystal oscillator was used in conjunction with a variable divider to give a highly accurate (better than 100 ppm) time delay that could be varied in 0.125 mS steps from 0.25 mS to 64 mS. The time delay unit was dc coupled so that additional time delay due to any ac coupling elements was not incurred. A single pole lowpass filter was used to smooth the output, and the associated pole's time delay taken into account in the experiment.

The preliminary set of experiments verified the "small signal" sinusoidal response of the circuit, i.e. L' and θ'. With 6 dB of input modulation, the amplitude and phase response of the loop at $1/v_g$ was measured from ω_N = 0.1 to 10 for delay phases of 0.78, 0.49, 0.19 and 0 radians. The EIFBAGC was operated using a 30 Hz closed loop bandwidth, a typical value for pilot SSB receivers. The amplitude response, L', agreed with the theoretical curves of figure 6.3 to within 0.5 dB worst case for all delay phases up to and including 0.49 radians. With a delay phase of 0.78 radians the loops amplitude response peaked 1.2 dB higher than predicted (at ω_N = 1.4). This error is attributed in part to the measuring technique used as the harmonics at $1/v_g$, although low, also peak around ω_N = 1.4 and are interpreted by the averaging voltmeter as a fundamental component. The small signal phase response of the loop was also in close agreement with the theoretical response. The worst

case deviation from figure 6.4 was less than 0.1 radians over a 8 radian

range with a delay phase of $\pi/4$ radians.

The measurement of the dc shift at $1/v_g$ as a function of frequency

was next performed for various depths of input modulation and a delay

phase of 0.49 radians. It was found in general that equation 6.15 tended

to slightly underestimate the magnitude of the dc shift. For example,

the maximum dc shift for a 30 dB input variation was underestimated by

0.7 dB.

The next set of measurements related to the output ripple, K_0.

The results are shown together with the theoretical predictions from the

feedforward model in figure 6.9. It is apparent that the measured output

variation is slightly greater than predicted by the feedforward model

below ω_m, but in general there is good agreement. Figure 6.10 is a record

of the output waveforms observed during the 30 dB input modulation tests.

The scaling factor on the vertical amplitude axis is the same for all

the graphs to allow relative comparison. The horizontal time axis was

adjusted to fit only 2 or 3 cycles of the output on each plot.

Figure 6.10 shows that up to about ω_N = 0.1, the ability of EIFBAGC

to suppress input variations is hardly impaired by time delay. Between

ω_N = 0.1 and ω_N = 10 the distortion introduced by EIFBAGC worsens with

increasing delay phase. Above ω_N = 10 the output is almost identical

to the input. The harmonics of the input at $1/v_g$ are evident in the

output envelope for the larger time delays, especially at ω_N = 0.3.

Note that ω_m is plotted as ω_N = 0.3 for no time delay (although it is,

in fact, infinite).
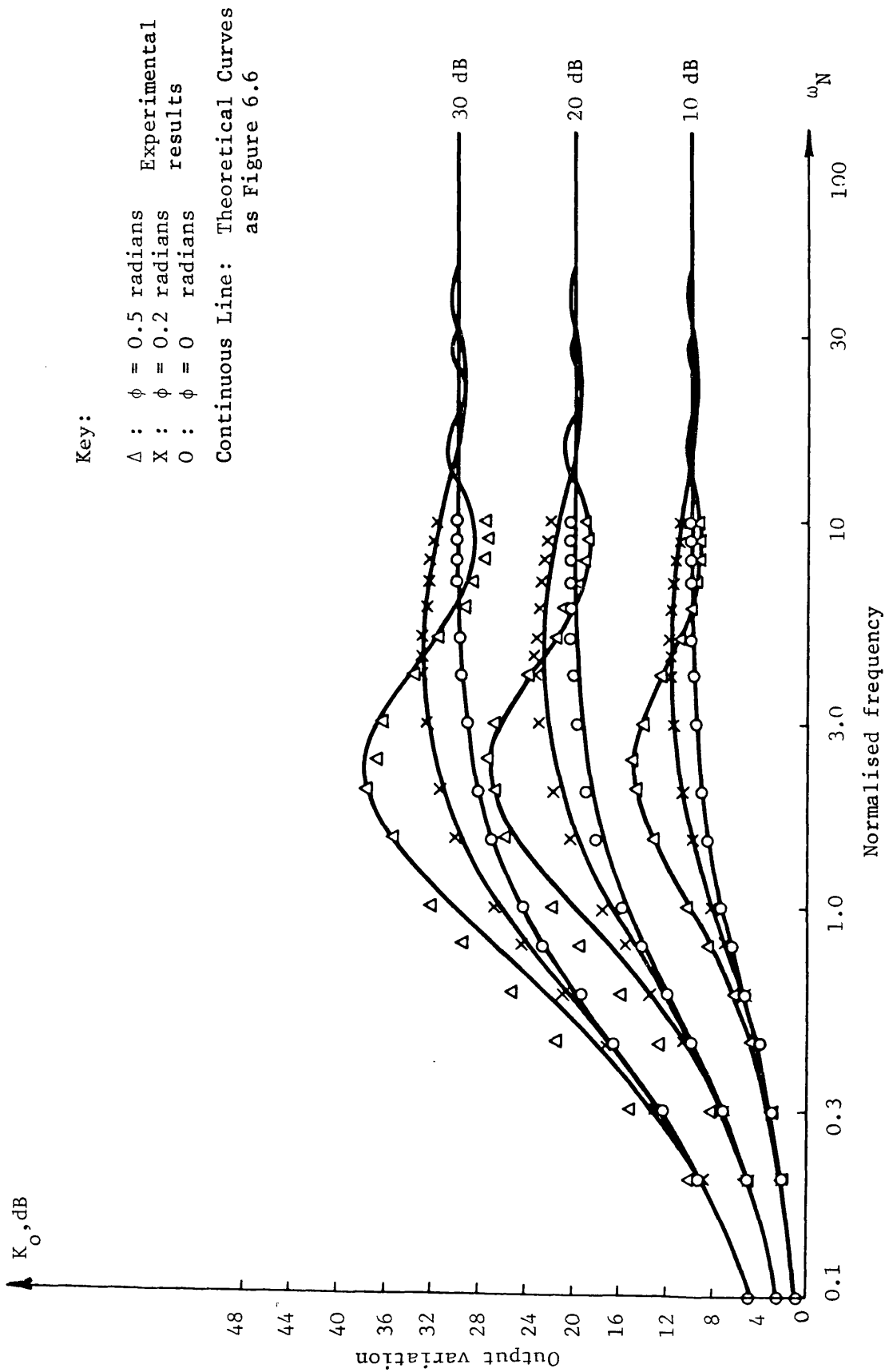
Figure 6.9 Output variation of experimental EIFBAGC circuit with time delay

6.26
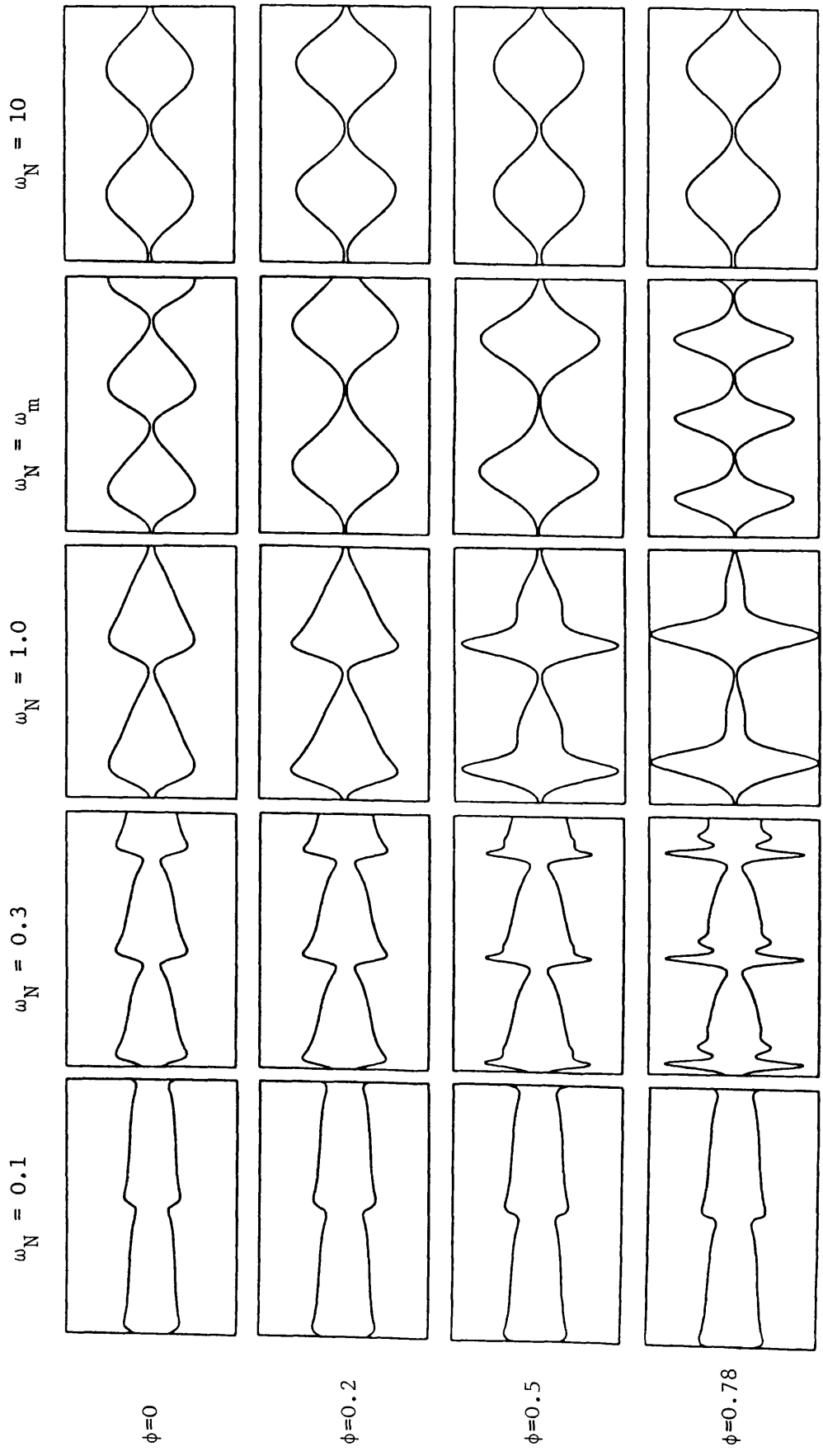
Figure 6.10 Recordings of output of experimental EIFBAGC circuit with time delay. Input excited sinusoidally, 30 dB peak to trough ratio

6.27

6.3.4 Subharmonic Generation

When subharmonics of the input occur at $1/v_g$ during sinusoidal

modulation, the circuit responds differently to successive cycles of the

input. This is shown in figure 6.11. This shows the observed output

waveform with zero delay phase and the observed output waveform with a

delay phase just above the value required for subharmonic generation to

occur. It has not been possible to theoretically analyse the effect

other than to note that subharmonic generation is a property of some

types of nonlinear systems (5.16). However, the following experimental

observations were made:

1) Subharmonics were only generated when the delay phase was

greater than $\pi/4$ radians (half the delay required for instability).

2) With a delay phase just greater than $\pi/4$ radians the loop only

generated the 1/2 harmonic of the input when it was deeply modulated

over a narrow range of frequencies centre on $\omega_N = 2$. At $\omega_N = 2$ with a

delay phase of $\pi/4$ radians the loop's amplitude response goes through

0 dB and the phase response is π radians.

3) Lower subharmonics were only generated for larger delay phases.

4) Subharmonics were only generated when the circuit was excited

periodically at the appropriate frequencies. There was no tendency to

generate subharmonics if the input were modulated by a single cycle of

a sinewave.
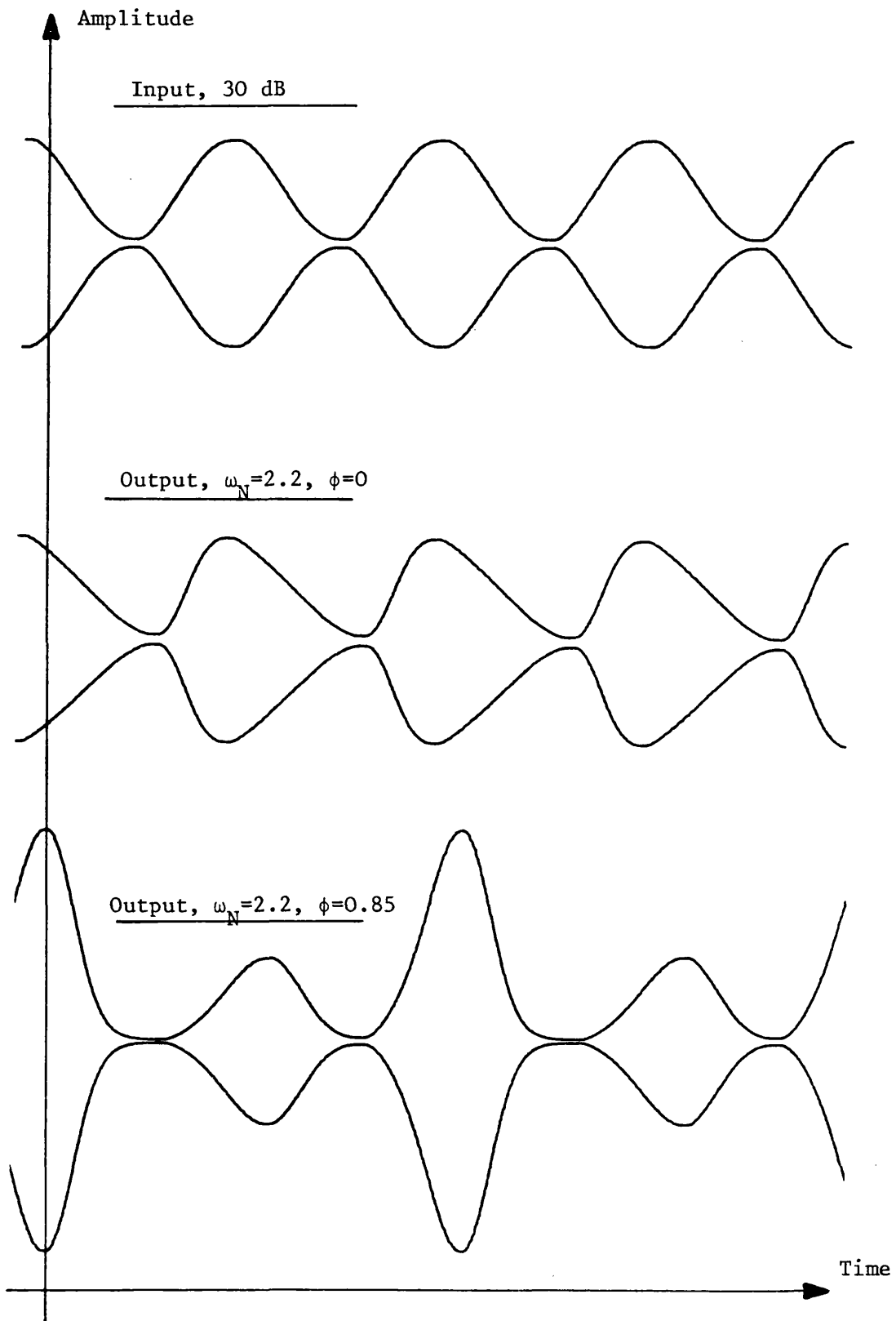
Figure 6.11 Illustration of subharmonic generation due to time delay

6.29

6.4 Response to Two Tones

This section concentrates on the deterioration of the ability of EIFBAGC to suppress 2 tone envelope variations, deterministic AGC test signal 2, due to time delay.

6.4.1 Theoretical Predictions

The input to the circuit is of the form:

$$r_2(t) = E(1 + R^2 + 2R \cos \omega_N t)^{\frac{1}{2}} \qquad (6.38)$$

where, as usual, ω_N is the tone separation frequency normalised to the EIFBAGC bandwidth without time delay, and R is the relative level of the 2 tones. The steady state envelope variations of the circuit's output can be written in general as:

$$v_o(t) = \frac{V_K(1 + R^2 + 2R \cos \omega_N t)^{\frac{1}{2}}}{FX((1 + R^2 + 2R \cos \omega_N t)^{\frac{1}{2}})} \qquad (6.39)$$

where FX represents the circuit's operation on the input signal's envelope. From the work in the previous section it would seem reasonable that FX can be approximated by a lowpass filtering operation combined with a dc shift. The lowpass filtering operation is likely to have the same amplitude and phase characteristic given by L' and θ' from equations 6.18 and 6.19 respectively. The problem with FX is analysing both the magnitude of the dc shift and how it fits into the equation. The solution of the dc shift has proved elusive, and because of its importance in predicting the output variation, a direct theoretical analysis has not been possible. Instead, practical measurements of the output ripple are presented in the next section.

6.4.2 Experimental Results

The experimental results were taken using the system described in section 6.3.3 and the 2 tone experimental technique described in section 5.4.4. The results are shown in figure 6.12 for delay phases of 0, 0.2 and 0.5. Once again, the EIFBAGC circuit used a 30 Hz bandwidth. The deterioration of the ability of the EIFBAGC circuit to suppress the envelope variations is apparent below ω_N = 1, the frequency region of interest. Significantly, for none of the practical measurements was the output ripple increased by more than 3 dB when ϕ = 0.2. A similar observation also applied during sinusoidal testing.

6.5 Response to Field Trial Data

This section describes the response of the precision EIFBAGC circuit with time delay to multipath fast fading.

6.5.1 Choice of Time Delay

For these results, the EIFBAGC circuit was subject to the same input waveform described in section 5.5.1. It was decided to operate the EIFBAGC circuit with a fixed amount of time delay and record the output waveform with different loop bandwidths. The question arose as to what would be a representative amount of time delay.

Lusignan (1.9) uses a 300 Hz wide pilot filter for his tone-above-band SSB system. Such a filter would have a maximum group delay of about 1 mS if it were first order, as described in section 6.1.3. However, Lusignan (ibid) states that the pilot filter has a delay of about 3 mS which suggests his pilot filter may be third order. As a consequence of the time delay work at Bath, Ball and Holmes (5.5) use

6.31
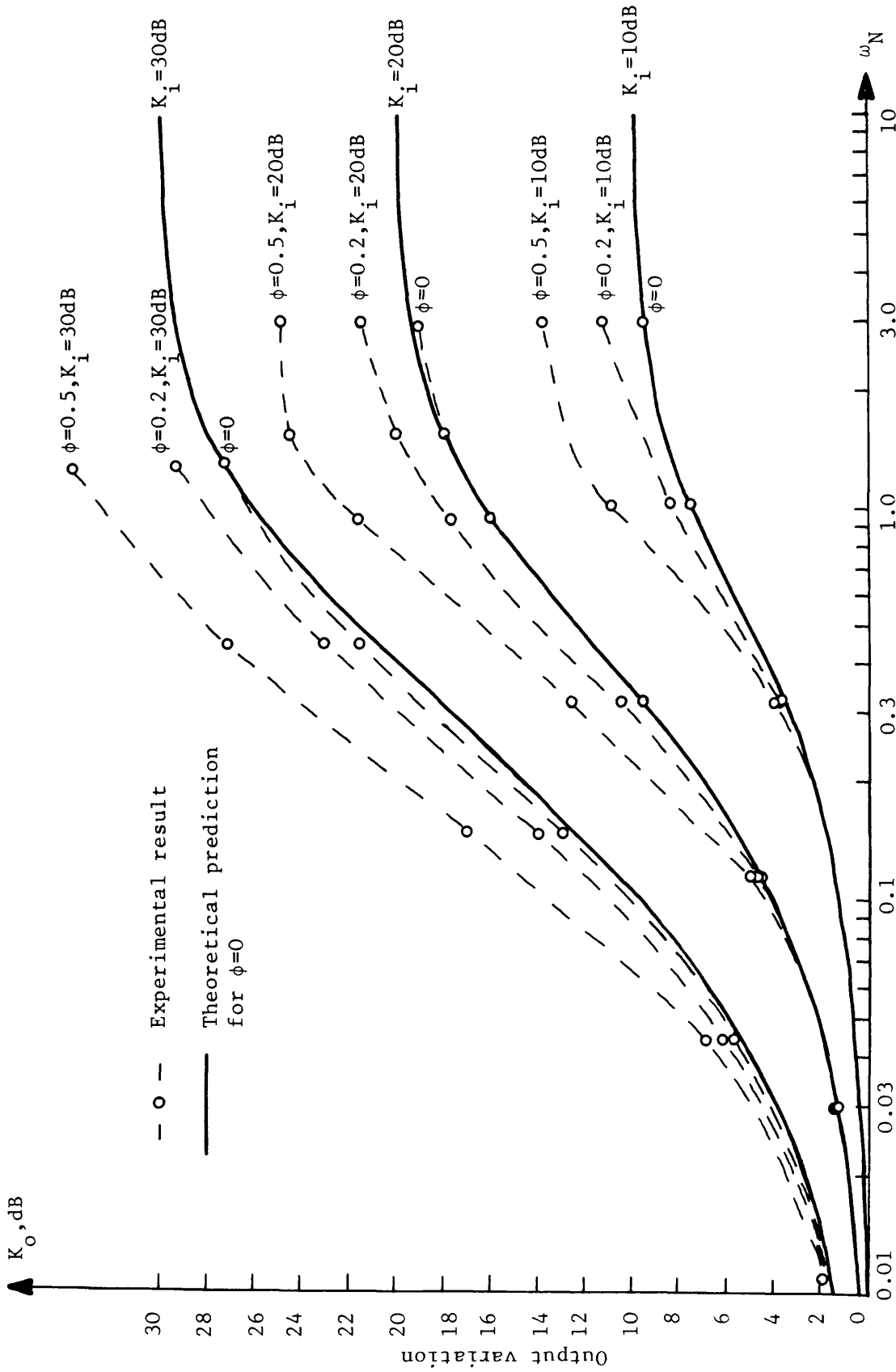
Figure 6.12 Practical measurements of the effect of time delay on the output ripple of the precision EIFBAGC circuit in response to 2 tones.

6.32

a first order pilot filter with a bandwidth of 500 Hz to limit the maximum group delay to about 640 µS in their pilot carrier SSB system. However, they also use an envelope detector smoothing filter that cuts of at 1.5 kHz which will add at least an extra 106 µS of group delay bringing the total time delay to 746 µS. McGeehan et al (1.8) use a 400 Hz bandwidth first order pilot filter with a maximum group delay of about 796 µS in their tone-in-band SSB system. The UHF SSB tone-in-band receiver described in chapter 4 used a pilot filter with a maximum group delay of 1 mS. This is a fairly representative amount of time delay and the results presented in the next section used 1 mS of pure time delay.

6.5.2 Response of Precision EIFBAGC Circuit with Time Delay

The field trial results were obtained using the system described in section 6.3.3 with 1 mS of time delay. For these results, the circuit was subject to the same input signal described in section 5.5.1, which allows direct comparison of these results to those presented in figures 5.18 to 5.24 without time delay. Plots of the output waveforms with time delay are shown in figures 6.13 to 6.18. Note that the vertical gains have been slightly increased to cause the peak input variation to just touch the positive and negative plot limits on the 1 Hz EIFBAGC output, figure 6.13.

The 1 Hz and 3 Hz EIFBAGC circuits are hardly affected by time delay, as shown by comparing figures 5.18 and 5.19 with 6.13 and 6.14. The 10 Hz circuit, figure 6.15, is only slightly affected by time delay which causes a very slight increase in the "sharpness" of the leading edge compared to figure 5.20 without time delay. However, the effect

6.33
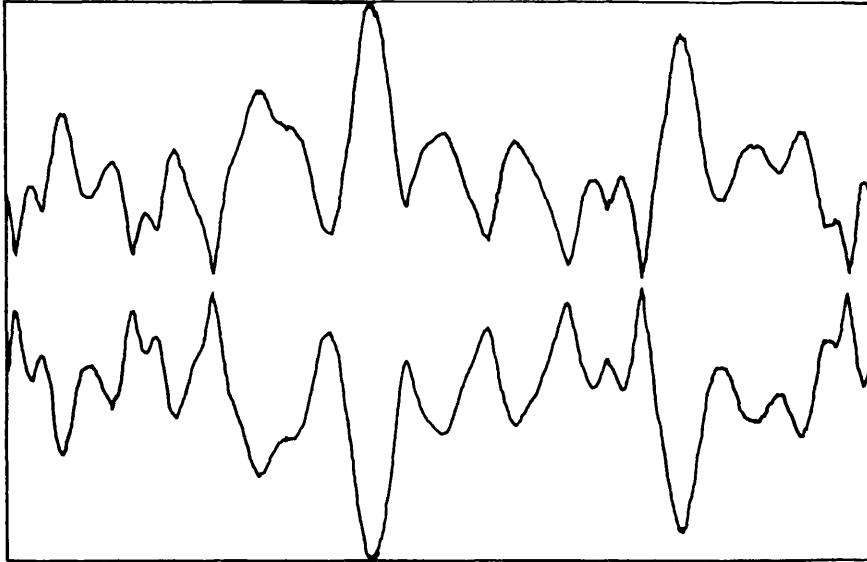
Figure 6.13   1 Hz EIFBAGC output, T = 1 mS, ϕ = 0.0063 radians

---
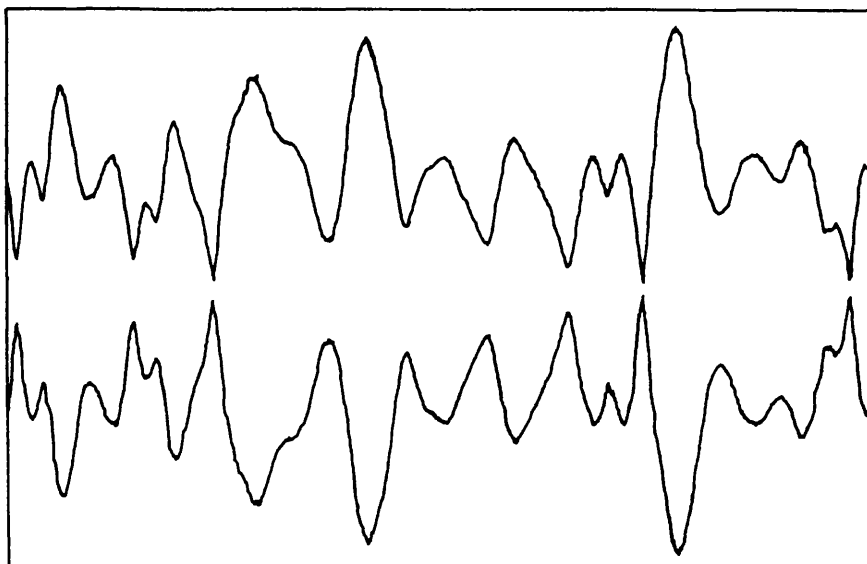
Figure 6.14   3 Hz EIFBAGC output, T = 1 mS, ϕ = 0.0188 radians
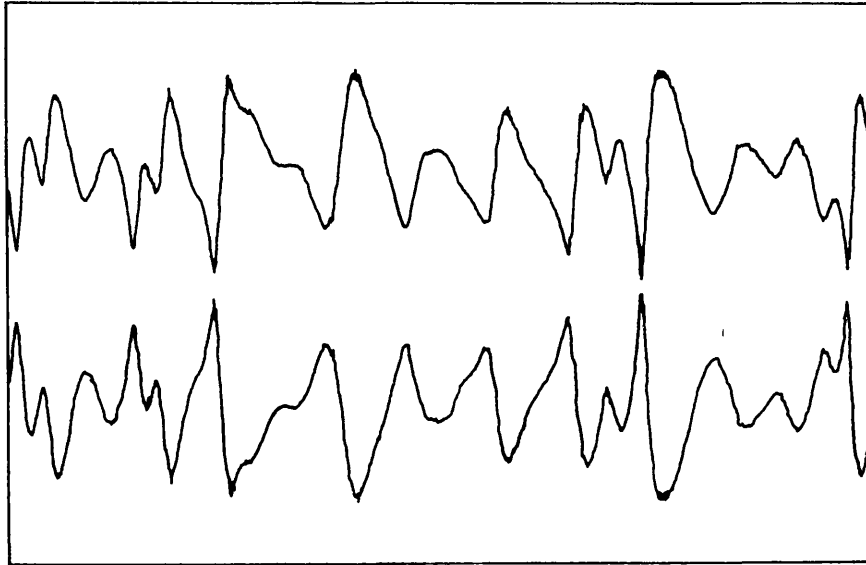
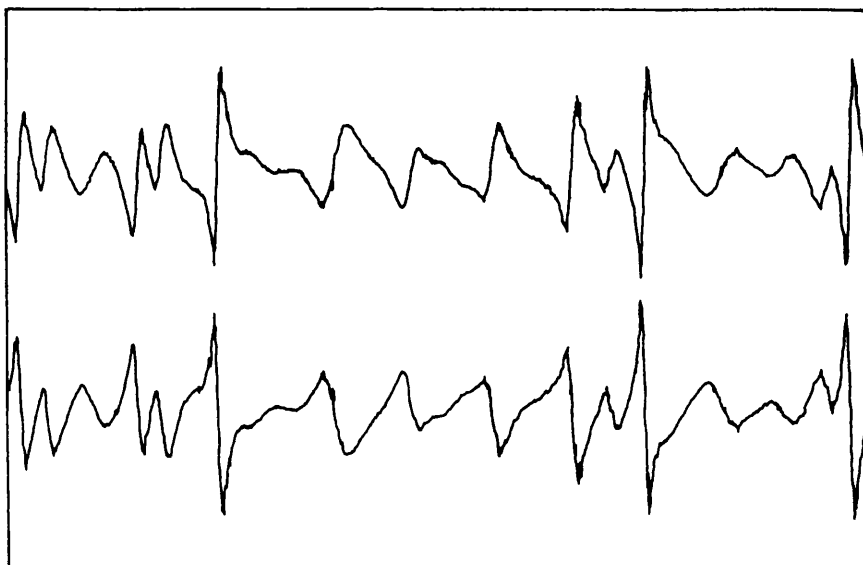Figure 6.15 10 Hz EIFBAGC output, T = 1 mS, ϕ = 0.063 radians

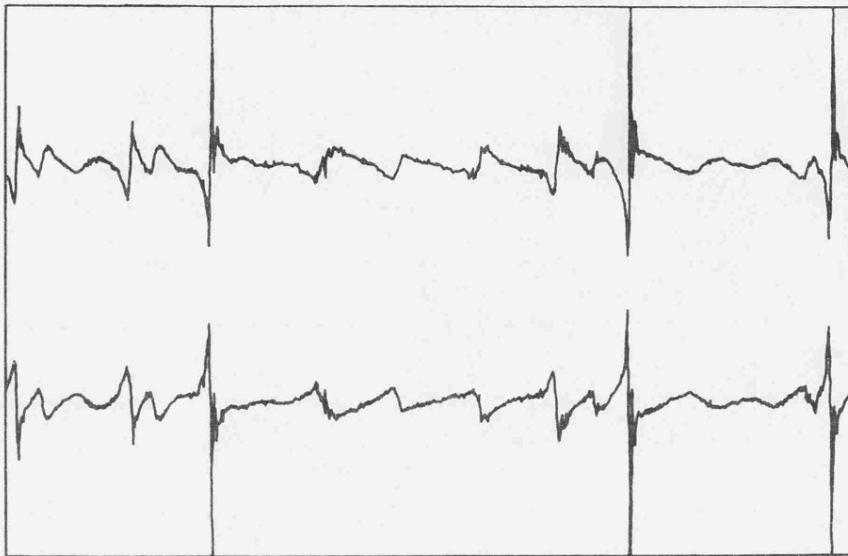Figure 6.16 30 Hz EIFBAGC output, T = 1 mS, ϕ = 0.188 radians

Figure 6.17   100 Hz EIFBAGC output, T = 1 mS, ϕ = 0.628 radians
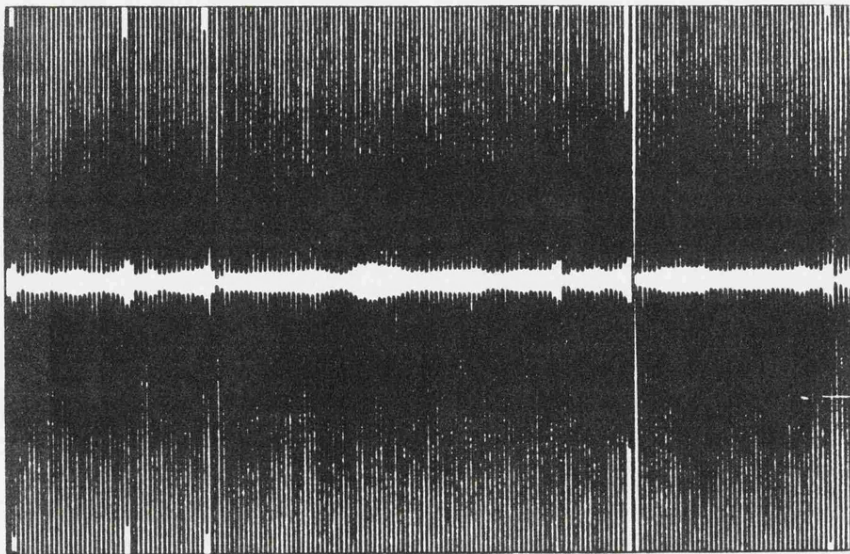

Figure 6.18   300 Hz EIFBAGC output, T = 1 mS, ϕ = 1.88 radians

of time delay causes a significant deterioration in the 30 Hz circuit's

output, figure 6.16, compared to figure 5.21 without time delay. The

most noticeable effect of time delay is the increase in the peak directly

after a deep fade. This effect is even more pronounced in the 100 Hz

circuit, figure 6.17. Finally, the 300 Hz circuit's output shown in

figure 6.18 is, as expected, unstable. Note that at no point could

good suppression of the fading be obtained. The 10 Hz EIFBAGC circuit

had the smallest output peaks, and this was the bandwidth chosen for

the equivalent circuit incorporated in the UHF SSB tone-in-band receiver

described in chapter 4.

In view of these results and the twin path observations, described

in section 6.4.2, it is suggested that EIFBAGC circuits operated in the

multipath environment should have delay phases of less than 0.2 radians.

This corresponds to an EIFBAGC bandwidth to first order pilot bandpass

filter bandwidth ratio of 1:10.

CHAPTER 7

COHERENT FEEDBACK AGC

The envelope detectors used in the EIFBAGC systems discussed so far have been conventional, wideband circuits of the precision rectifier type. These envelope detectors have no frequency discrimination properties i.e. they are incoherent and require an enhanced carrier or pilot for correct operation. While being satisfactory for most full carrier AM systems, they need to be preceded by bandpass filters for diminished carrier or pilot operation. The previous chapter discussed this topic and analysed the degrading effect of the bandpass filter's time delay on the dynamics of EIFBAGC. This chapter discusses the possible use of phase-locked loops (PLL) as coherent frequency discriminating envelope detectors. Such a system would allow the detection of diminished carrier or pilot envelopes in the presence of interfering modulation without incurring any time delay problems. However, it is necessary for the phaselocked loop to accurately track the phase of the incoming signal for correct envelope demodulation. This will be shown to be a major problem in the multipath environment.

7.1 Theory of Coherent AGC

This section describes the basic system and presents a novel model of coherent AGC. The model is used to show that the performance of coherent AGC is directly related to the phase tracking ability of the PLL. After considering the type of phase variations encountered in the mobile multipath environment, this section shows that coherent AGC is

7.1

likely to have a poor performance relative to incoherent techniques.

7.1.1 System Description

Section 3.2.1 showed that the general multipath received signal, $e_r(t)$, may be written as:

$$e_r(t) = r(t) \cos(\omega_c t + u(t)) \qquad (7.1)$$

where $r(t)$ and $u(t)$ describe the envelope and phase variations of the received carrier or pilot. This can be written in a more convenient form as:

$$e_r(t) = v_i(t)\underline{/\theta_i}(t) \qquad (7.2)$$

where $r(t)$ is represented by $v_i(t)$, $u(t)$ is represented by $\theta_i(t)$ and the symbol "$\underline{/x}$" represents $\cos(\omega_c t + x)$. This allows the notation of the earlier chapters to be used to describe envelope variations around the EIFBAGC circuit and a similar notation to Gardner's (7.1) to describe phase variations around the PLL.

The use of a PLL as a coherent envelope detector is well described elsewhere (7.2). A brief description of the complete coherent EIFBAGC system follows. Figure 7.1 shows the block diagram of the coherent EIFBAGC system to be investigated in this chapter. The input signal, $v_i(t)\underline{/\theta_i}(t)$, is applied to the multiplier section of the VGA. After amplification by H_o, the main output signal $v_o(t)\underline{/\theta_i}(t)$ is applied to the inputs of the phase sensitive detectors, PSD1 and PSD2 of the PLL. The PSD are linear multipliers with a gain factor K_d rad/V. The analysis neglects the sum (2f) output terms. The output of PSD1, $K_d v_o(t)\sin \theta_e(t)$, is filtered to determine the closed loop dynamics,
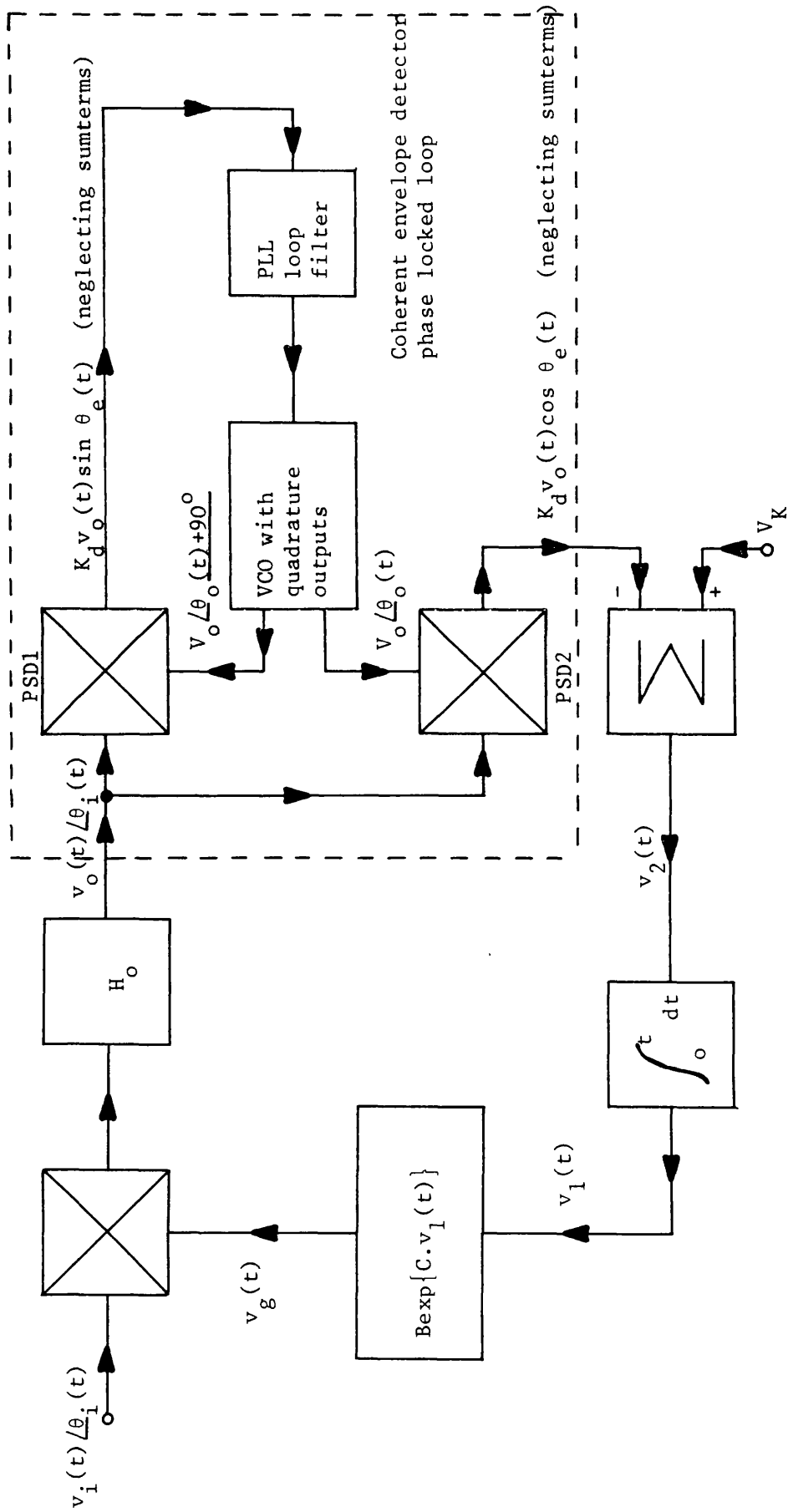
Figure 7.1   Block diagram of coherent EIFBAGC system

and applied to the input of the voltage controlled oscillator (VCO).

The 2 outputs of the VCO are in quadrature with a phase variation $\theta_0(t)$

and a peak voltage amplitude V_0. The bottom VCO output, $V_0 \underline{/\theta_0}(t)$, mixes

with the input to PSD2 to generate the signal for the summing junction

of the EIFBAGC circuit, $K_d v_0(t) \cos \theta_e(t)$.

Perfect envelope detection is obtained providing $\theta_e(t)$ is zero. In

this case the output of PSD2 is $K_d v_0(t)$ i.e. the PLL behaves as an

envelope detector with a gain K_d. The analysis of the response of

EIFBAGC performed in the earlier chapters then applies. However, if

$\theta_e(t)$ is not zero there is a complicated non-linear interaction between

the main EIFBAGC loop and the PLL. The PLL will then respond also to

envelope variations, the EIFBAGC loop will then respond to phase

variations, and in turn the response of each loop will affect the other.

This is the situation that arises in the multipath environment where

both $v_i(t)$ and $\theta_i(t)$ vary with time.

Usually, the analysis is simplified by assuming the EIFBAGC band-

width is much less than the PLL bandwidth. Gardner (4.3) states that

for deep-space missions the AGC noise bandwidth is narrower than the

PLL noise bandwidth by as much as 1000 to 1. Braun and Lindsey (7.3)

also assume the use of relatively narrow EIFBAGC bandwidths in their

study of the acquisition behaviour of the PLL. Although the coupled

AGC-Costas loop is not exactly the same as coupled AGC-PLL systems, the

work of Gagliardi (7.4) is relevant and discusses some steady state

tracking errors and the noise performance of coupled AGC-Costas loops.

His analysis also assumes the use of relatively narrow EIFBAGC bandwidths.

None of the aforementioned work presents a simple model of the

complicated circuit shown in figure 7.1 that can be used for general

analysis. The next section presents a "feedforward" model of coherent EIFBAGC that allows a better intuitive and mathematical understanding of its operation without any restrictions on relative bandwidths.

7.1.2 Feedforward Model of Coherent EIFBAGC

The feedforward model of coherent EIFBAGC may be derived as follows:

This analysis considers envelope variations around the gain control loop in figure 7.1. The output may be written as:

$$v_o(t) = v_i(t) \cdot v_g(t) \cdot H_o \qquad (7.3)$$

and $v_2(t)$ may be written as:

$$v_2(t) = \frac{d}{dt}\left[\frac{(\ln(v_g(t)/B))}{C}\right] \qquad (7.4)$$

But $v_2(t)$ is also given by:

$$v_2(t) = V_K - K_d\, v_o(t)\, \cos\, \theta_e(t) \qquad (7.5)$$

Equating equations 7.4 and 7.5 then substituting for $v_o(t)$ from equation 7.3 gives the main loop equation as:

$$\{v_i(t)K_d\, \cos\, \theta_e(t)\}\ v_g(t)H_o + \frac{d}{dt}\left[\frac{(\ln(v_g(t)/B))}{C}\right] - V_K = 0 \qquad (7.6)$$

Compare this to the main loop equation for conventional (incoherent) EIFBAGC, given by equation 5.9, i.e.:

$$v_i(t)v_g(t)H_o + \frac{d}{dt}\left[\frac{(\ln(v_g(t)/B))}{C}\right] - V_K = 0 \qquad (5.9)$$

Solving equation 5.9 in section 5.2.2 showed that $v_g(t)$ is simply a first order lowpass filtered and inverted version of $v_i(t)$. Comparison of

7.5

equation 5.9 with equation 7.6 shows that the only difference is the
multiplication of $v_i(t)$ by $K_d \cos \theta_e(t)$ in equation 7.6. Therefore it
can be immediately inferred in equation 7.6 that $v_g(t)$ is simply a first
order lowpass filtered and inverted version of $v_i(t)K_d \cos \theta_e(t)$. This
knowledge allows the derivation of a feedforward model of coherent
EIFBAGC in a similar manner to incoherent EIFBAGC. There are several
possible models, but the one shown in figure 7.2 is believed to be the
simplest. Although it incorporates feedback paths it is still referred
to as a feedforward model.

The output signal's envelope may be written from the model as:

$$v_o(t) = \begin{bmatrix} V_K \\ K_d \end{bmatrix} \frac{v_i(t)}{F1(v_i(t) \cos \theta_e(t))} \qquad (7.7)$$

where F1 represents the first order lowpass filtering operation, -3 dB
at CV_K rad/s. Note that no assumption has been made about the relative
EIFBAGC/PLL loop bandwidths and the only requirement for the validity of
equation 7.7 is that the denominator $d(t)$ is greater than zero. A
threshold circuit may be incorporated into the denominator of the divider
to prevent division by zero, as described in section 5.2.5.

7.1.3 Properties of the Feedforward Model

Equation 7.7 shows that the major problem with coherent EIFBAGC is
that the output signal's envelope is directly proportional to the filtered
inverse of the PLL phase error. If the phase error can be reduced to a
very small value then it can be seen that conventional EIFBAGC performance
will be obtained. However, any practical PLL will always exhibit some
phase error. This may be introduced by noise, modulation interference
(4.1) or multipath induced random phase modulation of the input. The
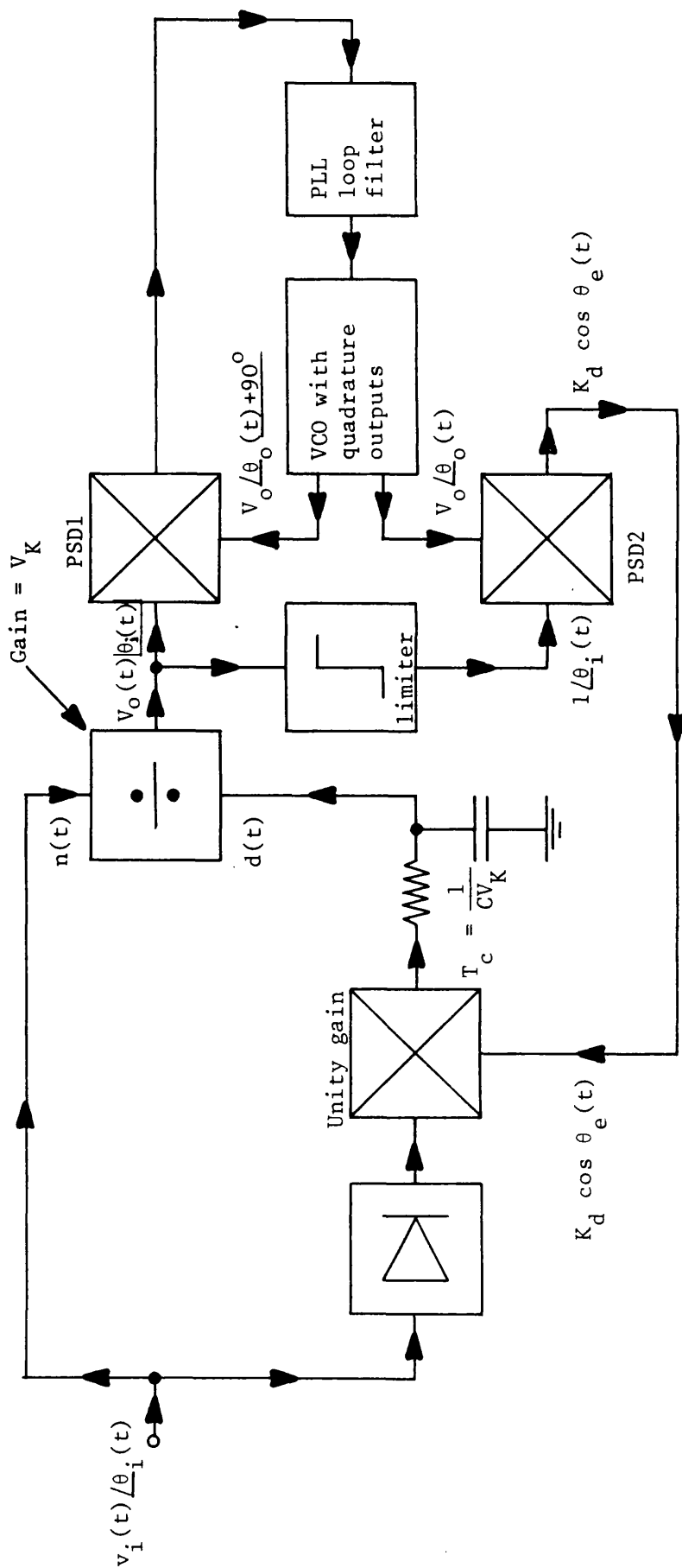
Figure 7.2   Feedforward model of coherent EIFBAGC

deterioration in EIFBAGC performance caused by this phase to envelope

conversion does not occur with incoherent envelope detection, such as

used in full carrier AM systems.

As stated earlier, one possible reason for using coherent envelope

detection in land mobile radio is to detect the envelope of the pilot

in pilot SSB systems. Whether or not coherent detection is preferable

to the use of bandpass filters and precision rectifiers is a complex

question. There are many aspects to this question, not the least of

which is the performance of coherent EIFBAGC in the multipath environment.

The feedforward model shows that the system's performance is very dependent

on the ability of the PLL to accurately track the random phase variations

of the incoming signal with a small phase error.

An exact theoretical analysis of the problem is elusive. After

considering the sort of phase variations the PLL is required to track

in the field, the rest of the chapter presents a series of practical

measurements of the response of precision PLL and coherent EIFBAGC systems

to multipath signals.

7.1.4 Multipath Phase Modulation

The various properties of the multipath signal's phase, u(t) and

du(t)/dt, its instantaneous frequency are described by Clarke (3.1) and

Jakes (3.2). The original work of Rice (7.5) provides more information

on the phase. The following observations have been made based on the

previous work.

The phase u(t) is uniformly distributed over the range $-\pi$ to π. The

higher rates of change of u(t) are associated with the deeper fades of

the received signal's envelope, r(t). This can be seen from the probability

density of du(t)/dt conditioned on the envelope level, r, given by Jakes

(ibid) as:

$$p \left[\frac{du(t)}{dt} \middle| r \right] = \frac{r}{\sqrt{2\pi b_2}} \exp \left[\frac{-r^2 \, du(t)/dt}{2b_2} \right] \tag{7.8}$$

where b_2 is the second moment of the multipath process and is given by:

$$b_2 = 0.75 \, b\omega_d^2 \tag{7.9}$$

For a fixed r, equation 7.8 is a Gaussian distribution with a standard

deviation $\sqrt{b_2}/r$. Therefore, the frequency deviations increase as r

decreases. Jakes (ibid) also gives equations for the PDF and power

spectrum of the random FM. However, the aforementioned result is the

most interesting and has the biggest implication for the phase tracking

ability of the PLL in the field.

Similar results can be obtained for the twin path situation. For

a received signal with one incoming component at $\omega_c - \omega_d$ and the other,

relative amplitude R, at $\omega_c + \omega_d$, the phase can be derived from

equation 2.11 as:

$$u(t) = \tan^{-1} \left[\left[\frac{R-1}{R+1} \right] \tan \omega_d t \right] \tag{7.10}$$

Differentiation of u(t) gives the instantaneous frequency as:

$$\frac{du(t)}{dt} = \frac{(R + 1)(R - 1)\omega_d}{((R + 1)^2 \cos^2 \omega_d t + (R - 1)^2 \sin^2 \omega_d t)} \tag{7.11}$$

The peak value of this, $\frac{\hat{du}(t)}{dt}$, occurs when $\omega_d t = 90°$, i.e. the trough

of the incoming fade. Then:

$$\frac{\hat{du}(t)}{dt} = \frac{(R + 1)}{(R - 1)} \omega_d \tag{7.12}$$

7.9

but $\dfrac{(R + 1)}{(R - 1)}$ is K_i, the peak to trough ratio of the fade. Therefore:

$$\frac{d\hat{u}(t)}{dt} = K_i \, \omega d \qquad\qquad (7.13)$$

Thus, for example, a 20 dB fade has a peak instantaneous frequency deviation of 10 x ω_d. Equation (7.10) shows that for the deeper fades the phase changes at the trough by up to π radians.

7.15 Expected PLL Performance

The PLL is not expected to operate with a small phase error in the multipath environment unless its bandwidth is considerably greater than the incoming fade rate. This is because the incoming signal exhibits rates of change of phase that greatly exceed maximum Doppler, ω_d. Furthermore, the response of the PLL is related to the drive level to PSD1 in figure 7.2. In the absence of the gain control loop the PLL is required to track the greatest rate of change of phase at the point where its response has been slowed down most. As shown in earlier chapters, even in the presence of relatively fast EIFBAGC systems the drive to PSD1 is still likely to suffer a large reduction corresponding closely in time to the input trough. Since the pilot is assumed to be transmitted well below peak modulation the use of limiters may not be considered.

However, the analysis of the PLL response is already complex without having to take into account the effect of correlated input envelope variations. In general, the envelope variations will degrade the PLL performance for reasons already described. The "best case" PLL performance may therefore be estimated by assuming the PLL is insensitive to input envelope variations. This approach is adopted later when considering the PLL response to twin path signals.

Some simplification of the calculation of the PLL response may be made if the PSD is assumed to possess a linear transfer characteristic as obtained using triangular or sawtooth PSD's. However, the work of Biswas et al (7.6) has shown that in the presence of noise or noisy fading signals the transfer characteristic of the triangular or sawtooth PSD tends to be approximately sinusoidal. Biswas et al (ibid) are also of the opinion that PLL will exhibit tracking difficulties in the presence of fading signals.

Weber (7.7) has analysed the approximate probability density of the phase error of an "on-tune" first order PLL in the presence of noise and Rayleigh fading. Significantly, he found that when the fading bandwidth is roughly equal to the average PLL bandwidth, the loop was essentially not tracking. In order to reduce the variance of the phase error to small values Weber (ibid) indicates the use of loop bandwidths between 10 and 100 times the incoming fade rate. However, his results are not easy to interpret and give little indication of the time varying nature of the phase error. Furthermore, these results are not directly applicable to the more widely used 2nd order PLL. A better indication of the expected PLL performance may be obtained by considering the phase variations of a twin path signal.

When subject to 2 input tones, a PLL will lock on to 1 (7.8). In the following work, u(t), the phase of the "carrier" as described by equation 7.10, is replaced by u'(t) where:

$$u'(t) = u(t) + \omega_d t \quad \text{for} \quad R < 1 \qquad (7.14)$$

$$u'(t) = u(t) - \omega_d t \quad \text{for} \quad R > 1 \qquad (7.15)$$

$$\text{and} \quad u'(t) = u(t) \pm \omega_d t \quad \text{for} \quad R = 1 \qquad (7.16)$$

A plot of u'(t) for various K_i (dB) is shown in figure 7.3. Note when $\omega_d t = 0$ or π, the input fade is at its peak and when $\omega_d t = \pi/2$ the input fade is at its trough. The maximum rate of change of phase occurs at the fade trough, and is given by $\pm (K_i - 1)\omega_d t$, (from equation 7.13 plus or minus $\omega_d t$). A PLL capable of tracking the rapid phase ramps (frequency steps) near the centre of figure 7.3 will obviously have little trouble with the slower phase ramps either side. The problem of estimating the PLL response to u'(t) can therefore be reduced to that of estimating its response to the peak rate of change of u'(t), i.e.

$$\frac{d\hat{u}'(t)}{dt} = \mp (K_i - 1)\omega_d \qquad (7.17)$$

Consider the use of a second order PLL with infinite dc gain using a sinusoidal PSD. When subject to a large frequency step, this kind of loop can never lose lock permanently (4.4). It may lose lock, slip cycles for a while, and then lock up once again. This is obviously undesirable. There is some frequency step limit below which the loop does not skip cycles but remains in lock: Gardner (4.4) terms this the "pullout" frequency, $\Delta\omega_{po}$. He gives an empirical relationship for $\Delta\omega_{po}$ as:

$$\Delta\omega_{po} = 1.8\,\omega_n(\zeta + 1) \qquad (7.18)$$

where ω_n is the natural frequency of the loop, and ζ is the damping factor, valid for $0.5 < \zeta < 1.4$. The minimum requirement of the PLL used in a coherent EIFBAGC system may be that it should not lose lock. In this case, the natural frequency, $\omega_n(\text{min})$, is given by equations 7.17 and 7.18 by:

$$\omega_n(\text{min}) > \frac{(K_i - 1)\omega_d}{1.8(\zeta + 1)} \qquad (7.19)$$

7.12
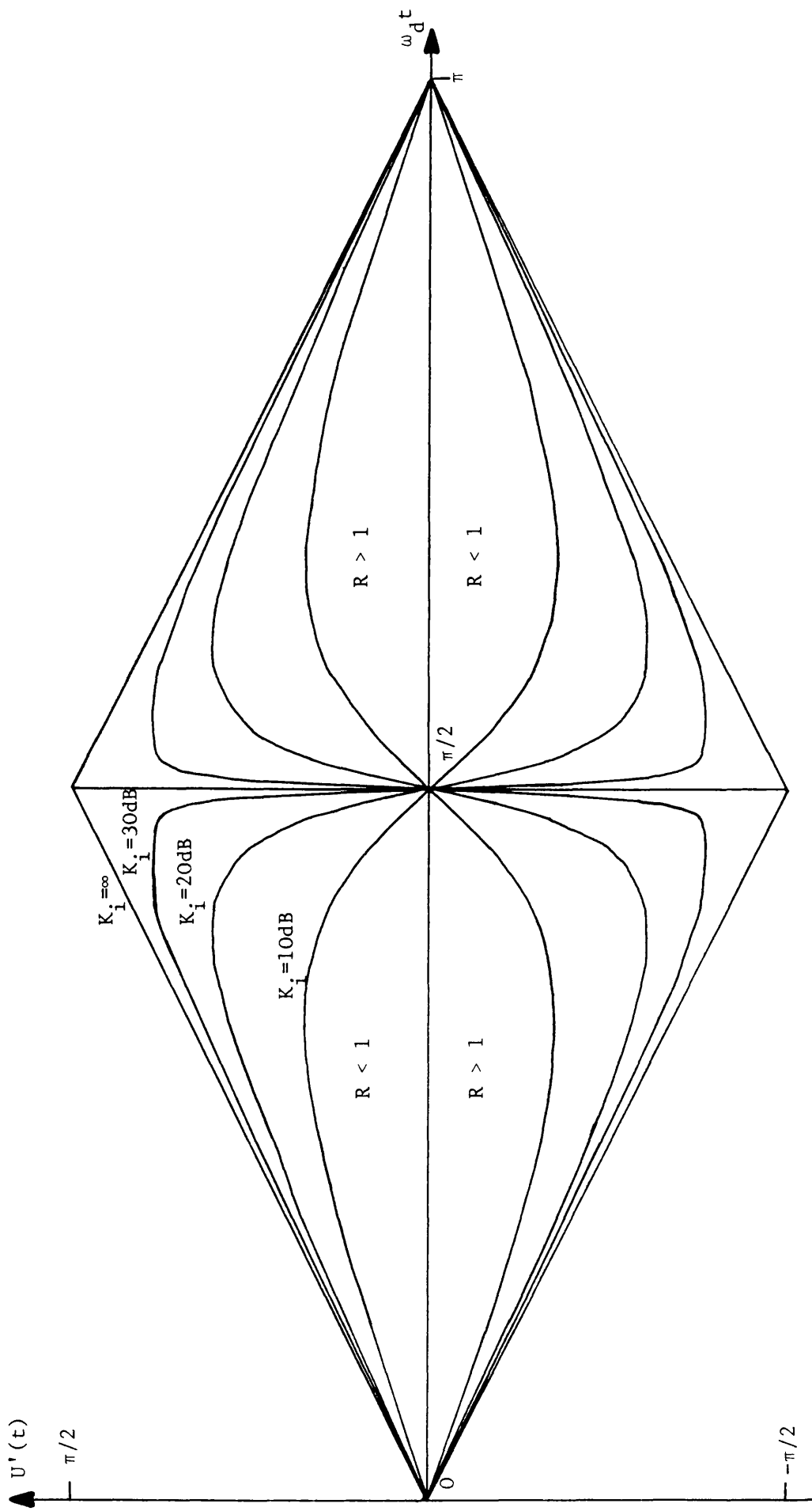
Figure 7.3 Plot of the phase variations of a twin path signal relative to the largest signal

7.13

Therefore, no matter how high ω_n is, there will always be a depth of fade below which the loop will lose lock. Gardner (ibid) also gives details of the peak phase error due to a frequency step. For values of θ_e between $-\pi/4$ and $\pi/4$ the maximum possible additional envelope modulation is 3 dB peak. The natural frequency, for $\zeta = 0.7071$, that gives less than 3 dB of envelope modulation via $\cos \theta_e$ is called ω_n (3 dB) and is given by:

$$\omega_n \ (3 \ dB) \ > \ \frac{(K_1 - 1)\omega_d}{1.7} \qquad\qquad (7.20)$$

It has been shown that a second order PLL will fail to satisfactorily track phase variations below a certain depth of fade, and deeper fades will always cause it to fall out of lock. The worst phase error will occur near the input fade trough. The implications of these results are considered in the rest of this chapter.

7.2 PLL Response to Field Trial Data

This section describes the results of practical measurements of a PLL response to field trial data. After explaining the design and construction of a precision PLL circuit, its performance in the multi-path environment is described and the results compared with theoretical predictions.

7.2.1 Precision PLL Circuit

A precision PLL was designed and built using conventional analogue and digital circuitry. The VCO was designed to operate at a nominal 1.67 kHz centre frequency with accurate in-quadrature outputs. The block diagram of the VCO is shown in figure 7.4. The sine and cosine analogue outputs are synthesised from digital coefficients stored in a

Voltage control input

Voltage controlled variable
frequency clock generator.
(XR2209)

External
clock
input

8 bit counter

(2 @ 4161B)

A_8 A_0

Read-Only-Memory
Even addresses:cosine
                    coefficients
Odd addresses: sine coeff-
                    icients
2 complete interleaved cycles
(2708 EPROM)

D_8 D_0

convert enable

convert enable

Digital to
analogue
convertor
(AD7524)

Sine
out

Cosine
out

Digital to
analogue
convertor
(AD7524)

Figure 7.4   Block diagram of quadrature VCO

programmable read only memory (PROM). The PROM contains the cosine coefficients. 2 complete cycles of sine and cosine coefficients are interleaved in the memory, and an address counter clock is required at 214 kHz to generate the 1.67 kHz analogue outputs. This form of VCO design allows the generation of outputs that are accurately 90° in quadrature, while incurring a minimal time delay penalty.

Figure 7.5 shows the block diagram of the complete PLL incorporating the aforementioned VCO. It is a second order type 2 PLL with a damping factor of 0.71 and 6 selectable values of natural frequency: 3 Hz, 10 Hz, 30 Hz, 100 Hz, 300 Hz and 1 kHz. The measured values of damping factor and natural frequency were within 10% of the designed value with the exception of the 1 kHz loop. This had an estimated ω_n of about 1.5 kHz with the notch switched in and was found to be underdamped. The notches were used to reduce the unwanted sum terms at the output of the multiplying PSD.

7.2.2 Typical Results

Some typical field trial results are shown in figures 7.6-7.12 inclusive. For these tests, the mobile was travelling at about 64 km/hr (40 mph) so that $2\omega_d$ is 54 Hz. The received signal strength was 30 dB above 1 μV. Before being input to the PLL, the signal was first passed through a 1 Hz EIFBAGC circuit that had negligible effect on the fast fading but provided the correct nominal input to the precision PLL. Note that whereas each run shown is of the same segment, lasting 205 mS, the vertical scale sometimes varies from figure to figure. When interpreting these results, the following information is useful.

7.16

.
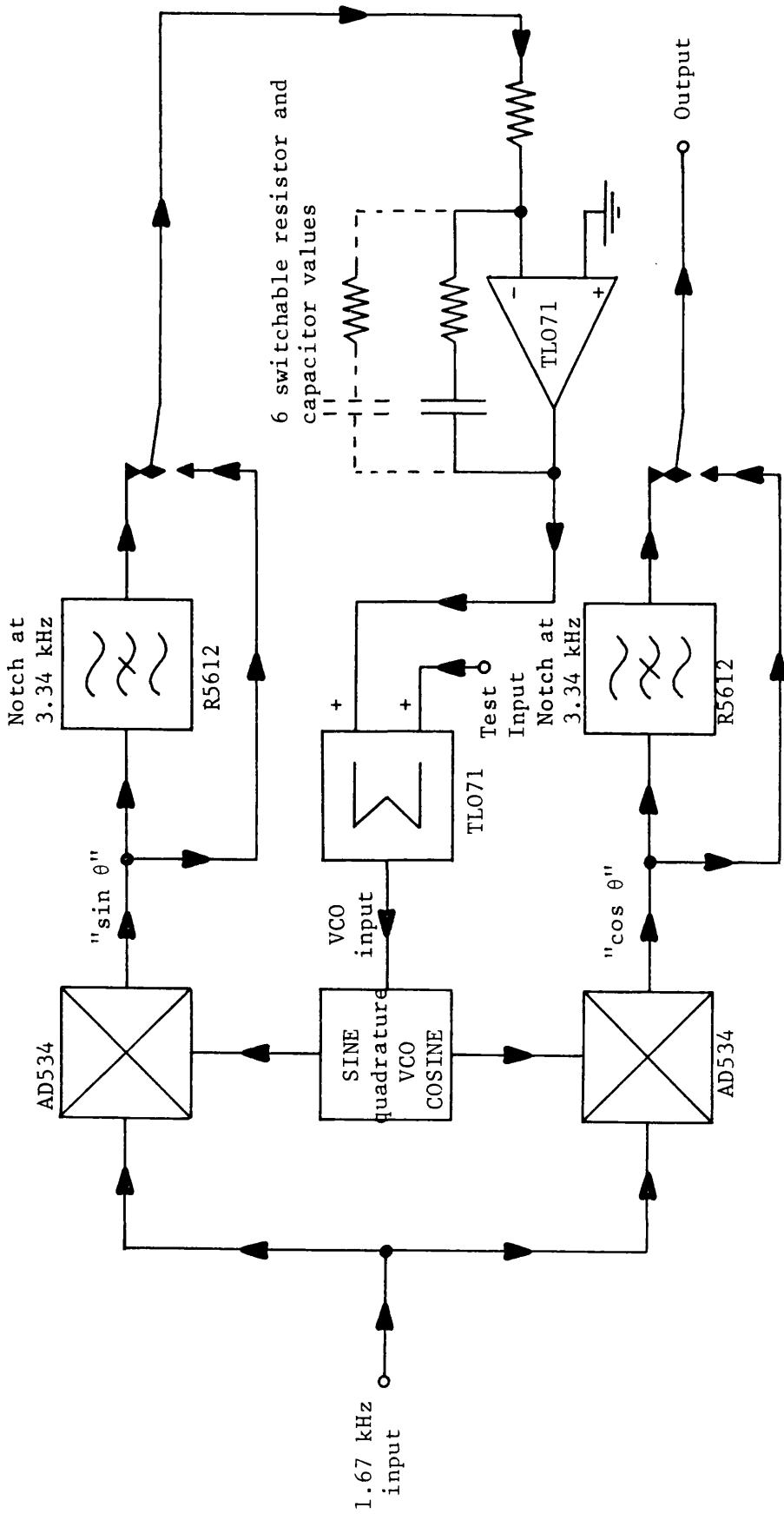
Figure 7.5 Block diagram of complete PLL

1) The VCO constant is 850 $r\ s^{-1}\ V^{-1}$ (135 Hz V^{-1}).

2) Both the sin θ and cos θ PSD have gains of 1 V r^{-1}. In the absence of fading, the cos θ output should be +1 V.

3) The envelope detector plot is obtained from a wideband precision rectifier circuit. Apart from the difference in vertical gains, the cos θ and envelope detector plots should be identical if the PLL were tracking the multipath FM with small phase error.

4) The straight line passing through the centre of the cos θ plot and near the bottom of the envelope detector plot corresponds to zero volts.

5) The deepest fade (second trough from start) was 30 dB peak to trough, 25 dB trough to peak with corresponding fall and rise times of 13.5 mS and 9.5 mS respectively.

6) The second deepest fade (second trough from end) was 20 dB peak to trough, 22 dB trough to peak with corresponding fall and rise times of 10 mS and 14 mS respectively.

7.2.3 <u>Discussion of Typical Results</u>

Figure 7.6, 3 Hz loop:

This PLL is seen to exhibit very poor phase tracking ability and consequently has a poor performance as an envelope detector. In fact, for the particular segment shown, the cos θ output spends more time below zero volts than above. At some points, the cos θ output appears to be tracking the envelope fading, but 180° out of phase.

Figure 7.7, 10 Hz loop:

This PLL is also seen to exhibit poor phase tracking ability, but manages to estimate that the envelope on the cos θ output spends more time above zero volts than below. There is, however, little resemblance
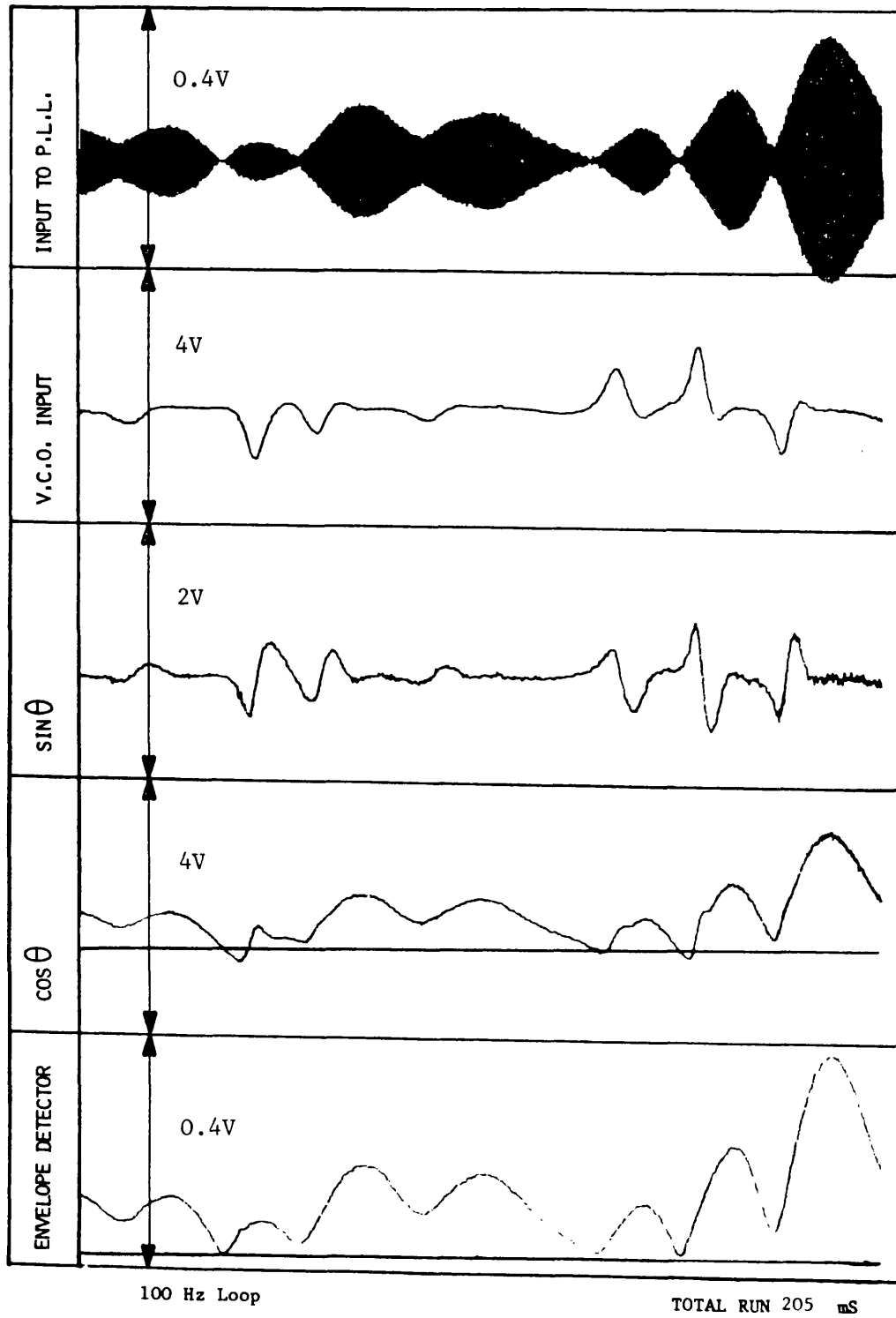
7.18
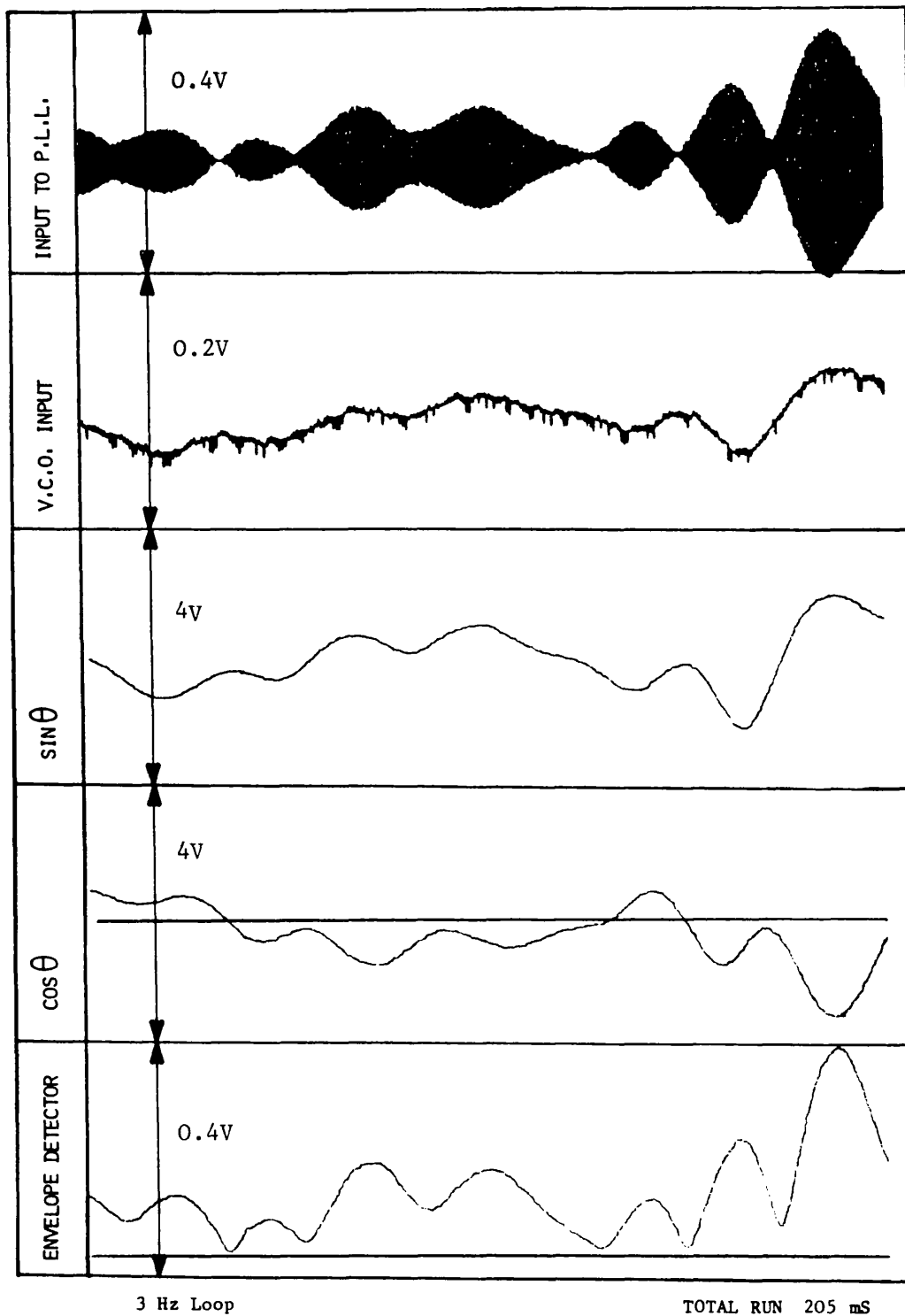
Figure 7.6 PLL response to field trial data, $\omega_n = 3$ Hz
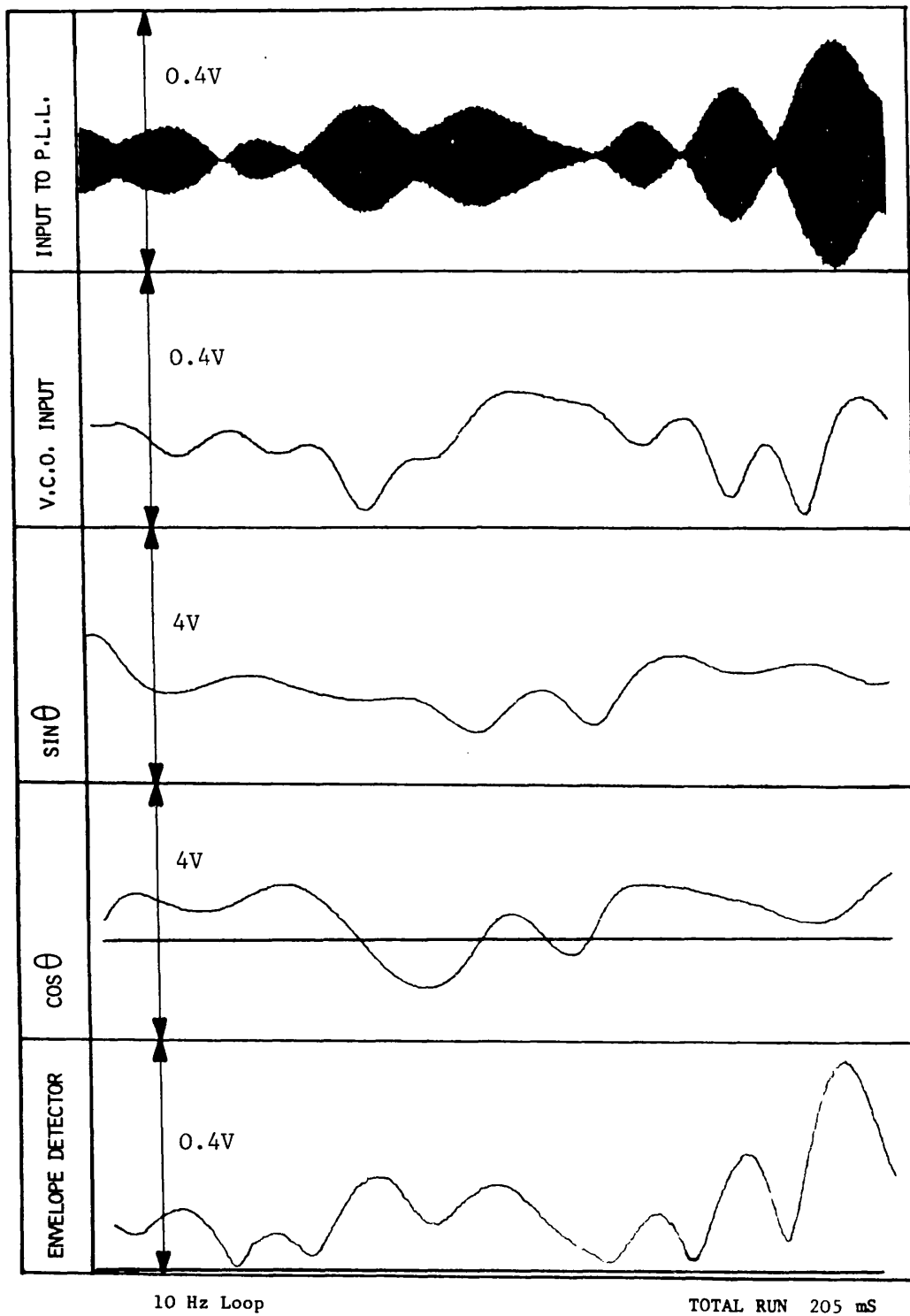
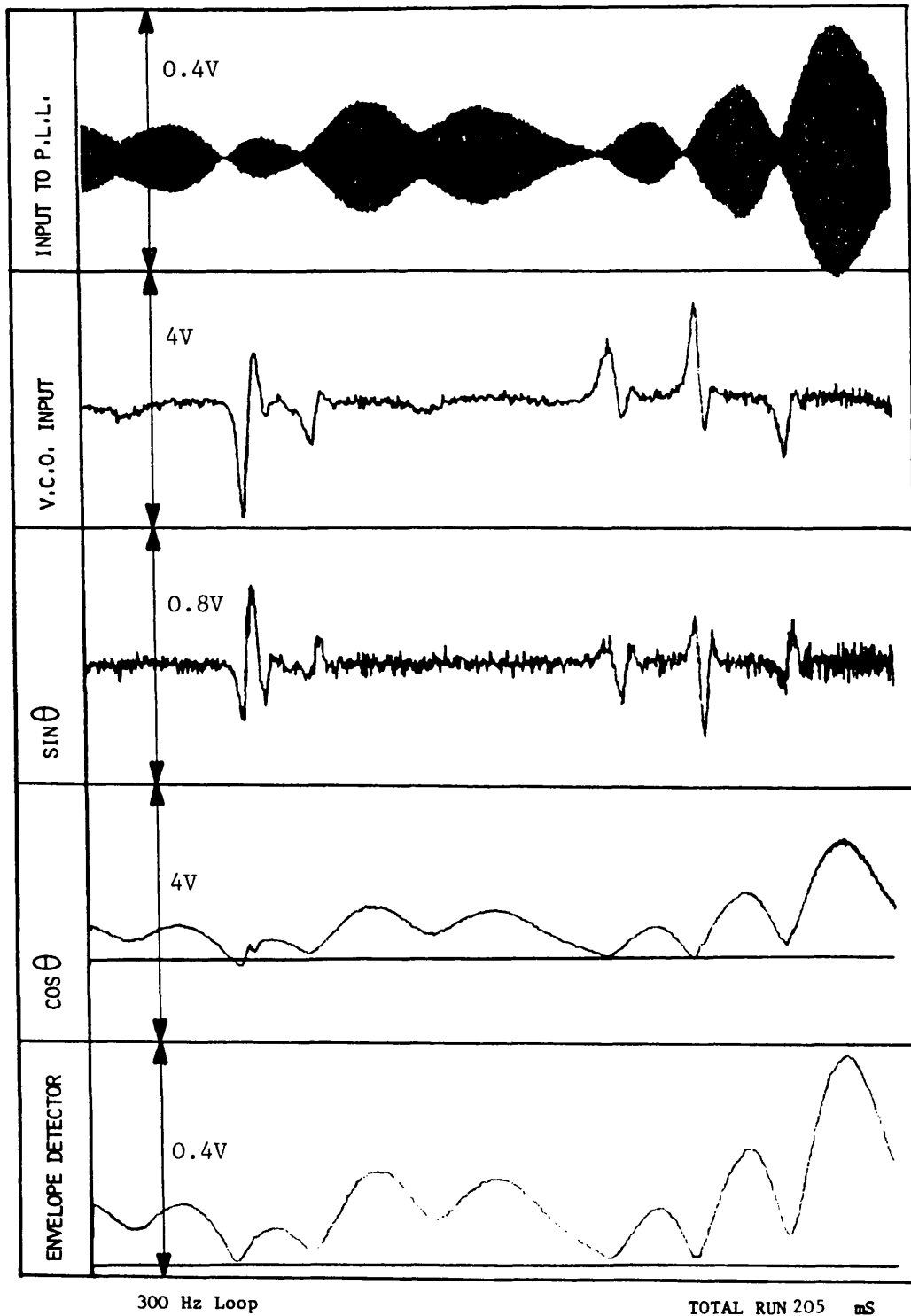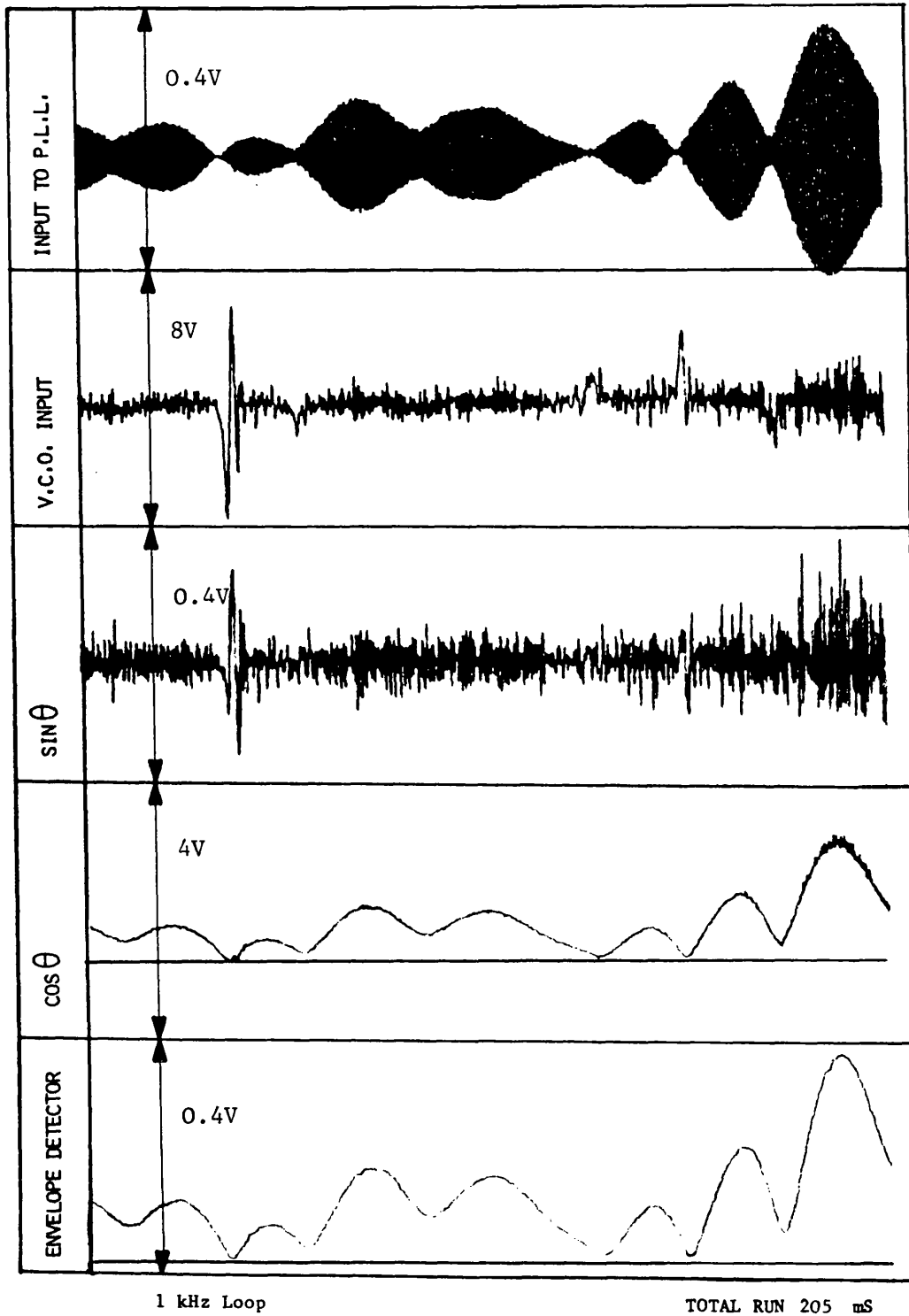Figure 7.7 PLL response to field trial data, $\omega_n = 10$ Hz

INPUT TO P.L.L. 0.4V

V.C.O. INPUT 2V

SIN θ 4V

COS θ 4V

ENVELOPE DETECTOR 0.4V

30 Hz Loop

TOTAL RUN 205 mS
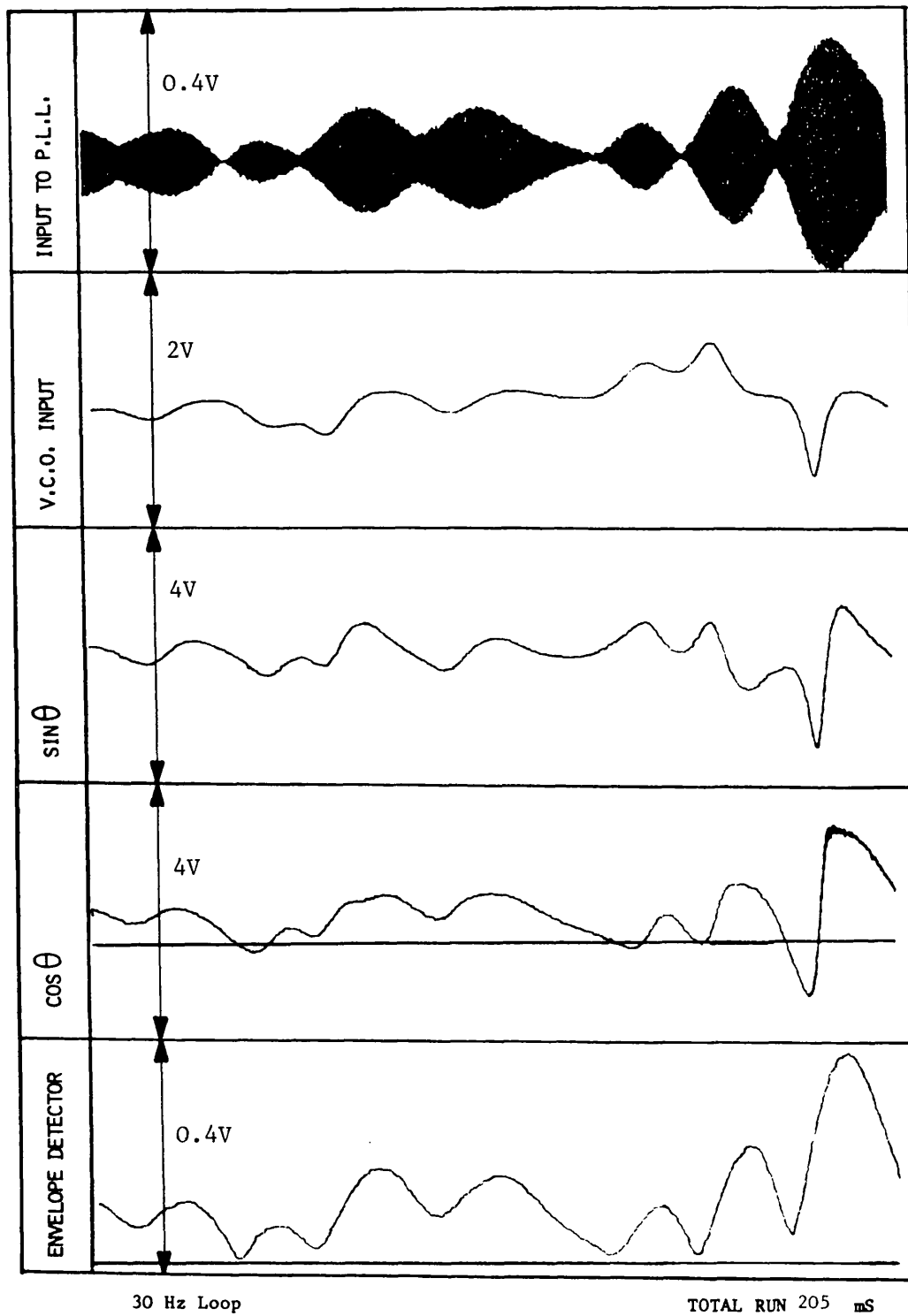
Figure 7.8   PLL response to field trial data, ω_n = 30 Hz

7.21

Figure 7.9   PLL response to field trial data, ω_n = 100 Hz

7.22

INPUT TO P.L.L. — 0.4V

V.C.O. INPUT — 4V

SIN θ — 0.8V

COS θ — 4V

ENVELOPE DETECTOR — 0.4V

300 Hz Loop   TOTAL RUN 205 mS

Figure 7.10   PLL response to field trial data, ω_n = 300 Hz

Figure 7.11 PLL response to field trial data, ω_n = 1 kHz

between cos θ and the envelope detector outputs.

Figure 7.8, 30 Hz loop:

This PLL begins to demonstrate the major problem with the use of coherent PLL envelope detectors, their poor performance at detecting the envelope near the trough of a fade.

Figure 7.9, 100 Hz loop:

The VCO input now begins to exhibit the "spiky" nature characterising relatively fast PLL as they attempt to track the rapid phase variations at the fade trough. However, even with peak to peak VCO deviations of over 200 Hz, the cos θ output is still observed to go negative.

Figure 7.10, 300 Hz loop:

This PLL is beginning to give a reasonable estimate of the signal's envelope at the expense of a relatively large ω_n (11 x ω_d). However, the cos θ output is still observed to go slightly negative during the deepest input fade, and close to zero at other points.

Figure 7.11, 1 kHz loop:

This PLL still generates a glitch on the cos θ envelope estimate not apparent on the envelope detector output, during the deepest input fade. At this point, the VCO exhibits a peak to peak deviation of over 850 Hz. The ratio of ω_n to ω_d is now 37, and the correspondingly large PLL noise bandwidth results in noticeable noise appearing on the cos θ output. The underdamped nature of the 1 kHz PLL is also apparent in the plots.

7.2.4 Comparison with Twin Path Predictions

If the input were a twin path (2 tone) signal, then in order that

the PLL does not lose lock during the 30 dB fade requires the use, from

equation 7.19, of an ω_n(min) of 270 Hz. In order to estimate the

envelope to within ± 3 dB requires, from equation 7.20, an ω_n (3 dB)

of 953 Hz. It is therefore not surprising that only the 1 kHz PLL gave

a good estimate of the signal's envelope.

One interesting observation was that a "best fit" twin path signal

gave a reasonable approximation of the peak frequency deviation of the

1 kHz PLL VCO when it was tracking the random FM. For example, the

20 dB fade near the end of the plot has a "best fit" twin path signal

with a frequency of 50 Hz (ω_d = 25 Hz). According to equation 7.13

such a twin path signal would exhibit a peak frequency deviation of

250 Hz. The measured VCO deviation in figure 7.11 is found to be 270 Hz

peak. Obviously many more measurements would be required to generalise

this result. However, it is significant that "best fit" deterministic

twinpath signals to the envelope of random multipath signals apparently

allow good estimation of the response of both AGC and PLL systems.

7.3 Coherent EIFBAGC Response to Field Trial Data

The precision PLL circuit was used to replace the precision rectifier

envelope detector in the EIFBAGC circuit described in section 5.2.6.

The complete coherent EIFBAGC circuit was then subject to the same input

waveform described in section 5.5.1. The output envelope recordings

described here therefore allow comparison with incoherent EIFBAGC response

and EIFBAGC with time delay presented in earlier chapters.

7.3.1 Typical Results and General Observations

Plots of the coherent EIFBAGC systems' output envelopes are presented for 3 EIFBAGC bandwidths in figures 7.12-7.29. The EIFBAGC bandwidths are 1 Hz, 30 Hz and 1 kHz with the results showing the use of all 6 PLL natural frequencies. The performance of the 1 Hz, 30 Hz and 1 kHz incoherent EIFBAGC systems can be seen by reference to figures 5.18, 5.21 and 5.24 respectively. The vertical gain on the plots 7.12-7.29 are the same as those in chapter 5, with each run lasting the same time, 819 mS. The following general observations have been made regarding these results:

Figures 7.12-7.17, 1 Hz AGC:

The 3 Hz, 10 Hz and 30 Hz PLL results all show an increase in the mean output level due to the reduction in the mean cos θ output. The 100 Hz, 300 Hz and 1 kHz PLL results show a negligible difference from the equivalent 1 Hz incoherent EIFBAGC output of figure 5.18.

Figures 7.18-7.23, 30 Hz AGC:

The poor phase tracking of the lower bandwidth PLL are apparent, especially near the fade troughs. Not until figure 7.21 where the 100 Hz PLL has a natural frequency greater than the EIFBAGC bandwidth is the output envelope contained within the vertical plot boundaries. The 300 Hz PLL and 1 kHz PLL results show a similar performance to the equivalent incoherent result in figure 5.21.

Figures 7.24-7.29, 1 kHz AGC:

The 1 kHz EIFBAGC is very sensitive to PLL errors in estimation of the envelope. Consequently, the 3 Hz PLL and 10 Hz PLL have resulted in complete system overload due to the poor phase tracking ability. The

7.27
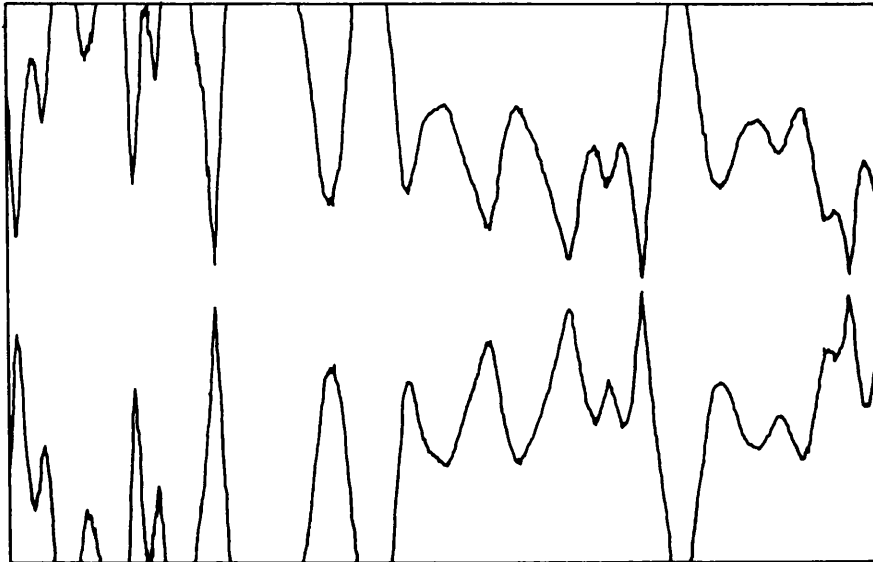
Figure 7.12   Coherent EIFBAGC output: 1 Hz AGC, 3 Hz PLL
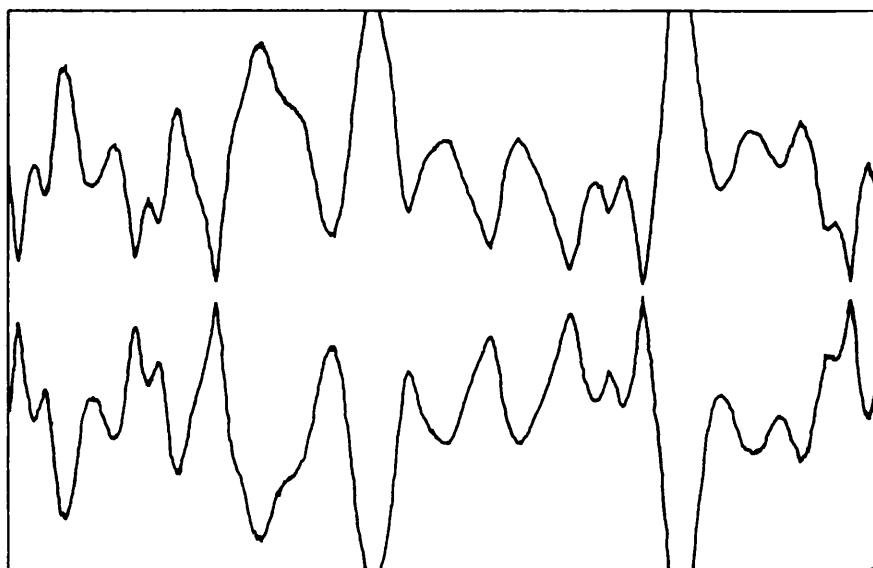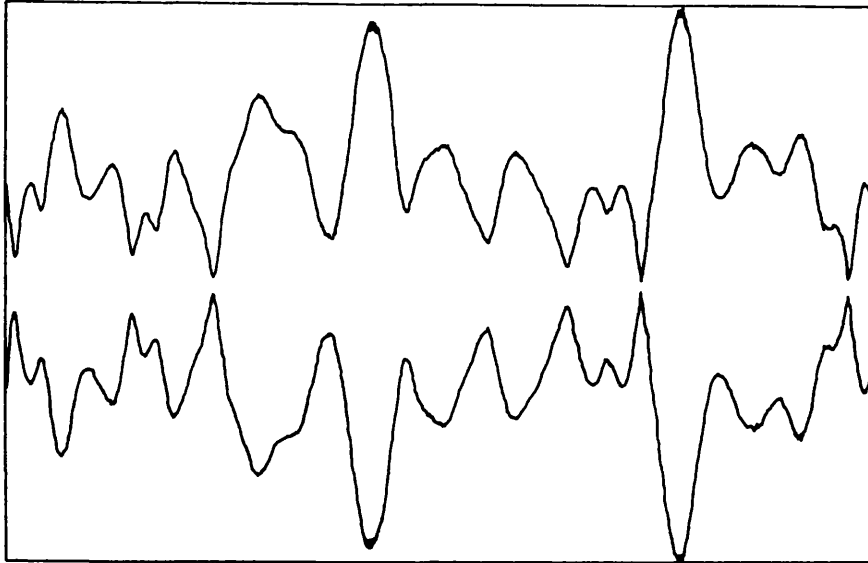

Figure 7.13   Coherent EIFBAGC output: 1 Hz AGC, 10 Hz PLL

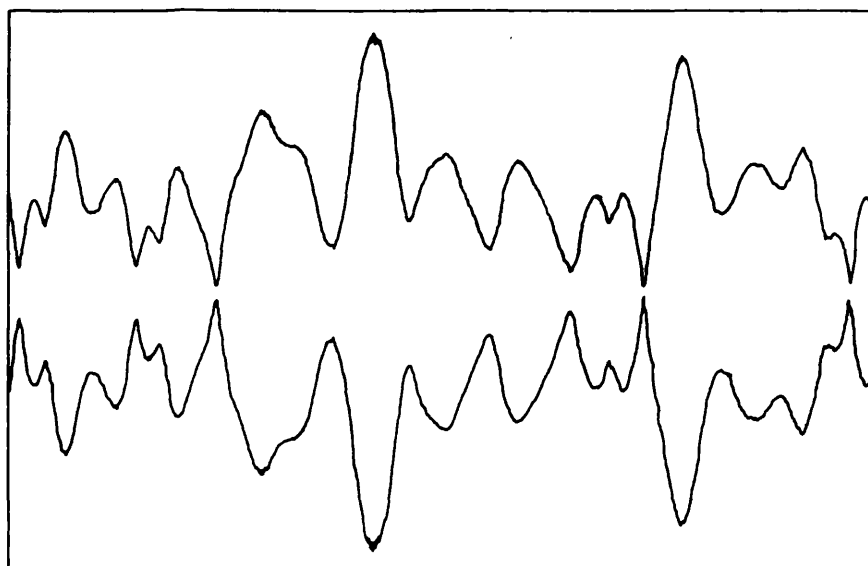Figure 7.14 Coherent EIFBAGC output: 1 Hz AGC, 30 Hz PLL

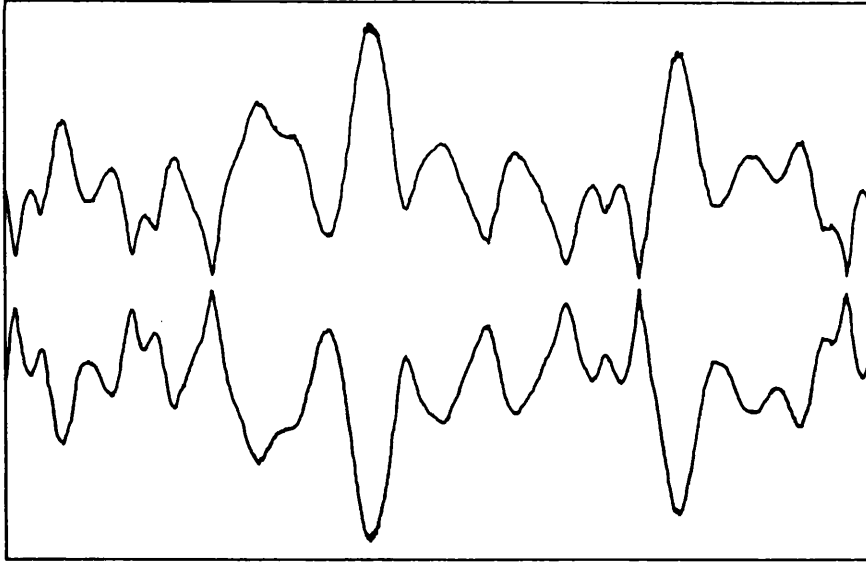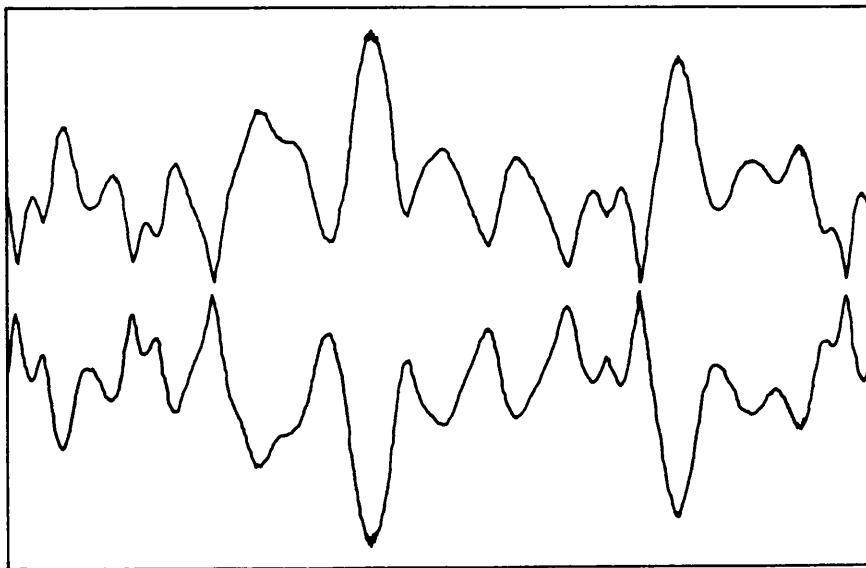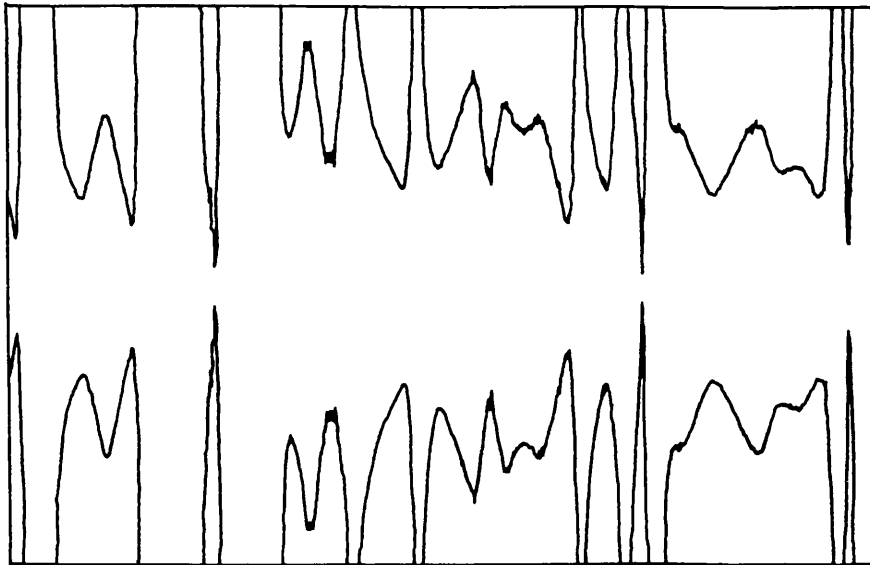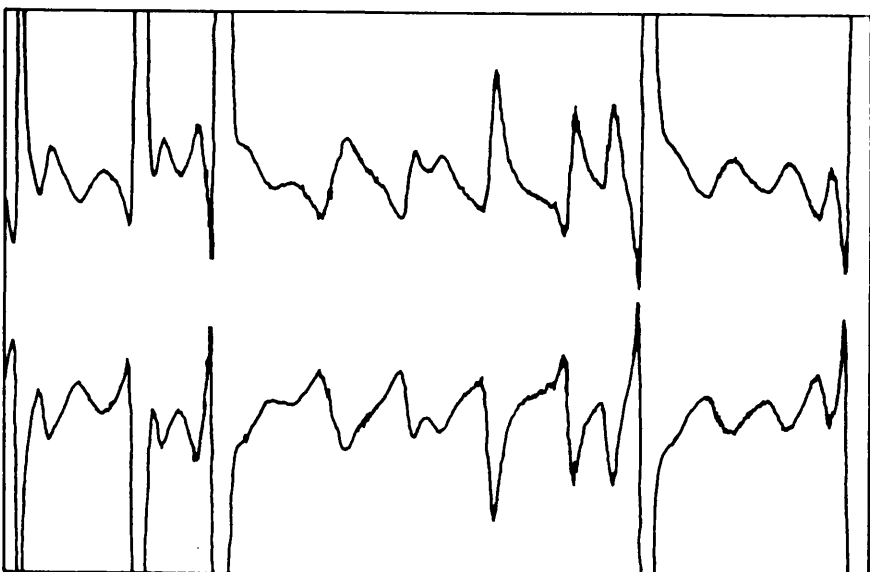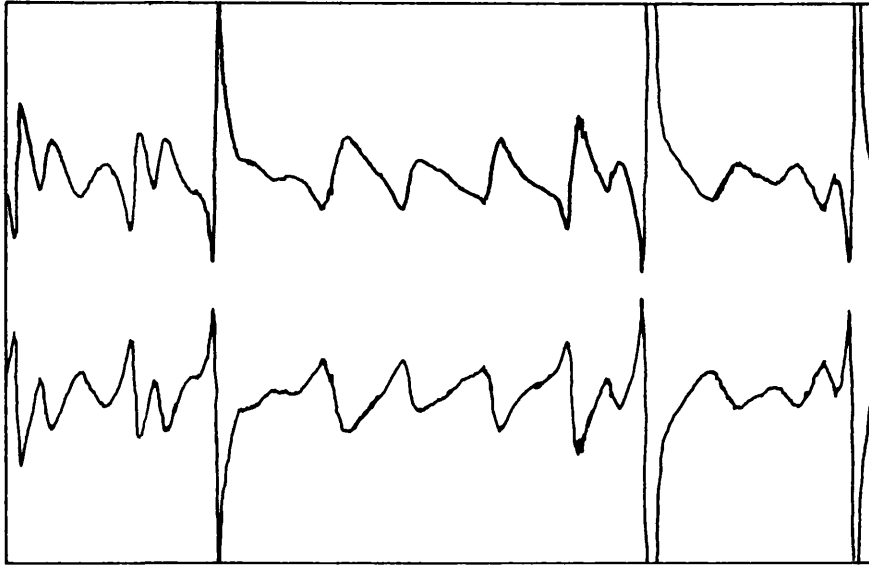Figure 7.15 Coherent EIFBAGC output: 1 Hz AGC, 100 Hz PLL

7.29

Figure 7.16   Coherent EIFBAGC output: 1 Hz AGC, 300 Hz PLL

Figure 7.17   Coherent EIFBAGC output: 1 Hz AGC, 1 kHz PLL

7.30

Figure 7.18 Coherent EIFBAGC output: 30 Hz AGC, 3 Hz PLL

Figure 7.19 Coherent EIFBAGC output: 30 Hz AGC, 10 Hz PLL

7.31

Figure 7.20 Coherent EIFBAGC output: 30 Hz AGC, 30 Hz PLL

Figure 7.21 Coherent EIFBAGC output: 30 Hz AGC, 100 Hz PLL
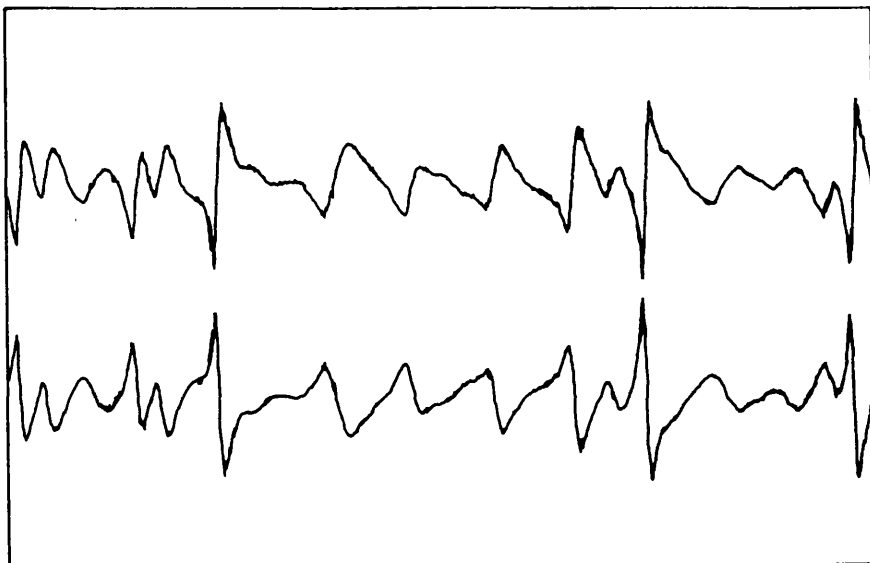
7.32

Figure 7.22   Coherent EIFBAGC output: 30 Hz AGC,   300 Hz PLL
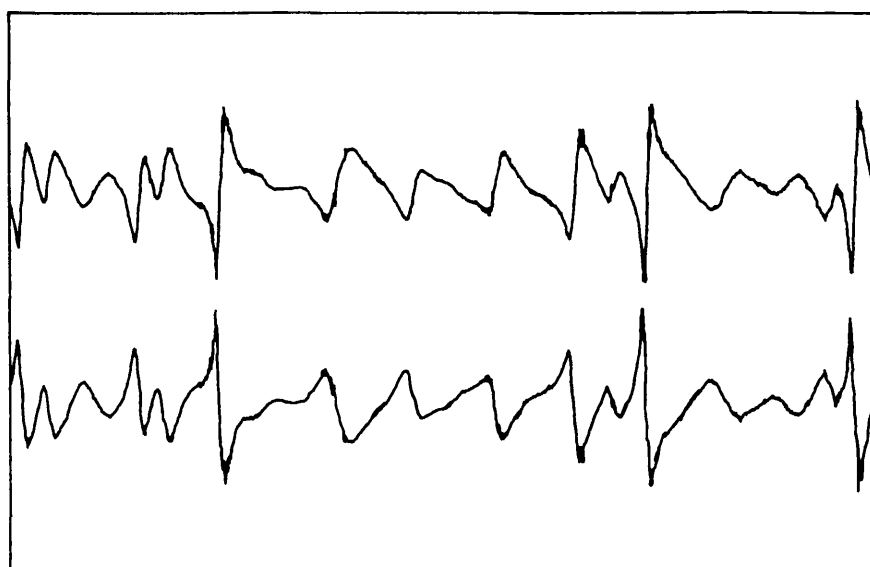

Figure 7.23   Coherent EIFBAGC output: 30 Hz AGC,   1 kHz PLL
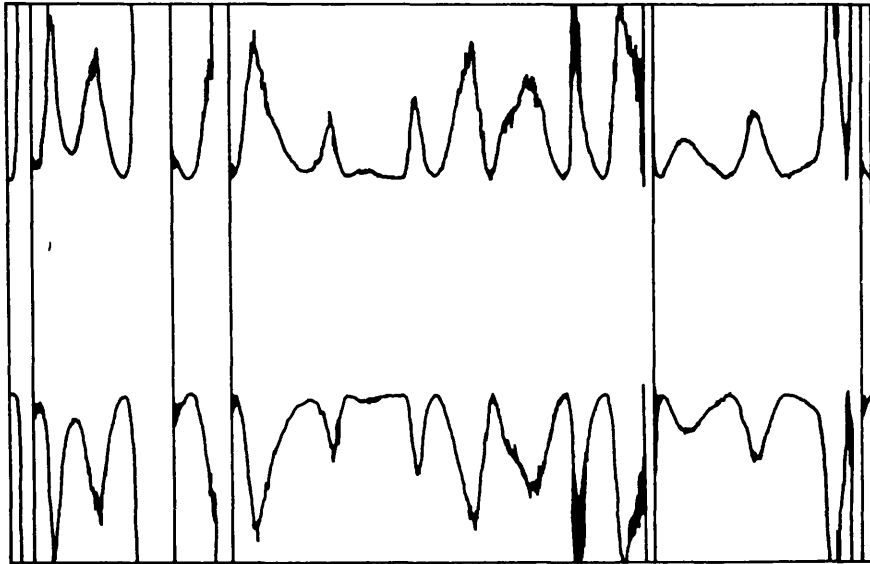
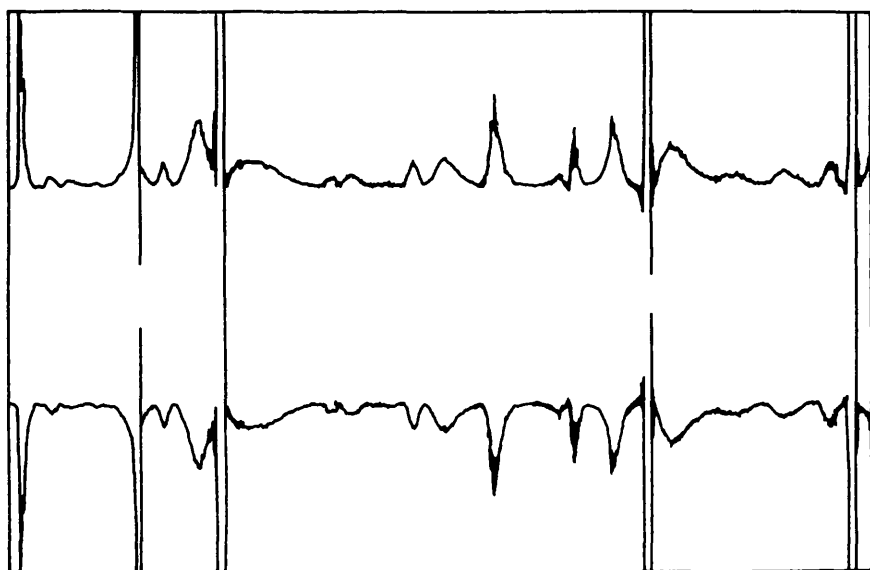Figure 7.24   Coherent EIFBAGC output: 1 kHz AGC, 3 Hz PLL

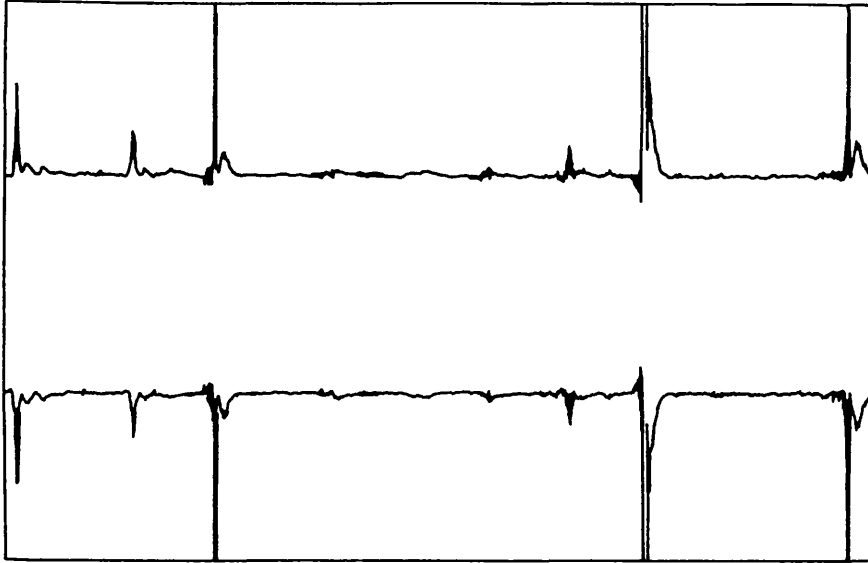Figure 7.25   Coherent EIFBAGC output: 1 kHz AGC, 10 Hz PLL

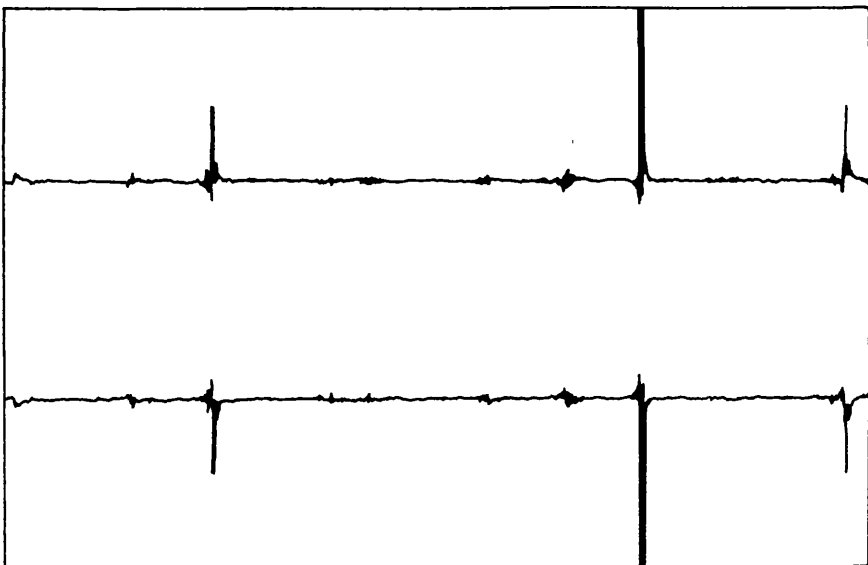Figure 7.26 Coherent EIFBAGC output: 1 kHz AGC, 30 Hz PLL

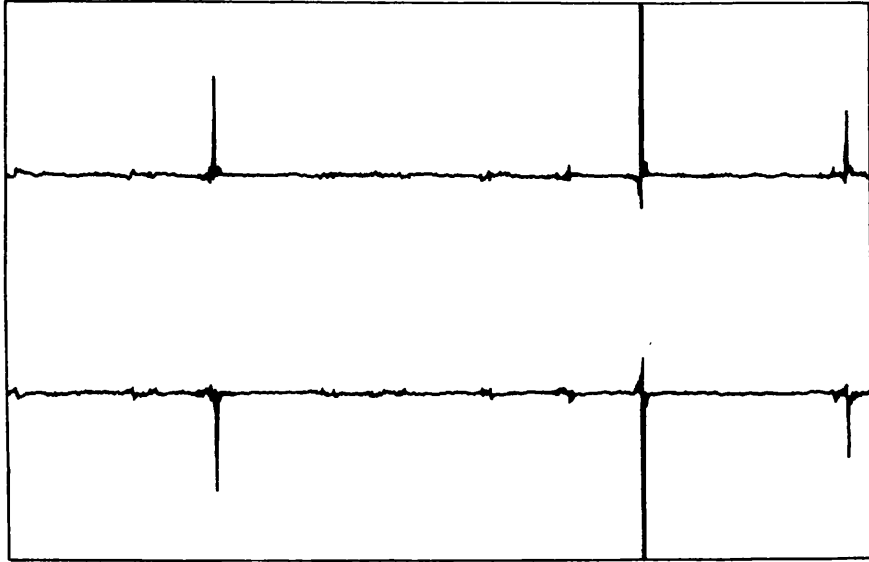Figure 7.27 Coherent EIFBAGC output: 1 kHz AGC, 100 Hz PLL

7.35

Figure 7.28   Coherent EIFBAGC output: 1 kHz AGC, 300 Hz PLL
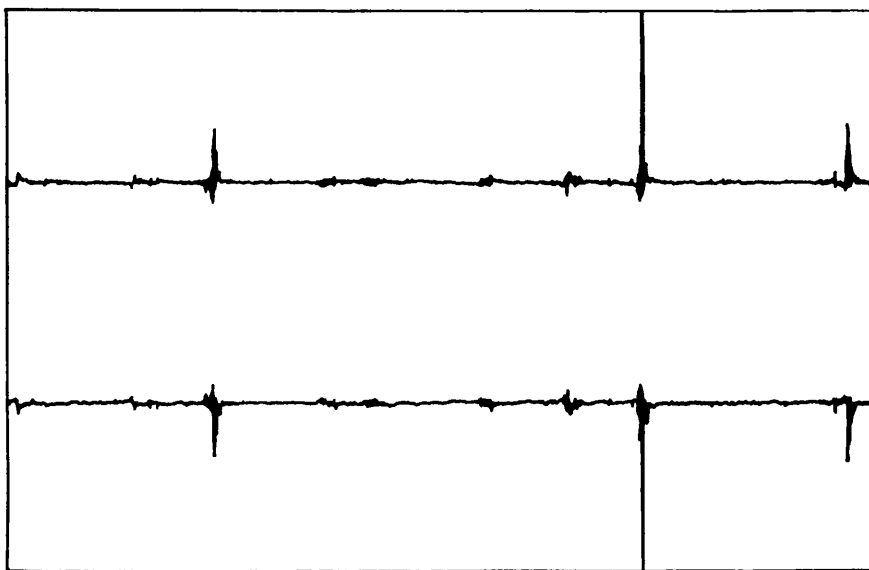

Figure 7.29   Coherent EIFBAGC output: 1 kHz AGC, 1 kHz PLL

7.36

30 Hz PLL result still shows large output spikes occurring just after the input has faded into a trough. The effect is reduced as the PLL ω_n is increased, but even with a 1 kHz PLL, the deepest fade has still resulted in a large output spike not apparent in the equivalent incoherent 1 kHz EIFBAGC result of figure 5.24. Evidently, the use of PLL ω_n in excess of 1 kHz are required to achieve the performance of the equivalent incoherent system.

A much longer section of field trial data was played back through the coherent EIFBAGC circuit and some general observations noted about its performance relative to incoherent EIFBAGC. The output was assessed on the following points basis:

Point	General Observation
1	Severe overload, latches up for > 10 fades
2	Occasional overload, 1-10 fades
3	Trough fade overload, < 1 complete fade
4	Severe trough fade peaking
5	Noticeable trough fade peaking
6	Slight degradation relative to incoherent EIFBAGC

The Doppler frequency for the run in question was about 22 Hz. The results are shown in table 7.1.

PLL ω_n \ AGC Bandwidth	1 Hz	3 Hz	10 Hz	30 Hz	100 Hz	300 Hz	1 kHz
3 Hz	2	1	1	1	2	2	2
10 Hz	2	2	2	1	1	1	2
30 Hz	6	4	3	1	1	2	2
100 Hz	6	6	5	4	2	3	3
300 Hz	6	6	6	6	3	3	3
1 kHz	6	6	6	6	5	3	3

Table 7.1   Observations of Coherent EIFBAGC Performance

The dark line drawn through table 7.1 represents the point where the PLL ω_n is equal to 30 times the EIFBAGC bandwidth. The following general observation has been made regarding these results:

The PLL ω_n should be about 30 times the EIFBAGC bandwidth for only a slight degradation in the multipath suppression performance relative to incoherent EIFBAGC systems.

7.3.2 Implications for Land Mobile Pilot SSB Receiver Design

The question originally posed in section 7.1.3 as to whether coherent (PLL) pilot detection is preferable to incoherent (bandpass filter/ precision rectifier) pilot detection is not satisfactorily answered by a consideration of the field trial results alone. The recommended PLL

ω_n to EIFBAGC bandwidth ratio of 30 is comparable to the recommended bandpass filter to EIFBAGC bandwidth ratio of 10. However, it should be noted that several other aspects of PLL performance (e.g. the effect of interfering modulation, out of lock situations etc.) need to be considered for a fuller comparison of coherent versus incoherent envelope detection.

It would seem logical to use the PLL incorporated into pilot SSB receivers for AFC purposes as the coherent envelope detector if a coherent EIFBAGC system were to be employed. However, the AFC PLL used in most pilot SSB receivers has an ω_n equal to or less than the EIFBAGC bandwidth (1.8,5.5). Obviously, using the AFC PLL as a coherent envelope detector would require the use of narrower EIFBAGC bandwidths.

Of course, this does not rule out the use of a second, independent wideband PLL, not used for receiver AFC purposes, as a coherent envelope detector. However, the increased complexity of such a PLL relative to the simpler bandpass filter/precision rectifier incoherent detector would probably rule out such an approach. Furthermore, the effect of modulation interference on such a wideband PLL would need to be carefully assessed as it is different to comparable effects in the incoherent case (4.1,7.8).

In view of these results it is suggested that coherent EIFBAGC is only used where relatively slow EIFBAGC bandwidths are acceptable, such as in deep space missions (4.3). The use of coherent systems in the multipath environment should be treated with great caution.
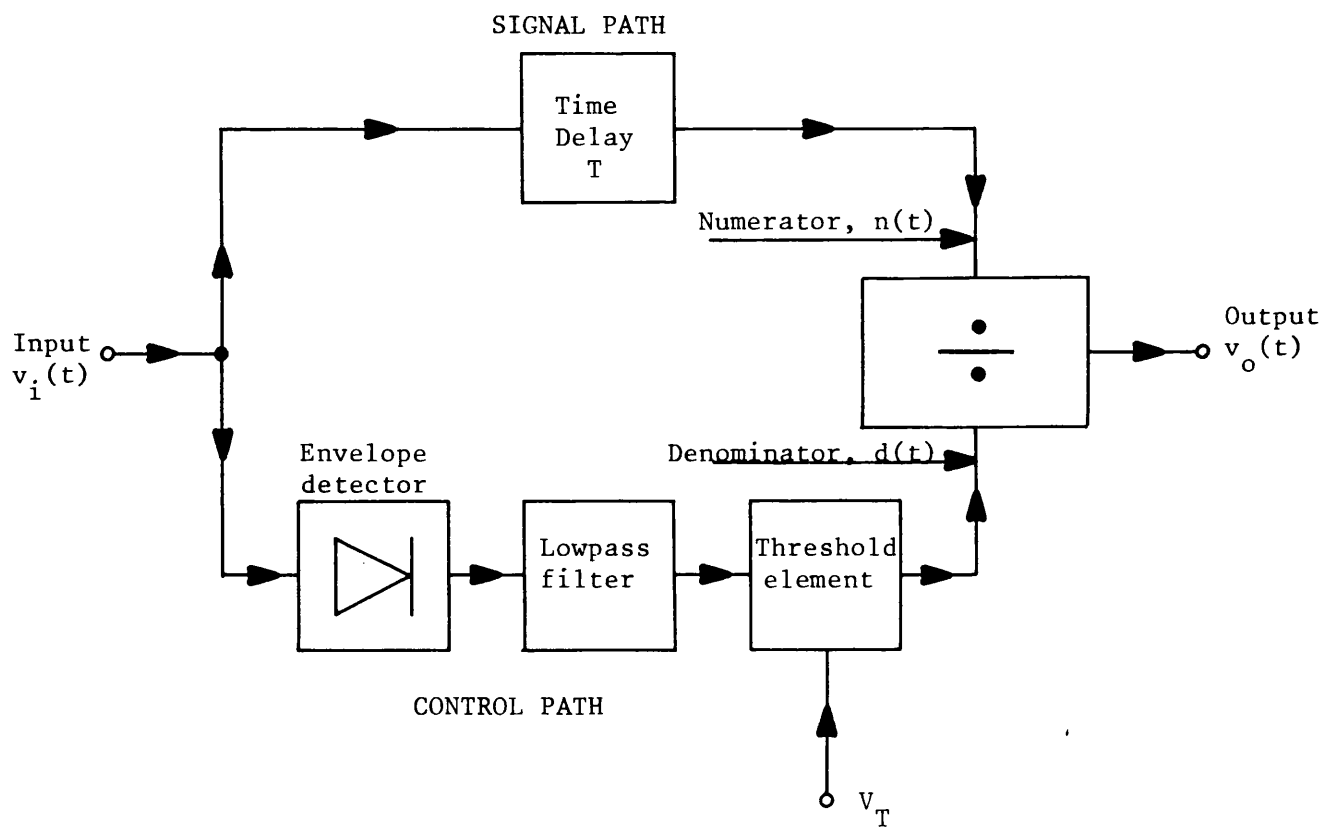
CHAPTER 8

LOWPASS FILTER FEEDFORWARD AGC

Feedforward AGC (FFAGC) is the generic name given to AGC systems

that operate by feeding forward, rather than backward, gain control

signals. Lowpass filter FFAGC (LFFAGC) refers to systems whose dynamics

are primarily determined by a post envelope detector lowpass filter.

LFFAGC systems can offer an improved dynamic performance relative to

feedback AGC. However, LFFAGC will be shown to exhibit an important

dynamic limitation and a more suitable form of FFAGC is proposed for

mobile radio operation.

8.1 Derivation from Feedback AGC

LFFAGC was first described by Hopper (8.1) in 1962 as a new form

of AGC. Here LFFAGC is shown to be a simple extension of the feed-

forward model of EIFBAGC and most of the analysis of EIFBAGC systems

presented in earlier chapters is applicable to LFFAGC.

8.1.1 Basic Configuration

Figure 2 shows the basic LFFAGC circuit configuration. Since there

is no selectivity before the envelope detector, an enhanced carrier

reference is required for correct operation and LFFAGC is most suitable

for full carrier AM systems. Note that there are several other possible

configurations of LFFAGC for use with full carrier AM systems. For

example, the input of the top path time delay element could be derived

from the output of the envelope detector instead of the complete signal

SIGNAL PATH

Time
Delay
T

Numerator, n(t)

Input
$v_i(t)$

Output
$v_o(t)$

Envelope
detector

Denominator, d(t)

Lowpass
filter

Threshold
element

CONTROL PATH

V_T

Note 1   Input and output signals are at IF.

Note 2 $v_i(t)$ and $v_o(t)$ refer to the input and output
signal's envelopes respectively.

Figure 8.1 Block diagram of LFFAGC system

8.2

as shown. However, the other possible configurations operate in a similar manner to figure 8.1, which is used in the subsequent analysis.

A comparison of figure 8.1 with the feedforward model of EIFBAGC incorporating a hard gain limiter, figure 5.6, shows that they are very similar. The 2 main differences between LFFAGC and EIFBAGC are:

1) The LFFAGC lowpass filter used to separate fading information from the required modulation need not be a first order RC filter. In general, higher order analogue or digital filters are used that possess a linear or approximately linear phase characteristic. High order, constant delay non-recursive digital filters (8.2) perform particularly well in this application. There are no time delay induced stability problems with LFFAGC (unlike EIFBAGC). The designer is therefore free to choose the lowpass filter amplitude characteristic required to meet a given specification.

2) The time delay element in the LFFAGC signal path allows the significantly high group delay of the bottom path to be compensated for at the divider inputs, giving good time correlation between fades on the signal and control path. Such time delay compensation is not possible in feedback systems. If the LFFAGC lowpass filter is linear phase then perfect time delay matching is theoretically possible between the 2 paths.

8.1.2 <u>Time Delay Matching</u>

If the lowpass filter has a linear phase characteristic over all frequencies of interest then the top path time delay, T, is obviously chosen to equal the lowpass filter's group delay. However, analogue

8.3

lowpass filters can, at best, only approximate a linear phase character-
istic (8.3). The time delay is then usually chosen to be a best fit to
the phase characteristic over the frequency range of interest. For
example, Rawling et al (8.4) designed their LFFAGC circuit with a 4th
order Butterworth lowpass filter. The top path time delay element was
designed to match the lowpass filter's group delay at 100 Hz, giving
maximum AGC effectiveness at fading frequencies around 100 Hz at the
expense of reduced lower frequency fade suppression.

If the envelope variations possess an infinitely wide spectrum and
a non-linear phase lowpass filter is used, then the choice of matching
time delay is not so obvious. This can be demonstrated by considering
the response of a LFFAGC circuit to a step input envelope change, where
the bottom path lowpass filter is a simple first order RC type. The
analysis of EIFBAGC to step input envelope changes applies here as
performed in section 5.2.4, with the inclusion of the matching time
delay. The output envelope, $v_0(t)$, may be written directly from equation
5.20 as:

$$v_0(t) = \frac{1 + Z\ H(t - T)}{1 + Z\ (1 - \exp(-t/T_c))} \qquad (8.1)$$

where the top path time delay, T, is incorporated in the numerator as
shown. Plots of $v_0(t)$ for positive and negative 20 dB input envelope
steps are shown in figures 8.2 and 8.3 respectively, for various values
of T. The choice of best matching time delay is not obvious and depends
on system requirements. A value of T such that:

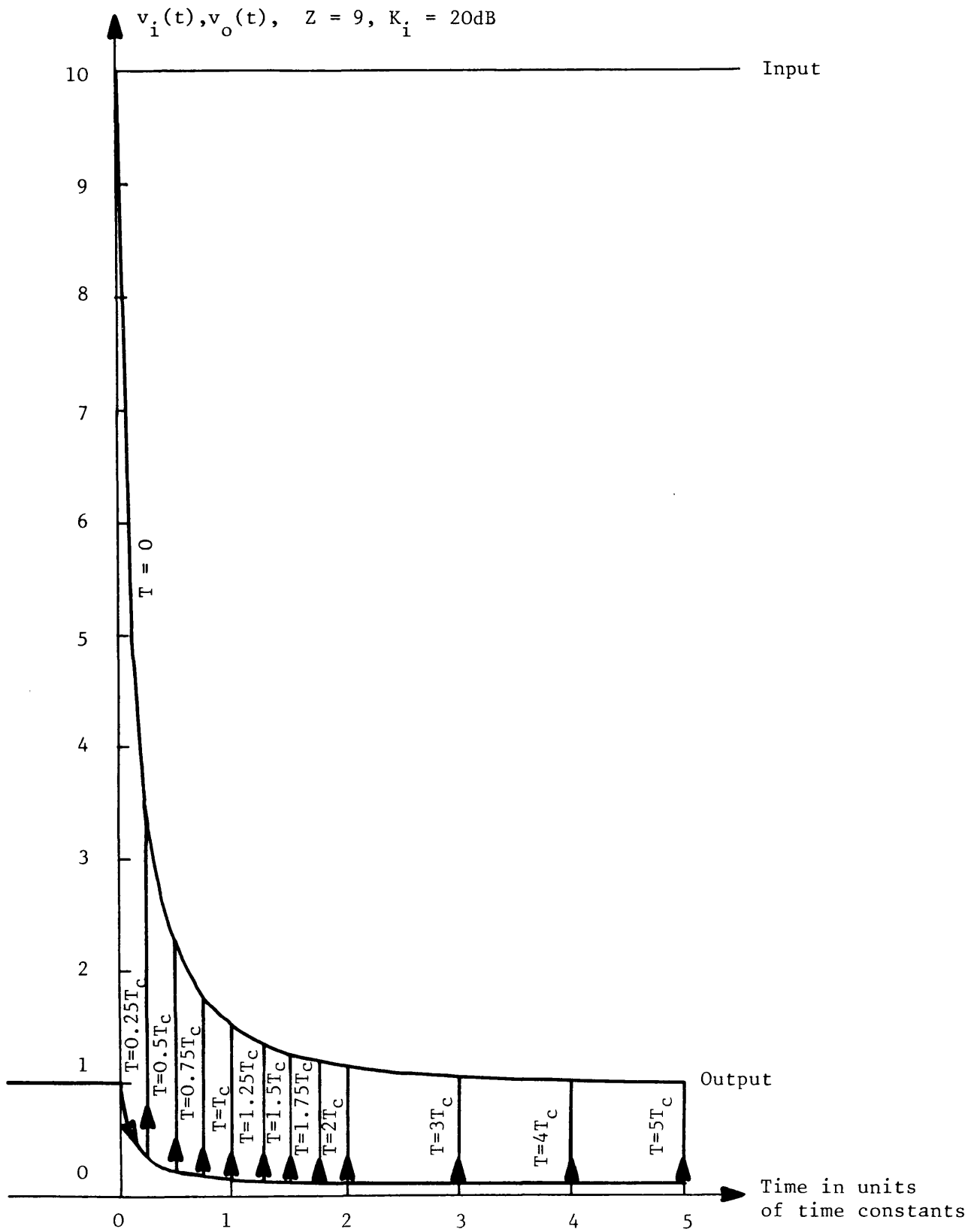$$\frac{T}{T_c} = \ln(0.5) = 0.6931 \qquad (8.2)$$

8.4

Figure 8.2   Response of LFFAGC with simple RC lowpass filter
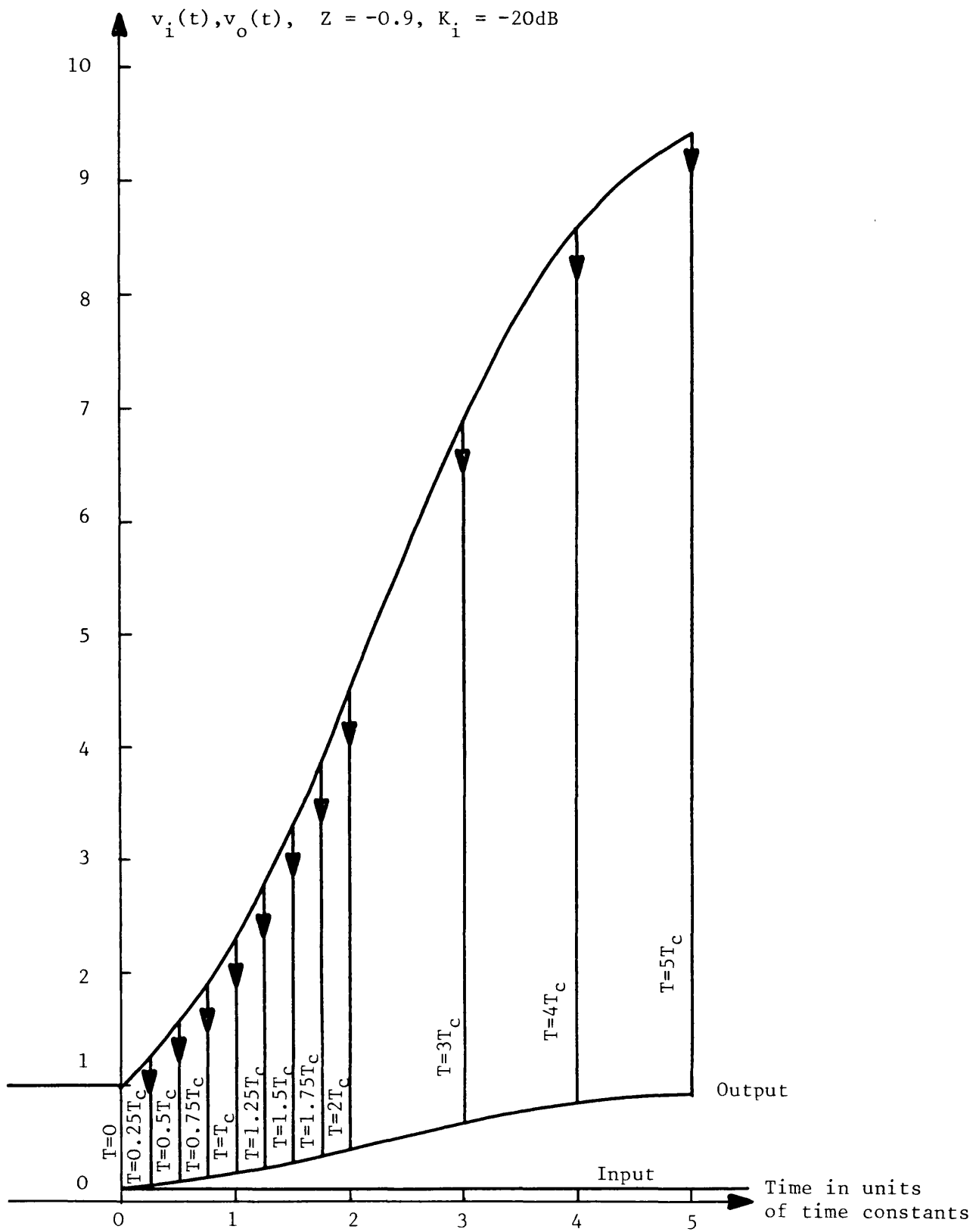to a positive 20 dB step change on input envelope

Figure 8.3 Response of LFFAGC with simple RC lowpass filter
to negative 20dB step change on input envelope

causes the maximum positive output overshoot to be the same for both

positive and negative input variations of the same peak to trough ratio.

The aforementioned first order LFFAGC circuit can form the basis of a

simple speech compression circuit, such as described by Price (8.5).

One of the assumptions behind any FFAGC circuit is that the user

can tolerate the processing time delay, T, which is typically less

than 10 milliseconds. With speech communication systems, such a small

time delay is unlikely to be noticed, although it may be a problem in

some "handshake" data communication systems. The time delay prevents

the circuits inclusion in any of the receiver feedback control circuits

(e.g. before a PLL PSD) unless they have a relatively low bandwidth.

FFAGC is usually regarded as a receiver "add on" circuit, coming after

most of the receiver processing circuitry.

8.1.3 Optimisation of the Lowpass Filter's Amplitude Response

LFFAGC circuits used for suppressing multipath fading generally

possess a lowpass filter that approximates to the ideal "brickwall" type.

As mentioned earlier, non-recursive linear phase digital filters give

the designer most freedom to choose the amplitude response to meet

the required specification while allowing for the possibility of perfect

time delay matching. It is convenient to describe the parameters of

such a filter, shown in figure 8.4.

The parameters are:

L_u : Upper limit to passband amplitude ripple

L_ℓ : Lower limit to passband amplitude ripple

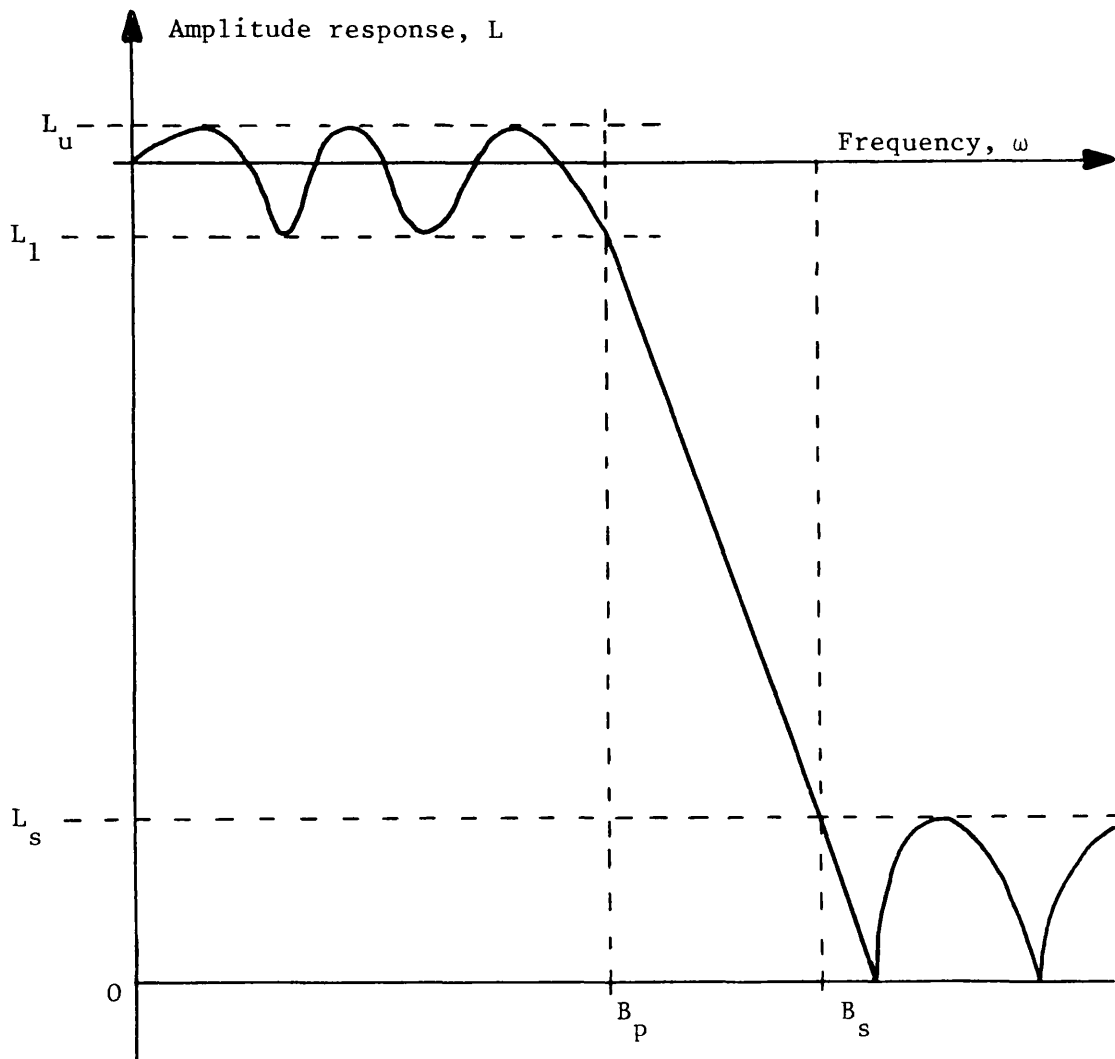L_s : Upper limit to stopband amplitude ripple

Figure 8.4   Description of lowpass filter parameters

B_p : Passband frequency limit

B_s : Stopband frequency limit

The design of non-recursive linear phase digital filters to meet a set
of prescribed parameters is described elsewhere (8.2). Later sections
of this chapter give formulae from which the parameters can be calculated
to meet a given fade suppression requirement.

8.1.4 Dynamic Range Considerations

Unlike FBAGC, all of the elements in a FFAGC system are subject
to the entire dynamic range of the input signal envelope variations.
The practical difficulties presented by this has restricted earlier
workers to operate LFFAGC with dynamic ranges of between 20 dB and
40 dB (8.1, 8.4). The obvious solution to the problem is to always
operate FFAGC in conjunction with a preceding slower acting FBAGC
circuit. The FBAGC circuit can then be used to suppress slow fading,
leaving the fast fading for the FFAGC circuit to suppress.

The dynamic range requirements of a FFAGC circuit can be evaluated
on a statistical basis. Assume the FFAGC circuit is preceded by a
slow acting FBAGC circuit that provides it with a Rayleigh fading
reference, with a mean envelope value V_K. The reference input power,
b, to the FFAGC circuit is then given by equation 3.7 as:

$$ b = \frac{2V_K^2}{\pi} \tag{8.3} $$

Theoretically, a Rayleigh fading signal has an infinitely wide amplitude
range. Practical considerations place a limit on both the upper and
lower input range of a FFAGC circuit. If the upper limit is r_u and

the lower limit is r_ℓ, it is possible to calculate the probability that the input signal's envelope, $r(t)$, will lie outside the FFAGC circuit's dynamic range. For the Rayleigh CDF from equation 3.5:

$$p(r(t) < r_u) = 1 - \exp\left[- \left[\frac{r_u}{V_K}\right]^2 \frac{\pi}{4}\right] \qquad (8.4)$$

$$p(r(t) > r_\ell) = \exp\left[- \left[\frac{r_\ell}{V_K}\right]^2 \frac{\pi}{4}\right] \qquad (8.5)$$

In general, a smaller upper limit is required than the lower limit to achieve equal probabilities of upper limit or lower limit overloading. For example, if r_u/V_K = 10 dB, then $p(r(t) < r_u)$ = 99.96%. For the same probability, $p(r(t) > r_\ell)$ = 99.96%, the lower limit is r_ℓ/V_K = -33 dB.

8.2 Response to Sinusoidal Modulation

This section analyses the response of LFFAGC to sinusoidal input envelope modulation, concentrating on the effects of lowpass filter imperfections. The aim is to develop a set of simple design equations for LFFAGC circuits using deterministic AGC test signal 1.

8.2.1 Predictions from EIFBAGC Analysis

For the purpose of mathematical convenience the time reference is taken to be after the time delay unit. The circuit's performance is now analysed above threshold and all circuit elements are assumed to be perfect except for the lowpass filter. The input signal's envelope is:

$$v_i(t) = E(1 + D \sin \omega_s(t + T)) \qquad (8.6)$$

The output signal's envelope can be written directly as:

$$v_o(t) = \frac{E(1 + D \sin \omega_s t)}{1 + LD \sin \omega_s(t + \tau)} \qquad (8.7)$$

assuming the divider is unity gain, where L is the lowpass filter's amplitude response at ω_s and τ is the differential time delay between the numerator and denominator envelopes at ω_s. That is, the lowpass filter's group delay at ω_s is $(T - \tau)$ sec. The ability of LFFAGC to suppress sinusoidal envelope variations can be calculted from the earlier work on EIFBAGC (5.20). The peak to trough ratio of the output ripple, $v_o(t)$, can be written down as:

$$K_o = \frac{1 - LD^2 \cos \omega\tau + D\sqrt{L^2D^2 \cos^2 \omega\tau + L^2 + 1 - 2L \cos \omega\tau - L^2D^2}}{1 - LD^2 \cos \omega\tau - D\sqrt{L^2D^2 \cos^2 \omega\tau + L^2 + 1 - 2L \cos \omega\tau - L^2D^2}} \qquad (8.8)$$

If equation 8.6 represents a wanted envelope variation then the harmonic distortion of $v_i(t)$ at $v_o(t)$ by the circuit can also be calculated from the earlier work on EIFBAGC. For values of $L \ll 1$ then the magnitude, A_n, of the nth harmonic of $v_i(t)$ at the circuit's output is given by:

$$A_n \simeq (D)^n (0.5L)^{n-1} \qquad (8.9)$$

from Appendix 5.

Equation 8.8 can be used for analysing LFFAGC circuits that use non-linear phase lowpass filters. The effect of the time delay mismatch, τ, can be eliminated by using linear phase lowpass filters as described in section 8.1.2. The next section describes the mathematical simplifications that result if $\tau = 0$.

8.11

8.2.2 Perfect Time Delay Matching Equations

When $\tau = 0$, K_o simplifies to K_o' where

$$K_o' = \frac{1 - LD^2 + D|(L - 1)|}{1 - LD^2 - D|(L - 1)|} \qquad (8.10)$$

Consider the use of a perfectly matched linear phase lowpass filter with the amplitude frequency characteristic shown by figure 8.4. The limitations of the passband amplitude ripple extremes (L_u and L_ℓ) are determined by the overall LFFAGC specification for output ripple. Equation (8.10) can be rearranged to give:

$$L_u = \frac{1 - D - K_o - DK_o}{D^2 - D - D^2K_o - DK_o} \qquad (8.11)$$

and

$$L_\ell = \frac{1 + D - K_o + DK_o}{D^2 + D - D^2K_o + DK_o} \qquad (8.12)$$

For example, consider the suppression of a 30 dB sinusoidal fade (D = 0.9387) to within 3 dB of output ripple with perfect time delay matching. Equation 8.11 gives L_u = 1.0187 (+ 0.16 dB) while equation 8.12 gives L_ℓ = 0.9742 (-0.23 dB). The input and output waveforms for this example are shown in figure 8.5. Notice that most of the output ripple occurs at a point corresponding to the input trough. Any absolute time delay difference, T, between the input and output waveforms is not shown for clarity.

The transition region of the LFFAGC circuit extends from B_p to B_s in figure 8.4. For frequencies above B_s the stopband attenuation requirement, L_s, is given by equation 8.9. In general, only a modest stopband attenuation is required. For example, a value of L_s of 0.1 (-20 dB) would cause about -26 dB of 2nd harmonic distortion to the
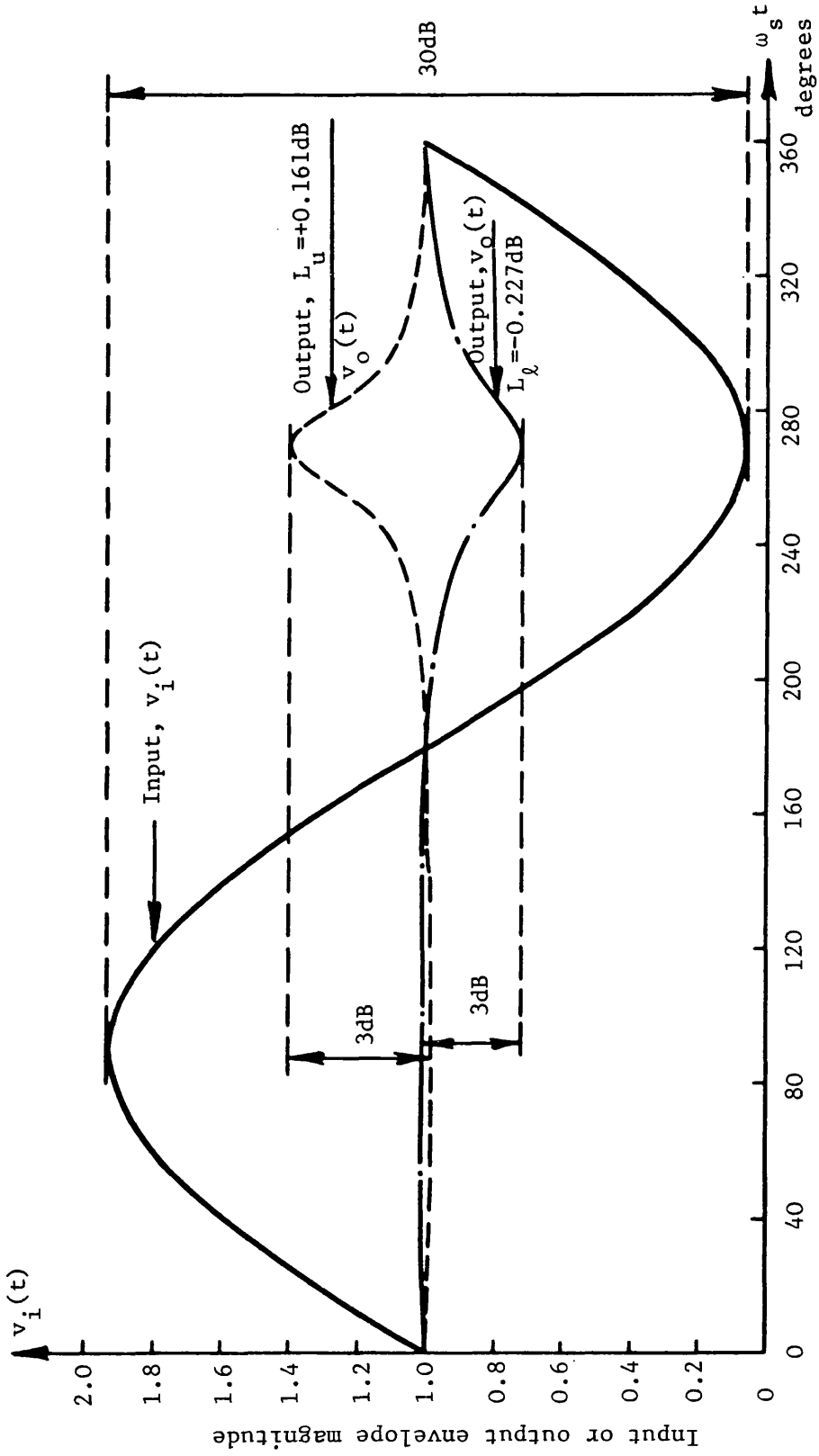
Figure 8.5   Input and output waveforms of the LFFAGC circuit described in the example of section 8.2.2

8.13

envelope of a 100% sinusoidally modulated input envelope.

8.3 Response to Two Tones

This section describes the response of LFFAGC to deterministic AGC
test signal 2. LFFAGC circuits are shown in general to possess a poor
2 tone envelope fade suppression ability and a technique is suggested
for improving the dynamic performance of FFAGC systems.

8.3.1 AGCSIM Predictions using Brickwall Filtering

The response of LFFAGC to deterministic AGC test signal 2 may
be simulated using AGCSIM, the computer programme described in Appendix 6.
Of most interest here are the results obtained using a "brickwall" post
envelope detector lowpass filter in an otherwise perfect LFFAGC system.
A series of runs were performed for 10 dB, 20 dB and 30 dB input fades
to assess the importance of the harmonics of the fundamental envelope
fade rate. The output envelope ripple decreases with increasing lowpass
filter cutoff frequency as shown in figure 8.6. Figure 8.7 shows some
of the computer plots obtained during the 30 dB runs, illustrating the
nature of the output envelope's ripple.

As may be expected, the suppression of the deeper fades with their
relatively high harmonic content requires a relatively high lowpass
filter cutoff frequency to achieve good fade suppression. A comparison
of the 20 dB and 30 dB input results demonstrates this. For example,
a 20 dB input fade is suppressed to better than 3 dB of output ripple
with the lowpass filter cutting off at 4 ω_f. However, a 30 dB input
fade requires the lowpass filter to cut off at 12 ω_f to achieve less
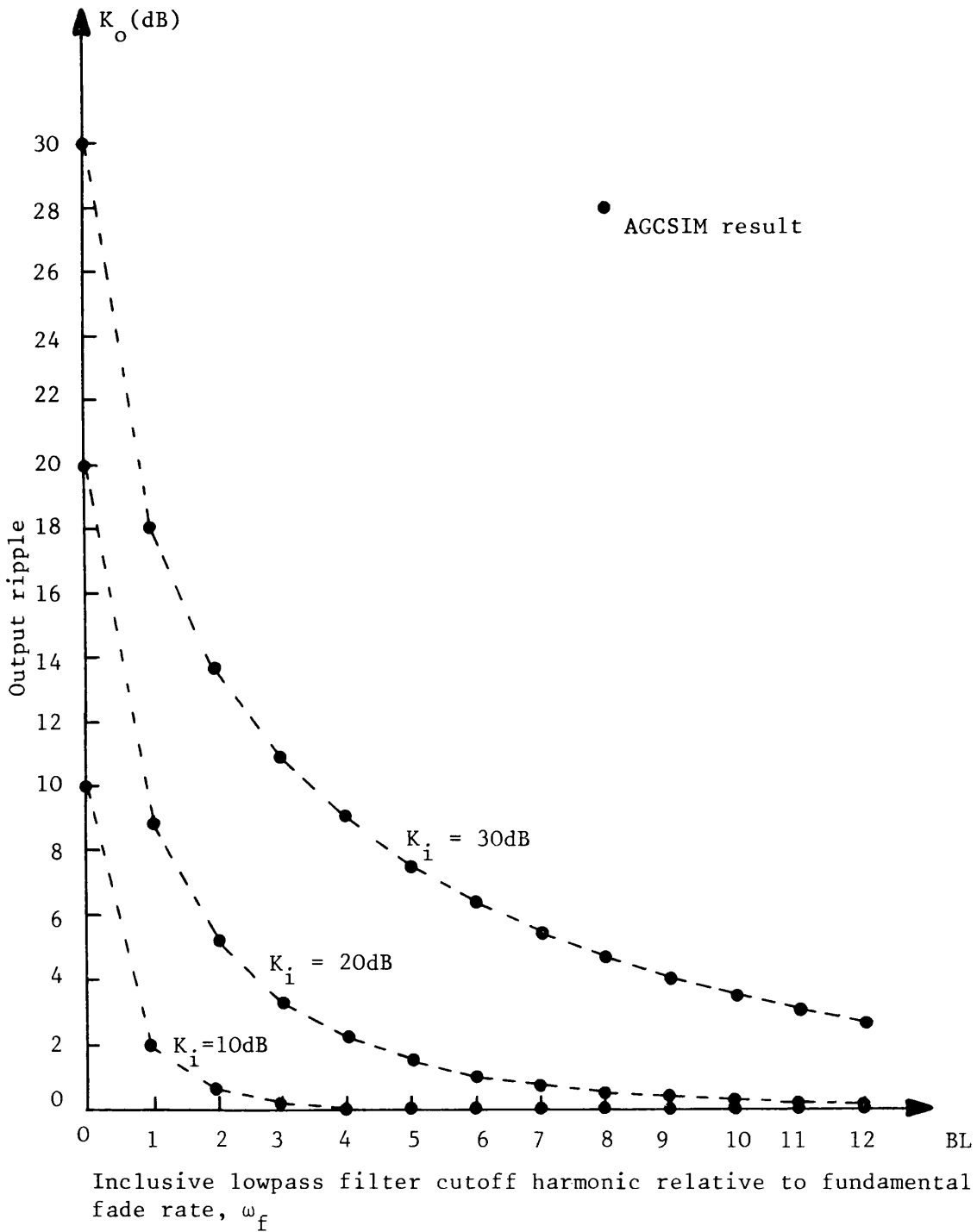than 3 dB of output ripple.

Figure 8.6 Output ripple versus brickwall lowpass filter cutoff
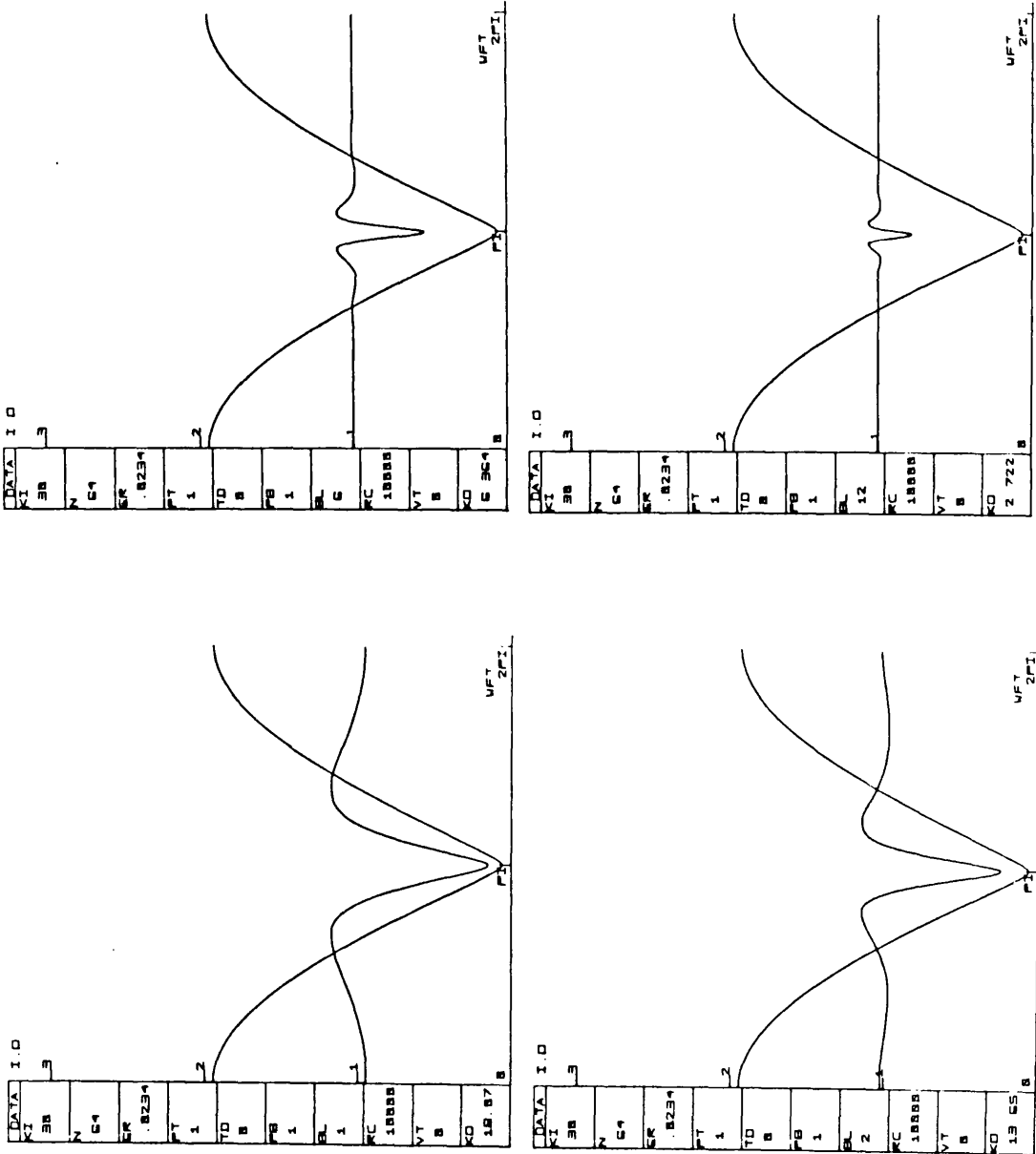   frequency for LFFAGC - AGCSIM results

Figure 8.7   Some results from AGCSIM for the 30dB input runs.   Note BL = inclusive brickwall
lowpass filter cutoff harmonic

8.16

In his analysis of the effect of filtering on the dynamics of
LFFAGC in response to a 2 tone input signal, Hopper (8.6) approximates
the input envelope spectrum by a Taylor series expansion up to the
second harmonic and includes only the dc and fundamental components
in his calculation of envelope suppression. Whilst this may be reasonable
for very shallow fades, the results presented in figure 8.6 from AGCSIM
show that the higher harmonics play an important part in the analysis
of the suppression of deeper fades.

8.3.2 An Improved Feedforward AGC System

LFFAGC has 2 main disadvantages for use in mobile radio systems:

1) It requires an enhanced carrier reference, being unsuitable
in the form described here for use with diminished carrier or pilot
SSB systems.

2) It still requires comparatively large lowpass filter bandwidths
to suppress deep twin path fades, although it is better than EIFBAGC
in this respect.

Both of these disadvantages are due to the main filtering operation
being performed after the envelope detector, in a similar manner to
EIFBAGC. These disadvantages can be overcome by determining the FFAGC
circuit's dynamics by a bandpass filter placed before the envelope
detector. Such an operation is uniquely possible with FFAGC systems,
since it would result in an unstable FBAGC system for reasons discussed
in chapter 6. The detailed theory and operation of FFAGC systems using
bandpass filters is discussed in the next 2 chapters.

CHAPTER 9

BANDPASS FILTER FEEDFORWARD AGC

Bandpass filter FFAGC (BFFAGC) refers to FFAGC systems whose dynamic performance is determined by a bandpass filter preceding the envelope detector. BFFAGC will be shown to be better than LFFAGC in several aspects and adaptable for use with most forms of AM-type modulation. After analysing some of the theoretical properties of BFFAGC, the rest of this chapter describes the design, construction and operation of a circuit for use with a TIB pilot SSB system.

9.1 Optimum Feedforward AGC System

This section describes the basic BFFAGC configuration used in the subsequent analysis. BFFAGC will be shown to be well suited to the suppression of multipath fading.

9.1.1 Basic Configuration

Figure 9.1 shows the block diagram of the BFFAGC circuit used in the following analysis. The input signal is assumed to consist of a carrier or pilot reference along with wanted modulation. The bandpass filter extracts the fading carrier or pilot reference from the composite received signal. The circuit then operates in a similar manner to LFFAGC. If the input were a full carrier AM signal or similar, then the circuit is required to operate at some IF. However, if the input is a tone-in-band (TIB) or tone-above-band pilot SSB signal the circuit can operate on the composite fading signal at baseband.

SIGNAL PATH

NOTE 1   Input and output may be at
         IF or audio - see main text

NOTE 2 $v_i(t)$ and $v_o(t)$ refer to the input and output
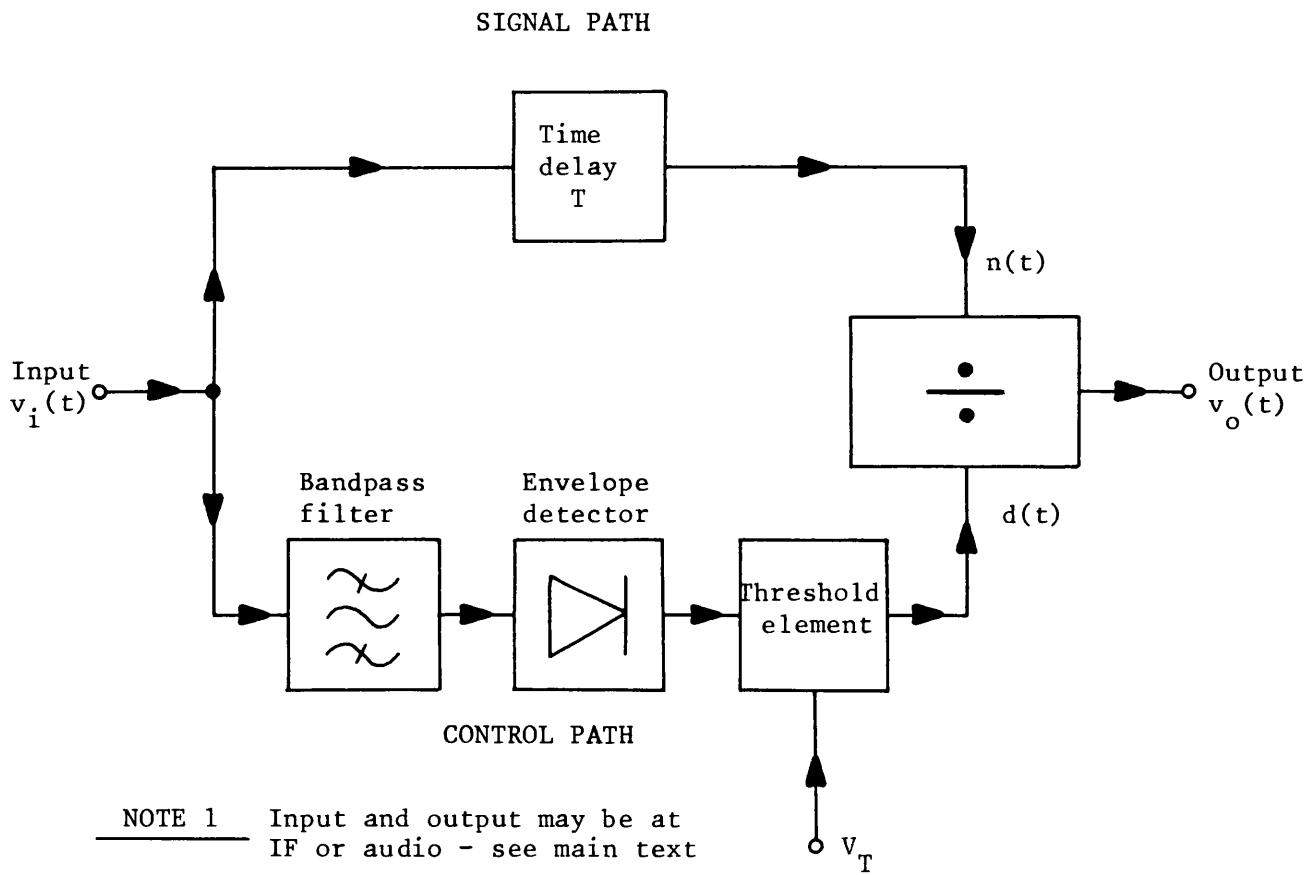   signal's envelopes respectively

Figure 9.1   BFFAGC circuit configuration

The bandpass filter is designed to be just wide enough to pass the "U" shaped incoming carrier or pilot reference spectrum (section 3.2.1) with negligible amplitude or phase distortion. As with LFFAGC, high order constant delay non-recursive digital filters (8.2) perform particularly well in this application. If the carrier or pilot reference spectrum can be exactly centred on the bandpass filter's passband then the filter's bandwidth need only be slightly greater than twice maximum Doppler, $2\omega_d$. BFFAGC is therefore ideally matched to the bandpass nature of pre-detection multipath signals, requiring the smallest control bandwidth of all the AGC systems under discussion to achieve a specified degree of 2 tone fade suppression.

9.1.2 Pre-detection and Post-detection Signal Comparison

Section 8.3.1 showed that the lowpass filter in LFFAGC requires a bandwidth much greater than $2\omega_d$ to include higher harmonics in the division process for good suppression of deep fades. However, suppose that for some reason (e.g. only shallow fade suppression required) acceptable performance could be obtained by using a lowpass filter with a bandwidth just greater than $2\omega_d$. The LFFAGC control bandwidth required to achieve the same maximum fade suppression frequency as BFFAGC appears to be the same. The following discussion shows this is not the case.

Figure 9.2 shows the spectrum of the output of the envelope detector of a LFFAGC circuit used in a full carrier AM system. The fundamental component of the envelope fading spectrum of the carrier is shown extending from dc to $2\omega_d$. Also shown is the spectrum of a tone originally transmitted at ω_ℓ representing the lowest frequency component of the wanted modulation. Evidently, the use of a brickwall
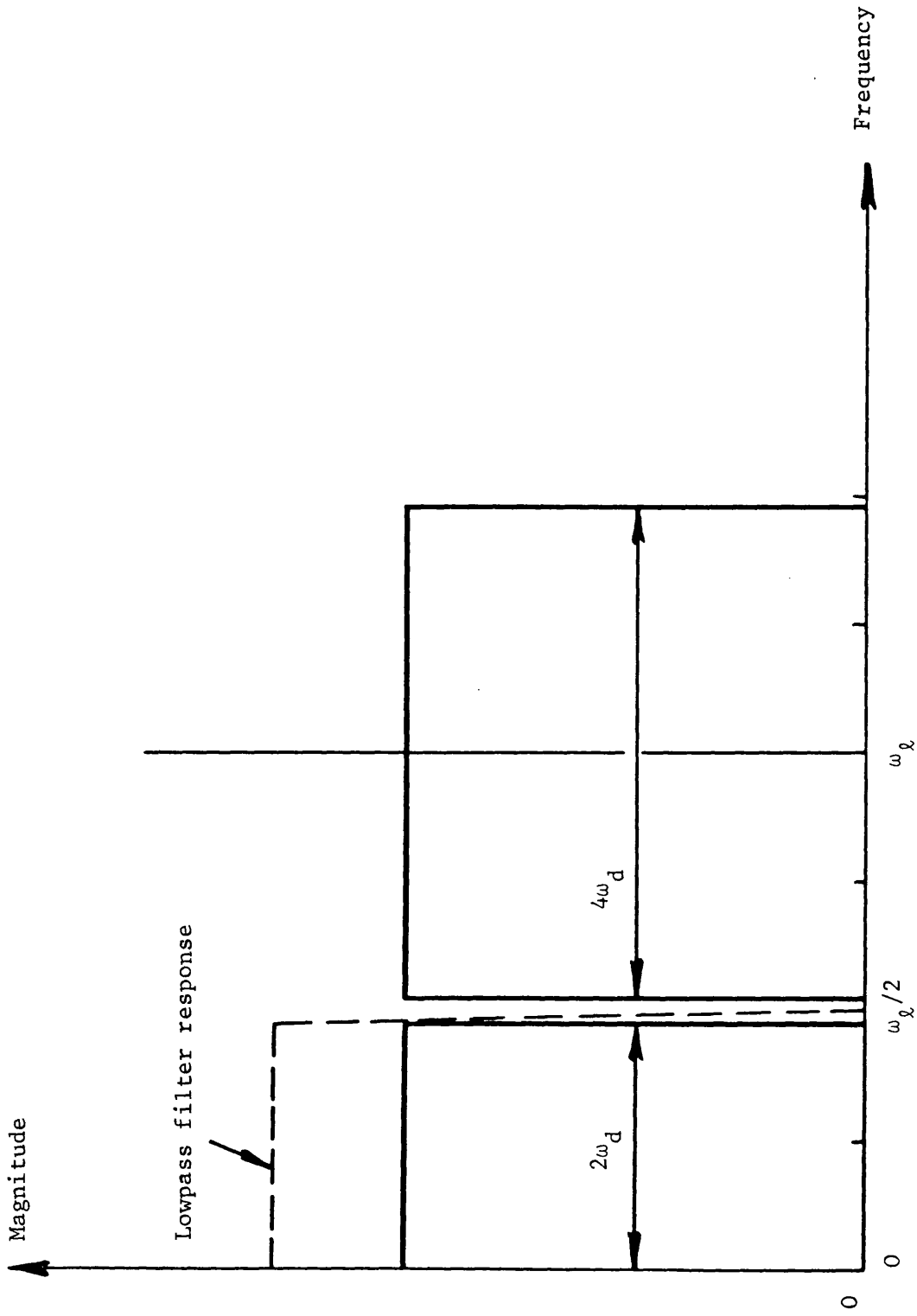
Figure 9.2   Illustration of the maximum frequency of operation of LFFAGC

9.4

lowpass filter will only allow fading with significant energy up to
$\omega_\ell/2$ to be suppressed. Thus, if $2\omega_d$ exceeds $\omega_\ell/2$ the spectra in
figure 9.2 will overlap making suppression of even the fundamental
component of the received signal's envelope variations impossible.
Compare this with the pre-envelope detection spectrum of the same
situation, shown in figure 9.3. It can be seen that unlike the output
of the envelope detector, the fading spectra of the input signals are
still well separated. Indeed, the Doppler spread can be doubled before
the carrier spectrum and modulation spectrum overlap. Therefore, BFFAGC
can suppress envelope fading at fade rates up to ω_ℓ instead of $\omega_\ell/2$ as
with LFFAGC. Of course, the argument is even more in favour of BFFAGC
if the LFFAGC circuit is required to suppress deep fades with their
higher harmonic content.

9.1.3   System Requirements

    The implementation of BFFAGC into an inband tone pilot SSB system
is relatively straightforward and is described in more detail in section
9.3. Other modulation systems such as full carrier AM have additional
requirements since the circuit must operate at some IF. A typical full
carrier AM receiver's final IF frequency may be 455 kHz and it would
be difficult to realise a useful linear phase bandpass filter that is
a few hundred Hertz wide centred on 455 kHz. Probably the simplest
solution is to convert the 455 kHz IF signal down to a much lower IF
(say 5 kHz centre frequency) and implement the circuit at this frequency.
Note that full carrier AM receivers often have a relatively poor final
demodulation frequency accuracy compared to SSB receivers. It may be
necessary to consider frequency control of the full carrier AM receiver's
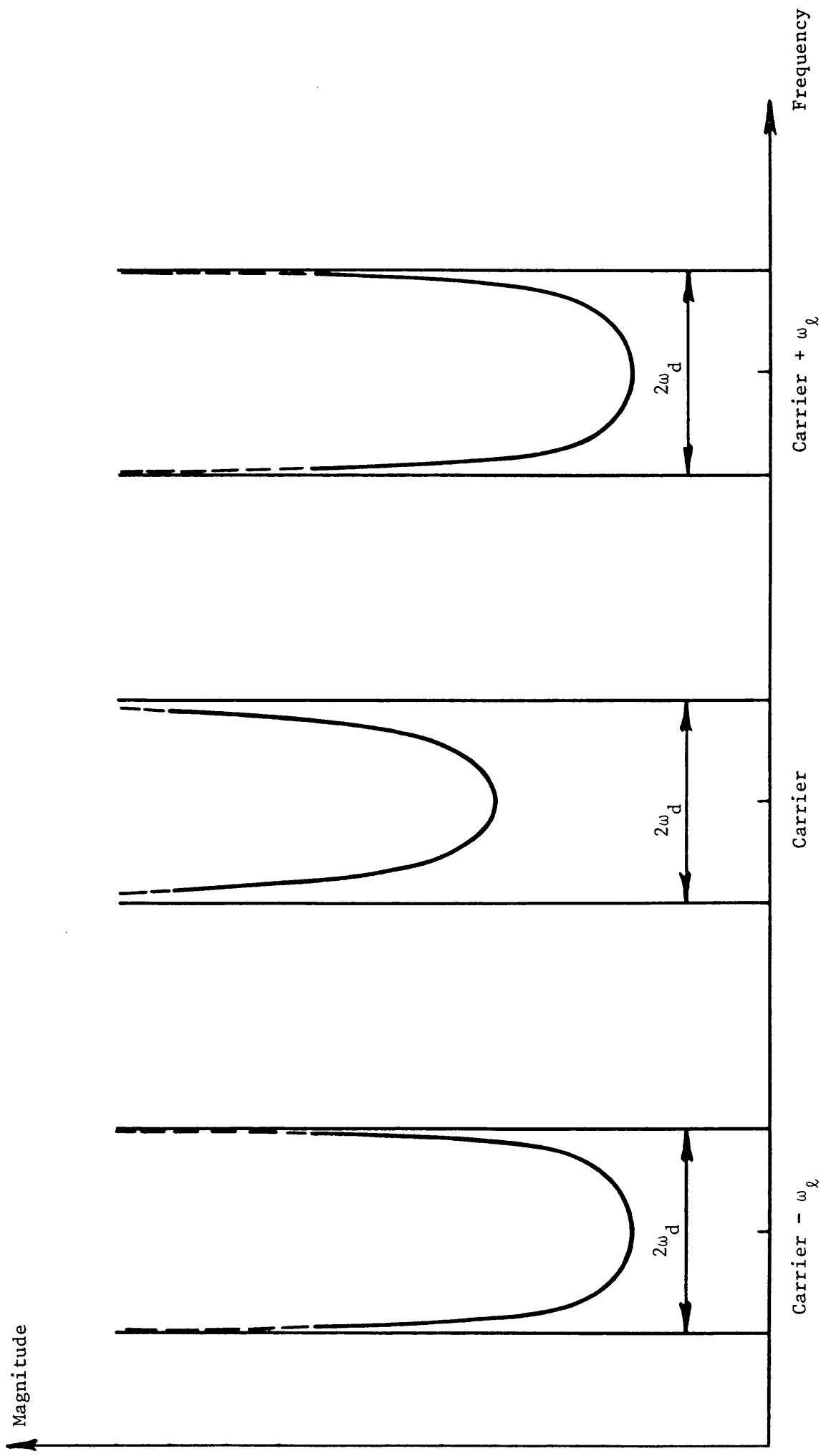local oscillators or synthesisers to enable the carrier to be positioned

Figure 9.3   Pre-envelope detection spectrum of the situation shown in figure 9.2

on the centre of the bandpass filter's passband.

9.1.4 Bandpass Filter Stopband Requirements

In general, the stopband requirements of the bandpass filters depend on the ratio of the carrier or pilot reference to peak modulation signal and for each modulation system (full carrier AM, double sideband diminished carrier, pilot SSB) this ratio will be different. However, it is fairly straightforward to evaluate the stopband requirements to meet a given specification. With full carrier AM systems, symmetrical attenuation of the wanted modulation sidebands of the carrier results in a directly proportional reduction in unwanted gain modulation by the BFFAGC circuit. With pilot SSB systems the interfering tone compression and modulation theory in section 5.4.3 can be used to evaluate the effects of residual speech energy after the bandpass filter.

9.2 Response to Two Tones

This section evaluates the passband requirements of the bandpass filter to meet a specified suppression of the envelope of deterministic AGC test signal 2. All of the circuit elements are assumed to be perfect except for the bandpass filter, and operation is investigated above threshold.

9.2.1 Asymmetrical Bandpass Filter Analysis

The following analysis of the bandpass filter's imperfections has been published elsewhere (9.1), this paper also being included in the published paper section. The analysis calculates the residual envelope modulation of the carrier or pilot reference, c(t), after it has passed through the BFFAGC circuit (neglecting the effects of the threshold

circuit). In the absence of fading the carrier or pilot reference at the input of the circuit is given by:

$$c(t) = E \cos \omega_p(t + T) \qquad (9.1)$$

where ω_p is either the in-band or above-band pilot tone baseband frequency or the final IF of another modulation system. The use of deterministic AGC test signal 2 results in $c(t)$ being represented by $c'(t)$ where:

$$c'(t) = E \cos(\omega_p(t + T) - \omega_1(t + T)) + RE \cos(\omega_p(t + T) + \omega_2(t + T)) \qquad (9.2)$$

This can be expressed as an amplitude and phase modulated signal as follows:

$$c'(t) = E(1 + R^2 + 2R \cos \omega_f(t + T))^{\frac{1}{2}} \cos(\omega_p(t + T)$$

$$+ \tan^{-1} \left[\frac{R \sin \omega_2(t + T) - \sin \omega_1(t + T)}{R \cos \omega_2(t + T) + \cos \omega_1(t + T)} \right] \qquad (9.3)$$

where
$$\omega_f = \omega_1 + \omega_2 \qquad (9.4)$$

The action of the bandpass filter on the envelope of $c'(t)$ is now analysed with the aid of figure 9.4. Figure 9.4a shows $c'(t)$, nominally at ω_p, split into 2 tones representing the signal described above. Figures 9.4b and 9.4c illustrate the terminology used to describe the bandpass filter's amplitude and phase response respectively. The filtered version of $c'(t)$ at the output of the bandpass filter is $F_b(c'(t))$ where:

$$F_b(c'(t)) = EB_1 \cos(\omega_p(t + \tau_1) - \omega_1(t + \tau_1)) + REB_2 \cos(\omega_p(t + \tau_2) + \omega_2(t +$$

$$(9.5)$$

By letting $P = B_2/B_1$ the envelope of $F_b(c'(t))$, $d(t)$, can be written as:

9.8

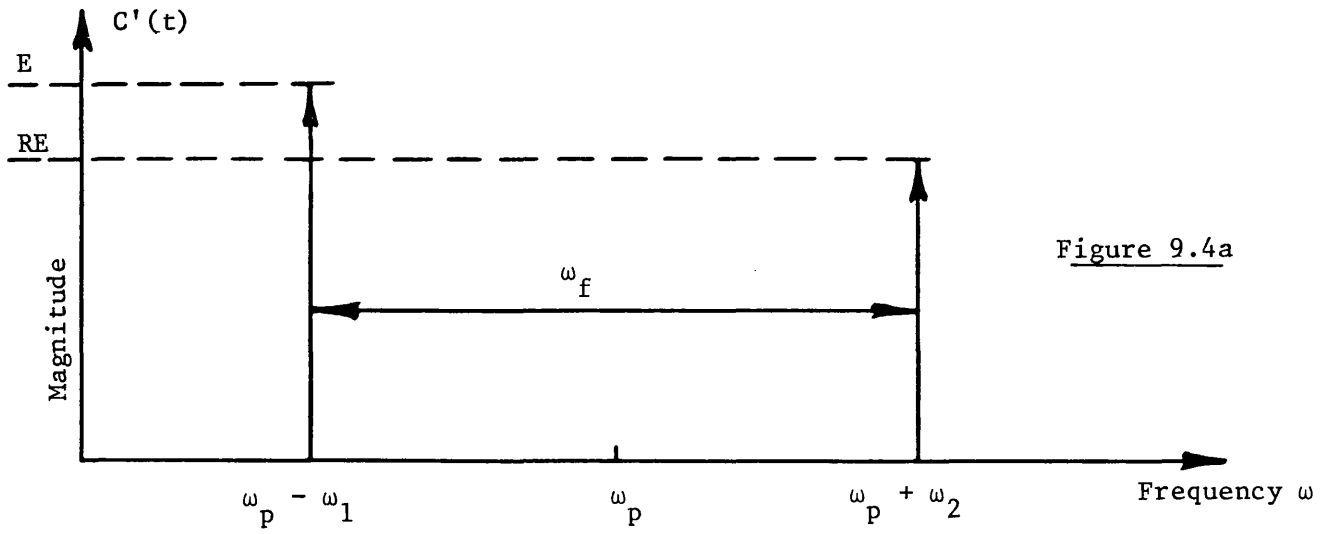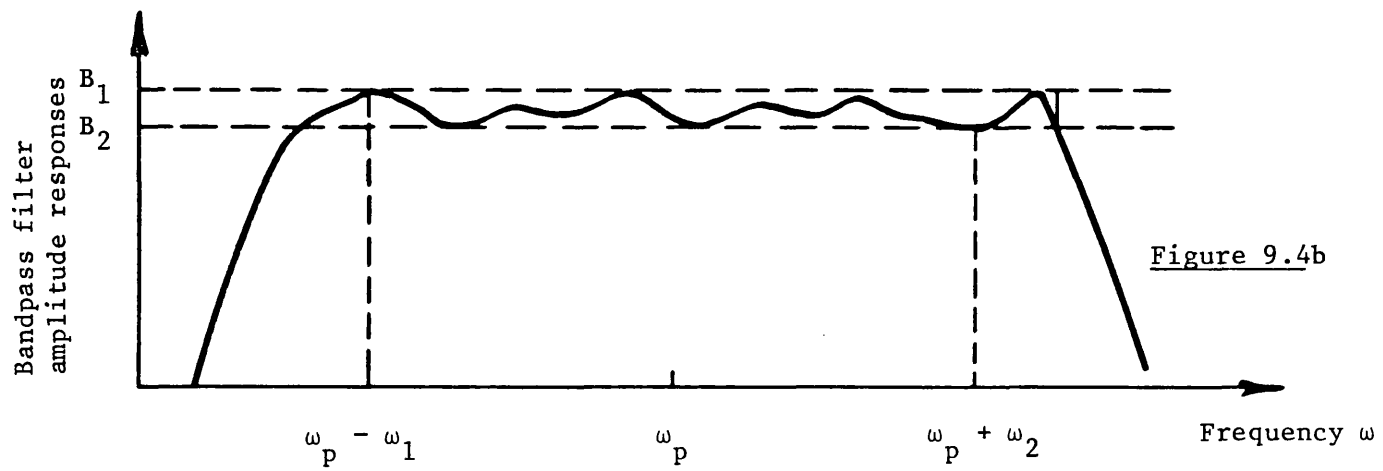Figure 9.4a

Figure 9.4b
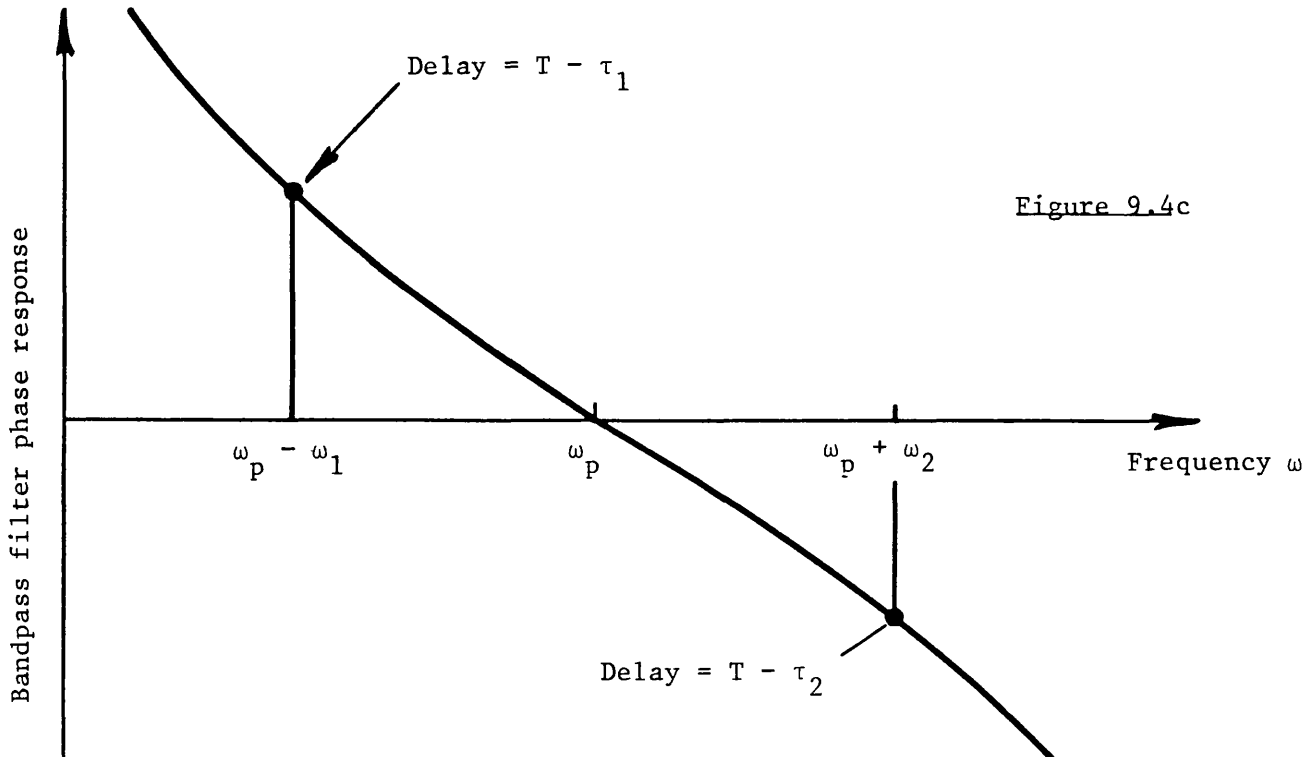
Figure 9.4c

Figure 9.4   Effect of the FFAGC bandpass filter on C'(t)

$$d(t) = B_1 E(1 + P^2R^2 + 2PR \cos(\omega_f t + \omega_1 \tau_1 + \omega_2 \tau_2 + \omega_p(\tau_2 - \tau_1)))^{\frac{1}{2}} \qquad (9.6)$$

The envelope of c'(t) at the output of the BFFAGC circuit, $v_o(t)$, can be derived from equations 9.3 and 9.6 as:

$$v_o(t) = \frac{1}{B1} \left[\frac{1 + R^2 + 2R \cos \omega_f t}{1 + P^2R^2 + 2PR \cos(\omega_f t + \omega_1 \tau_1 + \omega_2 \tau_2 + \omega_p(\tau_2 - \tau_1))} \right]^{\frac{1}{2}} \qquad (9.7)$$

The peak to trough ratio of equation 9.7, K_o, can be found by rewriting it in the form:

$$v_o(t) = \left[\frac{1 + R^2}{1 + P^2R^2} \right]^{\frac{1}{2}} \frac{1}{B_1} \left[\frac{1 + \left[\dfrac{2R}{1 + R^2} \right] \cos \omega_f t}{1 + \left[\dfrac{2PR}{1 + P^2R^2} \right] \cos(\omega_f t + \omega_1 \tau_1 + \omega_2 \tau_2 + \omega_p(\tau_2 - \tau_1))} \right]^{\frac{1}{2}}$$

$$(9.8)$$

Therefore equation 8.8 may be used to predict K_o of $v_o(t)$ providing that after the following substitutions are made:

$$L = \frac{P(1 + R^2)}{1 + P^2R^2} \qquad (9.9)$$

$$D = \frac{2R}{1 + R^2} \qquad (9.10)$$

and $\quad \omega\tau = \omega_1 \tau_1 + \omega_2 \tau_2 + \omega_p(\tau_2 - \tau_1) \qquad (9.11)$

the square root of K_o is taken

9.2.2 Perfect Time Delay Matching Equations

If the signal and control paths are perfectly matched in time delay then equation 9.7 can be simplified to:

$$v_o(t) = \frac{1}{B_1} \left[\frac{1 + R^2 + 2R \cos \omega_f t}{1 + P^2R^2 + 2PR \cos \omega_f t} \right]^{\frac{1}{2}} \qquad (9.12)$$

9.10

The output peak, J_{po}, may be written as:

$$J_{po} = \frac{1}{B_1} \left[\frac{1 + R^2 \mp 2R}{1 + P^2R^2 \mp 2PR} \right]^{\frac{1}{2}} = \frac{1}{B_1} \left[\frac{1 \mp R}{1 \mp PR} \right] \qquad (9.13)$$

The output trough, J_{to}, may be written as:

$$J_{to} = \frac{1}{B_1} \left[\frac{1 + R^2 \pm 2R}{1 + P^2R^2 \pm 2PR} \right]^{\frac{1}{2}} = \frac{1}{B_1} \left[\frac{1 \pm R}{1 \pm PR} \right] \qquad (9.14)$$

with the sign used (plus or minus) depending whether P is greater or less than unity. Therefore the ratio of J_{po} to J_{to}, called K_0'' is:

$$K_0'' = \left[\frac{1 \mp R}{1 \mp PR} \right] \left[\frac{1 \pm PR}{1 \pm R} \right] \qquad (9.15)$$

The sign ambiguity in equation 9.15 can be resolved by expanding it and reformulating so that:

$$K_0'' = \frac{1 - PR^2 + R|(P - 1)|}{1 - PR^2 - R|(P - 1)|} \qquad (9.16)$$

Examination of equation 8.10 for the single tone LFFAGC case and equation 9.16 shows that K_0' and K_0'' are identical expressions if L equals P and D equals R.

Depending on the relative position of the 2 tones inside the band-pass filter, P can take on 1 of 2 values, 1 slightly greater than unity and 1 slightly less than unity. The circuit will therefore tend to overestimate or underestimate the depth of fade respectively. Consequently, the passband ripple of the bandpass filter is only allowed to be at most half of the passband ripple of the lowpass filter in LFFAGC in order to achieve the same worst case degree of fade suppression. For

9.11

example, consider the suppression of a 30 dB 2 tone fade to within

± 3 dB of output ripple with perfect time delay matching. The most

stringent requirement placed on the bandpass filter's specification is

set in meeting the +3 dB output variation, and this in turn results (from

equation 9.16) in a maximum allowable passband ripple of P = 0.16 dB.

This value is the same as the maximum positive amplitude ripple in the

equivalent sinusoidal fading LFFAGC case. Equation 9.16 predicts that

the maximum negative output variation will be 2.2 dB. The input and

output waveforms for this example are shown in figure 9.5.

A comparison has been made between the slew rates of LFFAGC and

BFFAGC when they are suppressing 30 dB sinusoidal and 2 tone input

fades respectively (9.1). The LFFAGC circuit is shown to slew at

(148.6 x f_f) dB/sec where f_f is the input fade frequency in Hz. The

BFFAGC circuit is shown to slew at (431.02 x f_f)dB/sec. Thus, for the

same frequencies and depth of fade, BFFAGC slews much faster than the

LFFAGC circuit. Furthermore, since the BFFAGC circuit can operate at

twice the fading frequency of LFFAGC, the performance improvement is

even more dramatic.

The computer programme AGCSIM, described in Appendix 6, can be used

to simulate BFFAGC and has confirmed the predictions of the output ripple

made in equation 9.16.

9.3   The TIB Pilot SSB BFFAGC Circuit

The TIB Pilot SSB BFFAGC circuit was designed to operate on the

demodulated baseband output of the 457 MHz receiver described in chapter 4.

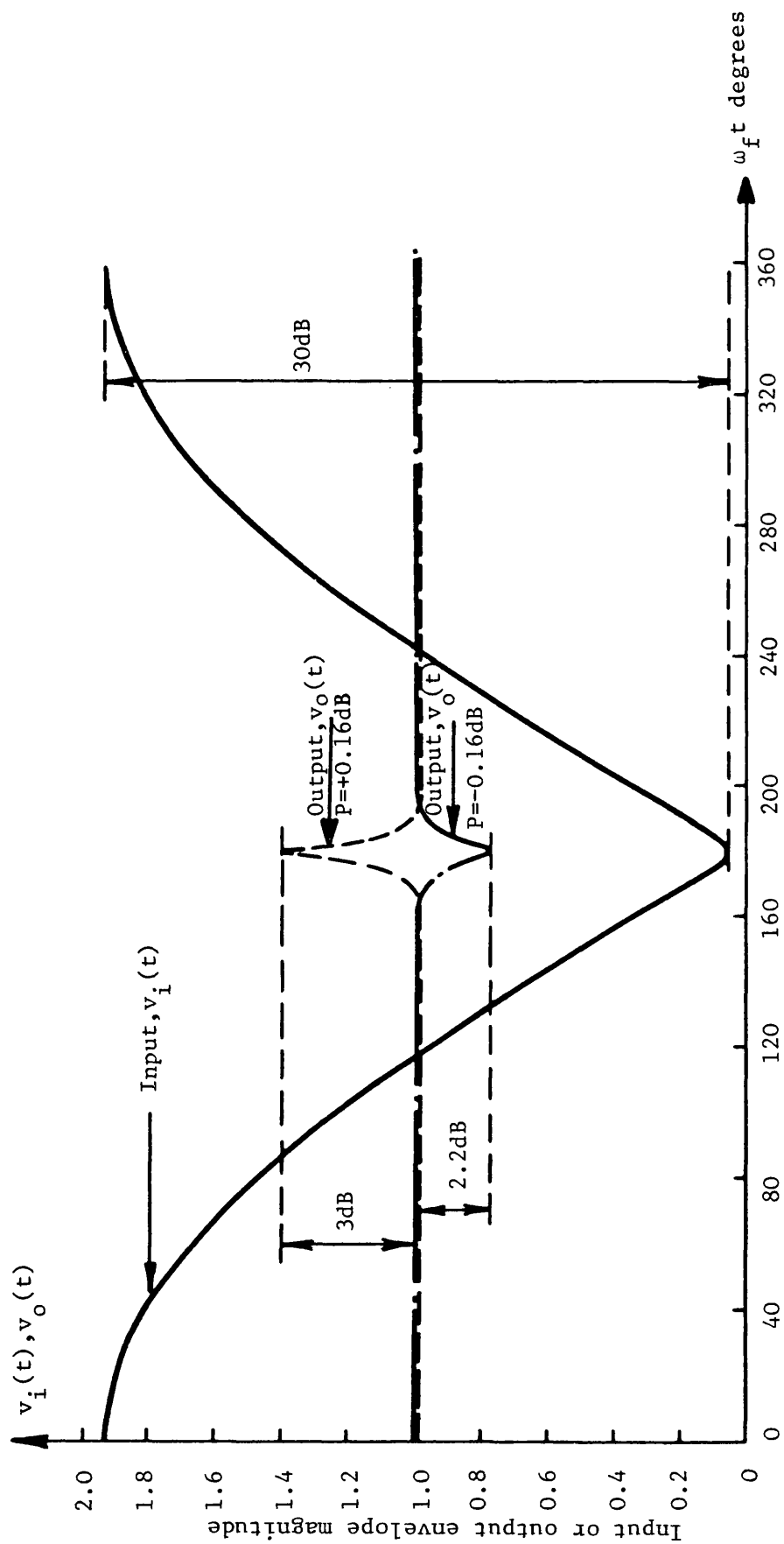A "hardware" approach was adopted, using conventional OP-AMP techniques

Figure 9.5 Input and worst case output waveforms of the BFFAGC circuit incorporating a bandpass filter with 0.16dB passband ripple for a 30dB 2 tone input envelope variation

along with the use of charge transfer device (CTD) technology to realise
the filters and time delay elements (9.2).

9.3.1 General Circuit Description

Figure 9.6 is a general block diagram of the BFFAGC circuit. The
input from the receiver consists of the composite 1.67 kHz pilot plus
speech signal. This is passed through a pre-amplifier and anti-aliasing
filter before being split into the 2 paths. The top path time delay
and bottom path bandpass filter both require clocks. These are derived
from a master crystal oscillator via programmable dividers. The
envelope detector is realised using a precision rectifier and lowpass
filter. The threshold circuit on the divider's denominator is controlled
by a separate unit that also monitors the denominator voltage. The
circuit's output then goes back into the receiver. Alternatively the
circuit can operate on tape recordings of the composite fading signal.

2 versions of the circuit were constructed. The first was a
prototype used to estimate various circuit parameters (such as an approp-
riate master oscillator frequency) and checked that acceptable performance
could be achieved. The second version of the circuit was laid out on
a set of printed circuit boards and is the version described in more
detail in the following text.

9.3.2 Programmable Clock Generator

A total of 4 independently programmable clocks were required to be
derived by direct division of a 4.131 MHz master oscillator. The master
oscillator was built using a crystal controlled CMOS 4049 gate oscillator.
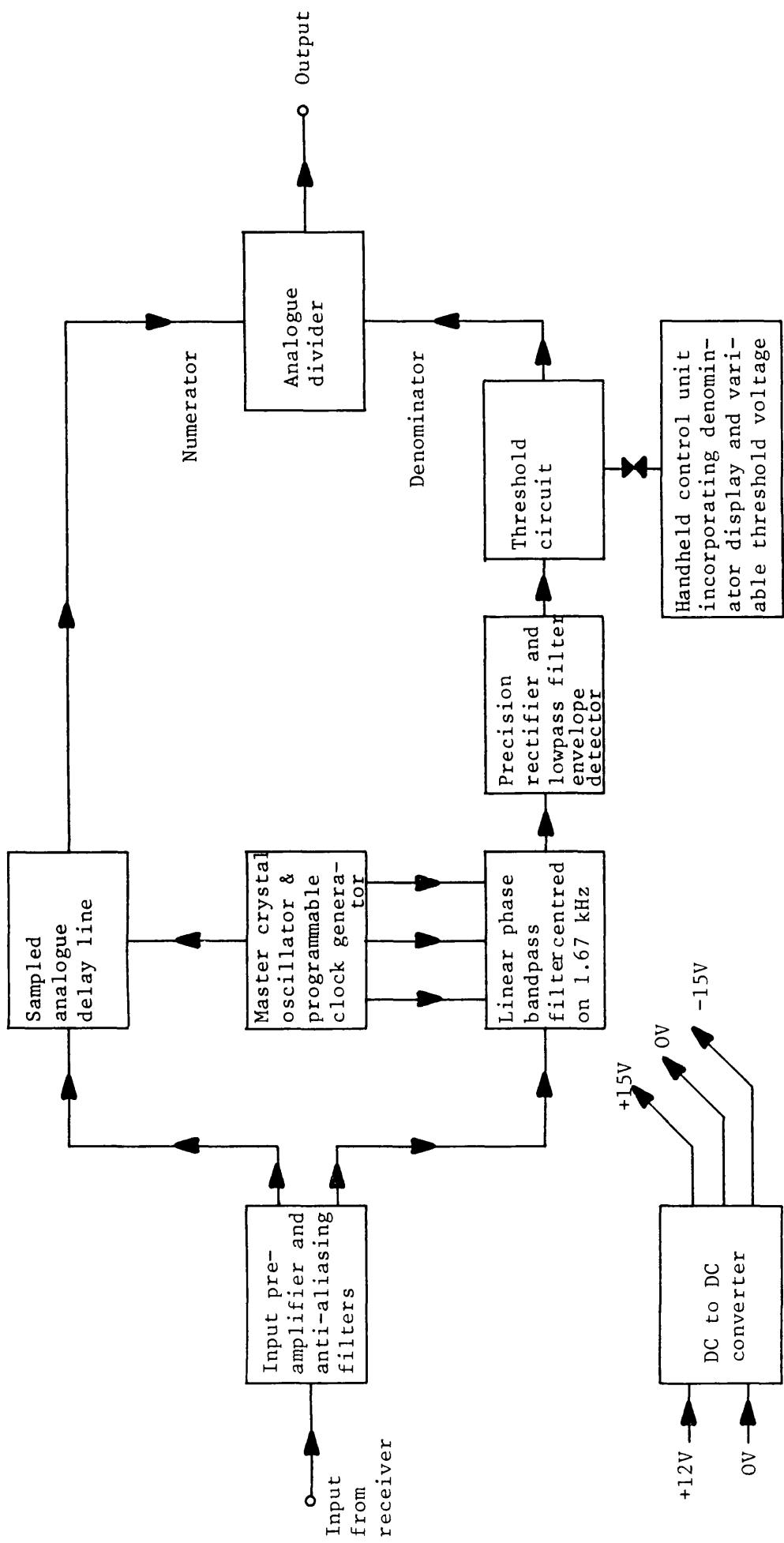The output of the master oscillator was divided to the required frequency

Figure 9.6 General block diagram of BFFAGC circuit

using CMOS 40103 programmable dividers. The 4 dividers could each be
independently programmed to divide between any number from 2 to 256 by
DIL switches. Each output was buffered and applied to the appropriate
device.

There is an important advantage in deriving the top path time delay
and bottom path bandpass filter's clock from the same master oscillator.
The time delay through all these devices is inversely proportional to
the clock frequency. Therefore, if the master oscillator frequency
drifts slightly then the resultant small change in top path delay time
is approximately matched by an equal bottom path time delay change.
The cancellation of the differential time delay drift is not exact since
the envelope detector incorporates a non-clocked lowpass filter, as does
the time delay device.

9.3.3 Input Circuitry and Time Delay

The anti-aliasing lowpass filter placed after the TL071 OP-AMP input
pre-amplifier is there primarily for the sampling analogue delay line.
The anti-aliasing filter used two TL071 OP-AMPs to form an active 4th
order Butterworth lowpass filter with a cut-off frequency of 8.8 kHz.
The output of the filter was split and buffered into 2 paths, 1
going to the bottom path bandpass filter and 1 going to the top path
time delay. The time delay element was realised using an SAD-512D, an
N-channel silicon gate bucket-brigade device. This was followed by a
further clock smoothing 4th order Butterworth lowpass filter, again
breaking at 8.8 kHz, before being put into the divider's numerator.
Care was taken to ensure that the 2 Butterworth filters introduced
negligible amplitude or phase distortion to the baseband (to 3 kHz)

signal for reasons that are discussed in the next chapter.

9.3.4 Bandpass Filter

The most frequency selective element of the bandpass filter was realised using an R5602-3 64 stage split electrode CTD transversal filter. There is no provision to alter its transfer characteristic and fortunately the pre-programmed device gave an acceptable performance. Its centre frequency is determined by an externally applied clock and it possesses a linear phase response. However, the device has a relatively low sampling rate, 4 times its centre frequency. The aliasing that occurs on its input and the clock output waveform could not be satisfactorily suppressed using conventional analogue lowpass filters. These would have introduced unacceptable amplitude and phase distortion into the bandpass filters transfer characteristic. Instead, it was noticed that relatively wide conventional analogue bandpass filters possessed negligible amplitude or phase distortion around their centre frequency, over the R5602-3 passband, while giving good attenuation of frequencies above the Nyquist rate. Therefore, 6 pole Chebyshev full octave bandpass filters were used as input anti-aliasing and output clock smoothing filters for the R5602-3.

The full octave bandpass filters were conveniently available as single chip devices, the R5606 full octave switched capacitor bandpass filter. Although the R5606 also required a clock to determine its centre frequency, it has a much higher sampling rate of 54 times its centre frequency. The input anti-aliasing and output clock smoothing filters required for the R5606 in turn, can therefore be realised using simple single pole RC low-pass filters. The circuit diagram of the complete bandpass filter is shown in figure 9.7.
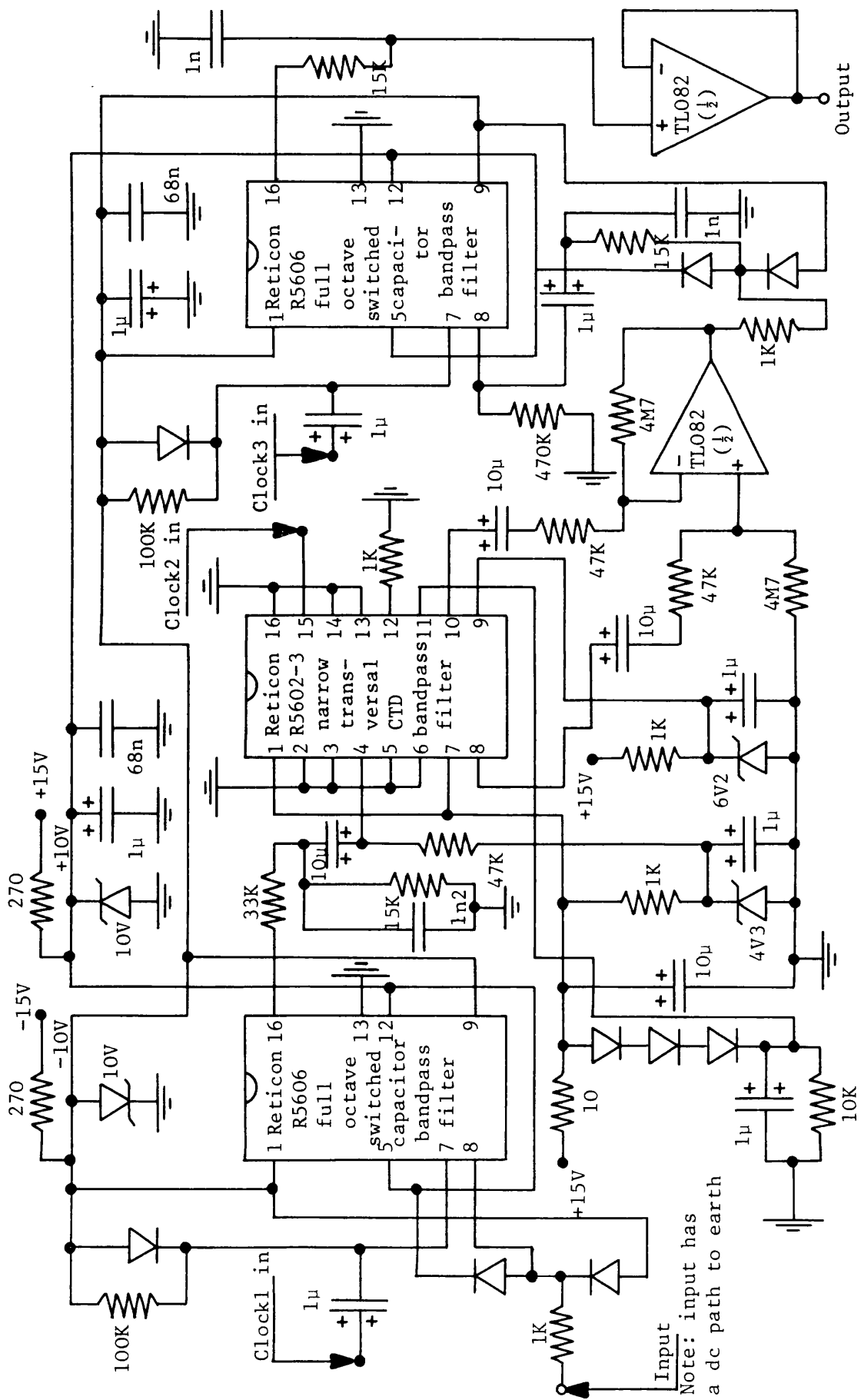
Figure 9.7 The bandpass filter circuit diagram

9.18

9.3.5 Envelope Detector, Threshold and Divider Circuits

The envelope detector following the bandpass filter was realised using a precision rectifier and lowpass filter. The precision rectifier was based on the same design as used in the EIFBAGC circuit described in section 5.2.6 (5.19), and was constructed using TL071 OP-AMP devices. The lowpass filter following the precision rectifier's primary task is to attenuate the unwanted components of the fullwave rectified pilot, leaving just the signal's envelope. Appendix 9 analyses the lowpass filter's requirement. (Note that the theory in Appendix 9 also applies to EIFBAGC circuits where the lowpass filter is the first order loop filtering operation). The residual components of the rectified pilot tone passing through the lowpass filter cause unwanted modulation of the numerator signal, and odd harmonics of the pilot tone to appear at the divider's ouput. Appendix 9 shows that to a first approximation, the ratio of the 3rd harmonic of the pilot tone to fundamental at the divider's output is given by:

$$\text{3rd Harmonic Distortion} = 20 \log_{10}(a/3) \text{ dB} \qquad (9.17)$$

where a is the gain of the lowpass filter at twice the pilot frequency, $2\omega_p$. A second order Butterworth lowpass filter was used in the circuit, -3 dB at 340 Hz, with an attenuation a = 0.0104 at 3.3 kHz. This gave a 3rd Harmonic of the pilot -49 dB with respect to the fundamental component at the divider's output.

The threshold circuit used on OP-AMP and diode to realise a "perfect" diode (9.3), the threshold voltage being applied externally from the hand held control unit. The analogue divider was built using an AD534JD laser trimmed precision multiplier IC.

9.19

9.3.6 Printed Circuit Board Layout

The aforementioned circuitry was assembled on 3 printed circuit boards (PCB) that could be incorporated into the back of the UHF SSB receiver. A photograph of the 3 boards before final assembly is shown in figure 9.8. The top board contains the master crystal oscillator and 4 programmable dividers. The divider programming switches are set at the values found by experiment to give the best circuit performance. The centre board has the input circuitry (top left), time delay device (top centre) and bandpass filter (bottom) built on it. The bottom board contains the envelope detector, threshold and divider circuits. The dc to dc converter enables all the circuitry to be powered off the UHF receiver's internal battery.

9.3.7 Hand-Held Control Unit

A small hand-held control unit was built to enable manual control of the threshold voltage and monitor the divider's denominator. The threshold voltage could be continuously adjusted from zero to twice the nominal dc denominator voltage. The unit could also disable the bottom path by applying a fixed control voltage to the denominator, preventing the circuit from suppressing any fading. The denominator and threshold voltages are displayed on 2 light emitting diode bar arrays.

The complete assembled and boxed PCB and hand held control unit are shown in the photograph in figure 9.9. After installing the main unit in the back of the UHF SSB receiver, the hand held control unit allowed convenient monitoring and control of the circuit's operation.
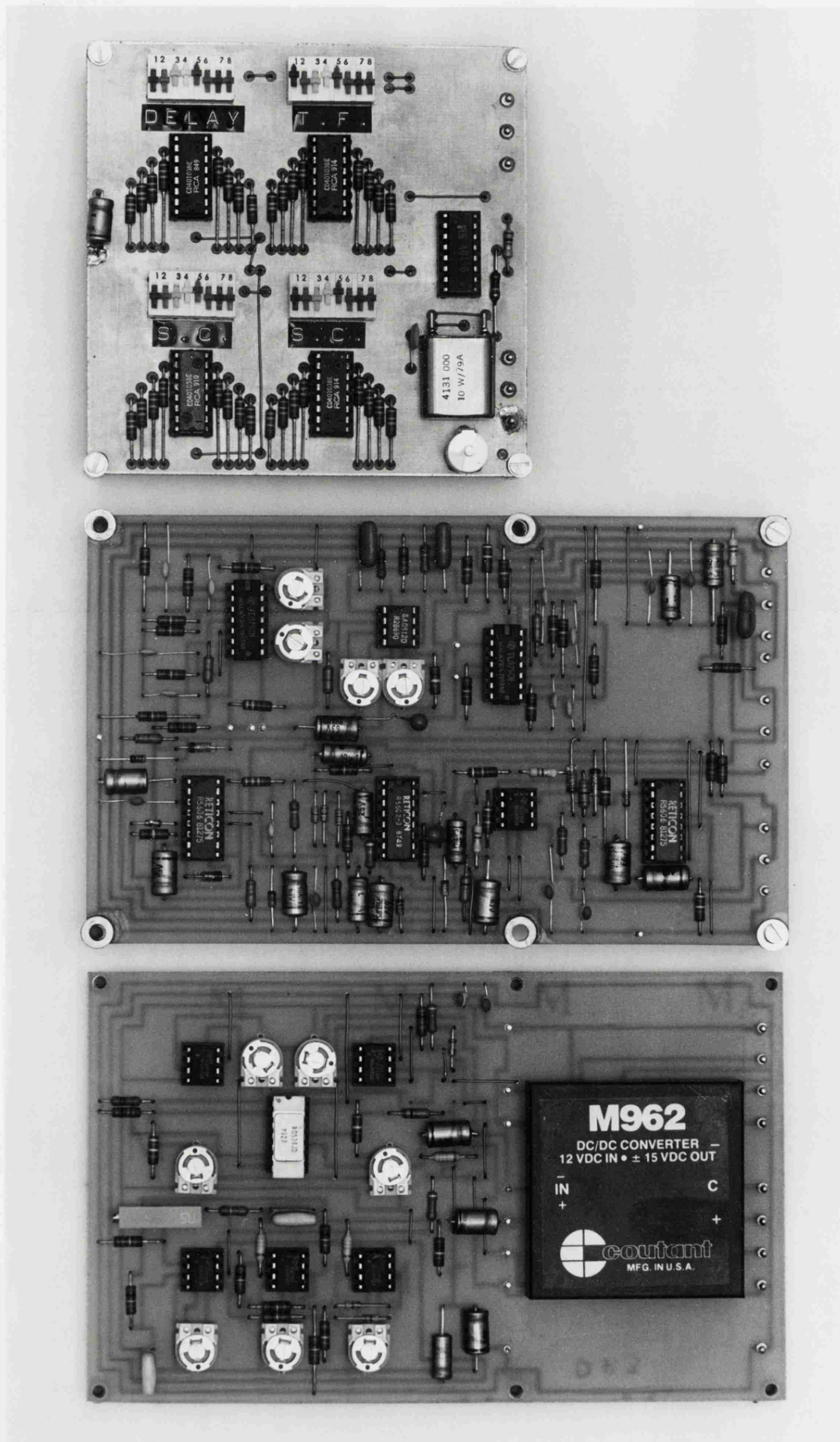
9.20

<u>Figure 9.8</u> Photograph of the 3 BFFAGC PCB before final assembly
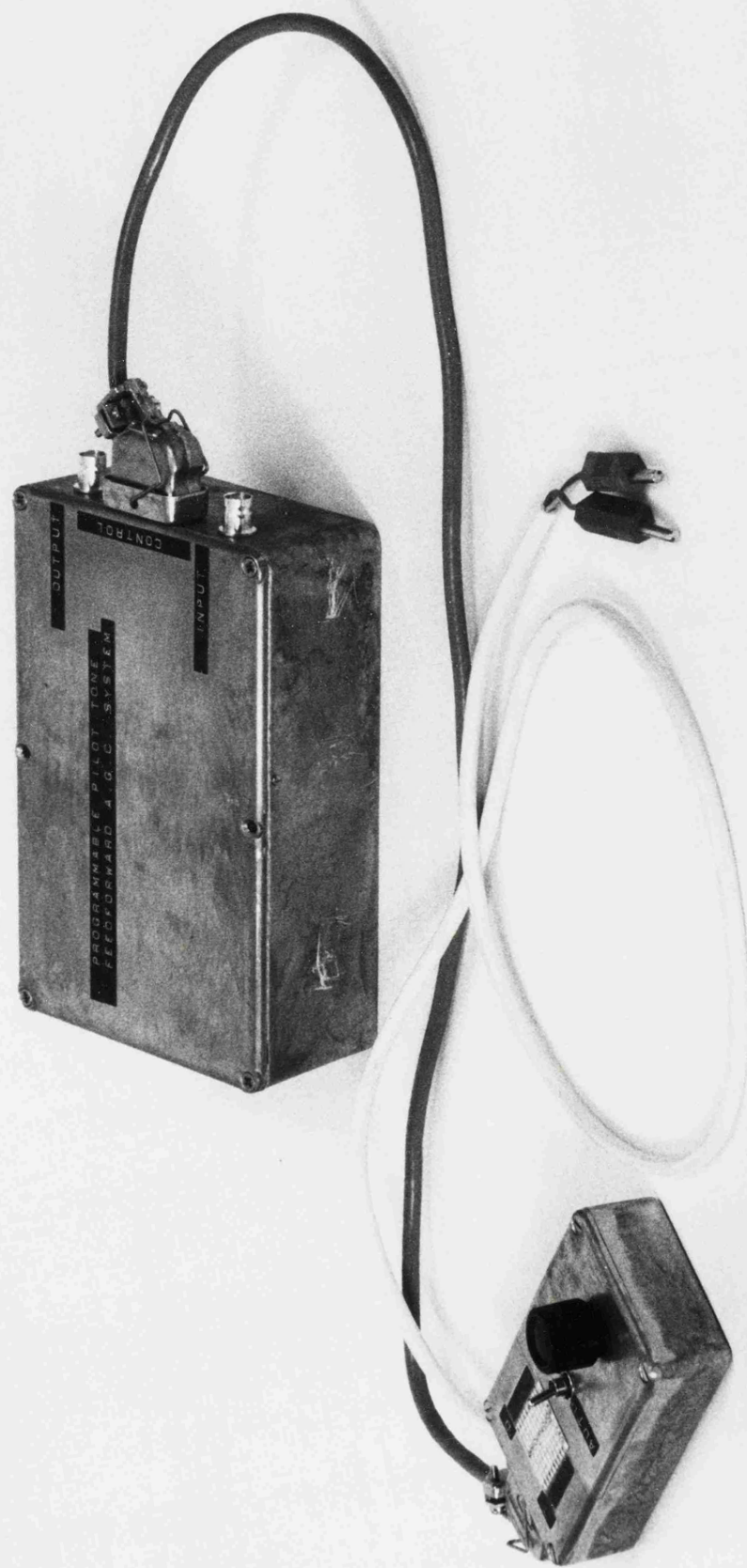
Figure 9.9 Photograph of the complete assembled BFFAGC circuit and hand-held control unit

9.3.8 Measured Circuit Performance

The following performance figures were obtained for the PCB version of the circuit shown in figures 9.8 and 9.9.

i) Static Performance

The nominal level of pilot tone delivered to the input of the circuit from the UHF SSB receiver is 0.5V peak to peak (0 dB reference), for which the circuit delivers 0 dB of pilot at the divider's output. With pilot and speech at the circuit's input, both signal and control paths had a +6 dB overload margin. With 0 dB of pilot at the input, the top path signal to noise ratio at the divider's numerator is 45 dB (55 dB for a peak speech tone). The bottom path signal to noise ratio at the divider's denominator is 55 dB. The total circuit's power consumption is 4.5 Watts at 12 Volts. The clock frequencies (master oscillator divide ratios) were set to the following values to the various devices:

   a) Delay line: 72.473 kHz ($\div$ 57). This results in a time delay of 7.065 mS.

   b) Transversal Bandpass Filter: 27 kHz ($\div$ 153). The filter then has a sampling frequency of 6.75 kHz.

   c) Switched Capacitor Bandpass Filter: 165.24 kHz ($\div$ 25).

ii) Bandpass Filter Characteristic

The amplitude/frequency response of the bandpass filter is shown in figure 9.10. Figure 9.10(a) shows the response in detail around the pilot frequency, while figure 9.10(b) shows the overall response. The response is not ideal for a BFFAGC circuit, but gave an acceptable dynamic performance.
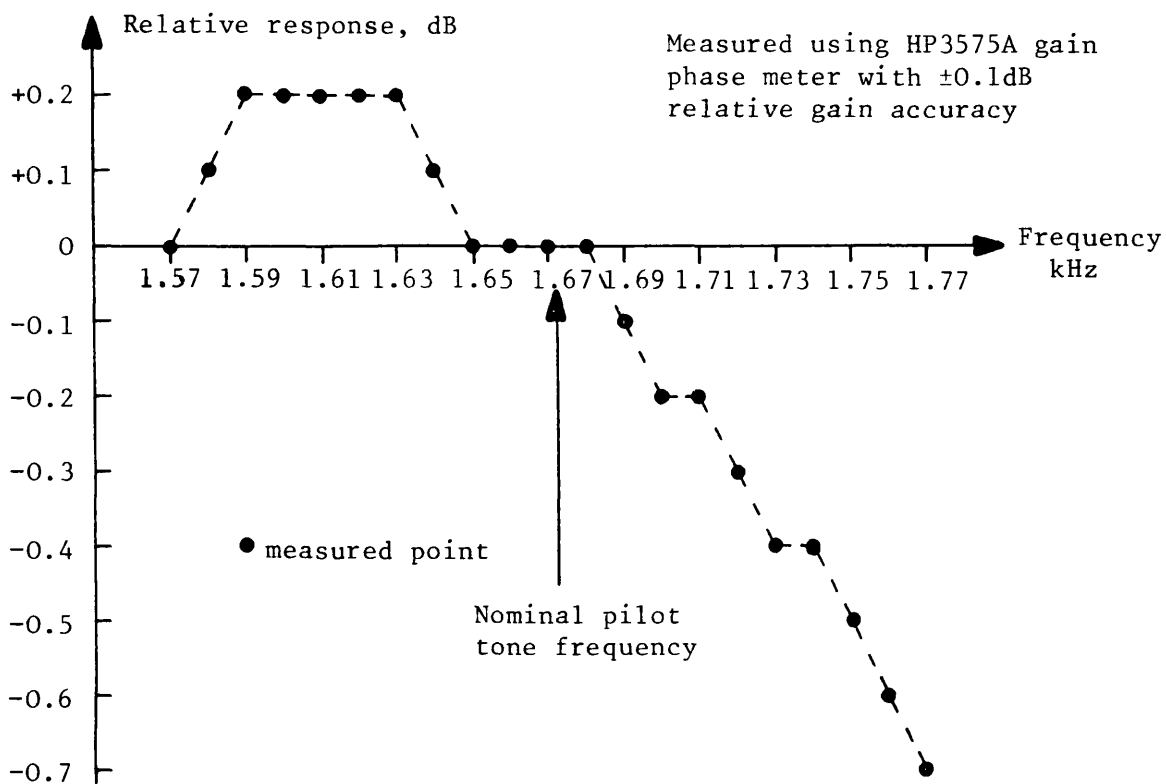
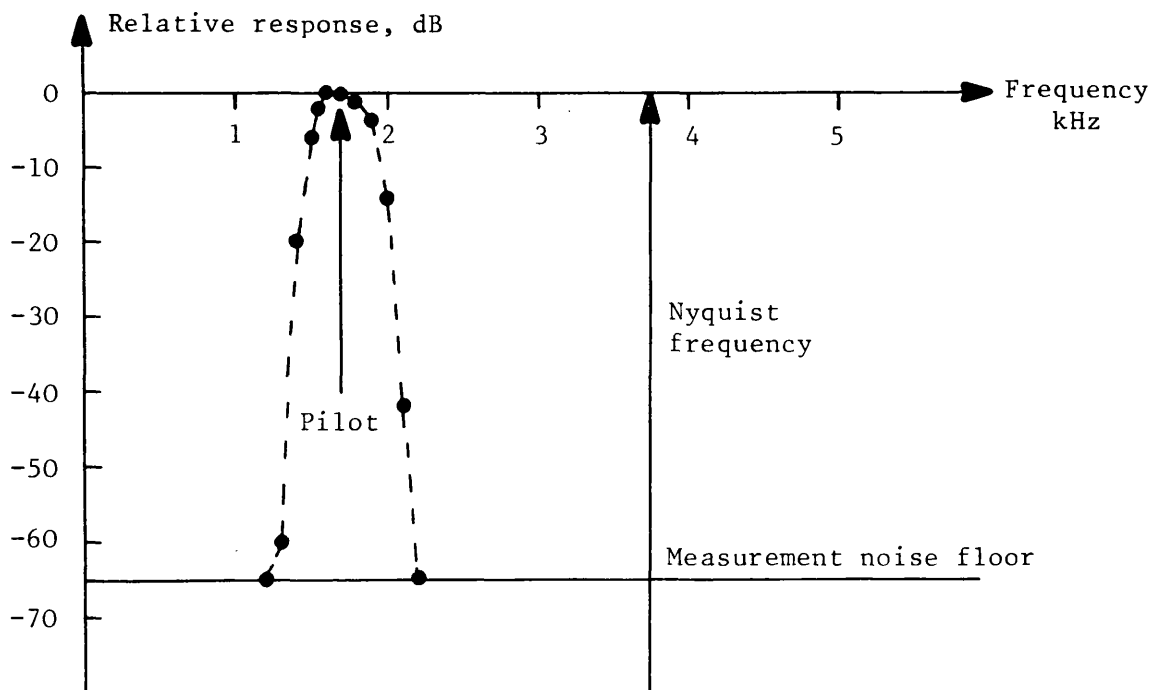Figure 9.10(a)   Response in detail

Figure 9.10(b)   Overall response

Figure 9.10   Amplitude frequency response of bandpass filter

iii) Dynamic Performance

The dynamic performance of the circuit is determined primarily by the bandpass filter, although the precision rectifier lowpass filter also had a slight effect. The 2 tone envelope fade suppression ability was measured as follows:

The output of 2 signal generators were summed together and connected to the circuit's input. Tone 1 was 500 mV peak to peak, tone 2 was 469 mV peak to peak generating a fade envelope 30 dB peak to trough. Table 9.1 gives the measured envelope output ripple in decibels for various tone frequencies.

The sinusoidal fade suppression ability of the circuit was also measured for a 30 dB fade with a pilot at 1.67 KHz. The residual envelope modulation was less than 3 dB for all frequencies below 94 Hz.

During the sinusoidal modulation and 2 tone tests the residual output envelope modulation was similar to those waveforms in figures 8.5 and 9.5, indicating a good top and bottom path time delay match. The main cause of the residual output envelope modulation was the bandpass filter, but the lowpass filter (9.4), circuit offset voltages and other imperfections also contributed to the overall measured results.

9.4 Response to Field Trial Data

This section describes some of the typical results obtained during field trials. The BFFAGC was installed in the back of the UHF SSB receiver for these results and the input and output waveforms were recorded in the field.

Tone 1 Frequency, kHz

	1.57	1.59	1.61	1.63	1.65	1.67	1.69	1.71	1.73	1.75	1.77
1.57	–	3.2	3.6	4.6	5.2	5.5	6.2	8.2	8.6	8.7	10
1.59	2.7	–	2.0	2.0	3.9	4.5	5.3	6.6	7.5	8.3	8.6
1.61	2.6	1.0	–	1.3	1.6	3.0	3.6	5.8	6.2	7.9	8.5
1.63	2.6	3.1	1.4	–	1.0	1.9	3.0	4.6	5.7	5.7	7.3
1.65	2.6	2.8	2.9	2.4	–	1.4	2.2	2.8	4.5	6.0	6.6
1.67	2.9	3.0	2.8	2.6	2.6	–	1.7	1.4	3.7	4.6	4.8
1.69	3.1	2.9	2.8	3.0	3.0	2.7	–	0.6	1.2	2.7	4.3
1.71	2.8	2.8	2.9	3.2	3.6	3.0	2.8	–	1.7	1.8	3.2
1.73	3.0	2.4	2.8	3.4	3.2	3.4	2.9	2.6	–	1.1	1.8
1.75	3.2	2.6	2.7	2.9	3.3	3.4	3.0	2.3	1.9	–	1.5
1.77	2.9	2.7	2.7	2.7	3.3	3.7	3.6	3.0	3.1	2.7	–

Tone 2 Frequency, kHz

Table 9.1   Measured 2 tone envelope fade suppression
30 dB input fade, output ripple in decibels

9.26

9.4.1 Typical Results

The results plotted in figures 9.11-9.20 were obtained as follows:

Both the 1.67 kHz and a 3 kHz tone representing a speech component were transmitted. The car containing the receiving system was driven at different speeds over the same piece of road, the plots all being taken at approximately the same position (driving from the west, just before the position marker (A) on figure 4.11). The received signal strength was about 30 dB above 1 μV and the BFFAGC threshold voltage was set to -20 dB below the average input signal level. The receiver's EIFBAGC circuit and PLL were switched in for these results.

In order to plot the results as shown, the recordings of the input and output composite waveforms were passed through 2 @ 400 Hz wide bandpass filters to separate the 1.67 kHz pilot and 3 kHz tone. They were then passed through a wideband envelope detector prior to plotting the envelopes as shown. Figures 9.11-9.19 show the general effects of increasing the car speed from 16 km/hr to 128 km/hr (10 mph to 80 mph). These plots were made by sampling the envelope at 100 μS per point with a total run time of 409.5 mS. Figure 9.20 shows a much longer run at 80-96 km/hr (50-60 mph), sampling the envelope at 2 mS per point with the total run time lasting 8.14 seconds. In all of these plots, the horizontal axis is time and both plus and minus the envelope is plotted linearly on the vertical axis.
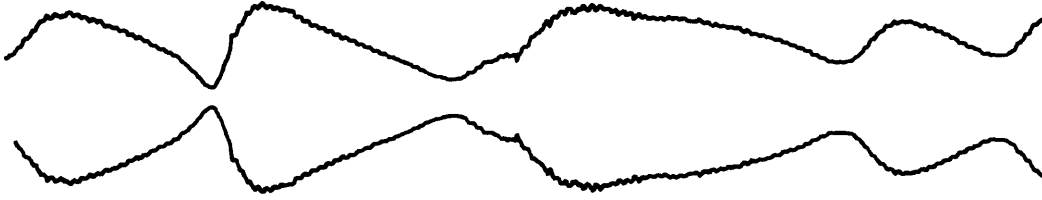
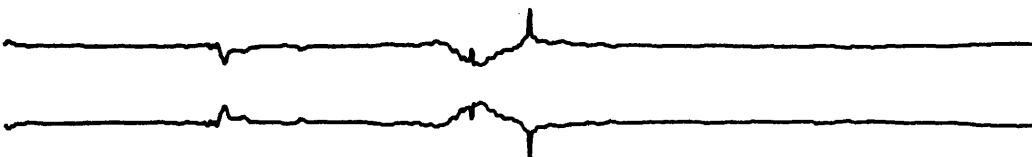Figure 9.11   BFFAGC 409.5 mS field trial result
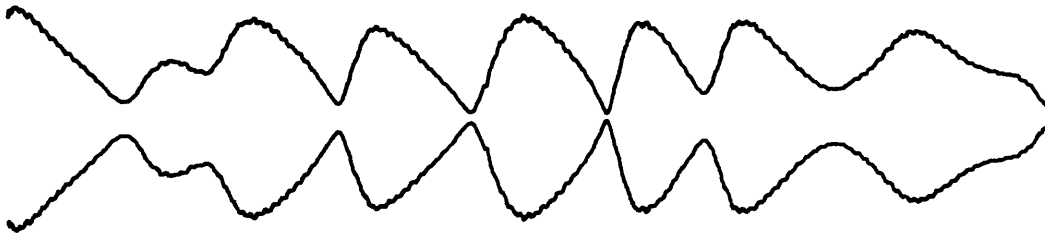
Figure 9.12   BFFAGC 409.5 mS field trial result

Figure 9.13 BFFAGC 409.5 mS field trial result

1.67 kHz PILOT INPUT

1.67 kHz PILOT OUTPUT

3 kHz TONE INPUT

3 kHz TONE OUTPUT

THRESHOLD −20 dB	SPEED 40 MPH	SIGNAL 30 dB ABOVE 1 μV

Figure 9.14 BFFAGC 409.5 mS field trial result

1.67 kHz PILOT INPUT

1.67 kHz PILOT OUTPUT
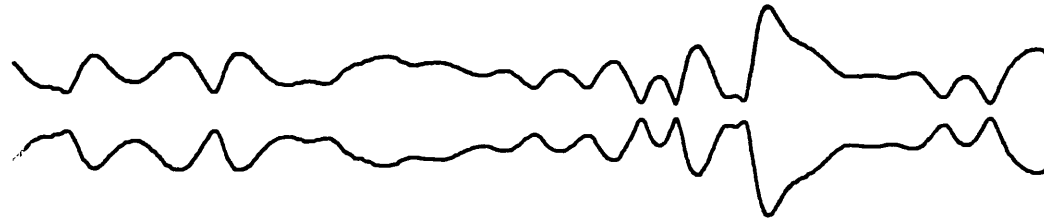
3 kHz TONE INPUT
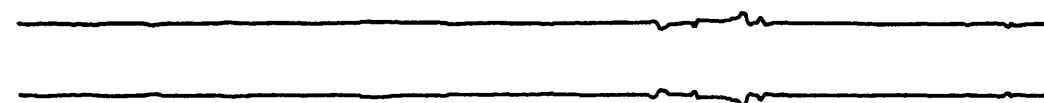
3 kHz TONE OUTPUT

THRESHOLD -20 dB	SPEED 50 MPH	SIGNAL 30 dB ABOVE 1 μV

Figure 9.15   BFFAGC 409.5 mS field trial result
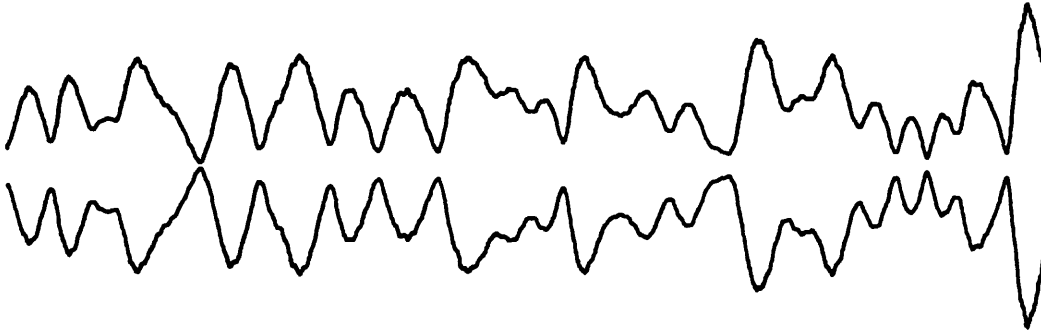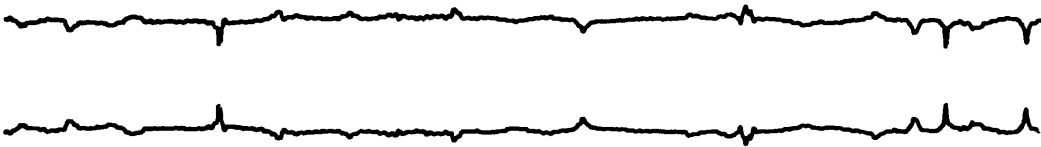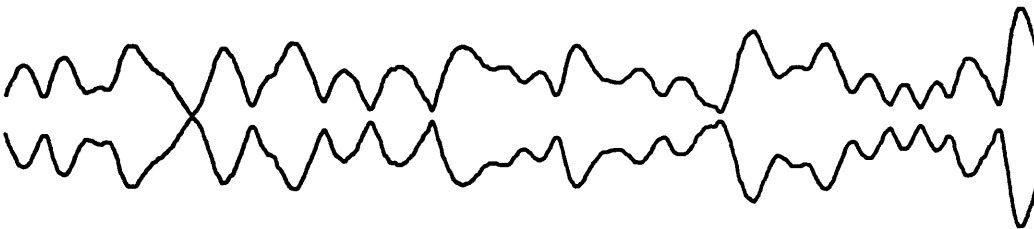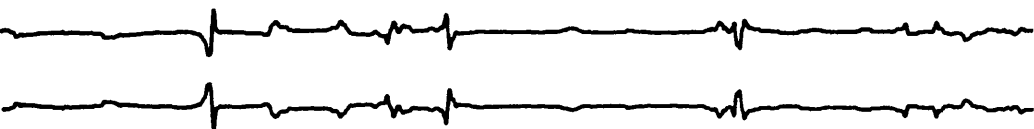
Figure 9.16   BFFAGC 409.5 mS field trial result
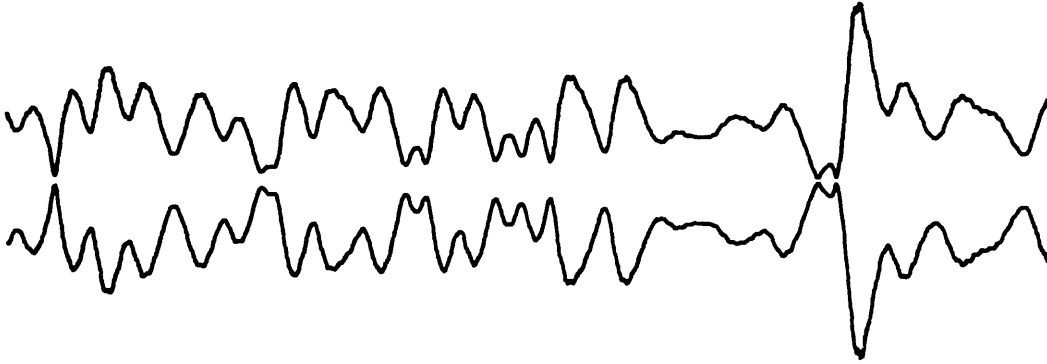
1.67 kHz PILOT INPUT

1.67 kHz PILOT OUTPUT
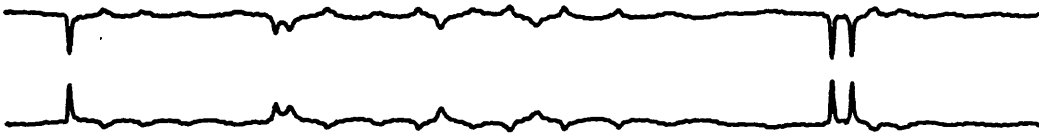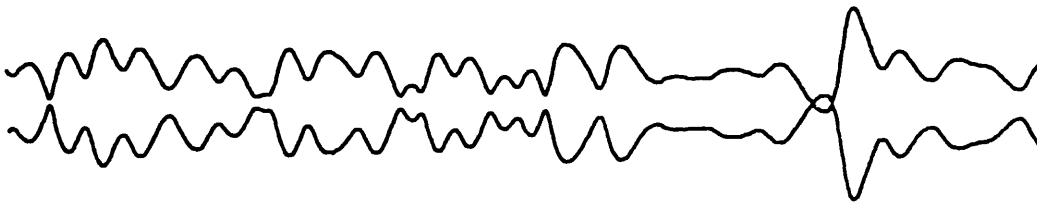
3 kHz TONE INPUT

3 kHz TONE OUTPUT

THRESHOLD −20 dB	SPEED 70 MPH	SIGNAL 30 dB ABOVE 1 μV

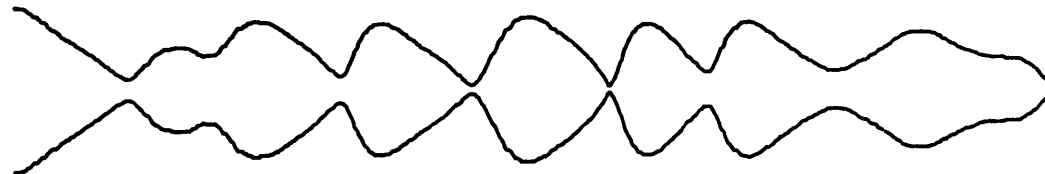Figure 9.17 BFFAGC 409.5 mS field trial result
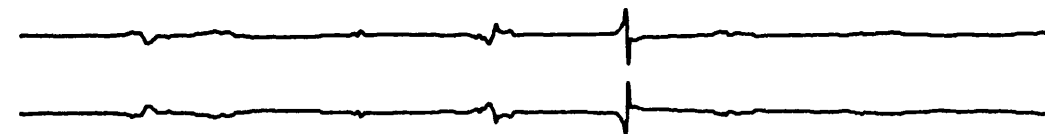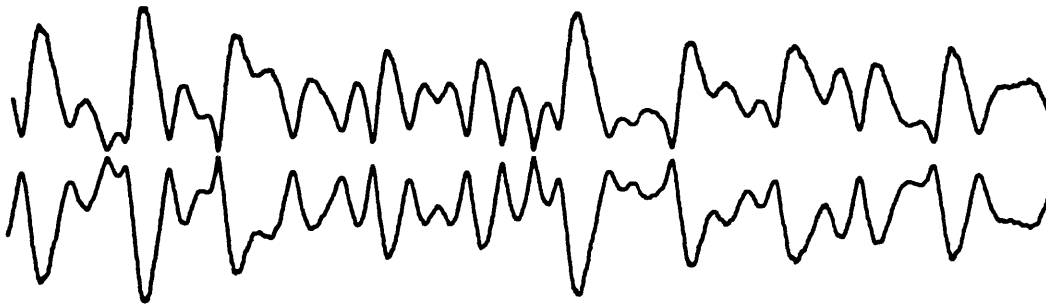
1.67 kHz PILOT INPUT

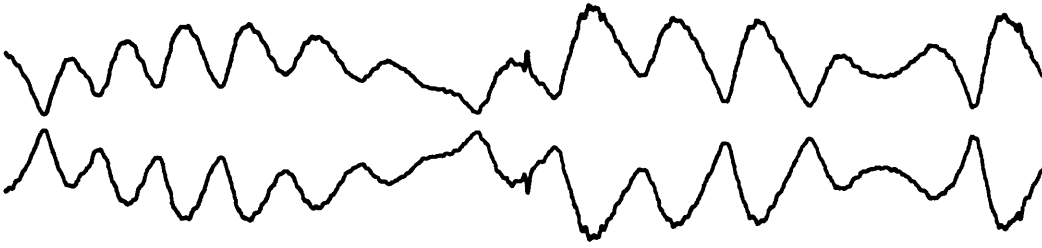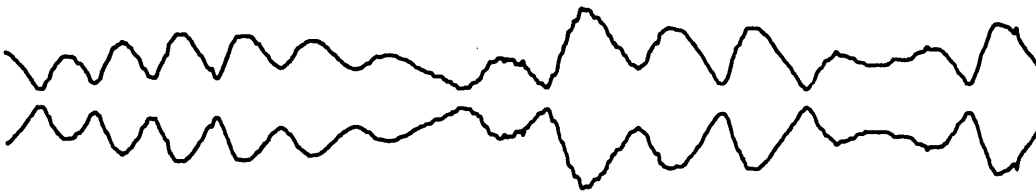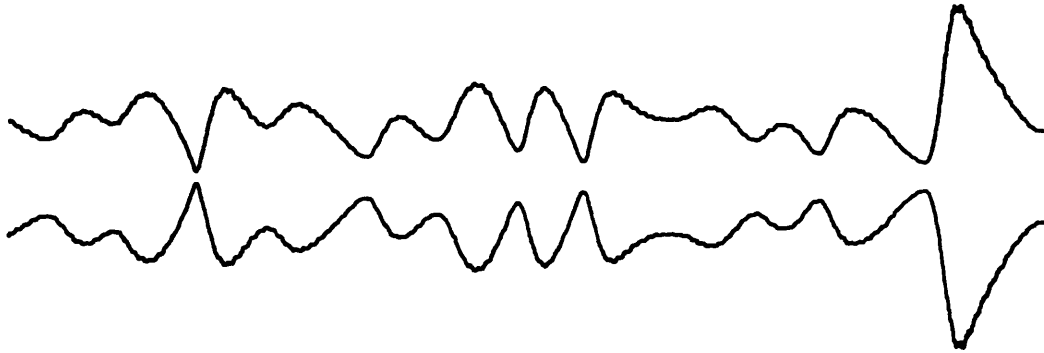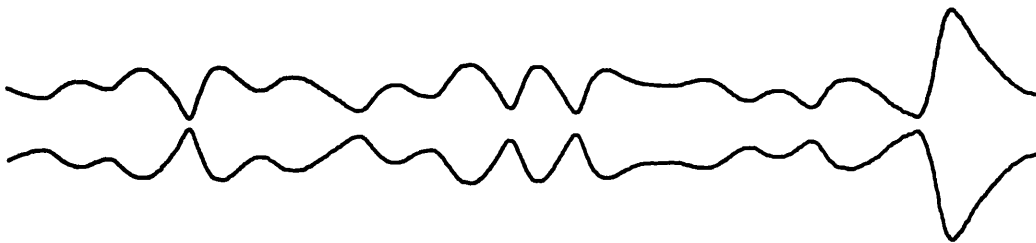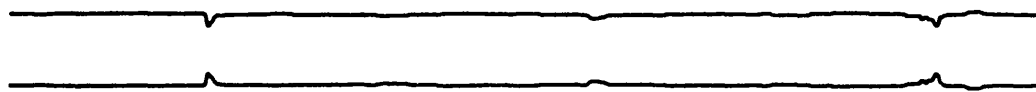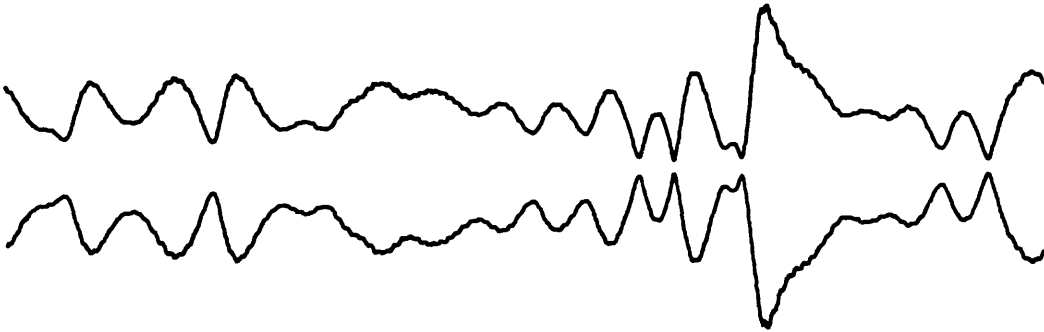1.67 kHz PILOT OUTPUT
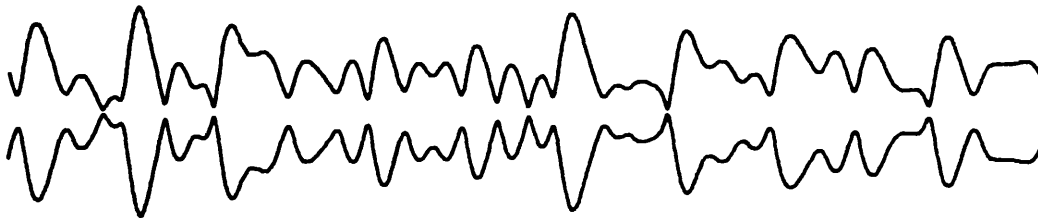
3 kHz TONE INPUT
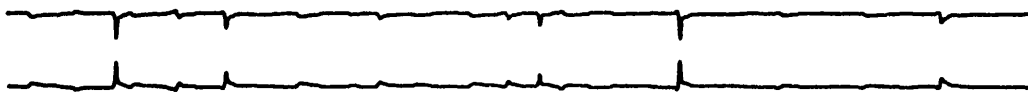
3 kHz TONE OUTPUT

| THRESHOLD -20 dB | SPEED 80 MPH | SIGNAL 30 dB ABOVE 1 μV |

Figure 9.18   BFFAGC 409.5 mS field trial result
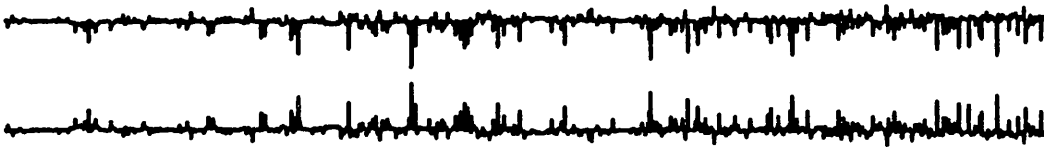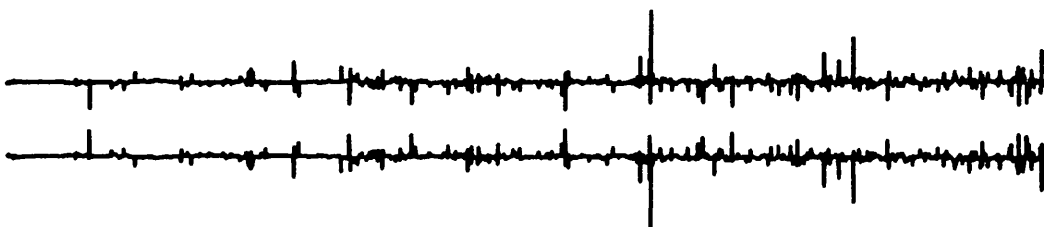
Figure 9.19 BFFAGC 8.19 s field trial result

9.4.2 Discussion of Results

The results presented in figures 9.11 to 9.20 show that the BFFAGC circuit gives good suppression of the pilot's envelope fading at all speeds up to 128 km/hr (80 mph). The main cause of the residual output envelope fading on the pilot is the threshold circuit that cuts in when the input fades below -20 dB. However, there are some very interesting anomalies between the plots of the pilot's and 3 kHz tone's envelopes. In general, the 3 kHz tone is seen to exhibit more residual envelope fading after the BFFAGC circuit than the pilot. This is most apparent in figure 9.20. The reasons for these discrepancies are discussed in more detail in the next chapter, but are briefly summarised below as being caused by:

1) Multipath time delay spread decorrelation effects

2) Receiver decorrelation effects

3) Noise

4) Other forms of interference (e.g. ignition)

It has been hitherto assumed that suppressing the envelope fading of the pilot automatically results in suppressing the envelope fading of the wanted signal. This is evidently not the case and the ultimate limitations of any AGC system with good pilot suppression dynamics are signal decorrelation effects.

9.4.3 Subjective Evaluation

The following observations were made regarding the field trials of the UHF SSB system incorporating BFFAGC during the transmission of speech:

9.37

The receiver's pilot tone notch circuit, which gave acceptable performance during static testing, was unable to satisfactorily attenuate the pilot during field trials and the problem was exacerbated by switching in the BFFAGC circuit. The reason for the problem is primarily the multipath induced random phase modulation on the pilot which the receiver's PLL was unable to track out. This is discussed in more detail in the next chapter. Obviously, the BFFAGC circuit has no effect on the phase of the incoming signal (other than pure time delay). However, it does render the multipath phase variations more audible by amplifying the received signal at the point where it has its greatest phase variation - the bottom of a fade. A simple solution to the problem used for the rest of the subjective tests was to pass the composite fading signal through a wider notch filter, the transmitter notch. The phase variations on speech signals were not found to be as subjectively noticeable as those on the pilot tone.

Without BFFAGC, the UHF SSB receiver's audio sounded distorted, having a distinctive "gravelly" or rough modulation characteristic during multipath propagation. Switching in the BFFAGC circuit caused a marked subjective improvement in speech quality, except in high noise environments. This BFFAGC improvement was found to be most noticeable on long vowel sounds, e.g. the word "are". Further investigation showed that there was little subjective gain in having the threshold more than -20 dB below the mean input level. Equation 8.5 shows that in the Rayleigh fading environment the signal's envelope spends over 99% of the time above this level.

The main subjective limitation in the use of BFFAGC appeared to be the effect of noise (and to a lesser extent, ignition interference). If the threshold was left on a low value during poor input signal to noise ratios, noise bursts occurred during the deep fades with characteristics similar to FM receiver-type noise bursts (or clicks). It was found to be preferable to raise the threshold as the received signal to noise ratio deteriorates and allow the deeper parts of fades to pass through the circuit unsuppressed. An approximate measure of the received signal to noise ratio is the receiver's EIFBAGC control line, and this raises the possibility of automatically increasing the threshold voltage as the received signal to noise ratio falls.

Before further subjective evaluations of BFFAGC are made, the complete UHF SSB system should incorporate a companding (compression and expansion) system. This has been shown to improve the subjective signal to noise ratio by between 7 dB and 11 dB in a similar SSB system (9.5). Combining this with inter-word muting would greatly reduce the effects of noise and interference. The BFFAGC circuit itself could be used to expand the received compressed signal if required.

9.4.4 Full Carrier AM Tests

Under the same operating conditions as described previously, a simple test was performed to show that BFFAGC can also be used with full carrier AM systems. The 1.67 kHz pilot tone was amplitude modulated with 300 Hz tone. The envelope of the received 1.67 kHz pilot is shown both before and after the BFFAGC circuit in the top 2 plots of figure 9.21. The bottom 2 plots show the 300 Hz modulation before and after the BFFAGC circuit, after passing the modulation through a 150 Hz highpass filter.

9.39
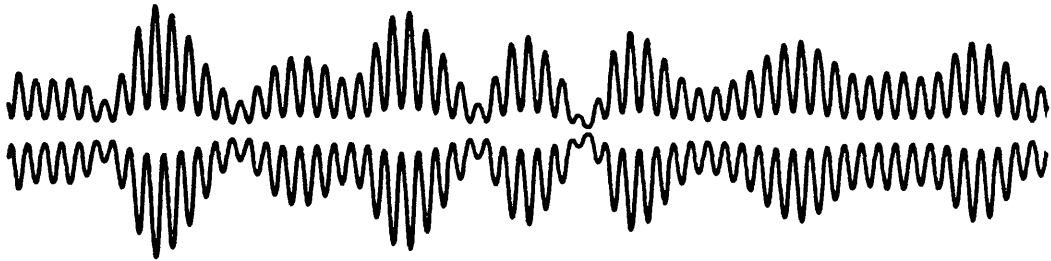
Figure 9.20   Full carrier AM field trial tests of BFFAGC,
                204.75 mS run
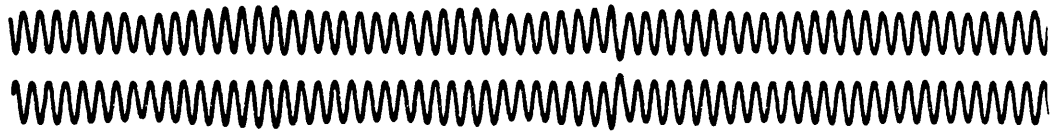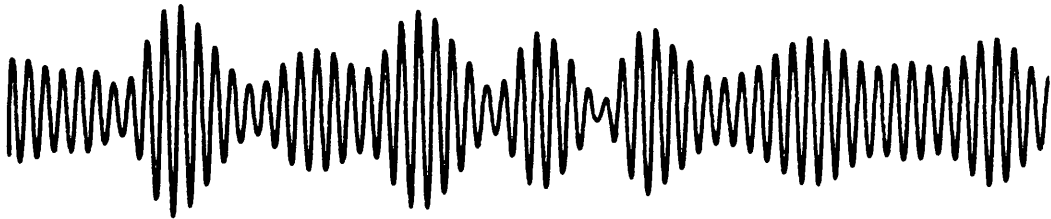
THRESHOLD −20 dB	SPEED 55 MPH	SIGNAL 40 dB ABOVE 1 μV

The sampling rate for the plots was 50 μS per point, with a total plot time of 204.8 mS. Evidently good suppression of the unwanted fading has been obtained.

CHAPTER 10

LIMITATIONS OF PILOT AGC

This chapter describes various performance limitations of feedback
and feedforward AGC systems using pilot AGC references, other than the
dynamic limitations already covered in earlier chapters. The aims are
to consider some of the significant factors behind the decorrelation
between fades of the pilot and wanted modulation, to analyse the effects
of noise and interference, and to discuss phase and phase control effects.

10.1 Multipath Time Delay Spread Decorrelation

It has been suggested (10.1) that due to the effects of Multipath
Time Delay Spread (MTDS) decorrelation alone, for microwave mobile radio
and deep fading, full carrier AM and pilot SSB communication channels
could not provide telephone quality signals, even with fast acting AGC
of any type. This section puts the problem of MTDS into perspective
using both simple worst case twin path models and statistical multipath
analysis.

10.1.1 Description

It has been assumed up to now that all of the energy reaching the
input of the receiver in the land mobile radio environment has arrived
via line-of-sight signals or signals that have been scattered or refracted
in the immediate vicinity of the vehicle. However, occasionally a
significant proportion of the received signal's energy arrives via 1
or more large reflectors some distance from the mobile. In such

circumstances it is possible that the envelope fading induced on the received signal is no longer "frequency flat", i.e. at any one instant of time, the depth of fade at different RF frequencies is dissimilar (3.2). This decorrelation between fades of the pilot reference and wanted modulation results in the wanted modulation suffering from residual unwanted fading at the output of an otherwise perfect AGC system.

10.1.2 Analysis using Twin Path Model

The following analysis assumes that the received signal consists of 2 components. One arrives from a nearby scattering source directly in front of the the mobile magnitude E_p. The other is assumed to arrive from a distant scattering source directly behind the mobile, magnitude RE_p with a relative arrival time delay, T_D, at $t = 0$. The received pilot at RF frequency ω_c may therefore be derived in a similar manner to equation 2.10 as $e_p(t)$ where :

$$e_p(t) = E_p(\cos(\omega_c t + \omega_c S/ct) + R\cos(\omega_c(t - T_D) - \omega_c S/ct)) \tag{10.1}$$

where S is the vehicle's speed and c the velocity of light. The pilot's envelope can be written as $r_p(t)$ where:

$$r_p(t) = E_p(1 + R^2 + 2R\cos(2\omega_c S/ct + \omega_c T_D))^{\frac{1}{2}} \tag{10.2}$$

Similarly, at a slightly different RF frequency $\omega_c + \Delta\omega$, a received signal will have an envelope given by $r_m(t)$ where:

$$r_m(t) = E_m(1 + R^2 + 2R\cos(2(\omega_c + \Delta\omega)S/ct + (\omega_c + \Delta\omega)T_D))^{\frac{1}{2}} \tag{10.3}$$

The BFFAGC divides the modulation signal's envelope, $r_m(t)$, by the pilot's envelope, $r_p(t)$, giving the output modulation signal's envelope $v'_{om}(t)$ as:

$$v'_{om}(t) = \frac{E_m}{E_p}\left[\frac{1 + R^2 + 2R\cos(2\omega_c S/ct + \omega_c T_D + 2\Delta\omega S/ct + \Delta\omega T_D)}{1 + R^2 + 2R\cos(2\omega_c S/ct + \omega_c T_D)}\right]^{\frac{1}{2}} \tag{10.4}$$

Subtracting $\omega_c T_D + 2\Delta\omega S/ct + \Delta\omega T_D$ from the top and bottom phases of equation 10.4 gives the output modulation signal's envelope, $v_{om}(t)$, where:

$$v_{om}(t) = \frac{E_m}{E_p}\left[\frac{1 + R^2 + 2R\cos 2\omega_d t}{1 + R^2 + 2R\cos(2\omega_d t - 2\Delta\omega S/ct - \Delta\omega T_D)}\right]^{\frac{1}{2}} \qquad (10.5)$$

since ω_d is equal to $\omega_c S/c$. The term $2\Delta\omega\,S/ct$ is the time variation of the excess time delay of the rear scattering source and for small values of t can be neglected to give:

$$v_{om}(t) = \frac{E_m}{E_p}\left[\frac{1 + R^2 + 2R\cos 2\omega_d t}{1 + R^2 + 2R\cos(2\omega_d t - \Delta\omega\,T_D)}\right]^{\frac{1}{2}} \qquad (10.6)$$

Therefore the effect of MTDS is to result in a time delay error in the division process. A comparison of equation 10.6 with equation 9.7 shows that if the substitution $P = 1$ and $\Delta\omega T_D = \omega_1\tau_1 + \omega_2\tau_2 + \omega_p(\tau_2 - \tau_1)$ is made, then the technique suggested in section 9.2.1 can be used to solve for the peak to trough ratio of $v_{om}(t)$. An estimate of the problem can be made by noting that the peak output of $v_{om}(t)$, $\hat{v}_{om}$, occurs approximately when:

$$2\omega_d t - \Delta\omega T_D = \pi \qquad \text{radians} \qquad (10.7)$$

which gives a peak output from equation 10.6 of:

$$\hat{v}_{om} = \frac{E_m}{E_p}\left[\frac{1 + R^2 - 2R\cos \Delta\omega T_D}{1 + R^2 - 2R}\right]^{\frac{1}{2}} \qquad (10.8)$$

which can be rearranged to give:

$$\Delta\omega = \frac{1}{T_D}\cos^{-1}\left[\frac{(\hat{v}_{om} E_p/E_m)^2(2R - 1 - R^2) + 1 + R^2}{2R}\right] \qquad (10.9)$$

10.3

For example, consider the maximum allowable wanted modulation to pilot frequency separation, $\Delta\omega$, when suppressing a 30 dB fade caused by 2 received signal components with $T_D = 1$ μS so that the peak of the residual modulation's ripple is less than 3 dB relative to the nominal output i.e. $(v_{om}E_p/E_m) = 3$ dB. Equation 10.9 gives $\Delta\omega \simeq 63.10^4$ radians/sec (10 kHz). Therefore MTDS is unlikely to cause significant residual output ripple in the UHF SSB system unless T_D is significantly greater than 1 μS. It is interesting to calculate what is the value of T_D required to affect the 3 kHz tone that has a $\Delta\omega$ of 1.33 kHz from the pilot. For the same 30 dB input to +3 dB peak output variation equation 10.9 gives $T_D = 7.5$ μS. Such a time delay will rarely be found in the field. It corresponds to a source over 2.2 km away.

10.1.3 Analysis using Multipath Model

A general statistical multipath analysis of the degrading effects of MTDS on FFAGC operation is complicated. A major problem is to decide upon what criteria the systems performance should be assessed. The early work of Gans and Yeh (10.1) applies mainly to full carrier AM systems and analyses the post FFAGC signal to signal suppression noise ratio. The signal suppression noise is defined as the alternating residual fading component of the envelope caused by MTDS after passing through an otherwise perfect FFAGC circuit. The results give a pessimistic estimate of the performance of full carrier AM systems since only low modulation depths are used and also the residual fading spectrum of the carrier is assumed to overlap into the wanted modulation spectrum. Care needs to be taken if the work is used to analyse the performance of a pilot SSB system. This is because the signal to signal suppression noise ratio of the envelope of an SSB signal is not directly

related to its effective overall signal to noise ratio. The ear is relatively insensitive to certain sorts of envelope variation on speech signals (10.2). The effective overall signal to noise ratio of the SSB signal is therefore likely to be higher than the signal to signal suppression noise ratio of its envelope.

Leland and Sollenberger (10.6) have analysed the effects of various impairment mechanisms on a combined feedforward AGC and AFC system. The system is assumed to be perfect and offer infinite suppression of multipath envelope and phase variations in the frequency flat Rayleigh fading environment. The analysis is based on a combination of theoretical work and a "Monte Carlo" computer simulation programme. The criterion used for assessing the effects of external impairment mechanisms is the signal to correction distortion ratio. Correction distortion is therein defined as the difference between the incoming signal's fading envelope and/or phase and the feedforward correction circuit's estimate of the fading envelope and/or phase. Once again, care should be taken when interpreting the results since in the absence of the envelope and frequency correcting system, the SSB signal is defined as possessing a 0 dB signal to correction distortion ratio. Nevertheless, based on this criterion Leland and Sollenberger (ibid) give theoretical results indicating that the distortion introduced by MTDS will be relatively modest (typically the signal to correction distortion ratio is greater than 20 dB) and quite limited in occurrence for a particular coverage area, although an experimental evaluation must be made to determine the subjective nature of the impairment.

In both the work of Gans and Yeh (ibid) and Leland and Sollenberger (ibid) it was pointed out that an important parameter in the calculation

of the performance of the feedforward system is the threshold level.

The effect of external system impairments such as MTDS are controlled

by the threshold circuit that places a limit on the maximum values of

the circuit's gain.

10.1.4 Significance of Results

In view of the results obtained in section 10.1.2 on the worst case

twin path model and the results obtained by Leland and Sollenberger (ibid),

it appears that Gans and Yeh (ibid) overestimated the problem of MTDS.

Furthermore, the use of TIB pilot SSB systems where the pilot is never

more than about 1.3 kHz from the furthest audio component greatly

minimises the decorrelation effects of MTDS.

10.2 Receiver Decorrelation

A far more serious problem than MTDS in relation to decorrelation

is the effect of filtering operations performed by the receiver prior

to BFFAGC processing. The original work of Hopper (8.6) attempted to

analyse the problem for shallow input fading (about 3.5 dB peak to trough)

This section presents a more general analysis of the problem using

techniques that can be simply applied to a practical receiver's filter.

10.2.1 Description

Usually, a practical superhet SSB receiver achieves its adjacent

channel selectivity through the use of high order crystal bandpass

filters at the IF. Unfortunately, this (and any other) filter

decorrelates fades of the pilot with the wanted modulation. The non-

flat group delay response of such a filter causes envelope variations

of the wanted modulation to arrive at a different time to the envelope

variations of the pilot. This is similar to the effect of MTDS

decorrelation. The amplitude response of such a filter is also usually

not perfectly flat in the passband and results in the depth of fade at

different frequencies being dissimilar. This is similar to the effect

of the BFFAGC bottom path bandpass filter exhibiting amplitude response

ripples in its passband.

10.2.2 UHF SSB Receiver's Filter

It is revealing to plot the characteristics of the UHF SSB receiver's

10.7 MHz crystal filter to estimate the magnitude of the decorrelation

effects. This is shown in figure 10.1. Figure 10.1(a) is a detailed

plot of the amplitude/frequency response and figure 10.1(b) a detailed

plot of the group delay/frequency response. The passband amplitude

ripple of the filter is 2 dB, as specified by the manufacturer. Care

was taken during these plots to prevent the source and measuring

instrument (an HP 3575A gain/phase meter) from affecting the filter's

matching circuitry. Most significant is the variation in group delay

across the passband of nearly 800 μS.

10.2.3 Analysis of Two Tone Response

As with the MTDS analysis, perfect suppression of the pilot's

envelope fading is assumed and the residual envelope fading of a wanted

modulation component at the output of a BFFAGC circuit is calculated. The

analysis requires the definition of 2 filter derived variables:

1) Relative Amplitude Decorrelation Factor, P_F. Over the range

$\pm 2\omega_d$ about either the pilot or wanted modulation component's frequency,

the amplitude response of the filter will vary by a small amount. This

is expressed as a dB variation with increasing frequency for both the
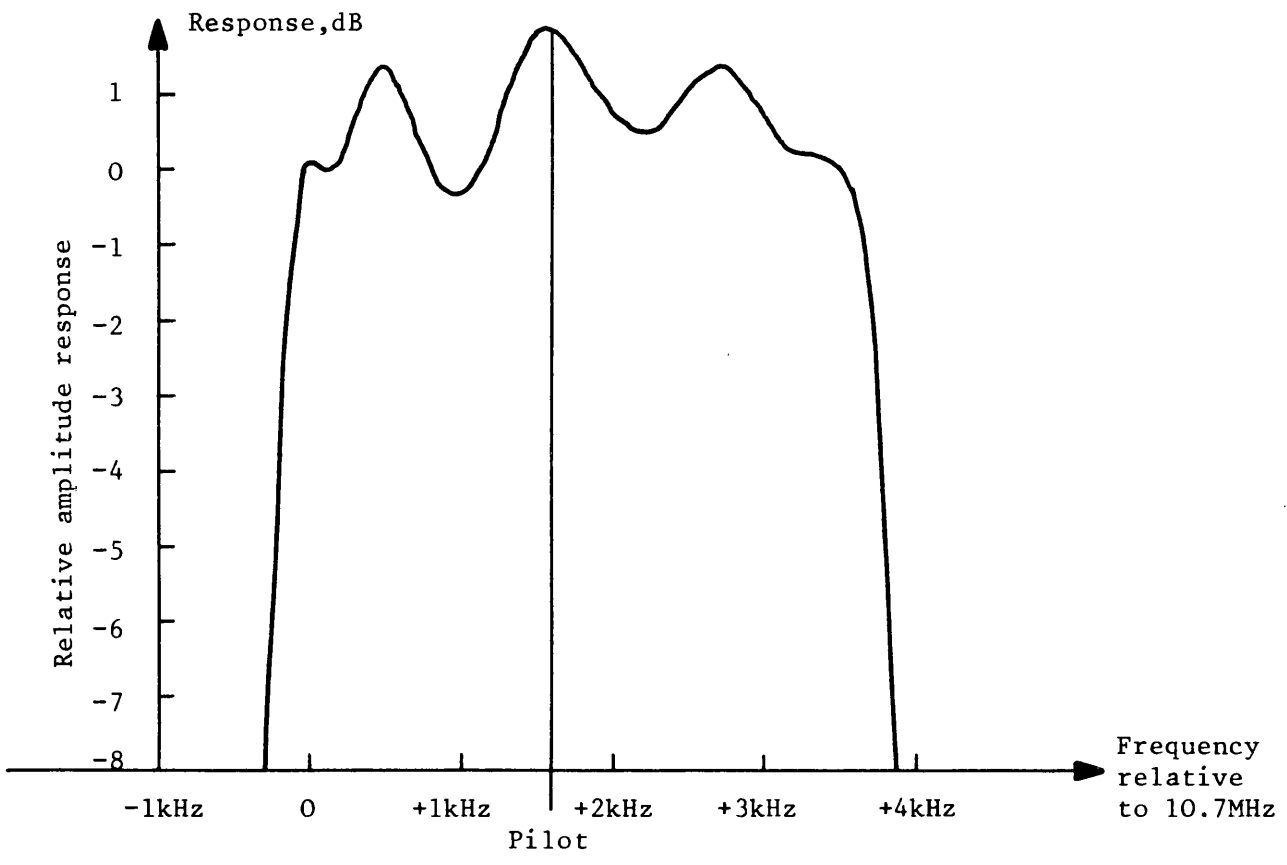
Figure 10.1(a)   Amplitude frequency response of 10.7 MHz crystal filter
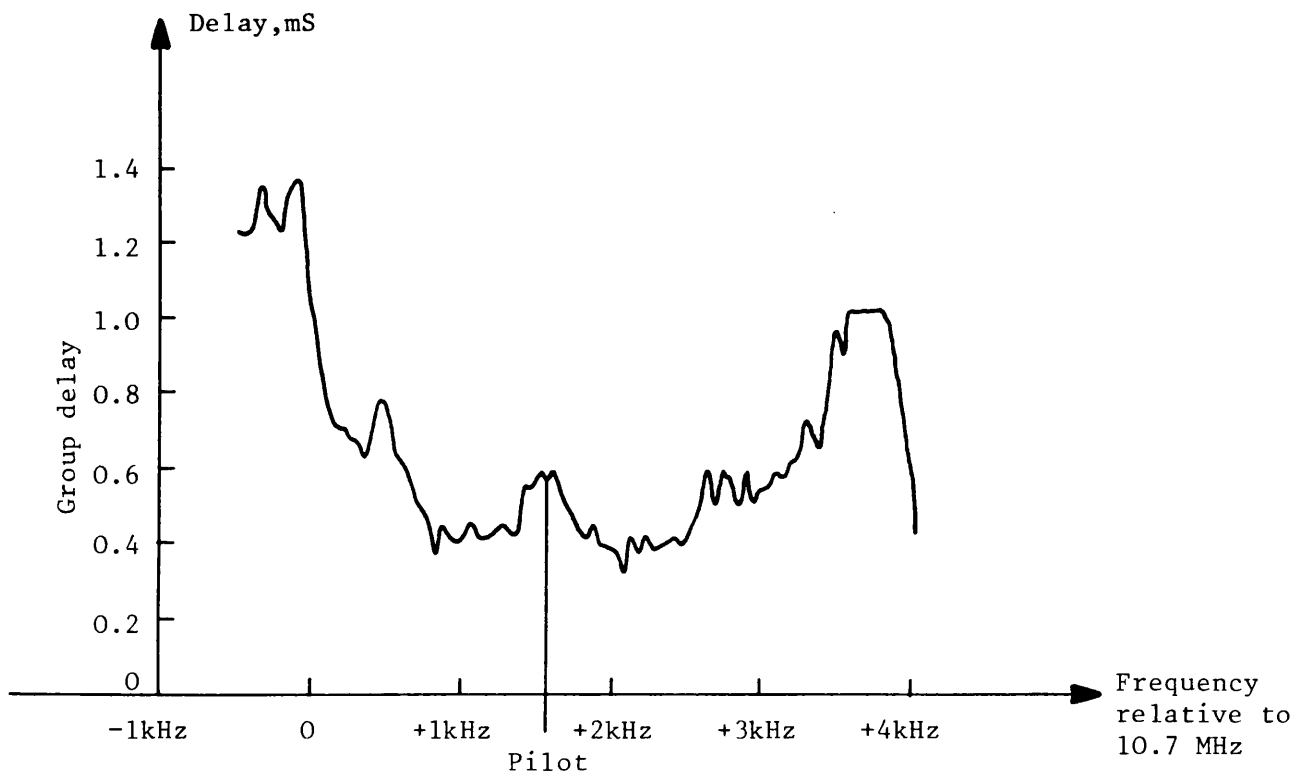
Figure 10.1(b)   Group delay frequency response of 10.7 MHz crystal filter

pilot and wanted modulation component. The difference between the 2 dB

variations is then expressed in a linear form as a number slightly

greater than or slightly less than unity. This is called P_F.

For example, consider the value of P_F for the pilot and a 3 kHz tone

when ω_d = 50 Hz. For the UHF SSB receiver's IF filter, figure 10.1(a),

the amplitude response varies by -0.2 dB from 1.62 kHz to 1.72 kHz. From

2.45 kHz to 3.05 kHz the amplitude response varies by -0.35 dB. The dB

difference is ± 0.15 dB. Therefore, this gives P_F = 1.0174 or 0.9829.

2) Relative Group Delay Decorrelation Factor, T_F. This is simply

the difference between the average group delay of the pilot and wanted

modulation component. It is assumed that there is no significant change

in group delay over the frequency range ± ω_d about either the pilot or

wanted modulation component's frequency.

With these definitions it follows that the wanted modulation term

suffers from a residual envelope fading, $v_{om}(t)$, at the output of an

otherwise perfect BFFAGC circuit of:

$$v_{om}(t) = \left[\frac{1 + P_F^2 R^2 + 2P_F R \cos(\omega_f t - \omega_f T_F)}{1 + R^2 + 2R \cos \omega_f t} \right]^{\frac{1}{2}} \qquad (10.10)$$

in response to a 2 tone test signal, relative level R, fade frequency

ω_f = $2\omega_d$. This equation can be seen to be similar to the inverse of

equation 9.7 and the technique suggested in section 9.2.1 can be used

to solve for the peak to trough ratio of $v_{om}(t)$.

It is interesting to compare a typical division phase error in

equation 10.10 with a division phase error from equation 10.6 relating to

twin path MTDS. The wanted modulation component is assumed to be at pilot

frequency + 2 kHz ($\Delta\omega$ = 12.57 kr/s) in this example. A 1 μS MTDS gives

10.9

a division phase error of $\Delta\omega T_d$ = 0.0126 radians (0.72°). The UHF SSB

receiver's filter has a relative group delay decorrelation factor at

pilot + 2 kHz of T_F = 400 µS. If the fade rate is assumed to be

100 Hz (ω_f = 628 r/s), then the division phase error due to the filter

is 0.25 radians (14.4°). Thus in this example, the effect of the filter

is 20 times greater than the effect of MTDS.

Note that the computer programme AGCSIM described in appendix 6

will calculate the impairments of MTDS, filter amplitude and/or phase

imperfections for the 2 tone test signal. The example programme

runs in appendix 6 illustrate the effects of time delay mismatches and

envelope decorrelation in the division process. The threshold can

greatly reduce the peak circuit's output as shown in the last example

in appendix 6.

10.2.4 Reducing the Effects

There are 2 known ways of reducing the effects of receiver

decorrelation:

1) Restricting the transmitted modulation signal's bandwidth.

This is the simplest of the 2 ways and merely involves designing the

complete system so that the receiver has a wider IF filter than the

transmitter. This is based on the observation that the worst decor-

relation effects occur at the edges of the crystal filter's passband.

This technique has been implemented in the UHF SSB system. A comparison

of the frequency response of the low level UHF SSB generator, figure 4.7,

with the receiver's IF filter, figure 10.1(a) illustrates this. The

transmitted modulation's frequency response is > 10 dB down below

250 Hz and above 3 kHz. Of course, implementation of this technique

requires the designer to observe transmitted modulation frequency response

requirements and receiver adjacent channel specifications.

2) Use a compensating filter. This filter would be inserted just before the BFFAGC input. It would possess a complementary characteristic to the IF crystal filter over the wanted modulation's passband such that the combined IF and compensating filter's amplitude and group delay response lay within specified linearity limits. Such a compensation filter would be uniquely characterised for each receiver IF crystal filter. The IF crystal filter characteristic may also vary significantly with temperature and a compensating filter should also vary with temperature in a complementary manner. This suggests the use of adaptive transversal filter equalisers under software control (10.3).

10.2.5 Comments on Other Pilot SSB Systems

The use of TIB pilot SSB allows fades of the pilot to be reasonably well correlated with fades of the wanted modulation. However, note the increased decorrelation that would occur using the filter characterised in figure 10 if the pilot were placed at the carrier position, 10.7 MHz (pilot carrier (1.7)) or at 10.7 MHz plus 3.5 kHz to 4 kHz (above band tone (1.9)). The following table compares the group delay decorrelation factor of the three systems.

System	Worst Case Pilot to Wanted Modulation Group Delay Decorrelation Factor over wanted Modulation Range 300 Hz - 3 kHz
TIB with Pilot at 1.67 kHz	260 µS
Pilot carrier	800 µS
Tone above band, Pilot at 3.75 kHz	700 µS

Furthermore, the amplitude decorrelation factor is also significantly larger for the pilot carrier and tone above band systems. Note especially the slope that would be imparted to the pilot carrier at 10.7 MHz in figure 10(a).

In a description of their pilot carrier SSB receiver Ball and Holmes (5.5) report on the problems of group delay decorrelation. This decorrelation was so severe that it affected the receiver's EIFBAGC system. In an attempt to reduce the effects the 10.7 MHz local oscillator was slightly offset in frequency to place the pilot carrier further inside the crystal filter's passband.

10.3 Noise and Interference

This section discusses some of the effects of receiver noise and external interference on BFFAGC systems. Some of the results can also be applied to EIFBAGC systems via the feedforward model developed in chapter 5.

10.3.1 Receiver Noise Effects on the Control Path

The receiver is assumed to add white (over the frequency range of interest), Gaussian noise to the pilot at the input of the BFFAGC circuit. The bandpass filter preceding the envelope detector extracts the pilot and also passes some noise. The output of the bandpass filter, $e_b(t)$, can be written as:

$$e_b(t) = E_p \cos \omega_p t + I_N \qquad (10.11)$$

where E_p is the pilot's magnitude, ω_p its frequency and I_N is the bandpass filtered noise. Rice (3.4) has analysed various properties of the envelope of $e_b(t)$ (and hence the input of the denominator's threshold

circuit), including its "Rician" PDF. He shows that if E_p is zero the envelope's PDF is Rayleigh distributed. If E_p is relatively large compared to the noise (SNR of $e_b(t)$ > 15 dB say) the envelope's PDF takes on a Gaussian shape with an average level E_p and a standard deviation equal to the RMS noise level.

In the absence of fading, the BFFAGC circuit's envelope detector output therefore suffers from 2 noise induced effects:

1) A noise derived dc component. The dc component of the envelope detector's output is no longer linearly related to the pilot's envelope at low SNR levels.

2) Random modulation. The random variations of the envelope detector's output that are passed by the threshold circuit are superimposed on to the divider's denominator. This causes random envelope modulation of the circuit's output.

Bennet (10.4) has discussed the dc component at the output of a linear half wave rectifier for various input signal to noise ratios in some detail. The noise derived dc component is only significant for relatively low input SNR. For example, the linear half wave rectifier envelope detector overestimates the dc component of the pilot's envelope by 3 dB when its input signal to noise ratio (i.e. the bandpass filter's output SNR) is -1.7 dB. That is, the RMS level of noise present is greater than the RMS level of pilot. Therefore it seems reasonable to assume that the envelope detector gives a linear estimate of the pilot's envelope at its input providing the input SNR is above 0 dB.

The extent of the problem of random gain modulation can be estimated for the UHF SSB system assuming the following receiver and BFFAGC parameters:

1. Peak speech modulation power to pilot ratio: 10 dB

2. Average speech modulation power to pilot ratio: 0 dB

3. Just acceptable average speech modulation power
    to noise ratio: 10 dB

4. Noise bandwidth of speech path: 3 kHz

5. Noise bandwidth of bandpass filter in BFFAGC circuit: 800 Hz

From the above figures, the pilot to noise ratio at the input to the envelope detector when the average speech modulation power to noise ratio is just acceptable is 15.7 dB. It is therefore reasonable to assume that the output of the envelope detector has a Gaussian PDF with a standard deviation 0.163 of the average (dc) level. This is the signal at the input of the threshold circuit. It will be assumed for now that the threshold circuit passes the envelope detector output directly on to the divider's denominator. The following information can therefore be inferred directly using Gaussian distribution tables:

1) The denominator stays within ± 3 dB of its average value 95.9% of the time.

2) 99.9% of the time the denominator stays above half the average value.

It should be noted that these denominator variations, although not too significant, will be greatly reduced by the threshold circuit. Typically, when the average speech modulation power to noise ratio is just acceptable the threshold voltage will be at 0 dB relative to the

10.14

denominator's average voltage, preventing any negative going noise
induced denominator variations from occurring.

It has been assumed up to now that there is no lowpass filter
following the envelope detector. The general effect of the post-envelope
detector lowpass filter will be to reduce the noise variations. If the
pre-lowpass filter SNR is above 15 dB say, then the post-lowpass filter
noise power will be reduced by the ratio of the lowpass filter's noise
bandwidth to the bandpass filters noise bandwidth. The noise induced
gain variations on a typical pilot SSB EIFBAGC system, with the post-
envelope detector noise bandwidth measured in a few tens of Hertz, will
be much lower than in the previous example of a BFFAGC system. Further
details of the noise analysis of a simple FBAGC system can be found
elsewhere (5.10). However, Ohlson (5.12) points out that the feed-
forward model of EIFBAGC can be used to analyse its noise performance and
suggests a technique for analysing the PDF of the output signal's envelope.

10.3.2   Effect of Fading-Noise Bursts

In section 9.4.3 the main subjective limitation in the use of BFFAGC
was reported to be the effect of noise "bursts" which occur when the input
signal fades into the noise. As indicated in section 10.3.1, the wanted
signal's envelope at the output of the BFFAGC circuit will remain
substantially constant apart from a small amount of noise-induced gain
modulation, providing the input is above the threshold voltage. The
noise will therefore appear to rise to the signal during a fade. This
is illustrated in figure 10.2 showing the input and output waveforms with
and without the threshold circuit operating. For any particular set of
operating conditions there is a threshold level which is the best
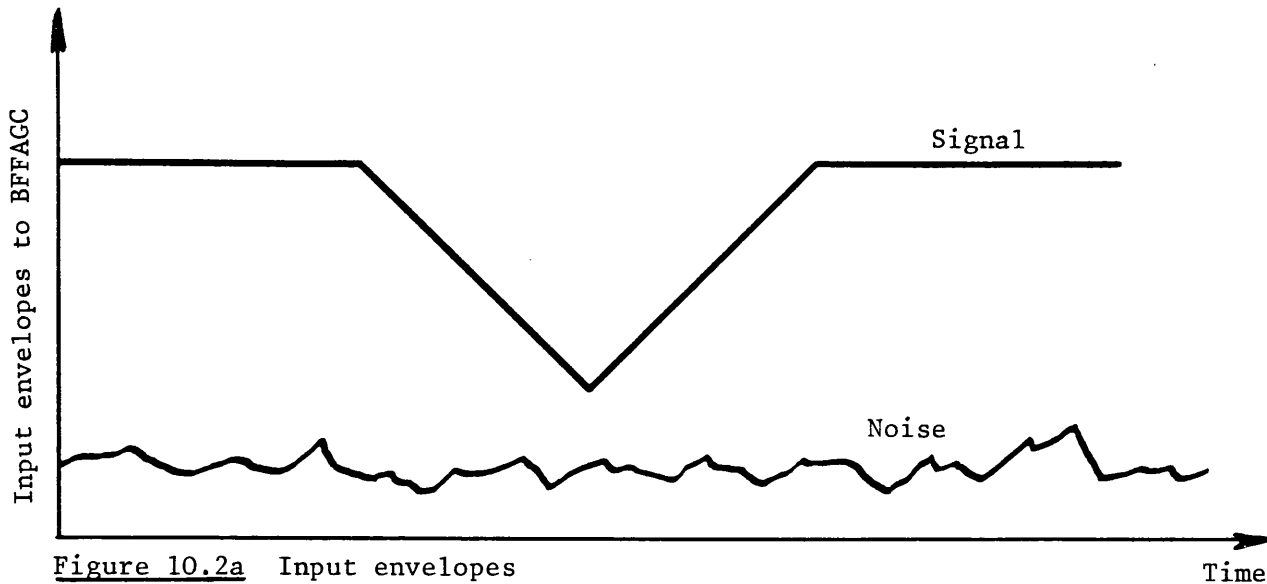
Figure 10.2a   Input envelopes
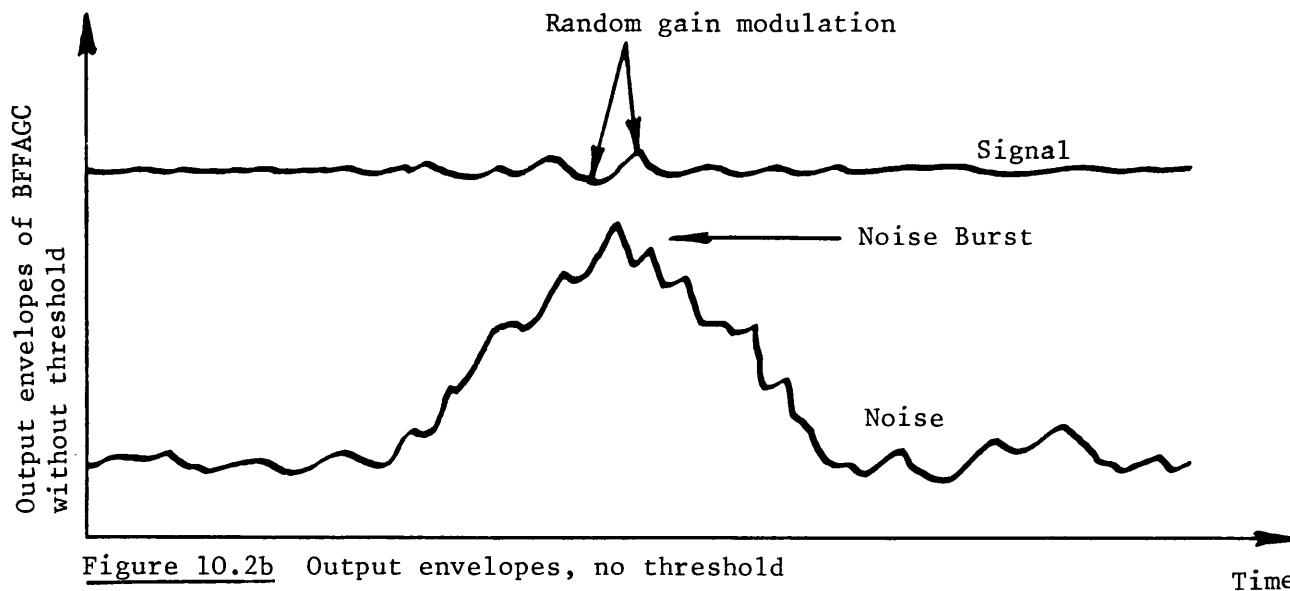
Figure 10.2b   Output envelopes, no threshold
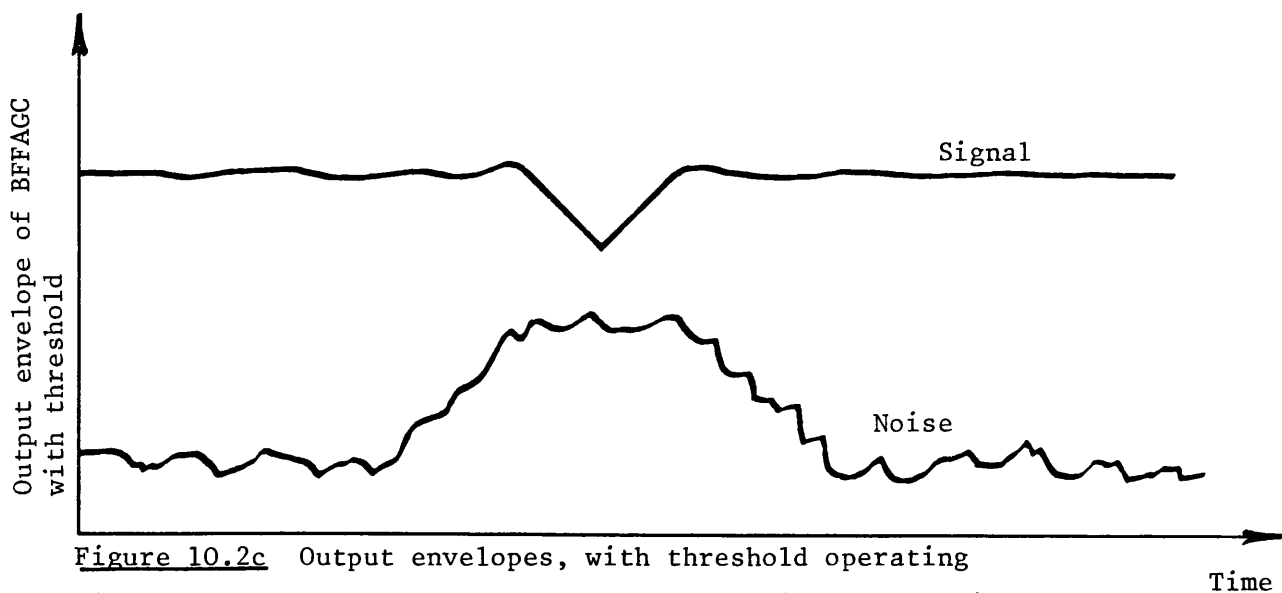
Figure 10.2c   Output envelopes, with threshold operating

Figure 10.2   Input and output envelopes of signal and noise,
illustrating the effect of a threshold circuit in
BFFAGC operation

subjective compromise between limiting the level of the noise bursts and passing too much envelope fading. In particular, it has been found to be best to raise the threshold voltage in the UHF SSB receiver's BFFAGC circuit from -20 dB with respect to the mean input level during good SNR reception to 0 dB when the average SNR is around 10 dB or less. An approximate measure of the average input SNR is the receiver's EIFBAGC control line. If, for a particular system, a "subjective law" can be found to relate the threshold level to input SNR, the BFFAGC circuit's threshold voltage level can be regulated via the EIFBAGC control line.

10.3.3 Ignition Interference

The general effects of ignition interference (and other forms of man-made noise) on the AGC circuitry in a receiver are not easily theoretically evaluated since the AGC circuitry's response also depends upon the modifications imparted to the interference by the preceding receiver circuitry. A practical investigation of the effects of ignition interference on the AGC circuitry would involve the whole receiver system under a variety of signal, interference noise, fading and threshold levels.

Ignition interference will cause compression and gain modulation of the AGC circuitry and for relatively low levels of interference, so that the receiver is operating in its linear range, it may be possible to evaluate these effects on a simple statistical basis. It is interesting to note that the suburban man made noise power level at 450 MHz is about the same level as typical receiver induced noise although it is about 15 dB higher in the urban environment (10.1). Therefore at signal levels where the ignition interference is likely to be significant the threshold circuit will be reducing the denominator's operating range,

diminishing the effects of ignition interference as well as receiver noise.

10.3.4 Co-channel Interference

Co-channel interference occurs when attempts are made to re-use radio channels with nominally the same frequencies in adjacent areas (10.5). An analysis of the various effects caused by interfering modulation and pilot signals on the performance of a combined feedforward AGC and AFC system has required the use of the Monte-Carlo computer simulation programme mentioned in section 10.1.3 (10.6). Leland and Sollenberger (ibid) state that an experimental subjective assessment of the results thus obtained is required and factors such as talker activity and particular hardware implementations of the equipment need to be taken into consideration. No doubt similar conclusions also apply to BFFAGC and EIFBAGC circuits.

However, it is possible to estimate some of the effects of co-channel interference when the wanted SSB signal, consisting of pilot and modulation, is received along with an interfering pilot at nominally the same frequency as the wanted pilot. Both pilots are assumed to be independent Rayleigh fading processes. For this situation, it is relatively simple to calculate the wanted to unwanted pilot ratio statistics. Assume that the specified level of the wanted pilot's envelope is r_ω and the specified level of the unwanted pilot's envelope is r_u, then from Gosling (10.5) the probability that $r_\omega > x r_u$ is given by:

$$p(r_\omega > x r_u) = \frac{1}{x^2 G^2 + 1} \qquad (10.12)$$

where G is the ratio of the average powers of the unwanted pilot to wanted pilot (usually G < 1).

For example, it is possible to calculate the probability that the wanted pilot level will exceed the unwanted pilot level by substituting x = 1 into equation 10.11. Gosling (ibid) suggests values of signal to interference ratios of 15 dB for SSB systems. Substituting G = 0.1778 into equation 10.11 shows that $p(r_\omega > r_u)$ is 84.9% in this case, i.e. the unwanted pilot's amplitude exceeds the wanted pilot's amplitude 15.1% of the time.

10.4 Phase and Phase Control Effects

This section discusses some of the problems of the SSB signal's phase variations and the effects of the receivers PLL circuitry.

10.4.1 Phase Variations

It has already been shown that the received multipath fading pilot may be written as:

$$e_p(t) = r(t) \cos(\omega_p t + u(t)) \tag{10.13}$$

where r(t) and u(t) are infinitely wide bandwidth random processes, but are so interrelated that the resulting pilot's bandwidth does not exceed $2\omega_d$. The action of a perfect pilot AGC circuit is to divide out the envelope variations leaving the pilot as:

$$e_p'(t) = E_p \cos(\omega_p t + u(t)) \tag{10.14}$$

Thus the pilot's spectrum is spread outside $2\omega_d$ since it is now simply phase modulated by u(t) alone. This is one of the reasons why it was found to be more difficult to satisfactorily notch out the pilot when

10.19

the BFFAGC circuit was switched into the UHF SSB system.

The random phase modulation is also superimposed upon the audio modulation signal's phase. However, subjectively it was found to be less noticeable on speech signals than on single tones. The ear is relatively insensitive to phase information (10.2) but the random phase modulation causes certain parts of the received speech to sound at times as if it were suffering from "wow and flutter".

Full carrier AM communications are not affected by this where the demodulation process is independent of the carrier's phase. FM systems are severely affected by these phase variations which are demodulated along with the wanted modulation causing an additional source of click-type interference (10.1).

10.4.2 PLL Frequency Averaging Properties

Chapter 7 showed that the typical PLL used in mobile SSB receivers with natural frequencies less than $2\omega_d$ have little ability to track out the multipath induced phase variations on the received signal. However, it is sometimes intuitively assumed that such a PLL will nevertheless perform the function of frequency averaging and accurately position the pilot's fading spectrum on the centre of the BFFAGC circuit's bandpass filter. The following experimental observation indicates that this may not be the case.

A recording was made of the multipath fading pilot from the UHF SSB receiver's output lasting 205 seconds. The receiver's PLL was disabled for this run, the high stability local oscillators preventing significant receiver drift. The recording started just as the vehicle arrived at

position B on figure 4.11. The vehicle turned around, stopped at B then proceeded off back to the University via position A. At position C the vehicle almost stopped as it turned into the University. The recording was played back through the precision PLL circuit described in section 7.2.1. The natural frequency of the PLL was set to 3 Hz, the same as the UHF receiver's PLL. A plot of the VCO voltage throughout this run is shown in figure 10.3. The vehicle speed varied up to a maximum of 64 km/hr (40 mph) on this run. The VCO voltages corresponding to nominal pilot frequency (centre line) and nominal pilot frequency $\pm \omega_d$ (33 Hz) are also plotted.

Figure 10.3 shows that the VCO frequency varies within the range $\pm \omega_d$, with a tendency to stay at more extreme values. Although further investigation of this phenomenon is required, the initial results suggest that the PLL offsets the pilot's spectrum from the centre of the bandpass filter. It may well be necessary to use wider BFFAGC bandpass filters in receivers using this form of frequency control.
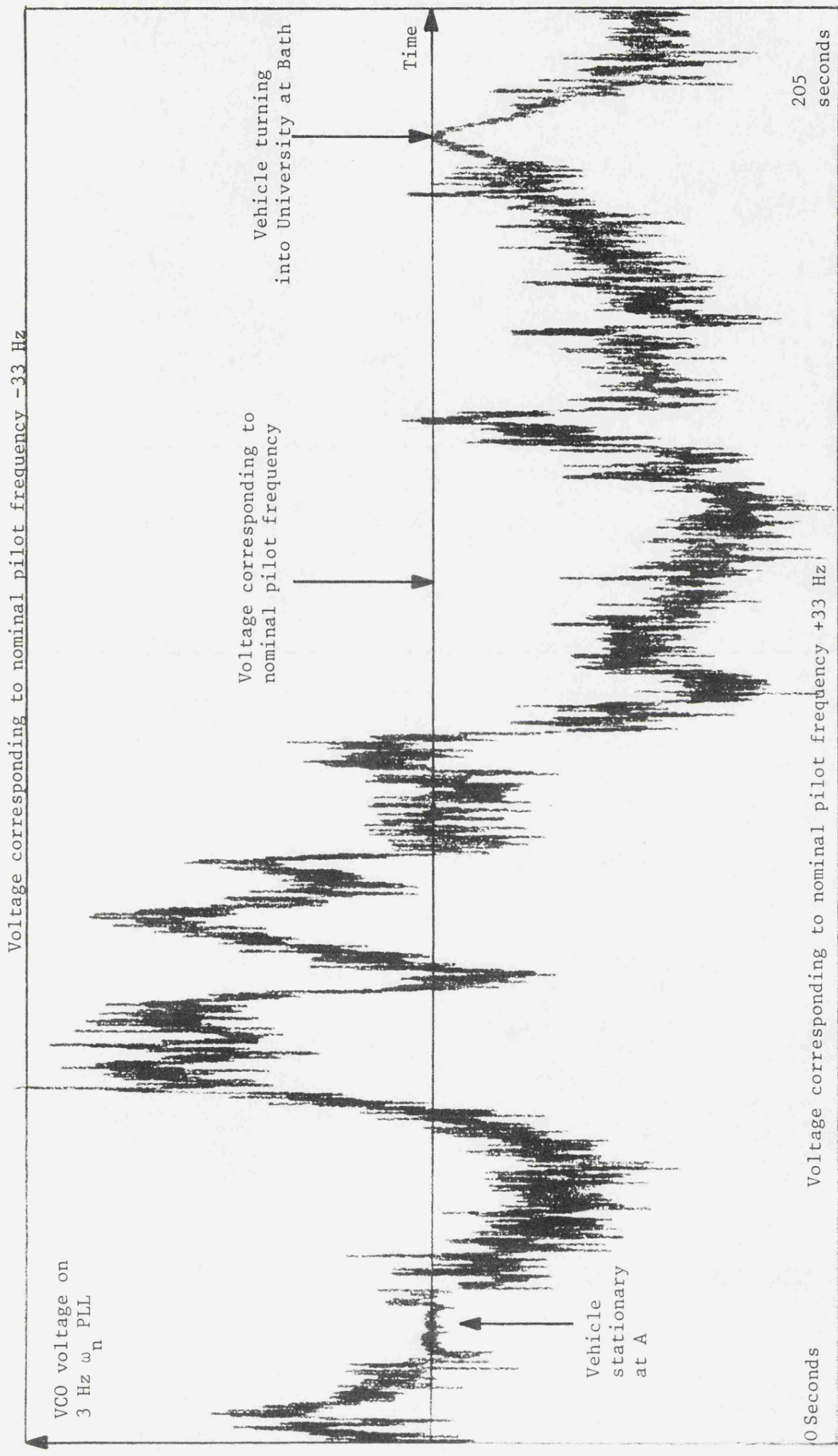
Figure 10.3 Plot of the VCO input voltage for the field trial described in section 10.4.2

Voltage corresponding to nominal pilot frequency +33 Hz

205 seconds

Time

Vehicle turning into University at Bath

Voltage corresponding to nominal pilot frequency

Voltage corresponding to nominal pilot frequency -33 Hz

VCO voltage on 3 Hz ω_n PLL

Vehicle stationary at A

0 Seconds

CHAPTER 11

CONCLUSIONS

This thesis has discussed the theoretical and experimental dynamic performance of a variety of AGC systems in the mobile multipath environment. Initially, deterministic test signals were developed to enable AGC systems to be analysed and designed on a worst case basis. These signals were then used to show that EIFBAGC generally has a poor dynamic performance and this is worsened by the effects of time delay and the use of coherent envelope detectors. LFFAGC was introduced and shown to offer improved dynamics but still require relatively large control path bandwidths to suppress deep fades. BFFAGC was then shown to be able to achieve a given performance specification for the narrowest required control bandwidth of all the AGC systems. Finally, the effects of decorrelation, noise and interference were shown to place limits on the ultimate performance of any AGC circuit.

In order to analyse the various AGC systems it was necessary to consider in detail the propagation-induced envelope variations they are required to suppress. Often only statistical descriptions of the incoming signal and its envelope variations were available. The non-linear nature of AGC, specifically the division process, necessitated the use of simple, deterministic signals in the analysis. A statistical comparison showed that the twin path (2 tone) test signal's envelope variations are likely to be more difficult for an AGC system to suppress than equivalent multipath envelope variations. Wherever possible,

therefore, the performance of an AGC system was analysed for twin path fading. The twin path fade was also shown to be representative of the aircraft communications situation, although this topic was not pursued further.

It was found that some modern theories of multipath propagation tended to neglect some important characteristics of the envelope. Specifically, the envelope is usually assumed to possess a power spectral density that is only significant up to twice maximum Doppler, $2\omega_d$. This assumption can lead to severe errors regarding the expected performance of AGC systems, especially their response to deep input fades. In order to illustrate this, the other deterministic AGC test signal used was based on a simple sinusoid. A comparison of the response of any of the AGC systems to sinusoidal and 2 tone envelope variations of the same fade rate demonstrates the importance of the higher frequency components of the incoming envelope.

The multipath performance of the various AGC systems was assessed by using recordings obtained from a 457 MHz UHF SSB system operating in the field. This system used a pilot tone-in-band reference and demonstrated that the original Wolfson VHF system could be operated at 457 MHz. Conventional transmitter and receiver design techniques were used and gave adequate system performance. The receiver was designed to have a wider IF filter than the transmitter to reduce the subjective effects of filter decorrelation on the performance of the BFFAGC circuit. The decision to collect multipath fading data from the field was vindicated by the demonstration of the various decorrelation, noise and interference effects not normally found in simple fading simulators.

It was shown that a variety of possible feedback AGC configurations existed, although invariably only their small signal performance was known. However, most of these were eliminated from further consideration by stipulating 5 simple requirements for a mobile radio's feedback AGC system to meet. EIFBAGC was found to meet all 5 requirements. In particular, it possessed a simple feedforward mathematical model that was used in all the subsequent analysis and gives a good conceptual understanding of its operation.

The division process inherent in AGC requires the denominator to follow the numerator's envelope variations very accurately for good fade suppression. The action of the first order denominator filtering operation in EIFBAGC results in poor suppression of deep input fades unless they occur at rates well inside the circuit's closed loop bandwidth. However, since it does possess only a first order roll-off characteristic, wanted envelope modulation frequencies should be well in excess of the EIFBAGC circuit's closed loop bandwidth to prevent their suppression and distortion. Thus it is found that EIFBAGC possesses a large frequency transition region between those unwanted envelope fading frequencies it will satisfactorily suppress and those wanted envelope modulation frequencies it will pass relatively undistorted. Typically, this frequency transition region extends over a 2 decade frequency range. An experimental precision EIFBAGC circuit was built which confirmed both the feedforward model and the theoretical sinusoidal predictions of the performance of EIFBAGC.

The twin path (2 tone) analysis of EIFBAGC required the use of a simple computer programme, called AGCSIM, based on the feedforward model. As expected, the 2 tone fade suppression ability of EIFBAGC

was worse than with equivalent sinusoidal input fading. An analysis of the effect of interfering tones showed that gain compression is more of a problem than gain modulation unless the interferer-pilot tone frequency difference was well within the EIFBAGC's closed loop bandwidth. Once again, the theoretical 2 tone predictions were confirmed by the experimental precision EIFBAGC circuit.

The performance of EIFBAGC in response to multipath field trial data was discussed in some detail. With the envelope fading encountered at UHF it was found that:

1) Unacceptably high closed loop bandwidths were required to achieve satisfactory suppression of the fading.

2) The 2 tone test signal is worst case on the following basis: An EIFBAGC system capable of suppressing twin path fading of a certain peak to trough ratio at a fade rate of $2\omega_d$ will always perform better in the multipath environment for fades of the same peak to trough ratio.

3) A "best-fit" single 2 tone fade cycle to a single multi-path input fade allowed accurate predictions of the EIFBAGC's response to the multipath fade.

Thus deterministic analysis of AGC systems enables their multipath performance to be assessed.

Full carrier AM receivers can be operated with EIFBAGC systems that are relatively unaffected by time delay since they do not require bandpass filters to extract the carrier. The closed loop EIFBAGC band-width is then only limited by the maximum acceptable speech compression and distortion constraints. However, a different situation arises with

pilot SSB systems. Here, the deleterious effects of time delay on the EIFBAGC dynamics caused by the pilot bandpass filter limit the upper closed loop bandwidth. The analysis of time delay effects derived the exact non-linear delay differential equation of the loop and presented an approximate feedforward model valid for sinusoidal input variations. The most significant effect of time delay is that it causes EIFBAGC systems to increase rather than suppress some sorts of input envelope variations, thus failing to meet the original AGC requirement of unconditional suppression. It was shown that only time delayless first order EIFBAGC systems possess the property of unconditional suppression (for step, sinusoidal and 2 tone input variation). Other effects such as subharmonic generation were shown to arise as a result of time delay, but are only significant for relatively large delay phases. Suggested operating delay phases are less than 0.2 radians, corresponding to an EIFBAGC closed loop bandwidth to first order pilot bandpass filter bandwidth ratio of 1:10 or more.

Using a typical SSB system time delay of 1 mS, it was shown that it was not possible to satisfactorily suppress the multipath fading encountered in the UHF SSB system with any closed loop EIFBAGC bandwidth. Low values of closed loop bandwidth had a naturally poor suppression of the fading while higher values resulted in excessive transient over-shoots and eventually instability.

Coherent envelope detectors using PLL offer the possibility of a significant reduction in the EIFBAGC loop's time delay by not requiring the use of a pilot bandpass filter. However, the PLL is required to accurately track the incoming pilot's phase for good detection of its envelope and this is a major problem in the multipath environment.

11.5

The "feedforward" model of coherent EIFBAGC demonstrates the circuit's tendency to convert the PLL tracking phase error into additional unwanted envelope variations. It was shown that a PLL will always lose lock to a deep enough twin path fade. Only PLL with bandwidths much greater than the incoming fade rate gave good estimates of the pilot's envelope although perfect envelope detection is never possible. The effects of the phase errors associated with the use of narrower PLL could be reduced by operating the EIFBAGC closed loop bandwidth well below the PLL bandwidth. A PLL ω_n to EIFBAGC closed loop bandwidth ratio of at least 30:1 is recommended. However, there are still other PLL effects to consider such as the out-of-lock situation and it is suggested that pilot SSB receivers should use incoherent bandpass filter/precision rectifier-type envelope detectors rather than coherent PLL envelope detectors.

None of the feedback AGC systems under discussion could give satisfactory suppression of the multipath fast fading encountered in the UHF SSB system. EIFBAGC is best suited to suppressing the large but relatively gradual variations of the incoming signal's envelope caused by slow fading. This then just leaves the multipath fast fading for feedforward AGC systems to suppress.

LFFAGC is a form of feedforward AGC most suited for use in full carrier AM systems. Its operation is based on a simple extension of the feedforward model of EIFBAGC, and much of the analysis of EIFBAGC can be easily adopted for use with LFFAGC. The main advantages of LFFAGC are the good time delay matching possible between numerator and denominator, and the reduction in the width of the transition region by using high order filters. The sinusoidal dynamic response of LFFAGC is very good - indeed, it is optimised for such sorts of

envelope variations. However, its 2 tone fade suppression ability is fairly poor for deep fades, demonstrating the importance of the higher frequency components of the input fading. LFFAGC is not suitable for use with pilot SSB systems and it was necessary to develop a new form of feedforward AGC-BFFAGC.

BFFAGC's good multipath envelope fade suppression ability can be explained by a simple observation regarding the statistical properties of multipath propagation. That is, before envelope detection the pilot is a narrow band signal while after envelope detection it is a wideband signal. BFFAGC can suppress twin path fading at up to twice the frequency that an equivalent LFFAGC circuit can operate. Furthermore, if the comparison is made using deep input fading the improvement is even more dramatic. Also unlike LFFAGC, BFFAGC can be incorporated into any system using a continuously transmitted pilot or carrier reference, even when it is transmitted below peak modulation.

The requirement for the bandpass filter to possess a very small passband ripple while having a linear phase characteristic means that non-recursive linear phase transversal filters are most suited to the task. An experimental BFFAGC circuit was built using commercially available IC filters and conventional analogue circuit techniques. This was found to have a good multipath envelope fade suppression ability at 457 MHz at vehicle speeds of up to at least 128 km/hr (80 mph). BFFAGC possesses almost perfect pilot AGC dynamics, but the field trial results demonstrated that other effects limit the ultimate dynamic performance of any AGC system - specifically, the effects of decorrelation, noise and interference.

The most noticeable subjective impairments to the post-BFFAGC audio signal were found to be noise bursts and the random phase modulation. The importance of a variable threshold circuit was demonstrated and a threshold level of about -20 dB below the mean input envelope rising to 0 dB in poor SNR situations is suggested. Nevertheless, even with these impairments BFFAGC was still found to offer a noticeable subjective improvement to the audio quality.

The decorrelation effects of MTDS are relatively insignificant for narrowband SSB systems, especially tone-in-band pilot SSB. However, far worse are the effects of receiver decorrelation caused by the crystal IF filter. The subjective effects of receiver decorrelation can be reduced to some extent by using a wider receiver IF filter. The problem is particularly acute for pilot carrier and tone-above-band SSB systems. One solution is to use an adaptive compensating pre-filter. Of course, the problem would be greatly reduced by using a low passband ripple linear phase IF filter and this may be made possible by some future advancements in transversal filter technology. The pilot-modulation decorrelation effects can then be reduced to the insignificant levels caused by MTDS.

Because of the use of relatively narrow bandpass filters on the control path, BFFAGC was found to be only slightly affected by receiver noise-induced gain compression and random modulation. Similar results also apply to EIFBAGC circuits using bandpass filter/precision rectifier type envelope detectors via the feedforward model. The main effect of receiver noise is, therefore, the subjective one of noise bursts already mentioned. The effects of external man-made noise need to be assessed for each system, but are not as significant at UHF as at the lower

frequencies. The threshold circuit places an upper limit to the noise induced gain variations, especially as it is raised during low SNR reception. Co-channel interference may be a major source of random gain modulation, especially at the levels of interference currently being considered to be acceptable. However, the subjective effects of both this and ignition-type interference still need to be assessed.

The random phase modulation of the incoming signal caused by multi-path propagation was found to be more of a problem on the pilot than the speech signal at 457 MHz. Nevertheless, this does raise some important questions relating to frequency control in the receiver. The work on coherent EIFBAGC showed that typical receiver PLL are unlikely to be able to significantly reduce the random phase modulation of the incoming signal at UHF. Furthermore, evidence was presented that suggested PLL also do not perform the apparently simpler task of frequency averaging - centering the pilot's spectrum on the bandpass filter. These observations could have important repercussions for system design at UHF.

This thesis has presented a unified treatment of the dynamics of AGC circuits incorporated into modern mobile radio receivers. The results indicate that conventional feedback techniques are not capable of satisfactorily suppressing envelope fast-fading and feedforward techniques are required as well. A combination of feedback and feed-forward AGC can meet an almost arbitrary receiver AGC performance specification. There is still a considerable amount of research to be done on pilot SSB mobile radio systems, but this thesis has attempted to answer some of the questions relating to automatic gain control.

CHAPTER 12

SUGGESTIONS FOR FUTURE WORK

This chapter briefly outlines a number of ideas and suggestions for future research on topics related to AGC and mobile radio.

12.1 Statistical Analysis

There is still further work to do concerning the statistical analysis of both the processes of multipath propagation and the response of AGC systems to such inputs. The most immediate questions relate to the statistical properties of the envelope at the output of an AGC system, including its PDF, CDF and power spectrum. According to Ohlson (5.12) the statistical characterisation of EIFBAGC to Rayleigh, Rician or log-normally distributed input envelopes requires more than just a knowledge of the first order statistics of the input. A general theory describing the division of an envelope function by a processed version of itself would allow the analysis of both FFAGC and FBAGC via the feedforward model.

12.2 Computer Simulation

An alternative approach to the problem of statistically analysing AGC can be made by using a combined computer simulation of multipath fading and AGC systems. Multipath fading can be simulated using techniques such as those described by Gladstone and McGeehan (2.6) or Leland and Sollenberger (10.6). A feedforward simulation similar to the AGCSIM programme would allow the response of several types of

feedback and feedforward AGC system to be evaluated. More sophisticated techniques would be required to simulate EIFBAGC with time delay and coherent AGC systems.

The simulation results could be presented in the form of statistical graphs of the type described by Gladstone and McGeehan (ibid). These may then be used as an independent check on a theoretical analysis or practical measurements of an AGC system. The simulation data corresponding to the AGC time domain input waveform could also be used as a pseudo-random test signal by replaying it in "real-time" through a D/A converter to external circuits.

12.3 Subjective Testing

The results obtained from either deterministic analysis, statistical analysis or computer simulation could be quantified subjectively to resolve a number of problems. For example, it would be particularly valuable to be able to relate an EIFBAGC system's bandwidth at a certain input fade rate to a subjective assessment of its performance. This would then enable decisions to be made, say, as to whether or not to incorporate FFAGC systems into receivers at the lower (VHF) PMR frequencies.

Other problems to be resolved by subjective testing include:

1) The basic effects of unwanted envelope fading and its suppression by various AGC systems.

2) The acceptable limits of the decorrelation effects of MTDS and the receiver's IF filters for various degrees of pilot fade suppression. This would be helpful, for example, in deciding whether a particular

receiver requires pre-BFFAGC compensating filters.

3) The effects of random gain modulation caused both by noise and interference. In particular, it would be interesting to compare the effects of co-channel interference on a pilot SSB system with an FM system under the same multipath fading conditions.

4) The effects of just multipath induced envelope modulation or just multipath induced phase modulation on an SSB system. It would be revealing to find out which was the worst and whether a good AGC system alone is sufficient signal processing in the receiver.

The emphasis in all the proposed subjective tests would be to resolve the effects of individual subjective impairments and discover how they combine to affect the overall system's performance.

12.4 Adaptive AGC systems

An adaptive AGC system is one in which the circuit parameters normally regarded as being "fixed" are varied in response to changing external conditions. A simple example of this has already been suggested, i.e. varying the threshold as the input SNR changes. A fully adaptive AGC system using feedforward techniques could, however, have not only the threshold but also several other parameters varied under circuit control. Suggested parameter variations and their relationship to external conditions include:

1) Independently variable pre and post envelope detection bandwidths. There is no need for the bandpass filter in a BFFAGC system to be wide enough to counteract multipath fading at the maximum expected fade rate if for much of the time the vehicle is driven more slowly. Thus the

12.3

pre-envelope detection bandwidth could be made directly proportional to the vehicle's speed (over certain limits). This may then reduce the random gain modulation effects of ignition interference in heavy traffic when the vehicle is likely to be travelling more slowly.

LFFAGC systems with insufficiently wide post envelope detection lowpass filters suffer from a "drop out" effect near the bottom of a deep fade similar to operation of the threshold circuit. This suggests varying the post-envelope detection bandwidth, perhaps in conjunction with the threshold voltage, not only as a function of input SNR but also other forms of interference. For example, if it were possible to measure the instantaneous level of co-channel interference, the post-envelope detection bandwidth and threshold level could be varied to reduce the random gain modulation, at the expense of reduced fade suppression, during areas of high interference.

2) Varying the division "law". During low input SNR or areas of high interference an alternative or supplementary technique to varying the threshold voltage and/or AGC bandwidth is to vary the division law. That is, the division process is deliberately made imperfect so as to result in finite output envelope variations. The simplest way of implementing this is to inject a small +ve dc offset voltage into the divider's denominator. This mainly affects the division process during the deepest part of an input fade, but it is a more gradual operation than the abrupt clamping action of the threshold circuit.

3) Variable parameter pre-BFFAGC IF compensating filter. It has already been suggested that this pre-BFFAGC filter may be required to vary with temperature as does the IF filter. However, a more ambitious system may attempt to compensate for the frequency selective fading effects

12.4

of MTDS using this filter. The main problem is to measure the instantaneous level of the incoming MTDS and its distribution across the received signal. This could be done by transmitting additional low level tones just outside the wanted modulation's spectrum as well as the main inband pilot tone. The fading on the additional pilots would be compared to that on the main pilot and the pre-BFFAGC compensating filter adjusted to compensate for the different arrival times of the envelope fading at different modulation frequencies.

12.5 Square Law Envelope Detectors

A square law envelope detector delivers a voltage proportional to the square of the input signal's envelope. In order to derive the envelope the square law envelope detector is followed by a square-rooting circuit. However, while the envelope is still in its squared form it possesses a unique characteristic. If the input to the detector were a narrowband process, bandwidth ω_f, then the squared output contains no envelope information above ω_f. This compares to a linear envelope detector that contains important spectral information well above ω_f. This is true for the case of bandlimited noise (12.1). It is also true for the 2 tone test signal. The output envelope of a linear envelope detector can be written in this case as:

$$r(t) = E(1 + R^2 + 2R \cos \omega_f t)^{\frac{1}{2}} \tag{12.1}$$

which contains important harmonics well above ω_f. However, the squared version of $r(t)$ is given by:

$$r(t)^2 = E^2(1 + R^2 + 2R \cos \omega_f t) \tag{12.2}$$

which contains zero spectral information above ω_f.

A major problem with conventional LFFAGC was shown to be its relatively poor performance when suppressing deep 2 tone fades, requiring the use of large post-envelope detector bandwidths to include many harmonics of the input envelope. However, if the linear envelope detector/ lowpass filter combination were replaced by a square law envelope detector/ lowpass filter/square root circuit combination it would have a greatly improved suppression of deep 2 tone fades. Square law envelope detectors could also be used in BFFAGC systems which also normally require large post-linear-envelope detector bandwidths. Note that the use of square law envelope detectors also requires a much larger bottom path dynamic range and additional dc coupled signal processing elements.

12.6 Diversity

One way of reducing the effects of multipath fading is to employ some form of diversity. This technique reduces the probability of a fade exceeding a certain depth by combining several received signals with uncorrelated fading envelopes. This normally involves the use of multiple transmitters or multiple receiver aerial systems together with special combining circuitry and is well described in the literature (12.2, 12.3,12.4). Besides reducing the range of the envelope fluctuations (like AGC) it results in an improved signal to noise ratio (unlike AGC). Unfortunately, its implementation is often too complex and expensive for the majority of PMR users, while certain practical difficulties are encountered in the aircraft situation. Nevertheless, Leland and Sollenberger (10.6) show theoretically that diversity can improve the reliability of communications with pilot SSB systems using feedforward signal processing. An important area of practical research is therefore into simple, econom- ically viable forms of diversity for pilot SSB systems with feedforward AGC.

12.7 Transparent Tone-in-Band SSB

The conventional inband tone pilot SSB system suffers from a disadvantage for some users. This is the fact that the baseband modulation channel is not user "transparent", i.e. the notches in the transmitter and receiver processing render part of the channel unusable. Furthermore, operation at the higher RF frequencies requires significant detrimental increases in notch width. However, as has already been demonstrated in chapter 10, there are a number of important advantages to be had in transmitting the pilot in the middle of the band compared to out-of-band pilot systems. Ideally, a pilot SSB system is therefore required that has the advantages of the inband tone system without losing any of the baseband spectrum. For this reason, "transparent tone-in-band" (TTIB) SSB modulation has been proposed.

TTIB operation is very simple. The baseband signal's spectrum (e.g. 300 Hz - 3 kHz) is split into 2 approximately equal frequency bands by suitable filtering (e.g. 300 Hz - 1.5 kHz and 1.5 kHz - 3 kHz). The upper frequency band is translated up in frequency by, say, 500 Hz. This is then added to the lower frequency band giving a signal extending from, e.g., 300 Hz - 1.5 kHz and 2 kHz - 3.5 kHz. This signal therefore has a "notch" 500 Hz wide into which the pilot can be added. The composite signal is then transmitted using conventional SSB techniques. The receiver extracts the pilot in the usual way for AFC, EIFBAGC and BFFAGC processing. The final stages of the receiver remove the pilot and perform a complementary downwards frequency translation of the upper half of the spectrum, regenerating the original 300 Hz - 3 kHz baseband signal. Thus TTIB gives the user a complete 300 Hz - 3 kHz channel from the baseband transmitter input to the baseband receiver output while possessing all the advantages of an inband pilot tone.

There is a small interference area in the centre of the received

signal's band due to practical filter roll-offs but this can be made

arbitrarily small by using high order filters. TTIB trades off trans-

mitted frequency spectrum bandwidth for notch width directly.

12.8 Feedforward Signal Regeneration

In the mobile multipath environment, the PLL circuits used in typical

SSB receivers have been shown to possess a relatively poor phase suppression

ability. Hence, as described in section 10.4, the output of a BFFAGC

circuit still suffers from the unwanted multipath induced phase modulation.

However, the phase variations can be suppressed by using feedforward AFC

techniques such as "heterodyne phase strippng" (12.2). Heterodyne phase

stripping removes the phase variations by using the received pilot as

a local oscillator in one of the receiver's frequency down conversion

operations. The unwanted phase variations of the pilot then simply

subtract from the unwanted phase variations of the complete received

signal. Unless the pilot is at the nominal carrier frequency, it needs

to be translated itself by a fixed oscillator prior to being used as the

down conversion local oscillator.

Feedforward Signal Regeneration (FFSR) simply extends the process

to include envelope suppression as well by BFFAGC techniques. Thus the

theoretical BFFAGC and feedforward AFC circuit of Leland and Sollenberger

is an FFSR system (10.6). At the higher RF frequencies FFSR is best

used in conjunction with TTIB and this appears to be a promising combination

for further research (12.5).

12.8

12.9 AFC Considerations

The final suggested area of research is into feedback automatic
frequency control systems for pilot SSB receivers. The FFAGC, feedforward
AFC and combined FFSR systems all require the multipath fading pilot's
spectrum to be extracted by a relatively narrow bandpass filter. As
indicated in section 10.4.2 it appears that conventional PLL may not
possess the required frequency averaging properties necessary to
accurately position the pilot's spectrum on the bandpass filter. Further
research is needed into this phenomenon to confirm that this is the
case. If it is so, then it may be possible to modify the receiver's PLL
or use other AFC techniques to perform the required frequency averaging.
The importance of the proposed work on the multipath performance of AFC
systems should not be underestimated since the results will affect the
design of many parts of a pilot SSB system.

REFERENCES

1.1 PANNEL, W.: "A study of the future frequency spectrum requirements
     for private mobile radio in the United Kingdom", Pye Tele-
     communications Ltd., Cambridge, 1976.

1.2 BARNES, D.M.: "A subjective evaluation of single sideband radio
     for use in private land mobile radio services - initial trials",
     Clerk Maxwell Commemorative Conference on Radio Receivers and
     Associated Systems, July 1981, Proc. No.50, IERE, pp.383-396.

1.3 LUSIGNAN, B.: "Single-sideband transmission for land mobile radio",
     IEEE Spectrum, July 1978, pp.33-37.

1.4 GOSLING, W.: "Protection ratio and economy of spectrum use in
     land mobile radio", IEE Proc. F, Commun., Radar and Signal
     Process., June 1980, Vol.127, No.3, pp.174-178.

1.5 Home Office Directorate of Radio Technology: "An interim report on
     subjective comparative tests of modulation methods for private
     mobile radio", Home Office Radio Regulatory Department, 1981.

1.6 COATES, R.F.W.: "Modern Communication Systems", Macmillan Press
     Ltd., 1975, Chapter 3, pp.90-122, and Chapter 5, pp.167-181.

1.7 WELLS, R.: "Radio telephones for the Home Office vhf single side-
     band trial", Clerk Maxwell Commemorative Conference on Radio
     Receivers and Associated Systems, July 1981, Proc.No.50, IERE,
     pp.363-371.

1.8   McGEEHAN, J.P., LIGHTFOOT, G., LYMER, A. and GOSLING, W.:
       "Optimisation of the Wolfson ssb radio receiver", Clerk Maxwell
       Commemorative Conference on Radio Receivers and Associated
       Systems, July 1981, Proc.No.50, IERE, pp.417-428.

1.9   LUSIGNAN, B.B.: "Convenience Circuits", Stanford University Technical
       Report No.30, June 1980, Stanford, CA94305.

1.10   - , "Fifty years of achievement: a history", Electronics, April
       17th 1980, Vol.53, No.9, p.425.

1.11   KTONAS, P.Y. and PAPP, N.: "Instantaneous envelope and phase
       extraction from real signals: theory, implementation, and an
       application to EEG analysis", Signal Processing (Netherlands),
       Oct. 1980, Vol.2, No.4, pp.373-385.

1.12   PAPPENFUS, E.W., BRUENE, W.D. and SCHOENIKE, E.O.: "Single Side-
       band Principles and Circuits", McGraw-Hill, 1964, Chapter 20,
       pp.315-339.

2.1   BULLINGTON, K.: "Radio propagation fundamentals", Bell Syst. Tech.
       J., May 1957, Vol.36, No.3, pp.593-626.

2.2   JAKES, W.C.: "Microwave Mobile Communications", Wiley-Interscience,
       1974, Chapter 2, pp.79-131.

2.3   LIVINGSTON, D.C.: "The Physics of Microwave Propagation", Prentice-
       Hall, 1970, Chapter 3, pp.19-58.

2.4   ALLSEBROOK, K. and PARSONS, J.D.: "Mobile radio propagation in
       .British cities at frequencies in the vhf and uhf bands", Proc.IEE,
       Feb. 1977, Vol.124, No.2, pp.95-102.

2.5   FRENCH, R.C.: "Radio propagation in London at 462 MHz", Radio and
      Electron. Eng., July 1976, Vol.46, No.7, pp.333-336.

2.6   GLADSTONE, K.J. and McGEEHAN, J.P.: "Computer simulation of multi-
      path fading in the land mobile radio environment", IEE Proc. G,
      Electron. Circ. and Syst., Dec. 1980, Vol.127, No.6, pp.323-330.

2.7   OSSANNA, J.F.: "A model for mobile radio fading due to building
      reflections: theoretical and experimental fading waveform power
      spectra", Bell Syst. Tech. J., Nov. 1964, Vol.43, pp.2935-2971.

2.8   BRIGGS, L.J. and LOWAN, A.N.: "Tables of Associated Legendre
      Functions", Columbia University Press, New York, 1945.

2.9   REED, H.R. and RUSSEL, C.M.: "Ultra High Frequency Propagation",
      Science Paperbacks (Chapman and Hall), 1965.

2.10 HARRIS, R.M.: "Characterization of the dynamical response of
      receivers to fading", Clerk Maxwell Commemorative Conference
      on Radio Receivers and Associated Systems, July 1981, Proc. No.50,
      IERE, pp.325-334.

3.1   CLARKE, R.H.: "A statistical theory of mobile-radio reception",
      Bell Syst. Tech. J., July-Aug. 1968, Vol.47, No.6, pp.957-1000.

3.2   JAKES, W.C.: "Microwave Mobile Communications", Wiley-Interscience,
      1974, Chapter 1, pp.11-78.

3.3   AULIN, T.: "A modified model for the fading signal at a mobile
      radio channel", IEEE Trans. Veh. Tech., Aug. 1979, Vol.VT-28,
      No.3, pp.182-203.

3.4   RICE, S.O.: "Mathematical analysis of random noise", Bell Syst.

Tech. J., Jan. 1945, Vol.24, No.1, pp.98-107;

"Statistical properties of a sine wave plus random noise", Bell

Syst. Tech. J., Jan. 1948, Vol.27, pp.109-157.

4.1   McGEEHAN, J.P. and LYMER, A.: "The problem of speech pulling and

its implications for the design of phaselocked SSB radio systems",

IEE Proc. F, Commun., Radar and Signal Process., Nov. 1981,

Vol.128, No.6, pp.361-369.

4.2   KRAUSS, H.L., BOSTIAN, C.W. and RAAB, F.H.: "Solid State Radio

Engineering", John Wiley and Sons, 1980, Chapter 8, pp.221-265.

4.3   GARDNER, F.M.: "Phaselock Techniques", John Wiley and Sons,

1979, Chapter 8, pp.144-164.

4.4   GARDNER, F.M.: "Phaselock Techniques", John Wiley and Sons,

1979, Chapter 4, pp.43-64.

5.1   OLIVER, B.M.: "Automatic volume control as a feedback problem",

Proc.IRE, April 1948, Vol.36, pp.466-473.

5.2   BANTA, E.D.: "Analysis of an automatic gain control (AGC)",

IEEE Trans. Auto. Control, April 1964, Vol.AC-9, pp.181-182.

5.3   GILL, W.J. and LEONG, W.K.S.: "Response of an AGC amplifier to two

narrow-band input signals", IEEE Trans. Comm. Tech., Aug. 1966,

Vol.COM-14, No.4, pp.407-416.

5.4   SIMPSON, R.S. and TRANTER, W.H.: "Baseband AGC in an AM-FM telemetry

system", IEEE Trans. Comm. Tech., Feb. 1970, Vol.COM-18, No.1,

pp.59-63.

5.5   BALL, J.R. and HOLMES, D.W.J.: "An ssb with pilot receiver for
       mobile radio", Clerk Maxwell Commemorative Conference on Radio
       Receivers and Associated Systems, July 1981, Proc. No.50,
       IERE, pp.429-435.

5.6   VICTOR, W.K. and BROCKMAN, M.H.: "The application of linear servo
       theory to the design of AGC loops", Proc.IRE, Feb. 1960, Vol.48,
       pp.234-238.

5.7   MOSKOWITZ, J.: "Linear feedback AGC with input-level-invariant
       response times", J. Acoust. Soc. Am., Dec. 1977, Vol.62, No.6,
       pp.1449-1456.

5.8   HUGHES, R.S.: "Design automatic gain control loops the easy way",
       EDN, Oct. 5, 1978, pp.123-128.

5.9   PLOTKIN, S.: "On nonlinear AGC", Proc. IEEE, Feb. 1963, Vol.51,
       p.380.

5.10   SCHACTER, H. and BERGSTEIN, L.: "Noise analysis of an automatic gain
       control system", IEEE Trans. Auto. Control, July 1964, Vol.AC-9,
       pp.249-255.

5.11   RICKER, D.W.: "Nonlinear feedback system for the normalisation of
       active sonar returns", J. Acoust. Soc. Am., Feb. 1976, Vol.59,
       No.2, pp.389-396.

5.12   OHLSON, J.E.: "Exact dynamics of automatic gain control", IEEE Trans.
       Comm., Jan. 1974, Vol.COM-22, pp.72-75.

5.13   WILLIAMS, N.A.F.: "Automatic gain control systems", Wireless World,
       Sept. 1977, Vol.83, pp.60-61.

5.14 GREEN, D.N.: "Nonlinear analysis of an AGC circuit", Proc. 1980

IEEE Int. Symp. on Circuits, April 1980, Part 1, p.233.

5.15 HEALEY, M.: "Principles of Automatic Control", English Universities

Press Ltd., 1975, Chapter 5, pp.64-87 and Chapter 7, pp.118-130.

5.16 HEALEY, M.: "Principles of Automatic Control", English Universities

Press Ltd., 1975, Chapter 9, pp.167-193.

5.17 MOORE, J.B.: "AGC noise considerations in receiver design",

Electronics, May 1945, Vol.18, No.5, pp.116-118.

5.18 KRAUSS, H.L., BOSTIAN, C.W. and RAAB, F.H.: "Solid State Radio

Engineering", John Wiley and Sons, 1980, Chapter 9, pp.266-294.

5.19 GRAEME, J.G., TOBEY, G.E. and HUELSMAN, L.P.: "Operational Amplifiers,

Design and Applications", McGraw-Hill Kogakusha Ltd., 1971,

Chapter 7, pp.236-281.

5.20 McGEEHAN, J.P. and BURROWS, D.F.: "Large signal performance of

feedback automatic gain control systems", IEE Proc. F, Commun.,

Radar and Signal Process., April 1981, Vol.128, No.2, pp.110-117.

6.1 PAINTER, W.A.: "An hf packset receiver-transmitter using direct

conversion", Clerk Maxwell Commemorative Conference on Radio

Receivers and Associated Systems, July 1981, Proc.No.50, IERE,

pp.199-211.

6.2 GRAEME, J.G., TOBEY, G.E. and HUELSMAN, L.P.: "Operational Amplifiers,

Design and Applications", McGraw-Hill Kogakusha Ltd., 1971,

Chapter 8, pp.282-326.

6.3   KUO, F.F.: "Network Analysis and Synthesis", John Wiley and Sons, 1966, Chapter 8, pp.212-252.

6.4   BURROWS, D.F. and McGEEHAN, J.P.:"Time delay in receiver AGC systems", Clerk Maxwell Commemorative Conference on Radio Receivers and Associated Systems, July 1981, Proc.No.50, IERE, pp.73-88.

7.1   GARDNER, F.M.: "Phaselock Techniques", John Wiley and Sons, 1979, Chapter 2, pp.8-24.

7.2   GARDNER, F.M.: "Phaselock Techniques", John Wiley and Sons, 1979, Chapter 9, pp.165-197.

7.3   BRAUN, W. and LINDSEY, W.C.: "Acquisition behaviour of coupled AGC and phase-locked loop systems", Proc. Natl. Telecom. Conf., Dec. 1975, Vol.2, Session 30, pp.12-15.

7.4   GAGLIARDI, R.M.: "Coupled AGC-Costas loops with AM/PM conversion", IEEE Trans. Comm., Jan. 1980, Vol.COM-28, No.1, pp.122-127.

7.5   RICE, S.O.: "Statistical properties of a sine wave plus random noise", Bell Syst. Tech. J., Jan. 1948, Vol.27, pp.109-157.

7.6   BISWAS, B.N., RAY, S.K., BHATTACHARYA, A.K., SARKAR, B.C. and BANERJEE, P.: "Phase detector response to noisy and noisy fading signals", IEEE Trans. Aero. and Electron. Sys., March 1980, Vol.AES-16, No.2, pp.150-156.

7.7   WEBER, W.J.: "Performance of phase-locked loops in the presence of fading communication channels", IEEE Trans. Comms., May 1976, Vol.COM-24, pp.487-499.

7.8   KLIGER, I.E. and OLENBERGER, C.F.: "Phase-lock loop jump phenomenon
        in the presence of two signals", IEEE Trans. Aero. and Electron.
        Sys., Jan. 1976, Vol.AES-12, No.1, pp.55-64.

8.1   HOPPER, A.L.: "An experimental fast acting AGC circuit", IRE
        Convention Record-Veh. Comm., Vol.10, pt.8, 1962, pp.13-20.

8.2   ANTONIOU, A.: "Digital Filters: Analysis and Design", McGraw-Hill,
        1979, Chapter 9, pp.218-253.

8.3   KUO, F.F.: "Network Analysis and Synthesis", John Wiley and Sons,
        1966, Chapter 13, pp.365-412.

8.4   RAWLING, A.J., McGEEHAN, J.P. and GOSLING, W.:"Forward feeding AGC
        with extended signal delays", Proc. Conf. Radio Receivers and
        Associated Systems, 1978, IERE, pp.85-92.

8.5   PRICE, S.: "The G4BWE speech processor", Rad. Comm., Oct. 1980,
        pp.1018-1024.

8.6   HOPPER, A.L.: "Forward acting automatic gain control", Nat. Electron.
        Conf., Oct. 1963, Vol.19, pp.358-370.

9.1   McGEEHAN, J.P. and BURROWS, D.F.: "Performance limits of feedforward
        automatic gain control in mobile radio receivers", IEE Proc. F,
        Commun., Radar and Signal Process., Nov. 1981, Vol.128, No. 6,
        pp.385-392.

9.2   McGEEHAN, J.P. and BURROWS, D.F.: "The impact of CCD technology
        on feedforward automatic gain control systems for mobile radio
        communications", EUROCON '80, March 1980, Stuttgart, pp.184-188.

9.3   MILLMAN, J. and HALKIAS, C.C.: "Integrated Electronics: Analogue

and Digital Circuits and Systems", McGraw-Hill Kogakusha, 1972,

Chapter 16, pp.537-592.

9.4   BURROWS, D.F. and McGEEHAN, J.P.: "The use of feedforward automatic

gain control for reducing fast fading in single sideband mobile

radio systems", Proc. Int. Conf. Radio Spectrum Conservation

Techniques, July 1980, IEE, London, pp.22-25.

9.5   McGEEHAN, J.P. and BATEMAN, A.: "Subjective performance of amplitude

companding in SSB mobile radio systems", Electron. Lett., 29th

Oct. 1981, Vol.17, No.22, pp.859-860.

10.1 JAKES, W.C.: "Microwave Mobile Communications", Wiley-Interscience,

1974, Chapter 4, pp.161-307.

10.2 HILL, P.C.J.: "Simultaneous Subliminal Signalling in Conventional

Sound Circuits", BBC Engineering, May 1972, pp.14-25.

10.3 HAWKSFORD, M.J. and REZAEE, N.: "Adaptive mean-square-error trans-

versal equaliser", IEE Proc. F, Commun., Radar and Signal Process.,

Oct. 1981, Vol.128, No.5, pp.296-304.

10.4 BENNET, W.R.: "Response of a linear rectifier to signal and noise",

Bell Syst. Tech. J., Jan. 1944, Vol.23, pp.97-113.

10.5 GOSLING, W.: "A simple mathematical model of co-channel and

adjacent channel interference in land mobile radio", IEEE Trans.

Veh. Tech., Nov. 1980, Vol.VT-29, No.4, pp.361-364.

10.6 LELAND, K.W. and SOLLENBERGER, N.R.: "Impairment mechanisms for SSB mobile communications at UHF with pilot-based Doppler/fading correction", Bell Syst. Tech. J., Dec. 1980, Vol.59, No.10, pp.1923-1942.

12.1 RANDALL, R.B.: "Application of B and K equipment to frequency analysis", Bruel and Kjaer, Sept. 1977, Appendix B, pp.224-228.

12.2 PARSONS, J.D., HENZE, M., RATLIFF, P.A. and WITHERS, M.J.: "Diversity techniques for mobile radio reception", Radio and Electron. Eng., July 1975, Vol.45, No.7, pp.357-367.

12.3 PARSONS, J.D. and RATLIFF, P.A.: "Diversity reception for vhf mobile radio", Radio and Electron. Eng., May 1973, Vol.43, No.5, pp.317-324.

12.4 GOSLING, W., MARTIN, J.D., HOLBECHE, R.J. and ALLEN, G.: "Sideband diversity: a new application of diversity particularly suited to land mobile radio", Radio and Electron. Eng., March 1978, Vol.48, No.3, pp.133-139.

12.5 McGEEHAN, J.P., BATEMAN, A.J. and BURROWS, D.F.: "The use of "transparent" tone-in-band (TTIB) and feedforward signal regeneration (FFSR) in single sideband communication systems", to be published at "Communications 82", IEE, April 1982.

APPENDICES

PEAK FADE RATE OF TWIN PATH SIGNALS

The fade rate of a twin path signal is defined from equations 2.8, 2.9 and 2.14 as ω_f where:

$$\omega_f = \left[\frac{X_1 - St}{((X_1 - St)^2 + Y_1^2)^{\frac{1}{2}}} - \frac{X_2 - St}{((X_2 - St)^2 + Y_2^2)^{\frac{1}{2}}} \right] \omega_d \qquad (A1.1)$$

The peak fade rate occurs when:

$$\frac{d\omega_f}{dt} = 0 \qquad (A1.2)$$

To solve this, consider first:

$$\frac{d}{dt}\left[\frac{X - St}{((X - St)^2 + Y^2)^{\frac{1}{2}}} \right] =$$

$$\frac{((X - St)^2 + Y^2)^{\frac{1}{2}}(-S) - (X - St)\frac{1}{2}((X - St)^2 + Y^2)^{-\frac{1}{2}} \cdot 2(X - St)(-S)}{(X - St)^2 + Y^2} =$$

$$\frac{S(X - St)^2((X - St)^2 + Y^2)^{-\frac{1}{2}} - S((X - St)^2 + Y^2)^{\frac{1}{2}}}{(X - St)^2 + Y^2} \qquad (A1.3)$$

Multiplying the top and bottom of (A1.3) by $((X - St)^2 + Y^2)^{\frac{1}{2}}$ gives:

$$\frac{d}{dt}\left[\frac{X - St}{((X - St)^2 + Y^2)^{\frac{1}{2}}} \right] =$$

$$\frac{S(X - St)^2 - S((X - St)^2 + Y^2)}{((X - St)^2 + Y^2)^{3/2}} = \frac{- SY^2}{((X - St)^2 + Y^2)^{3/2}} \qquad (A1.4)$$

Therefore, it follows that:

$$\frac{d\omega_f}{dt} = \left[\frac{SY_2^2}{((X_2 - St)^2 + Y_2^2)^{3/2}} - \frac{SY_1^2}{((X_1 - St)^2 + Y_1^2)^{3/2}}\right] \omega_d \quad (A1.5)$$

To solve (A1.2) then:

$$\frac{Y_2^2}{((X_2 - St)^2 + Y_2^2)^{3/2}} - \frac{Y_1^2}{((X_1 - St)^2 + Y_1^2)^{3/2}} = 0 \quad (A1.6)$$

that is:

$$Y_2^2((X_1 - St)^2 + Y_1^2)^{3/2} - Y_1^2((X_2 - St)^2 + Y_2^2)^{3/2} = 0 \quad (A1.7)$$

or:

$$Y_2^2((X_1 - St)^2 + Y_1^2)^{3/2} = Y_1^2((X_2 - St)^2 + Y_2^2)^{3/2} \quad (A1.8)$$

Raising both sides to the power $2/3$ gives:

$$Y_2^{4/3}((X_1 - St)^2 + Y_1^2) = Y_1^{4/3}((X_2 - St)^2 + Y_2^2) \quad (A1.9)$$

which can be rewritten as:

$$Y_2^{4/3}(X_1^2 + (St)^2 - 2X_1 St + Y_1^2) - Y_1^{4/3}(X_2^2 + (St)^2 - 2X_2 St + Y_2^2) = 0 \quad (A1.10)$$

Expanding (A1.10) gives an equation of the form:

$$A(st)^2 + Bst + C = 0 \quad (A1.11)$$

A3

where

$$A = Y_2^{4/3} - Y_1^{4/3} \qquad \text{(A1.12)}$$

$$B = 2X_2 Y_1^{4/3} - 2X_1 Y_2^{4/3} \qquad \text{(A1.13)}$$

$$C = Y_2^{4/3}X_1^2 + Y_2^{4/3}Y_1^2 - Y_1^{4/3}X_2^2 - Y_1^{4/3}Y_2^2 \qquad \text{(A1.14)}$$

There are therefore 2 solutions to the peak fade rate when:

$$St = \frac{-B \pm \sqrt{B^2 - 4AC}}{2A} \qquad \text{(A1.15)}$$

providing $Y_1 \neq Y_2$.

If $Y_1 = Y_2 = Y$ then the fade rate peaks just once. The time it peaks is given by equation (A1.11) as:

$$St = \frac{Y^{4/3}X_2^2 + Y^{4/3}X_1^2}{2(X_2 Y^{4/3} - X_1 Y^{4/3})} \qquad \text{(A1.16)}$$

which simplifies to:

$$St = \frac{X_1 + X_2}{2} \qquad \text{(A1.17)}$$

i.e., the peak fade rate then occurs when the vehicle is equidistant from each scattering source.

If 1 source is directly in front and 1 source directly behind the vehicle so that $Y_1 = Y_2 = 0$, then:

$$\omega_f = \left[\frac{X_1 - St}{((X_1 - St)^2)}^{\frac{1}{2}} - \frac{X_2 - St}{((X_2 - St)^2)}^{\frac{1}{2}} \right] \omega_d \qquad \text{(A1.18)}$$

A4

Using "| |" to represent "magnitude of" then:

$$\omega_f = \left[\frac{X_1 - St}{|X_1 - St|} - \frac{X_2 - St}{|X_2 - St|} \right] \omega_d \qquad (A1.19)$$

Therefore, providing the vehicle is in between the 2 sources then:

$$\omega_f = 2\omega_d \qquad (A1.20)$$

When the vehicle is not in between them, then:

$$\omega_f = 0 \qquad (A1.21)$$

APPENDIX 2

THE PEAK SLEW RATE OF THE ENVELOPE

The peak slew rate of $r(t)$, termed $\hat{r}(t)_{slew}$ in decibel form is found as follows:

$$r(t) = 10 \log_{10} (1 + R^2 + 2R \cos \omega_f t) \qquad (A2.1)$$

The rate is given by the time derivative of $r(t)$ i.e.:

$$\frac{d}{dt} r(t) = \frac{-20}{\ln 10} \left[\frac{R\omega_f \sin \omega_f t}{1 + R^2 + 2R \cos \omega_f t} \right] \quad dB/sec \qquad (A2.2)$$

The peak rate occurs when the time derivative of equation A2.2 is equal to zero i.e. when:

$$\frac{-20}{\ln 10} \left[\frac{(1 + R^2 + 2R \cos \omega_f t)(R\omega_f^2 \cos \omega_f t) + (R\omega_f t \sin \omega_f t)(2R\omega_f \sin \omega_f t)}{(1 + R^2 + 2R \cos \omega_f t)^2} \right] = 0$$

$$(A2.3)$$

that is:

$$(1 + R^2 + 2R \cos \omega_f t)\cos \omega_f t + 2R \sin^2 \omega_f t = 0 \qquad (A2.4)$$

so:

$$\cos \omega_f t = \frac{-2R}{(1 + R^2)} \qquad (A2.5)$$

Using the principle value of (A2.5) corresponding to the positive going edge of the fade gives:

A6

$$\omega_f t = 2\pi - \cos^{-1}\left[\frac{-2R}{(1 + R^2)}\right] \qquad (A2.6)$$

Substitution of (A2.6) into (A2.2) gives the peak slew rate as:

$$\hat{r}(t)_{slew} = \frac{20 \,\omega_f \, R \, \sin\left[\cos^{-1}\left[\frac{-2R}{1 + R^2}\right]\right]}{\ln(10)\left[1 + R^2 - \left[\frac{4R}{(1 + R^2)}\right]\right]} \quad dB/sec \qquad (A2.7)$$

APPENDIX 3

THE SOLUTION OF EQUATION 5.12

This is the equation describing the response of EIFBAGC to a sinu-soidal input variation. It is written:

$$\frac{V_K(1 + D \sin \omega_s t)}{(1 + LD \sin(\omega_s t - \theta))} - \frac{LD\omega_s \cos(\omega_s t - \theta)}{C(1 + LD \sin(\omega_s t - \theta))} - V_K = 0 \qquad (A3.1)$$

multiplying through by $C(1 + LD \sin(\omega_s t - \theta))$ and expanding gives:

$$CV_K D \sin \omega_s t - LD \omega_s \cos \omega_s t \cos \theta - LD \omega_s \sin \omega_s t \sin \theta$$

$$- CV_K LD \sin \omega_s t \cos \theta + CV_K LD \cos \omega_s t \sin \theta = 0 \qquad (A3.2)$$

Equating the $\cos \omega_s t$ terms to zero gives:

$$- LD \omega_s \cos \theta + CV_K LD \sin \theta = 0 \qquad (A3.3)$$

Hence:

$$\tan \theta = \frac{\omega_s}{CV_K} \qquad (A3.4)$$

i.e.:

$$\theta = \tan^{-1} \left[\frac{\omega_s}{CV_K} \right] \qquad (A3.5)$$

Let

$$\frac{\omega_s}{CV_K} = \omega_N \qquad (A3.6)$$

then equating the $\sin \omega_s t$ terms to zero gives:

$$1 - \omega_N L \sin \theta - L \cos \theta = 0 \qquad (A3.7)$$

therefore:

$$L = \frac{1}{\omega_N \sin \theta + \cos \theta} \qquad (A3.8)$$

However, $\cos \theta$ and $\sin \theta$ are related to $\tan \theta$ by the following 2 formulae:

$$\cos \theta = \frac{1}{(1 + \tan^2 \theta)^{\frac{1}{2}}} \qquad \text{(A3.9)}$$

$$\text{and:} \quad \sin \theta = \frac{\tan \theta}{(1 + \tan^2 \theta)^{\frac{1}{2}}} \qquad \text{(A3.10)}$$

Substituting for tan θ from A3.4 via A3.9 and A3.10 into A3.8 gives:

$$L = \frac{1}{\dfrac{\dfrac{\omega^2}{N}}{\dfrac{(1 + \omega^2)^{\frac{1}{2}}}{N}} + \dfrac{1}{\dfrac{(1 + \omega^2)^{\frac{1}{2}}}{N}}} \qquad \text{(A3.11)}$$

which simplifies to:

$$L = \frac{1}{\dfrac{(1 + \omega^2)^{\frac{1}{2}}}{N}} \qquad \text{(A3.12)}$$

APPENDIX 4

THE PEAK AND TROUGH POSITION OF EQUATION 5.25

The peak and trough position of equation 5.25 occurs when its differential equals zero. Thus since:

$$v_o = V_K \left[\frac{1 + D \sin \omega_N t}{1 + LD \sin(\omega_N t - \theta)} \right] \tag{A4.1}$$

then $\dfrac{dv_o(t)}{dt} = 0$ is required. Calculating $\dfrac{dv_o(t)}{dt}$ and equating the numerator to zero gives:

$$(1 + LD \sin(\omega_N t - \theta))(\omega_N D \cos \omega_N t) - (1 + D \sin \omega_N t)(\omega_N LD \cos(\omega_N t - \theta)) = 0 \tag{A4.2}$$

Expanding the brackets, dividing by $\omega_N D$ and simplifying gives:

$$\cos \omega_N t + LD \sin(\omega_N t - \theta) \cos \omega_N t - L \cos(\omega_N t - \theta)$$
$$- LD \sin \omega_N t \cos(\omega_N t - \theta) = 0 \tag{A4.3}$$

Expanding the terms involving products of sines and cosines and simplifying gives:

$$\cos \omega_N t - LD \sin \theta - L \cos(\omega_N t - \theta) = 0 \tag{A4.4}$$

Expanding the $L \cos(\omega_N t - \theta)$ term and rearranging gives:

$$(1 - L \cos \theta) \cos \omega_N t - (L \sin \theta) \sin \omega_N t = LD \sin \theta \tag{A4.5}$$

This can be written in polar form as:

$$(1 - 2L \cos \theta + L^2)^{\frac{1}{2}} \sin \left[\omega_N t - \tan^{-1} \left[\frac{L \sin \theta}{1 - \cos \theta} \right] + N\pi \right] = LD \sin \theta \tag{A4.6}$$

From Appendix 3, L and θ can be substituted for functions of ω_N in the first order EIFBAGC system to give:

$$\left[\frac{\omega_N^2}{(1 + \omega_N^2)} \right]^{\frac{1}{2}} \sin(\omega_N t - \tan^{-1}\left[\frac{1}{\omega_N} \right] + N\pi) = \frac{\omega_N D}{(1 + \omega_N^2)} \qquad (A4.7)$$

i.e.

$$\sin\left(\omega_N t - \tan^{-1}\left[\frac{1}{\omega_N} \right] + N\pi \right) = \frac{D}{(1 + \omega_N^2)^{\frac{1}{2}}} \qquad (A4.8)$$

The principle values of the solution to this equation are chosen to give:

$$\beta_{po} = \tan^{-1}\left[\frac{1}{\omega_N} \right] - \sin^{-1}\left[\frac{D}{(1 + \omega_N^2)^{\frac{1}{2}}} \right] + 2\pi \qquad (A4.9)$$

$$\beta_{to} = \tan^{-1}\left[\frac{1}{\omega_N} \right] + \sin^{-1}\left[\frac{D}{(1 + \omega_N^2)^{\frac{1}{2}}} \right] + \pi \qquad (A4.10)$$

APPENDIX 5

APPROXIMATE SOLUTION OF A_n, HARMONICS OF EQUATION 5.25

Equation 5.25 can be written as:

$$v_o(t) = \frac{n(t)}{d(t)} = V_K \frac{(1 + D \sin \omega_N t)}{(1 + LD \sin (\omega_N t - \theta))} \qquad (A5.1)$$

The solution required occurs for $\omega_N > 1$ so that $\theta \to 90°$.

Therefore (A5.1) can be approximated by:

$$v_o(t) \simeq \frac{n(t)}{d(t)} = V_K \frac{(1 + D \sin \omega_N t)}{(1 - LD \cos \omega_N t)} \qquad (A5.2)$$

If $\quad n(t) = V_K(1 + D \sin \omega_N t) \qquad (A5.3)$

and $\quad d(t) = (1 - LD \cos \omega_N t) \qquad (A5.4)$

then the approximate solution works by expanding $\frac{1}{d(t)}$ as a series and multiplying this by $n(t)$. The series of $\frac{1}{d(t)}$ is only solved here for 3 terms, i.e.:

$$\frac{1}{d(t)} = 1 + LD \cos \omega_N t + L^2 D^2 \cos^2 \omega_N t \qquad (A5.5)$$

which can be rewritten as:

$$\frac{1}{d(t)} = 1 + LD \cos \omega_N t + 0.5 L^2 D^2 + 0.5 L^2 D^2 \cos 2\omega_N t \qquad (A5.6)$$

multiplying equation A5.6 by A5.3 gives the approximation to $v_o(t)$ as:

$$v_o(t) \simeq V_K(1 + D \sin \omega_N t)(1 + LD \cos \omega_N t + 0.5 L^2 D^2 + 0.5 L^2 D^2 \cos 2\omega_N t)$$

$$(A5.7)$$

Expanding the brackets of equation A5.7 and dropping all dc terms since only the harmonics are required gives:

$$\frac{v_o(t)}{V_K} = LD \cos \omega_N t + 0.5L^2D^2 \cos 2\omega_N t + D \sin \omega_N t$$
$$+ LD^2 \sin \omega_N t \cos \omega_N t + 0.5L^2D^3 \sin \omega_n t$$
$$+ 0.5L^2D^3 \sin \omega_N t \cos 2\omega_N t \tag{A5.8}$$

If $L < 1$, as is the case for $\omega_N > 1$, then the terms that predominate in the calculation of the magnitudes of the various harmonics in the above equation give:

$$A_1 = D \tag{A5.9}$$

$$A_2 = 0.5LD^2 \tag{A5.10}$$

$$A_3 = 0.25L^2D^3 \tag{A5.11}$$

From which the general approximation for A_n is inferred as:

$$A_n = (D)^n (0.5L)^{n-1} \tag{A5.12}$$

A13

APPENDIX 6

TWO TONE AUTOMATIC GAIN CONTROL SIMULATION

PROGRAMME: AGCSIM

AGCSIM is a programme written in 12K extended basic. It runs on a "Research Machines" 380Z microcomputer and also requires an interface unit and XY plotter to record results. It uses feedforward techniques to analyse the response of AGC systems to the envelope of a 2 tone test signal. It can therefore be used to analyse the response of EIFBAGC (via the feedforward model) or feedforward AGC systems proper. This appendix outlines some of the characteristics of the programme along with operating details. The main equations defining the programmes operation are also presented, allowing similar programmes to be written for other machines.

The programme's structure and operation is best understood by reference to figure A6.1. This shows a block diagram of the feedforward circuit modelled by the programme, along with defining equations. The user inputs the various quantities as shown, the programme aiding this with prompts. Once all the variables are entered, the programme runs, plotting the data and input and output waveform shapes calculating them over 360 points i.e. 1 point every degree of the fundamental frequency. The numerical outputs that are plotted are:

IP o— → PT —A— TD —B— → ÷ —→ o OP

PB —C— BL —D— RC —E— VT —F—

ER - see main text

N FFT
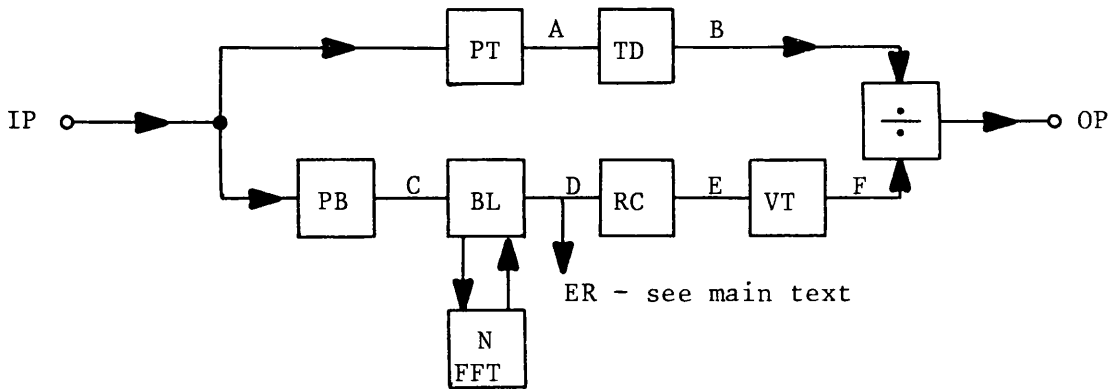
$$IP = (1 + R^2 + 2R \cos(2\pi T))^{\frac{1}{2}}: \quad \text{user inputs peak to trough ratio, KI, in dB.}$$

$$A = (1 + (PTR)^2 + 2PTR \cos(2\pi T))^{\frac{1}{2}}: \quad \text{user inputs PT, a decorrelation quantity on the top path fade. Input unity for perfect correlation.}$$

$$B = (1 + (PTR)^2 + 2PTR \cos(2\pi T - TD))^{\frac{1}{2}}: \quad \text{user inputs TD, a differential time delay. Input zero for perfect matching other than RC filtering.}$$

$$C = (1 + (PBR)^2 + 2PBR \cos(2\pi T))^{\frac{1}{2}}: \quad \text{user inputs PB, a decorrelation quantity on the bottom path fade. Input unity for perfect correlation.}$$

D   Comprised of an N point FFT of C, truncated (i.e. brickwall filtered) at BL coefficient (inclusive). Input N (usually 64) and BL. Note that FFT give dc and all cosine coefficients up to $(N/2-1)$ therefore $BL \leq (N/2-1)$.

E   Modified coefficients of FFT by first order lag. Time constant is RC relative to fade rate, i.e. input $RC = 0.1$ for $\omega_N = 10$ etc.

F   Threshold version of E. User inputs VT, time domain value at F never goes below VT.

OP = B/F. Division takes place in time domain on a point by point basis over 360 intervals of one fade cycle.

Figure A6.1   Structure of AGCSIM

1. ER. This is the value of the point C, the time domain waveform, divided by the equivalent value of the FFT of C the frequency domain representation, at PI. It is a measure of the programme's accuracy and, ideally, should be 0 dB. It is used mainly for check purposes and is not usually of great use.

2. KO. This is the most useful programme result. It is the ratio of the peak to trough output variation in decibels.

The accuracy of the programme's ability to calculate KO deteriorates as the input variation, KI, increases and N decreases. A measure of the programme's accuracy may be made by setting PT and PB to unity, TD to zero and RC to 10,000. If the user inputs KI and N, the programme will respond with a finite value of KO. Ideally this should be 0 dB since the output should possess no variation. In practice, it is found that large values of N are required to get acceptable programme accuracies. For example, in most of the work presented in this thesis, N = 64 was used. This gives a programme error of 0.2276 dB for a 30 dB input variation. Some typical programme outputs are shown overleaf.
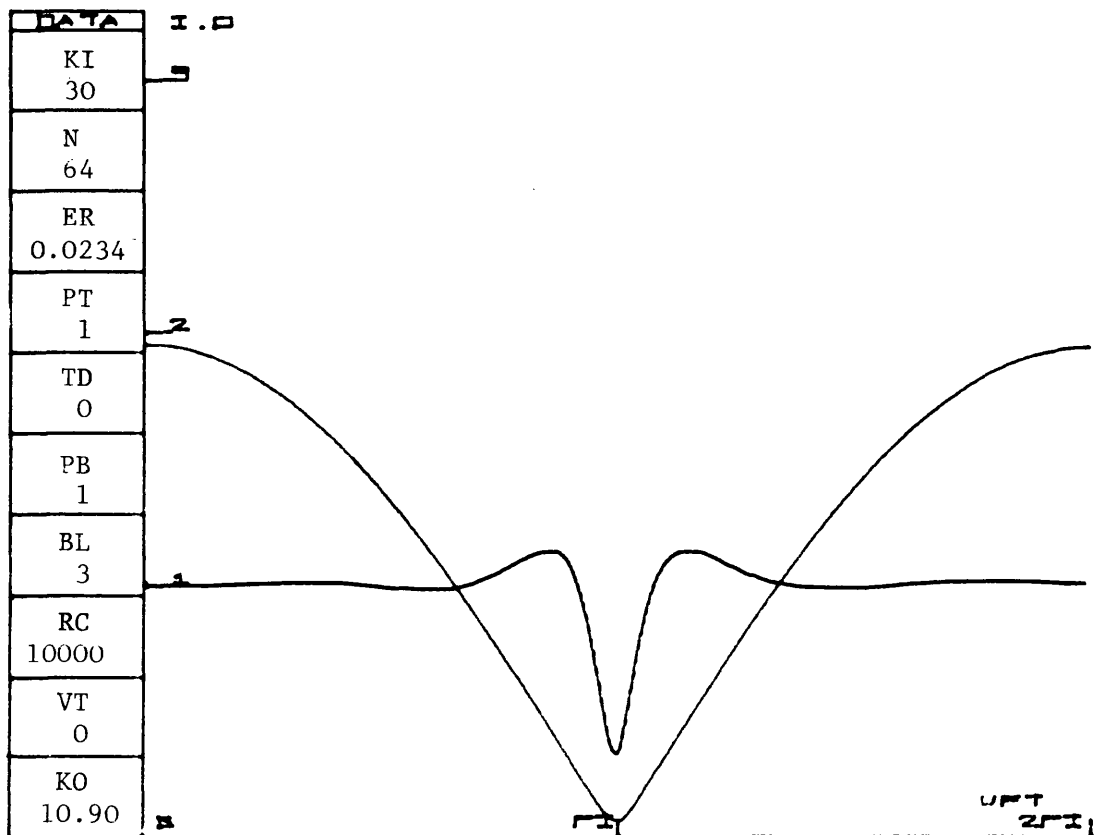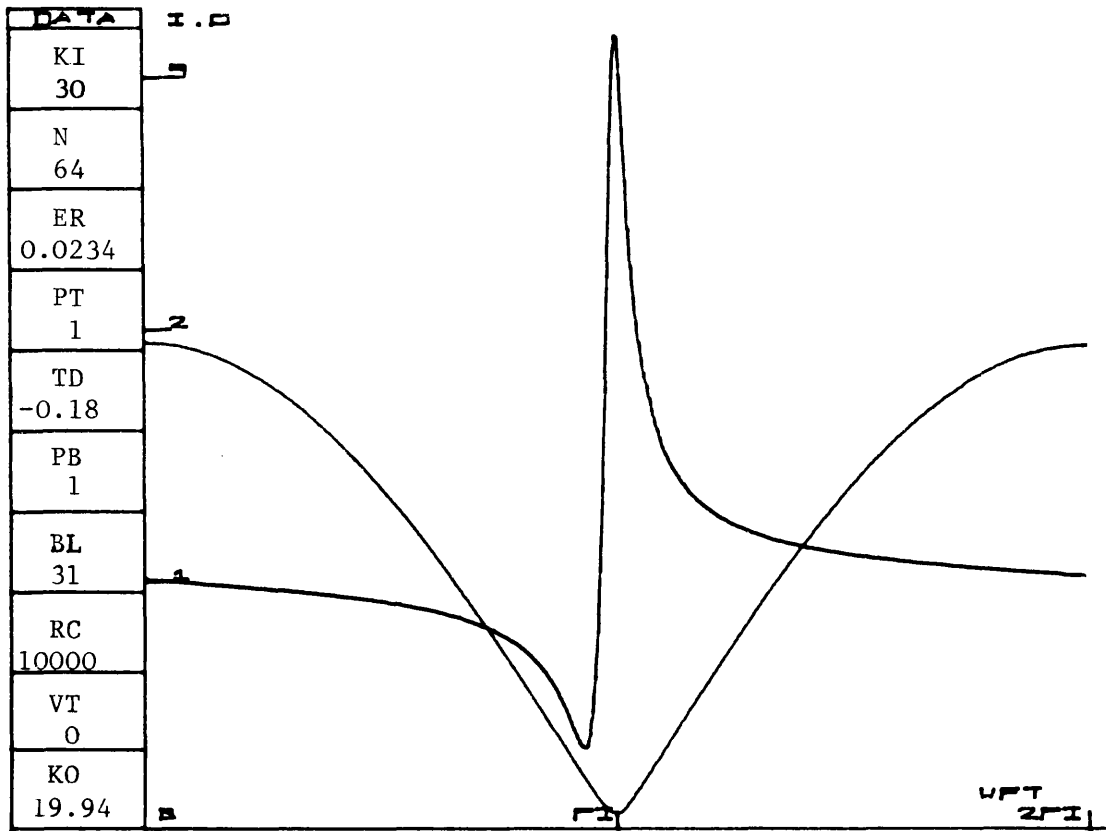
DATA	
KI	30
N	64
ER	0.0234
PT	1
TD	-0.18
PB	1
BL	31
RC	10000
VT	0
KO	19.94

DATA	
KI	30
N	64
ER	0.0234
PT	1
TD	0
PB	1
BL	3
RC	10000
VT	0
KO	10.90

Figure A6.2   Some typical AGCSIM results

DATA   1.0

KI	30
N	64
ER	0.0234
PT	0.87
TD	0
PB	1
BL	31
RL	100000
VT	0
KO	10.05

DATA   1.0

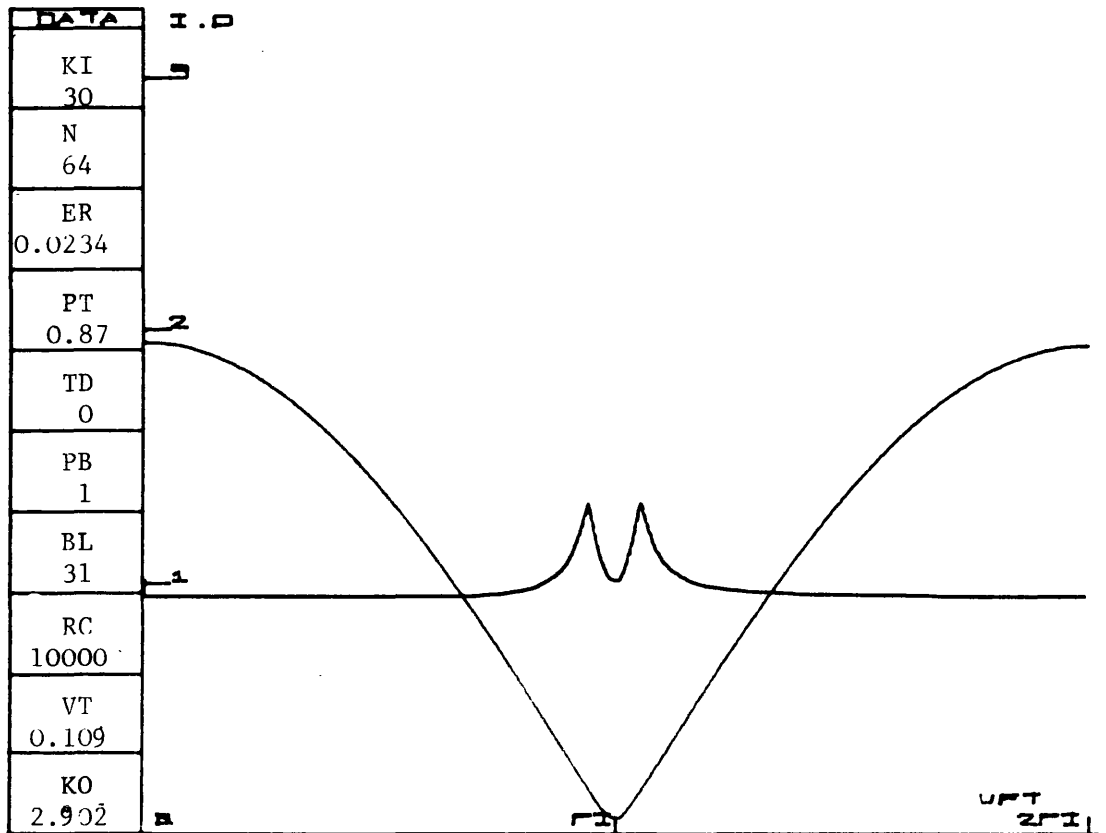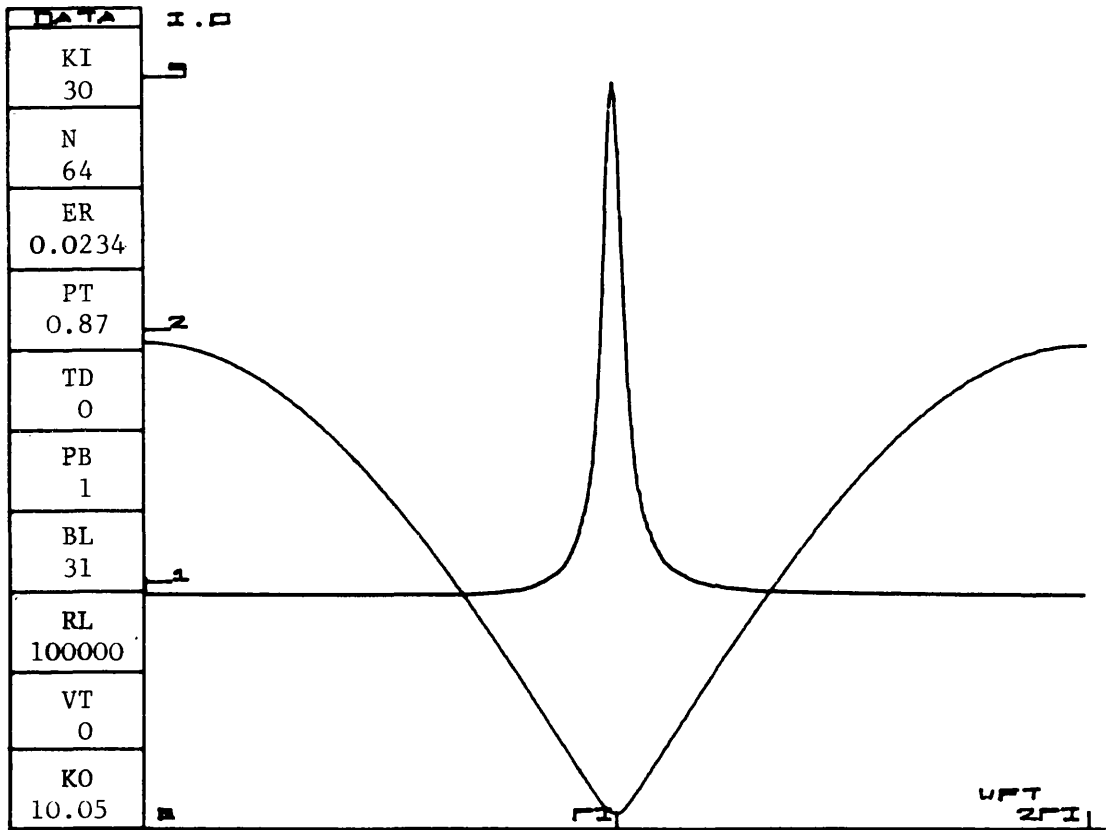| KI | 30 |
N	64
ER	0.0234
PT	0.87
TD	0
PB	1
BL	31
RC	10000
VT	0.109
KO	2.902

Figure A6.3   Some typical AGCSIM results

SOLUTION OF EQUATION 6.12 FOR DC AND FUNDAMENTAL COMPONENTS

Equation 6.12 is:

$$- \frac{LD\omega_S \cos(\omega_S t - \theta)}{C(A + LD \sin(\omega_S t - \theta))} - V_K + \frac{V_K(1 + D \sin(\omega_S t - \omega_S T))}{(A + LD \sin(\omega_S t - \omega_S T - \theta))} \simeq 0 \qquad (A7.1)$$

multiplying through by:

$$C(A + LD \sin(\omega_S t - \theta))(A + LD \sin(\omega_S t - \omega_S T - \theta)) \qquad (A7.2)$$

gives:

$$(-LD\omega_S \cos(\omega_S t - \theta))(A + LD \sin(\omega_S t - \omega_S T - \theta))$$

$$- CV_K(A + LD \sin(\omega_S t - \theta))(A + LD \sin(\omega_S t - \omega_S T - \theta))$$

$$+ CV_K(A + LD \sin(\omega_S t - \theta))(1 + D \sin(\omega_S t - \omega_S T)) \simeq 0 \qquad (A7.3)$$

expanding gives:

$$- ALD\omega_S \cos(\omega_S t - \theta)$$

$$- \frac{L^2 D^2 \omega_S}{2} \sin(2\omega_S t - 2\theta - \omega_S T) + \frac{L^2 D^2 \omega_S}{2} \sin \omega_S T$$

$$- CV_K A^2 - CV_K ALD \sin(\omega_S t - \omega_S T - \theta) - CV_K ALD \sin(\omega_S t - \theta)$$

$$- \frac{CV_K L^2 D^2}{2} \cos \omega_S T + \frac{CV_K L^2 D^2}{2} \cos(2\omega_S t - 2\theta - \omega_S T)$$

$$+ CV_K A + CV_K AD \sin(\omega_S t - \omega_S T) + CV_K LD \sin(\omega_S t - \theta)$$

$$+ \frac{CV_K LD^2}{2} \cos(\theta - \omega_S T) - \frac{CV_K LD^2}{2} \cos(2\omega_S t - \theta - \omega_S T) \simeq 0 \qquad (A7.4)$$

From which the various components are equated to zero to solve for A,
L and θ. Note that the second harmonic components do not equate to
zero due to the approximation at $v_g(t)$. Equating the dc components to
zero gives:

$$\frac{L^2D^2\omega_S}{2} \sin \omega_S T - CV_K A^2 - \frac{CV_K L^2D^2}{2} \cos \omega_S T + CV_K A$$

$$+ \frac{CV_K LD^2}{2} \cos(\theta - \omega_S T) = 0 \qquad (A7.5)$$

Making the substitutions:

$$\omega_N = \frac{\omega_S}{CV_K} \qquad (A7.6)$$

and $\quad \phi = CV_K T \qquad (A7.7)$

Equation A7.5 simplifies to:

$$A^2 - A - 0.5(L^2D^2\omega_N \sin(\phi\omega_N) - L^2D^2\cos(\phi\omega_N)$$

$$+ LD^2\cos(\theta - \phi\omega_N)) = 0 \qquad (A7.8)$$

Since A $\geq$ 1, then the solution is:

$$A = 0.5 + 0.5 \sqrt{1 + 2(L^2D^2\omega_N \sin(\phi\omega_N) - L^2D^2\cos(\phi\omega_N) \ldots}$$

$$\overline{\ldots + LD^2\cos(\theta - \phi\omega_N))} \qquad (A7.9)$$

Thus providing L and θ were known, A could be calculated. It is there-
fore required to solve for L and θ to generate equations that are
independent of A. This will not be performed here, but instead equations
will now be derived for L and θ that are only weakly dependent on A.

Equating the fundamental components of equation A7.4 to zero and
expanding gives:

$- ALD\omega_S \cos \omega_S t \cos \theta - ALD\omega_S \sin \omega_S t \sin \theta$

$- CV_K ALD \sin \omega_S t \cos(\theta + \omega_S T) + CV_K ALD \cos \omega_S t \sin(\theta + \omega_S T)$

$- CV_K ALD \sin \omega_S t \cos \theta + CV_K ALD \cos \omega_S t \sin \theta$

$+ CV_K AD \sin \omega_S t \cos \omega_S T - CV_K AD \cos \omega_S t \sin \omega_S T$

$+ CV_K LD \sin \omega_S t \cos \theta - CV_K LD \cos \omega_S t \sin \theta = 0$ \hfill (A7.10)

The coefficients of $\sin \omega_S t$ are, after substitution for ω_N and ϕ:

$- ALD\omega_N \sin \theta - ALD \cos(\theta + \phi\omega_N) - ALD \cos \theta + LD \cos \theta$

$\hspace{6cm} + AD \cos \phi\omega_N = 0$ \hfill (A7.11)

which simplifies to:

$- AL\omega_N \sin \theta - AL \cos(\theta + \phi\omega_N) + L(1 - A)\cos \theta + A \cos \phi\omega_N = 0$ \hfill (A7.12)

Similarly, the coefficients for $\cos \omega_S t$ are, after substitution for

ω_N and ϕ:

$- AL\omega_N \cos \theta + AL \sin(\theta + \phi\omega_N) + (A - 1)L \sin \theta - A \sin \phi\omega_N = 0$ \hfill (A7.13)

From (A7.12) and (A7.13) two equations can be formed:

$$L = \frac{A \cos(\phi\omega_N)}{A\omega_N \sin \theta + A \cos(\theta + \phi\omega_N) + (A - 1)\cos \theta}$$ \hfill (A7.14)

and:

$$L = \frac{A \sin(\phi\omega_N)}{A \sin(\theta + \phi\omega_N) - A\omega_N \cos \theta + (A - 1) \sin \theta}$$ \hfill (A7.15)

Equating the two and cross multiplying gives:

$A \cos(\phi\omega_N)(A \sin(\theta + \phi\omega_N) - A\omega_N \cos \theta + (A - 1) \sin \theta)$

$\hspace{0.5cm} = A \sin(\phi\omega_N)(A\omega_N \sin \theta + A \cos(\theta + \phi\omega_N) + (A - 1)\cos \theta)$ \hfill (A7.16)

Expanding this gives:

$$A\cos(\phi\omega_N)\sin\theta\cos(\phi\omega_N) + A\cos(\phi\omega_N)\cos\theta\sin(\phi\omega_N)$$

$$- A\omega_N\cos(\phi\omega_N)\cos\theta + (A-1)\cos(\phi\omega_N)\sin\theta - A\omega_N\sin(\phi\omega_N)\sin\theta$$

$$- A\sin(\phi\omega_N)\cos\theta\cos(\phi\omega_N) + A\sin(\phi\omega_N)\sin\theta\sin(\phi\omega_N)$$

$$- (A-1)\cos\theta\sin(\phi\omega_N) = 0 \qquad\qquad (A7.17)$$

which simplifies to:

$$A\sin\theta + (A-1)\cos(\phi\omega_N)\sin\theta - A\omega_N\sin(\phi\omega_N)\sin\theta$$

$$- A\omega_N\cos(\phi\omega_N)\cos\theta - (A-1)\sin(\phi\omega_N)\cos\theta = 0 \qquad\qquad (A7.18)$$

Thus:

$$\sin\theta(A - A\omega_N\sin(\phi\omega_N) + (A-1)\cos(\phi\omega_N))$$

$$+ \cos\theta(-(A-1)\sin(\phi\omega_N) - A\omega_N\cos(\phi\omega_N)) = 0 \qquad\qquad (A7.19)$$

therefore:

$$\tan\theta = \frac{A\omega_N\cos(\phi\omega_N) + (A-1)\sin(\phi\omega_N)}{A - A\omega_N\sin(\phi\omega_N) + (A-1)\cos(\phi\omega_N)} \qquad\qquad (A7.20)$$

Hence:

$$\theta = \tan^{-1}\left[\frac{A\omega_N\cos(\phi\omega_N) + (A-1)\sin(\phi\omega_N)}{A - A\omega_N\sin(\phi\omega_N) + (A-1)\cos(\phi\omega_N)}\right] + N\pi \qquad (A7.21)$$

Now to find L. Into equation A7.14, θ is substituted from A7.20 using the formulae:

$$\cos\theta = \frac{1}{(1 + \tan^2\theta)^{\frac{1}{2}}} \quad\text{and}\quad \sin\theta = \frac{\tan\theta}{(1 + \tan^2\theta)^{\frac{1}{2}}} \qquad (A7.22)$$

which gives:

$$L = \cfrac{A\cos(\phi\omega_N)}{A\omega_N\cfrac{\tan\theta}{(1+\tan^2\theta)^{\frac{1}{2}}} + \cfrac{A\cos(\phi\omega_N)}{(1+\tan^2\theta)^{\frac{1}{2}}} - \cfrac{A\tan\theta\sin(\phi\omega_N)}{(1+\tan^2\theta)^{\frac{1}{2}}} + \cfrac{(A-1)}{(1+\tan^2\theta)^{\frac{1}{2}}}} \qquad (A7.23)$$

i.e.:

$$L = \frac{A\cos(\phi\omega_N)(1+\tan^2\theta)^{\frac{1}{2}}}{(A\omega_N - A\sin(\phi\omega_N))\tan\theta + A\cos(\phi\omega_N) + (A-1)} \qquad (A7.24)$$

If:

$$\tan\theta = \frac{X}{Y} = \frac{A\omega_N\cos(\phi\omega_N) + (A-1)\sin(\phi\omega_N)}{A - A\omega_N\sin(\phi\omega_N) + (A-1)\cos(\phi\omega_N)} \qquad (A7.25)$$

then:

$$L = \frac{A\cos(\phi\omega_N)(1 + \frac{X^2}{Y^2})^{\frac{1}{2}}}{(A\omega_N - A\sin(\phi\omega_N))\frac{X}{Y} + A\cos(\phi\omega_N) + (A-1)} \qquad (A7.26)$$

i.e.:

$$L = \frac{A\cos(\phi\omega_N)(X^2 + Y^2)^{\frac{1}{2}}}{(A\omega_N - A\sin(\phi\omega_N))X + AY\cos(\phi\omega_N) + (A-1)Y} \qquad (A7.27)$$

Substituting for X and Y from A7.25 gives:

$$L = \frac{A\cos(\phi\omega_N)((A - A\omega_N\sin(\phi\omega_N) + (A-1)\cos(\phi\omega_N)^2}{(A\omega_N - A\sin(\phi\omega_N))(A\omega_N\cos(\phi\omega_N) + (A-1)\sin(\phi\omega_N))} \quad \ldots\ldots$$

$$\ldots\ldots\frac{+ (A\omega_N\cos(\phi\omega_N) + (A-1)\sin(\phi\omega_N))^2)^{\frac{1}{2}}}{+ (A\cos(\phi\omega_N) + (A-1))(A - A\omega_N\sin(\phi\omega_N) + (A-1)\cos(\phi\omega_N)}$$

$$(A7.28)$$

Expanding the numerator of L, L_N, gives:

$$A \cos(\phi\omega_N)(A^2 - A^2\omega_N\sin(\phi\omega_N) + A(A - 1)\cos(\phi\omega_N) - A^2\omega_N\sin(\phi\omega_N)$$

$$+ A^2\omega_N^2 \sin^2 \phi\omega_N - A(A - 1)\omega_N \sin(\phi\omega_N)\cos(\phi\omega_N)$$

$$+ A(A - 1)\cos \phi\omega_N - A(A - 1)\omega_N \sin(\phi\omega_N)\cos(\phi\omega_N)$$

$$+ (A - 1)^2 \cos^2(\phi\omega_N) + A^2\omega_N^2 \cos^2(\phi\omega_N)$$

$$+ (A - 1)^2 \sin^2 (\phi\omega_N) + 2A(A - 1)\sin(\phi\omega_N)\cos(\phi\omega_N))^{\frac{1}{2}} \qquad (A7.29)$$

which simplifies to:

$$L_N = A \cos(\phi\omega_N)(A^2 + (A - 1)^2 - 2A^2\omega_N \sin(\phi\omega_N)$$

$$+ 2A(A - 1)\cos(\phi\omega_N) + A^2\omega_N^2)^{\frac{1}{2}} \qquad (A7.30)$$

Similarly, the denominator of L, L_D, can be expanded to give:

$$L_D = A^2\omega_N^2 \cos(\phi\omega_N) + A\omega_N(A - 1)\sin(\phi\omega_N) - A^2\omega_N \sin(\phi\omega_N)\cos(\phi\omega_N)$$

$$- A(A - 1)\sin^2(\phi\omega_N) + A^2 \cos(\phi\omega_N) + A(A - 1)$$

$$- A^2\omega_N \cos(\phi\omega_N)\sin(\phi\omega_N) - A(A - 1)\omega_N \sin(\phi\omega_N)$$

$$+ A(A - 1)\cos^2(\phi\omega_N) + (A - 1)^2 \cos(\phi\omega_N) \qquad (A7.31)$$

which simplifies to:

$$L_D = 2A(A - 1)\cos^2(\phi\omega_N) + (A^2 + (A - 1)^2 + A^2\omega_N^2)\cos(\phi\omega_N)$$

$$- 2A^2\omega_N \cos(\phi\omega_N)\sin(\phi\omega_N)$$

Substitution of L_N and L_D to form L in the next equation gives:

$$L = \frac{A(A^2 + (A - 1)^2 - 2A^2\omega_N \sin(\phi\omega_N) + 2A(A - 1)\cos(\phi\omega_N) + A^2\omega_N^2)^{\frac{1}{2}}}{(A^2 + (A - 1)^2 - 2A^2\omega_N \sin(\phi\omega_N) + 2A(A - 1)\cos(\phi\omega_N) + A^2\omega^2_N)}$$

$$(A7.32)$$

Therefore

$$L = \frac{A}{(A^2 + A^2\omega_N^2 + (A - 1)^2 - 2A^2\omega_N \sin(\phi\omega_N) + 2A(A - 1)\cos(\phi\omega_N))^{\frac{1}{2}}}$$

$$(A7.33)$$

We now have explicit equations for both L and θ. Unfortunately, they are both functions of A and also do not allow simple solution by direct substitution. However, both L and θ are only weakly dependent on A and since A $\simeq$ 1 the solutions are thought to be acceptable, especially as the main text does not use them in their full form. The equations for L, θ and A are rewritten thus:

$$L = \frac{1}{(1 + \omega_N^2 + ((A - 1)/A)^2 - 2\omega_N \sin(\phi\omega_N) + 2((A - 1)/A)\cos(\phi\omega_N))^{\frac{1}{2}}}$$

(A7.34)

$$\theta = \tan^{-1}\left[\frac{\omega_N \cos(\phi\omega_N) + ((A - 1)/A)\sin(\phi\omega_N)}{1 - \omega_N \sin(\phi\omega_N) + ((A - 1)/A)\cos(\phi\omega_N)}\right] + N\pi$$

(A7.35)

$$A = 0.5 + 0.5 \sqrt{1 + 2(L^2 D^2 \omega_N \sin(\phi\omega_N) - L^2 D^2 \cos(\phi\omega_N) + LD^2 \cos(\theta - \phi\omega_N))}$$

(A7.36)

APPENDIX 8

SOLUTION OF EQUATION 6.33

This equation can be written in full as:

$$\frac{\sqrt{\left(\frac{L'}{A}\right)^2 D^2 \cos^2\theta + \left(\frac{L'}{A}\right)^2 + 1 - 2\left(\frac{L'}{A}\right)\cos\theta - \left(\frac{L'}{A}\right)^2 D^2}}{1 - \left(\frac{L'}{A}\right) D^2 \cos\theta} \leqslant 1 \qquad (A8.1)$$

That is:

$$\left(\frac{L'}{A}\right)^2 D^2 \cos^2\theta + \left(\frac{L'}{A}\right)^2 + 1 - 2\left(\frac{L'}{A}\right)\cos\theta - \left(\frac{L'}{A}\right)^2 D^2$$

$$\leqslant 1 - 2\left(\frac{L'}{A}\right) D^2 \cos\theta + \left(\frac{L'}{A}\right)^2 D^4 \cos^2\theta \qquad (A8.2)$$

which simplifies to:

$$\left(\frac{L'}{A}\right)(D^2 \cos^2\theta - D^4 \cos^2\theta - D^2 + 1) \leqslant 2\cos\theta - 2D^2 \cos^2\theta \qquad (A8.3)$$

therefore:

$$\left(\frac{L'}{A}\right) \leqslant \frac{2(1 - D^2)\cos\theta}{(1 - D^2)(1 + D^2 \cos^2\theta)} \qquad (A8.4)$$

hence:

$$\left(\frac{L'}{A}\right) \leqslant \frac{2\cos\theta}{1 + D^2 \cos^2\theta} \qquad (A8.5)$$

The maximum value of D is given by equation 6.24 as:

$$D = \left(\frac{A}{L'}\right) \qquad (A8.6)$$

Substitution into equation A8.5 for D gives:

$$\left(\frac{L'}{A}\right) \leqslant \frac{2 \cos \theta}{1 + \left(\frac{A}{L'}\right)^2 \cos^2 \theta} \qquad (A8.7)$$

which expands to give:

$$\left(\frac{L'}{A}\right)^2 - 2 \left(\frac{L'}{A}\right) \cos \theta + \cos^2\theta \leqslant 0 \qquad (A8.8)$$

which simplifies to:

$$\left[\left(\frac{L'}{A}\right) - \cos \theta\right]^2 \leqslant 0 \qquad (A8.9)$$

Hence the relationship between L, A and θ for unconditional suppression is:

$$\left(\frac{L'}{A}\right) \leqslant \cos \theta \qquad (A8.10)$$

APPENDIX 9

POST PRECISION RECTIFIER LOWPASS FILTER REQUIREMENTS

Let the (non fading) pilot tone reference at the input of the precision fullwave rectifier be c(t) where:

$$c(t) = E \cos \omega_p t \qquad (A9.1)$$

The dc (envelope) component of c(t) is obtained by the precision fullwave rectifier taking the absolute value of c(t). The output of the precision rectifier can be written as the Fourier series:

$$|c(t)| = \frac{2E}{\pi} \left[1 - \sum_{n=1}^{\infty} \left[\frac{2}{(4n^2 - 1)} \cos (2n\omega_p t) \right] \right] \qquad (A9.2)$$

Passing this through a lowpass filter results in attenuation of the ac components, with proportionally more attenuation of the higher harmonics. Therefore, to a good approximation the output of the lowpass filter (for convenience, possessing a dc gain of $\pi/2$) is given by d(t) where:

$$d(t) \simeq E \left(1 - \frac{2a}{3} \cos(2\omega_p t - PS) \right) \qquad (A9.3)$$

where a is the lowpass filter's gain at $2\omega_p$ and PS its phase shift. Since a << 1 then the act of dividing d(t) into the top path may be approximated, using a 2 term Taylor series expansion, as multiplying the numerator, n(t), to give a divider output:

$$\text{Divider Output} \simeq \frac{1}{E} \left[1 + \frac{2a}{3} \cos(2\omega_p t - PS) \right] n(t) \qquad (A9.4)$$

This amplitude modulation causes a 3rd harmonic of the pilot tone to appear at the divider output. With just pilot tone at the numerator:

$$n(t) = E \cos \omega_p t \qquad\qquad\qquad\qquad (A9.5)$$

the divider output is therefore:

$$\text{Divider Output} \simeq \left(1 + \frac{2a}{3} \cos(2\omega_p t - PS)\right) \cos \omega_p t \qquad (A9.6)$$

which can be expanded, since a << 1, to:

$$\text{Divider Output} \simeq \cos \omega_p t + \frac{a}{3} \cos(3\omega_p t - PS) \qquad (A9.7)$$

Therefore to a first approximation, the ratio of the 3rd harmonic of the pilot tone to fundamental is given by:

$$\text{3rd Harmonic Distortion} = 20 \log_{10} (a/3) \qquad dB \qquad (A9.8)$$

PUBLISHED PAPERS

Paper 1:   McGEEHAN, J.P. and BURROWS, D.F.: "Large signal performance

of feedback automatic gain control systems", IEE Proc. F,

Commun., Radar and Signal Process., April 1981, Vol.128, No.2,

pp.110-117.

Paper 2:   McGEEHAN, J.P. and BURROWS, D.F.: "Performance limits of feed-

forward automatic gain control in mobile radio receivers",

IEE Proc. F, Commun., Radar and Signal Process., Nov. 1981,

Vol.128, No.6, pp.385-392.

These two papers are included at the end of this section.

Also published by the author:

1.   BURROWS, D.F. and McGEEHAN, J.P.: "The application of feedforward

automatic gain control to mobile radio receivers as a means of

reducing multipath interference", Colloquium on Modern Techniques

for Combatting Multipath Interference in Radio, Radar and Sonar

Systems, Nov. 1979, digest No. 1979/62, IEE Electronics Division.

2.   McGEEHAN, J.P. and BURROWS, D.F.: "The impact of CCD technology on

feedforward automatic gain control systems for mobile radio

communications", EUROCON '80, March 1980, Stuttgart, pp.184-188.

3.   BURROWS, D.F. and McGEEHAN, J.P.: "The use of feedforward automatic

gain control for reducing fast fading in single sideband mobile

radio systems", Proc. Int. conf. Radio Spectrum Conservation

Techniques, July 1980, IEE, London, pp.22-25.

4. BURROWS, D.F. and McGEEHAN, J.P.: "Time delay in receiver AGC systems",
    Clerk Maxwell Commemorative Conference on Radio Receivers and
    Associated Systems, July 1981, Proc.No.50, IERE, pp.73-88.

5. BURROWS, D.F. and McGEEHAN, J.P.: "Feedback and feedforward automatic
    gain control for suppressing multipath induced signal fading",
    Colloquium on Multipath Interference in Radio, Radar and Sonar
    Systems, May 1981, Digest No. 1981/41, IEE Electronics Division.

6. McGEEHAN, J.P., BURROWS, D.F. and WHIPP, S.J.: "Bandwidth invariant
    feedback automatic gain control systems for SONAR", Electronics
    for Ocean Technology, Birmingham, Sept. 1981, IERE, Proc. No.51,
    pp.249-261.

7. McGEEHAN, J.P., BATEMAN, A.J. and BURROWS, D.F.: "The use of
    "transparent" tone-in-band (TTIB) and feedforward signal regeneration
    (FFSR) in single sideband communication systems", to be published
    at "Communications 82", IEE, April 1982.

Large signal performance of feedback automatic gain control systems

J.P. McGeehan, B.Eng., Ph.D., C.Eng., M.I.E.E., and D.F. Burrows, B.Sc.

Indexing terms: Control systems, Feedback, Signal processing, Nonlinear systems, Closed-loop systems, Mobile radio

Abstract: Feedback automatic gain control (FBAGC) is used to maintain the mean level of one or more signals throughout a signal processing system at a fixed value. The paper is particularly concerned with the application of FBAGC to receiver design and discusses the problem of attempting to suppress large unwanted envelope variations of an incoming signal without distorting any wanted modulation. A simple feedforward model of FBAGC systems predicts their effect on deep sinusoidal variations of the input signal's envelope. Experimental results confirming the predictions are presented, and a method of determining the parameters of an undefined AGC system given. Finally, the fundamental problems of FBAGC dynamics are discussed, and a technique is suggested for greatly improving them.

List of principal symbols

A_1, A_2, B, C = circuit element gains
D = magnitude of input sinewave
k = output ripple
L = loop amplitude response
V = mean input level
V_k = loop reference voltage
v_g = loop control voltage
v_i = loop input signal
v_o = loop output signal
v_{in} = input voltage to exponentiator
ω_f = angular fade frequency
ω_n = normalised frequency
θ = loop phase response

1 Introduction

Feedback automatic gain control (FBAGC) is the name given to a nonlinear closed-loop control system used to suppress mean level variations of a signal's envelope. Although FBAGC is used extensively in the fields of sonar, instrumentation and radio communications in general, perhaps the most demanding requirements are in the area of mobile radio. FBAGC is used in amplitude modulation (AM) type receivers such as full-carrier AM, double sideband diminished carrier and single sideband (SSB) to maintain the output at a sensibly constant level despite the input signal undergoing random unwanted amplitude variations. Fading of the input signal level is conventionally considered as consisting of two types: slow and fast. The slow variations can be very large, up to 120 dB, and are a result of changing transmitter/receiver distances and gross variations in the terrain. The fast variations are the smaller, but relatively more rapid sort, occurring principally as a result of multipath interference. This paper is particularly concerned with the performance of FBAGC in the presence of this 'fast fading'. It will attempt to quantify the performance of FBAGC in the presence of input variations of a depth and frequency commonly encountered in the field, and to determine the limit on the performance that can be expected from simple FBAGC systems. This is particularly timely because of the recent upsurge of interest in the use of single sideband as a modulation form at VHF and UHF in the UK and USA [1, 2, 3].

Considerable effort has been directed towards understanding FBAGC and optimising its performance. To this end

various forms of AGC have been proposed and their characteristics analysed. The early work of Oliver [4], and more recently Simpson [5] and Banta [6], assumed a linear relationship between the amplifier gain and the applied control voltage, obtaining some interesting results under small signal conditions. However, this form of FBAGC has input-level-variant dynamics, and some attention has been paid to overcoming this problem by using amplifiers with a gain characteristic dependent on the Nth power of the control voltage. The analysis and design of FBAGC circuits using this control law has been described by Victor and Brockman [7] and more recently in the sonar field by Ricker [8]. These loops are claimed to have input-level-invariant dynamics but need log/antilog circuitry to obtain the required control law. Moskowitz [9] has described an alternative method to give input-level-invariant loop dynamics using two 'complementary' linear feedback networks. However, both this and the previous method are too complex, and a much simpler technique for maintaining the loop dynamics input-level-invariant will be discussed and compared to an input-level-variant system.

Most bipolar gain-controlled amplifier stages, as used in modern radio receivers, have a gain characteristic which varies exponentially with control voltage, resulting in a gain which, when expressed in dB, is a linear function of the control voltage. In a purely theoretical paper, Ohlson [10] put forward a model and analysis for such a system under moderate signal variations. No practical results were presented, but it is clear that the exponential gain control law together with an integrator for a loop filter should provide constant loop dynamics under moderate signal variations. Williams [11] has also claimed that the use of the exponential gain control law alone results in input-level-invariant dynamics.

In order to be completely general, in what follows both an input-level-variant and an input-level-invariant system are analysed and the resulting mathematical models used to predict the large signal performance of FBAGC. Several systems employing FBAGC circuits will be presented and the results obtained from them compared with the theoretical predictions.

2 Theory of feedback automatic gain control

A general FBAGC configuration which relies on a carrier or pilot reference signal for its operation is shown in the block diagram of Fig. 1. The input to the system consists of a carrier or reference signal which undergoes both wanted and unwanted multiplicative amplitude variations. The envelope detector following the variable gain amplifier extracts a signal from the output proportional to the magnitude of the envelope. This is then compared to a fixed reference signal and the resulting difference signal filtered to extract the low-frequency

variations. The filter output is then used to control the gain of the amplifier so as to suppress these unwanted variations.

Fig. 2 is a block diagram valid for the consideration of envelope variations. The variable gain amplifier has been replaced by a unity gain linear multiplier. The envelope detector is no longer required and the summing junction is followed by an integrator to perform the lowpass filtering operation. The circuit element H can be either linear or nonlinear and sets the 'control law' of the multiplier.

2.1 Input-variant FBAGC systems

Assume, as the simplest case, that the element H is a linear amplifier of gain A_1 and that at DC the integrator has a large gain A_2, then the static equations of the loop are

$$v_o = v_i v_g \tag{1}$$

$$v_g = A_1 A_2 (V_k - v_o) \tag{2}$$

Therefore

$$v_o = v_i A_1 A_2 (V_k - v_o) \tag{3}$$

Hence

$$v_o = \frac{A_1 A_2 v_i V_k}{1 + A_1 A_2 v_i} \tag{4}$$

and from eqn. 1

$$v_g = \frac{A_1 A_2 V_k}{1 + A_1 A_2 v_i} \tag{5}$$

Thus, as $A_2 \to \infty$, eqns. 4 and 5 become

$$v_o = V_k \tag{6}$$

and

$$v_g = \frac{V_k}{v_i} \tag{7}$$

It can be seen from eqns. 6 and 7 that the static action of this class of FBAGC is to maintain the output at a fixed value V_k
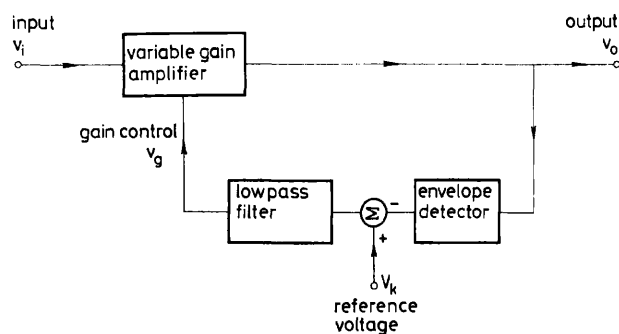

input
V_i

output
V_o

variable gain amplifier

gain control
V_g

lowpass filter

envelope detector

V_k
reference voltage

Fig. 1 *General FBAGC configuration*

input
V_i

multiplier

output
V_o

gain control
V_g

H
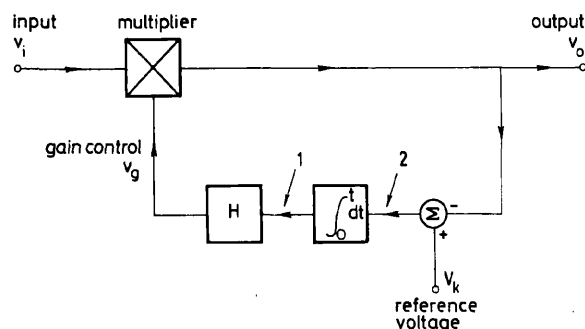
$\int_0^t dt$

1

2

V_k
reference voltage

Fig. 2 *Envelope equivalent of Fig. 1*

by dividing the input by itself. Using the above information the dynamic performance of the loop can be determined.

The differential equation at point 2 in Fig. 2 is

$$\frac{\dot{v}_g}{A_1} = V_k - v_o \tag{8}$$

but $v_o = v_i v_g$ from eqn. 1 so that the main loop equation becomes

$$\frac{\dot{v}_g}{A_1} + v_i v_g - V_k = 0 \tag{9}$$

The signal used for analysing the dynamics will be

$$v_i = V(1 + D \sin \omega_f t) \tag{10}$$

where $|D| < 1$.

Eqns. 6 and 7 show that v_g is the inverse of the input under static conditions. Therefore, when subject to the above input, the steady-state voltage at v_g is given by

$$v_g = \frac{V_k}{V(1 + LD \sin (\omega_f t - \theta))} \tag{11}$$

where L and θ represent the effective loop filtering operation at ω_f. Substituting for v_i and v_g from eqns. 10 and 11 into eqn. 9 gives

$$- \frac{V_k L D \omega_f \cos (\omega_f t - \theta)}{A_1 V (1 + LD \sin (\omega_f t - \theta))^2}$$

$$+ \frac{V_k (1 + D \sin \omega_f t)}{(1 + LD \sin (\omega_f t - \theta))} - V_k = 0 \tag{12}$$

The fundamental terms of eqn. 12 can be solved for L and θ, giving the results

$$L = \frac{1}{(1 + \omega_n^2)^{1/2}} \tag{13}$$

and

$$\theta = \tan^{-1}(\omega_n) \tag{14}$$

where

$$\omega_n = \frac{\omega_f}{A_1 V} \tag{15}$$

Clearly, these are the amplitude and phase equations of a first-order lowpass filter. The action of the linear FBAGC loop just described is, therefore, to a good approximation, to divide the input by a filtered version of itself. This action is shown in Fig. 3, an equivalent feedforward model of Fig. 2, where H is an amplifier of gain A_1. The condition for this circuit equivalent to be valid is that the denominator is greater than zero, i.e.

$$LD < 1 \tag{16}$$

Since the -3 dB point of the filter in Fig. 3 is a function of the input signal, specifically the 'mean' level V, the linear FBAGC system described herewith is a system whose dynamic response is input-variant. Now consider the circuit with H as a simple nonlinear element.

2.2 Input-invariant FBAGC systems

The circuit element H is given the transfer function

$$v_{out} = B \exp (C v_{in}) \tag{17}$$

If the loop integrator is again assumed to have a gain A_2 at DC, where A_2 tends to infinity, the static equations of the

loop are given by

$$v_o = v_i v_g \tag{18}$$

and

$$v_g = B \exp (A_2 C(V_k - v_o)) \tag{19}$$

These equations can be solved to give

$$v_o + \frac{\ln (v_o)}{A_2 C} = V_k + \frac{\ln (v_i)}{A_2 C} + \frac{\ln (B)}{A_2 C} \tag{20}$$

so that, providing $v_i, v_o \neq 0$ as $A_2 \to \infty$,

$$v_o = V_k \tag{21}$$

and, from eqn. 18,

$$v_g = \frac{V_k}{v_i} \tag{22}$$

Thus, as in the input-level-variant case, eqns. 21 and 22 show the static action of this exponential law FBAGC is to maintain the output at a fixed value V_k by dividing the input by itself. The dynamic performance of this loop can now be calculated in a similar manner as before.

The differential equation at point 2 in Fig. 2 is

$$\frac{d}{dt}\left[\frac{(\ln (v_g/B))}{C}\right] = V_k - v_o \tag{23}$$

However, $v_o = v_i v_g$ so that the main loop equation is

$$v_i v_g + \frac{d}{dt}\left[\frac{(\ln(v_g/B))}{C}\right] - V_k = 0 \tag{24}$$

Using the same input test signal as before, i.e.

$$v_i = V(1 + D \sin \omega_f t) \tag{25}$$

then, in steady state,

$$v_g = \frac{V_k}{V(1 + LD \sin (\omega_f t - \theta))} \tag{26}$$

and

$$\frac{d}{dt}\left[\frac{(\ln (v_g/B))}{C}\right] = -\frac{LD\omega_f \cos (\omega_f t - \theta)}{C(1 + LD \sin (\omega_f t - \theta))} \tag{27}$$

therefore the full equation for the loop is, from eqn. 24,

$$\frac{V_k(1 + D \sin \omega_f t)}{(1 + LD \sin (\omega_f t - \theta))} - \frac{LD\omega_f \cos (\omega_f t - \theta)}{C(1 + LD \sin (\omega_f t - \theta))}$$

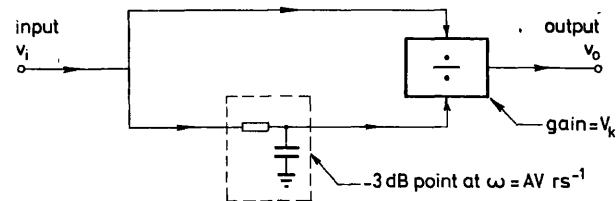$$- V_k = 0 \tag{28}$$

Fig. 3 *Feedforward equivalent of Fig. 2 where H is an amplifier*
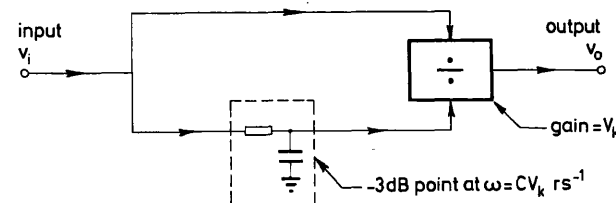
Fig. 4 *Feedforward equivalent of Fig. 2 where H is an exponentiator*

This equation can be solved for L and θ, giving the results

$$L = \frac{1}{(1 + \omega_n^2)^{1/2}} \tag{29}$$

and

$$\theta = \tan^{-1}(\omega_n) \tag{30}$$

where

$$\omega_n = \frac{\omega_f}{CV_k} \tag{31}$$

Fig. 4 is therefore a valid feedforward equivalent of exponential law FBAGC. This particular result has also been proposed by Ohlson [10]. The condition for validity is as before:

$$LD < 1 \tag{32}$$

so that division by zero is avoided. However, there is an important difference between the results obtained here and those obtained in Section 2.1. Here, the lowpass filter has a fixed -3 dB point which is independent of the level of the input signal. Exponential law FBAGC circuits incorporating a simple integrator as lowpass filter have input-level-invariant dynamics. If the analysis were now repeated with an RC lowpass filter replacing the integrator, then the circuit's dynamics would be found to have a partial dependency on the input signal level. Among exponential law FBAGC circuits, only those of type one (one integrator) are input-level-invariant.

2.3 Response of FBAGC to sinusoidal modulation

The models depicted in Figs. 3 and 4 can be used to analyse the sinusoidal response of FBAGC. In general, if the input of the circuit is subjected to sinusoidal modulation at a frequency ω_n (normalised to the -3 dB point), of the form

$$v_i = 1 + D \sin \omega_n t \tag{33}$$

then the output of the circuit v_o is given by

$$v_o = \frac{V_k(1 + D \sin \omega_n t)}{1 + LD \sin (\omega_n t - \theta)} \tag{34}$$

If $\omega_n \ll 1$, then $L \simeq 1$ and $\theta \simeq 0$, so that the output will remain approximately constant at a value of V_k. If $\omega_n \gg 1$, then the output will be given by

$$v_o = V_k(1 + D \sin \omega_n t) \tag{35}$$

For intermediate frequencies there exists a transition region where FBAGC introduces suppression and distortion of the input modulation. Two characteristics of the input envelope during this transition region are now analysed. They are

(i) the residual output ripple, particularly relevant for $\omega_n < 1$

(ii) the harmonic distortion, particularly relevant for modulation frequencies greater than $\omega_n = 1$.

2.3.1 Residual output ripple:
The output of the FBAGC circuit is subject to a residual modulation given by eqn. 34. The output ripple is defined by k, where

$$k = \frac{v_o(\text{maximum})}{v_o(\text{minimum})} \tag{36}$$

Eqn. 34 is solved for k in Appendix 7.1. The general solution is given by

$$k = \frac{1 - LD^2 \cos\theta + D\sqrt{L^2D^2 \cos^2\theta + L^2 + 1 - 2L\cos\theta - L^2D^2}}{1 - LD^2 \cos\theta - D\sqrt{L^2D^2 \cos^2\theta + L^2 + 1 - 2L\cos\theta - L^2D^2}} \tag{37}$$

The relationship between L, θ and ω_n is that of a first-order lowpass filter, and Appendix 7.2 solves eqn. 37 for this case in particular, giving

$$k = \frac{1 + D\sqrt{\dfrac{\omega_n^2}{\omega_n^2 + 1 - D^2}}}{1 - D\sqrt{\dfrac{\omega_n^2}{\omega_n^2 + 1 - D^2}}} \tag{38}$$

Fig. 5 is a graph of the residual output modulation ripple as a function of ω_n for several values of input modulation depth.
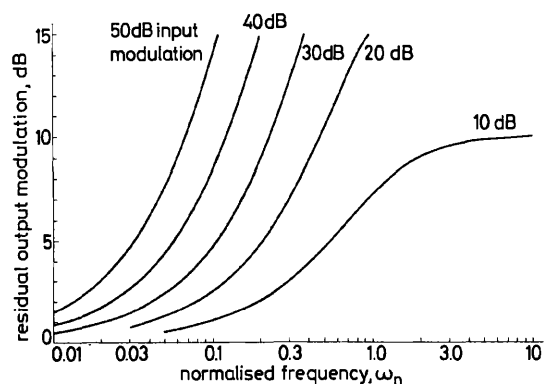
Fig. 5 *Residual output modulation ripple as a function of normalised input frequency for several values of input modulation depth*

It is clear from these theoretical curves that deep modulation depths are only suppressed adequately if they occur at frequencies well below $\omega_n = 1$. For comparison purposes, theoretically computed output envelope shapes are plotted in Fig. 6 as a function of ω_n.

2.3.2 Output harmonic distortion: The second characteristic of the output envelope to be considered is the harmonic dis-
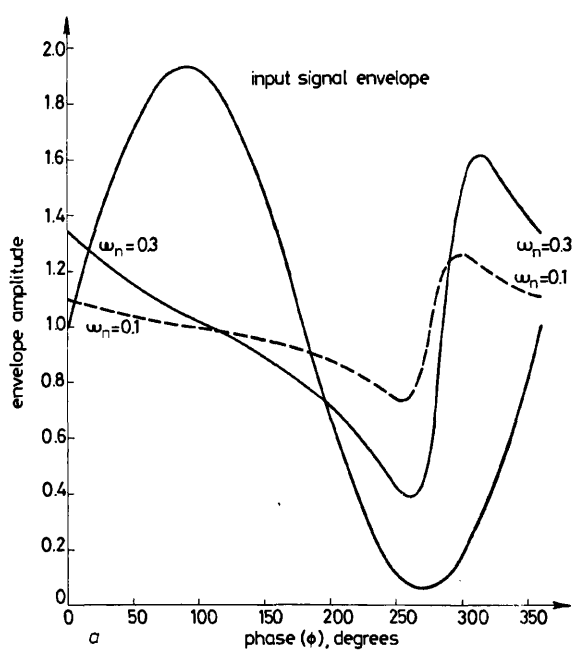
tortion introduced by FBAGC. The harmonics of eqn. 34 have been analysed using a 64-point discrete Fourier transform, and

the theoretical curves for $D = 1$ (100% fading) are presented in Fig. 7. A good empirical fit to the harmonic curves for fading frequencies at $\omega_n > 1$ is given by

$$\text{level of Nth harmonic} = (D)^N(\tfrac{1}{2}L)^{N-1} \tag{39}$$

and is also plotted in Fig. 7. Eqn. 39 and Fig. 7 indicate that large wanted amplitude variations are not distorted only if they occur at frequencies well above $\omega_n = 1$.
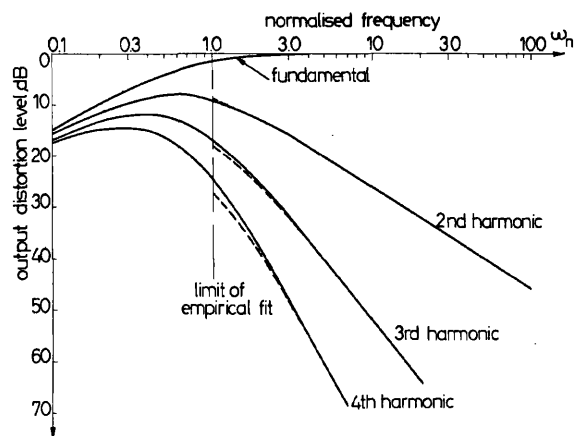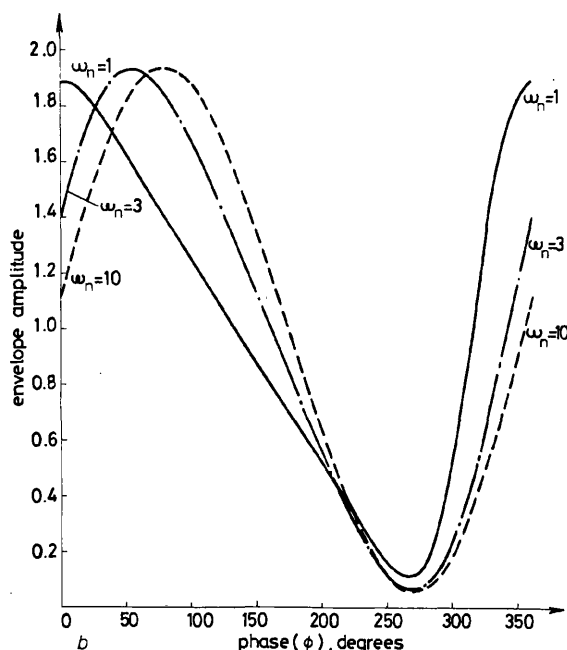

Fig. 7 *Harmonic distortion introduced by feedback automatic gain control*

$D = 1$ (100% modulation)
———— computed curves
— — — empirical fit

3 Experimental verification of theory

To verify the FBAGC theory presented thus far and the resulting equivalent feedforward models, measurements have been made on three distinct forms of FBAGC system, namely
(i) the envelope equivalent circuit of Fig. 2, where the

Fig. 6 *Computed output envelope shapes as a function of normalised frequency*

a $\omega_n = 0.1, 0.3$ *b* $\omega_n = 1, 3, 10$

circuit element H is an exponentiator (here, the 'carrier' is at DC and all circuit elements are DC coupled)

(ii) a full AM receiver with an IF signal of 10.7 MHz and constructed from commercially available exponential control law integrated circuits and a coherent detector

(iii) a UHF phaselocked pilot-tone SSB receiver.

The investigation has been confined to loops which have input-signal-level-invariant dynamics, i.e. exponential control-law/integrator systems, since it is these systems which are likely to prove by far the most important in radio communication and sonar applications.

3.1 Envelope equivalent circuit

A block diagram of the envelope equivalent circuit is shown in Fig. 8. The circuit operated over a 40 dB dynamic range of input from 0.1 to 10 V with no measurable variation of the output during the static tests. During dynamic testing, the circuit performed as predicted theoretically when subjected to an input test signal of the form $(1 + D \sin \omega_f t)$, and the main features of the results are summarised below.
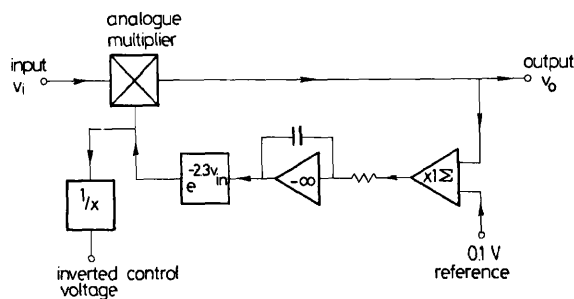
Fig. 8 *Block diagram of DC carrier circuit*

Although the waveforms observed around the loop during deep fade modulations were nonsinusoidal, the inverted control voltage signal was found to be a sinusoidal lowpass filtered version of the input signal. This confirms that the basic action of a FBAGC system is to divide an input by a filtered version of its own modulus. The calculated closed-loop band-width was 100 Hz, and the measured bandwidth was 106.6 Hz for 40 dB input variations. This was obtained by plotting the amplitude and phase response between the input and the inverted (sinusoidal) control voltage. With smaller input variations from −20 to −10 dBV and +10 to +20 dBV, the closed-loop bandwidth was measured at 101.4 and 108.4 Hz, respectively, i.e. a 6.5% variation in closed-loop bandwidth corresponded to a 30 dB variation in mean input level, demonstrating level-invariance of AGC characteristics. Fig. 9 shows
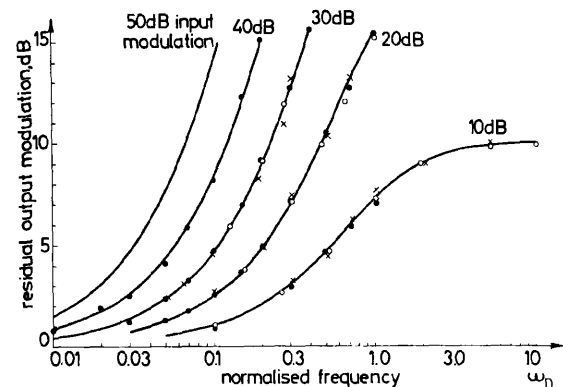
Fig. 9 *Measured output ripple as a function of normalised frequency*

———— theoretical curves
● ● ● envelope equivalent circuit
o o o AM receiver
x x x SSB receiver

the measured output ripple against frequency for various values of modulation depth. Computed points assume a closed-loop bandwidth of 105 Hz. Theoretical curves of Fig. 5 present an interesting comparison. Fig. 10 shows measured values of harmonic distortion in the output envelope introduced by FBAGC as a function of frequency; theoretical curves are again plotted for comparison. There is good agreement between theory and practice, with the exception of the second-harmonic curve at high frequencies. Here, the inherent second-harmonic distortion within the circuit causes the curve to level at −28 dB.
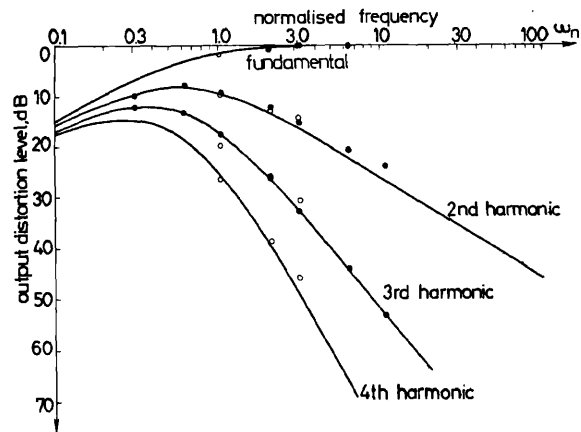
Fig. 10 *Measured output harmonic distortion for FBAGC*

———— theoretical curves
● ● ● envelope equivalent circuit
o o o AM receiver

3.2 Full-carrier AM receiver

For this set of measurements the 10.7 MHz IF strip, detector and AGC circuits of a full-carrier AM receiver were constructed from commercial integrated circuits as shown in Fig. 11. Three SL1612C devices were used in the IF strip in order to produce an extremely linear dB/V gain control characteristic as required by Section 2.2. An SL624 was used as a coherent detector [12] which permitted low-level detection, hence giving the required large dynamic range. Balanced outputs from the mixer drive the AGC circuit, an integrator and level-shifting network. The value of capacitor in the integrator gave a loop bandwidth of 25 Hz, a typical value in VHF AM systems.

Static measurements showed the output of the receiver constant to within 1 dB for changes in input levels greater than 100 dB. To measure the closed-loop bandwidth of the system and verify the dynamic characteristics of the FBAGC, the input signal to the IF strip was amplitude-modulated sinusoidally to a depth of 30 dB, i.e. $D = 0.939$, and output-ripple-observed at various modulation frequencies. The first point plotted on Fig. 9, corresponding to an output ripple of 4.6 dB, fitted the 30 dB theoretical curve if a value of 26 Hz was assumed for the closed-loop bandwidth. Based on this value, the remaining experimental points for output ripple and harmonic distortion were plotted on the normalised theoretical curves of Figs. 9 and 10, respectively. Again, good agreement is observed between theory and practice.

3.3 UHF pilot tone SSB receiver

A 457 MHz in-band pilot tone SSB receiver was constructed incorporating an exponential control-law/integrator FBAGC system as shown in the block diagram of Fig. 12. Although it is not intended to describe pilot tone SSB systems here, since they are described adequately elsewhere [13], it is necessary to state that the pilot tone is positioned in a notch in the audio spectrum at 1.67 kHz. As with the AM receiver, the IF amplifiers possessed a linear dB/V gain control characteristic to obtain constant loop bandwidth over all usable input signal

114

levels to the receiver. The main difference between the FBAGC in this receiver and a normal full-carrier AM receiver is the inclusion of a bandpass audio filter. This is used to extract the 1.67 kHz pilot tone reference signal from the audio and has a bandwidth approximately forty times that of the FBAGC's closed-loop bandwidth.

The FBAGC circuit maintained the tone level at the output of the receiver to within 0.2 dB over an input range of 120 dB (1 μV to 1 V). The receiver's FBAGC was designed to have a closed-loop bandwidth of 10 Hz. By using the technique described in Section 3.2, the measured value obtained was 11 Hz. Fig. 9 gives experimental points for output ripple as a function of frequency. Close agreement is again noted between theory and practice for this particular FBAGC system. In all three experiments the observed output envelope waveforms were similar to those shown in Fig. 6.

4 Conclusions

Two types of FBAGC have been analysed, i.e. the linear control-law/integrator system and the exponential control-law/integrator system. The exponential/integrator system with linear dB/V gain control characteristics is evidently the most useful for receiver applications, having well defined static and dynamic performance independent of the mean input signal level to the receiver. Theoretical and experimental confirmation of the large signal equivalent feedforward model of FBAGC systems has also been presented.

FBAGC is unfortunately found to have a large frequency transition region between the envelope fading frequencies it will suppress satisfactorily and the envelope modulation frequencies that it will pass undistorted. This transition region commences from about 0.1 of the closed-loop bandwidth (30 dB of input fade modulation to 4.6 dB of output ripple)
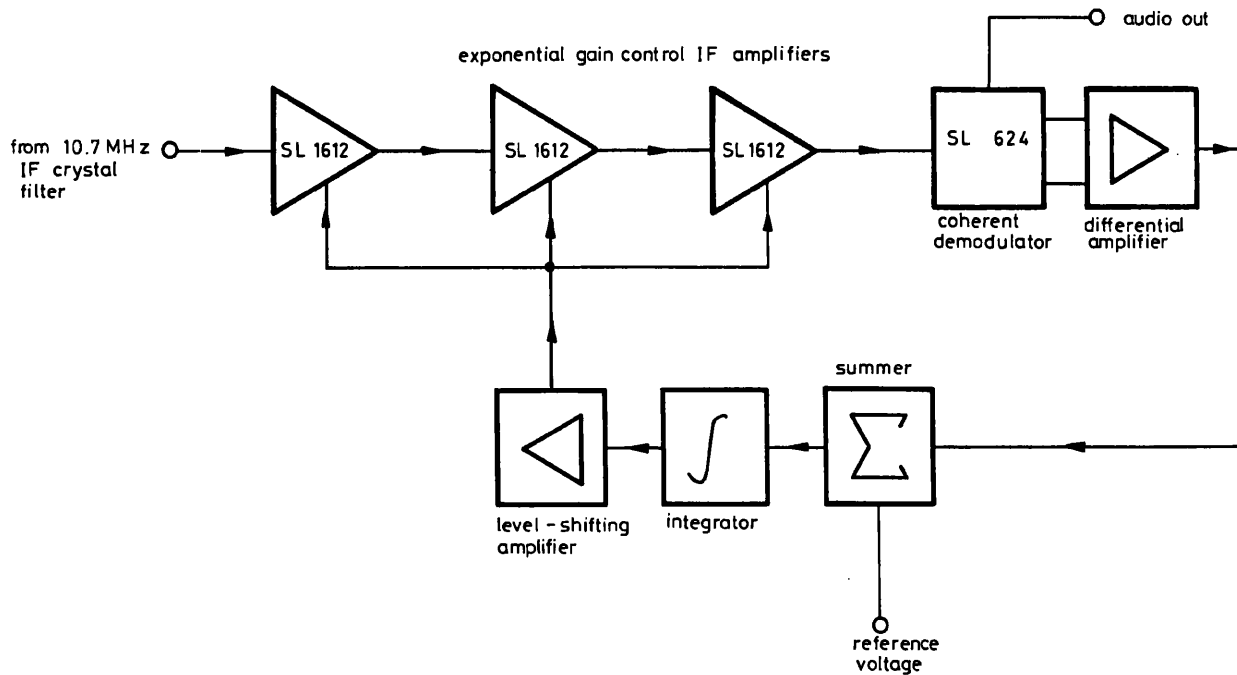

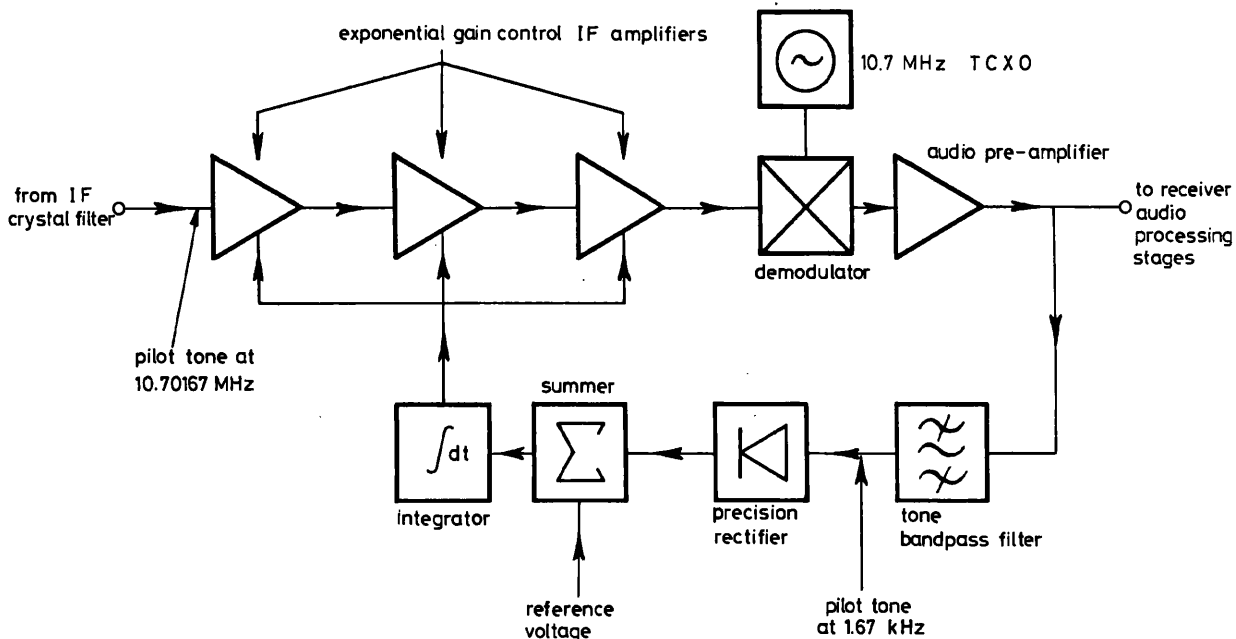**Fig. 11** *IF and FBAGC control circuitry of VHF AM receiver*

Fig. 12 *IF and FBAGC control circuitry of UHF pilot tone SSB receiver*

to about 10 times the loop bandwidth (5% of second-harmonic distortion for 100% modulation on the input). Although these definitions are somewhat arbitrary they are representative of typical design parameters for optimum FBAGC performance. Over the transition region, deep modulation on the input will be partially suppressed but also grossly distorted. However, at no frequency will the output ripple of the receiver exceed the peak to trough fade depth at the input, providing the FBAGC loop is first-order [4]. This necessarily eliminates the use of 2nd- and higher-order loops to reduce the transition region [16]. The large transition region of about 100:1 that occurs with FBAGC limits fade rates which can be suppressed to a few hertz in the presence of speech. FBAGC is, therefore, contrary to views expressed elsewhere [14, 15], unsatisfactory for suppressing fast fading that arises as a result of multipath interference in VHF and UHF land mobile ratio systems under certain conditions of use. To resolve this difficulty, the authors have subsequently investigated a supplementary form of AGC which operates by feeding control signals forward rather than back. The technique, called feedforward AGC, is capable of reducing the transition region from 100:1 to 2:1 [17, 18], and will be the subject of an early publication.

5 Acknowledgments

6 References

1 McGEEHAN, J.P., RICHARDSON, J.H., and GOSLING, W.: 'The Wolfson SSB mobile radio system'. 3rd world telecommunication forum, Pt. 2, Geneva, 1979, pp. 2.3.4.1–2.3.4.5
2 WELLS, R.: 'SSB for VHF mobile radio at 5 kHz channel spacing'. Proceedings of conference on radio receivers and associated systems, IERE, London, 1978, pp. 29–36
3 WILMOTTE, R.M., and LUSIGNAN, B.B.: 'UHF Task Force report – spectrum efficient technology for voice communications'. Federal Communications Commission, Washington, 1978
4 OLIVER, B.M.: 'Automatic volume control as a feedback problem', Proc. IRE, 1948, 36, pp. 466–473
5 SIMPSON, R.S., and TRANTER, W.H.: 'Baseband AGC in an AM-FM telemetry system', IEEE Trans., 1970, COM-18, pp. 59–63
6 BANTA, E.D.: 'Analysis of an automatic gain control (AGC)', ibid., 1964, AC-9, pp. 181–182
7 VICTOR, W.K., and BROCKMAN, M.H.: 'The application of linear servo theory to the design of AGC loops', Proc. IRE, 1960, 48, pp. 234–238
8 RICKER, D.W.: 'Non-linear feedback system for the normalisation of active sonar returns', J. Acoust. Soc. Am., 1976, 59, pp. 389–396
9 MOSKOWITZ, J.: 'Linear feedback AGC with input-level-invariant response times', ibid., 1977, 62, pp. 1449–1456

10 OHLSON, J.E.: 'Exact dynamics of automatic gain control', IEEE Trans., 1974, COM-22, pp. 72–75
11 WILLIAMS, N.A.F.: 'Automatic gain control systems', Wireless World, 1977, 83, pp. 60–61
12 BRYANT, J.M.: 'Radio communications handbook' (The Plessey Co. Ltd., 1977), pp. 25–32
13 GOSLING, W., McGEEHAN, J.P., and HOLLAND, P.G.: 'Receivers for the Wolfson single sideband VHF land mobile radio system', Radio & Electron. Eng., 1979, 49, pp. 321–325
14 LUSIGNAN, B.B.: 'AGC, AFC, tone select circuits for narrow-band mobile radio'. Intelcom 79, International telecommunication exposition, Dallas, Texas, 1979
15 'Single sideband for land mobile radio demonstrated', Wireless World, 1979, 85, p. 95
16 BURROWS, D.F., and McGEEHAN, J.P.: 'Time delay in receiver AGC systems'. Clark Maxwell commemorative conference on radio receivers and associated systems, IERE (to be published July 1981)
17 McGEEHAN, J.P., and BURROWS, D.F.: 'The impact of CCD technology on feedforward automatic gain control systems for mobile radio communications'. 4th European conference on electrotechnics, Eurocon 80, Stuttgart, 1980, pp. 184–188
18 BURROWS, D.F., and McGEEHAN, J.P.: 'The use of feedforward automatic gain control for reducing fast fading in single sideband mobile radio systems'. IEE Conf. Publ. 188, 1980, pp. 22–25

7 Appendixes

7.1 Solution of eqn. 34 for k

Eqn. 34 states that

$$v_o = \frac{V_k(1 + D \sin \omega_n t)}{1 + LD \sin (\omega_n t - \theta)}$$

and k is defined by

$$k = \frac{v_o(\text{maximum})}{v_o(\text{minimum})}$$

Instead of differentiating the above equation to solve for k (a lengthy technique giving an indirect solution) the following method is used. Eqn. 34 is rewritten as

$$y = \frac{1 + D \sin \omega_n t}{1 + LD \sin (\omega_n t - \theta)}$$

by letting $y = v_o/V_k$ and is solved for $\omega_n t = f(y)$ as follows.

Let $x = \tan [\omega_n t/2]$ such that $\sin \omega_n t = 2x/(1 + x^2)$ and $\cos \omega_n t = (1 - x^2)/(1 + x^2)$. Then

$$y = \frac{1 + 2Dx/(1 + x^2)}{1 + LD\left[\dfrac{2x \cos \theta}{1 + x^2} - \dfrac{(1 - x^2)}{1 + x^2} \sin \theta\right]}$$

which, rearranging, gives

$$x^2(y + yLD \sin \theta - 1) + x(2LDy \cos \theta - 2D) +$$
$$+ y - yLD \sin \theta - 1 = 0$$

and hence

$$x = \frac{2D(1 - yL \cos \theta) \pm \sqrt{4D^2(1 - 2Ly \cos \theta + y^2 L^2 \cos^2 \theta) - 4(y + yLD \sin \theta - 1)(y - yLD \sin \theta - 1)}}{2(y + yLD \sin \theta - 1)}$$

which simplifies to

$$x = \frac{D(1 - yL \cos \theta) \pm \sqrt{y^2(L^2 D^2 - 1) + 2y(1 - LD^2 \cos \theta) + D^2 - 1}}{y + yLD \sin \theta - 1}$$

and, since $x = \tan [\omega_n t/2]$, then

$$\omega t = 2 \tan^{-1}\left[\frac{D(1 - yL \cos \theta) \pm \sqrt{y^2(L^2 D^2 - 1) + 2y(1 - LD^2 \cos \theta) + D^2 - 1}}{y(1 + LD \sin \theta) - 1}\right]$$

Having solved for $\omega t = f(y)$ it is obvious that the peak and troughs of y, and hence v_o, occur when there are two solutions to $f(y)$, i.e. when the square root in the above equation equals zero. If the value of y at these points (maxima or minima) is y_m, then

$$y_m^2(L^2D^2 - 1) + 2y_m(1 - LD^2 \cos \theta) + D^2 - 1 = 0$$

so that

$$y_m = \frac{LD^2 \cos \theta - 1 \pm D\sqrt{L^2D^2 \cos^2\theta + L^2 + 1 - 2L \cos \theta - L^2D^2}}{L^2D^2 - 1}$$

Since $L^2D^2 - 1 < 0$ and $LD^2 \cos \theta - 1 < 0$, then

$$y_m = \frac{1 - LD^2 \cos \theta \pm D\sqrt{L^2D^2 \cos^2\theta + L^2 + 1 - 2L \cos \theta - L^2D^2}}{1 - L^2D^2}$$

and hence, from the definition of k,

$$k = \frac{1 - LD^2 \cos \theta + D\sqrt{L^2D^2 \cos^2\theta + L^2 + 1 - 2L \cos \theta - L^2D^2}}{1 - LD^2 \cos \theta - D\sqrt{L^2D^2 \cos^2\theta + L^2 + 1 - 2L \cos \theta - L^2D^2}}$$

7.2 First-order solution of k

Now

$$k = \frac{1 - LD^2 \cos \theta + D\sqrt{L^2D^2 \cos^2\theta + L^2 + 1 - 2L \cos \theta - L^2D^2}}{1 - LD^2 \cos \theta - D\sqrt{L^2D^2 \cos^2\theta + L^2 + 1 - 2L \cos \theta - L^2D^2}}$$

and, for first-order systems,

$$L = \frac{1}{(1 + \omega_n^2)^{1/2}}, \quad \theta = \tan^{-1}\omega_n$$

and hence

$$L = \cos \theta$$

so that

$$k = \frac{1 - L^2D^2 + D\sqrt{L^4D^2 + L^2 + 1 - 2L^2 - L^2D^2}}{1 - L^2D^2 - D\sqrt{L^4D^2 + L^2 + 1 - 2L^2 - L^2D^2}}$$

i.e.

$$k = \frac{1 - L^2D^2 + D\sqrt{(1 - L^2D^2)(1 - L^2)}}{1 - L^2D^2 - D\sqrt{(1 - L^2D^2)(1 - L^2)}}$$

$$= \frac{1 + D\sqrt{\dfrac{(1 - L^2)}{(1 - L^2D^2)}}}{1 - D\sqrt{\dfrac{(1 - L^2)}{(1 - L^2D^2)}}}$$

Substituting L for ω_n, then

$$k = \frac{1 + D\sqrt{\dfrac{1 - \dfrac{1}{1 + \omega_n^2}}{1 - \dfrac{D^2}{1 + \omega_n^2}}}}{1 - D\sqrt{\dfrac{1 - \dfrac{1}{1 + \omega_n^2}}{1 - \dfrac{D^2}{1 + \omega_n^2}}}}$$

which simplifies to

$$k = \frac{1 + D\sqrt{\dfrac{\omega_n^2}{\omega_n^2 + 1 - D^2}}}{1 - D\sqrt{\dfrac{\omega_n^2}{\omega_n^2 + 1 - D^2}}}$$

Performance limits of feedforward automatic gain control in mobile radio receivers

J.P. McGeehan, B.Eng., Ph.D., C.Eng., M.I.E.R.E., M.I.E.E., and D.F. Burrows, B.Sc.

Abstract: In the paper, two forms of feedforward automatic gain control circuit, i.e. lowpass and bandpass, are described and their performance limits discussed in respect of nonideal circuit parameters, receiver pre-filtering decorrelation and propagation-medium time delay spread. The bandpass filter limited dynamics configuration is shown to have twice the fade suppression bandwidth of the lowpass filter limited dynamics form and is particularly suited for use in VHF and UHF full carrier AM and SSB mobile radio receivers. A series of field trials in which a bandpass limited dynamics feedforward automatic gain control circuit was fitted to the audio output of a 457 MHz SSB mobile radio system is described.

1   Introduction

A significant problem at VHF and UHF in land mobile radio communications is multipath propagation of the transmitted signal. This results in a quasistationary interference pattern of signal peaks and troughs being set up over the required coverage area. It can be shown that, when there is no direct line-of-sight signal between the transmitter and receiver, such that any energy reaching the receiver is by way of a number of indirect paths, then the envelope statistics are Rayleigh distributed [1]. Fades of 30 dB or more below the mean level are encountered, and a vehicle driving through this fading pattern at 112 km/h (70 miles/h) can experience signal fluctuations at rates of up to twice Doppler, i.e. 33 per second at 160 MHz and 93 per second at 450 MHz. An AM-type receiver [such as full carrier AM or single sideband (SSB)] has these envelope variations impressed directly onto the demodulated output. This fast fading distorts speech and can severely degrade data communications.

However, it is not just in the land mobile radio field that communications are degraded by fast fading. For example, low flying aircraft using UHF full carrier AM systems suffer severe multipath induced envelope fast fading during inter-aircraft communications, even though they may be flying less than 1 km apart [2]. Although received signal strengths will be extremely high in this case, intelligibility can be severely degraded. This is because conventional receiver feedback AGC (FBAGC) circuits can only suppress deep unwanted fading at up to a few times per second in the presence of speech. Any attempt to 'speed up' FBAGC can result in distortion of the speech information [3] and possible fading enhancement or instability in the presence of time delay [4].

One way of reducing multipath-induced distortion is to employ some form of diversity. This technique reduces the probability of a fade exceeding a certain depth by combining several received signals with uncorrelated fading envelopes. This normally involves the use of multiple transmitters or multiple receiver aerial systems together with special combining circuitry and is well described in the literature [5]. Besides reducing the range of the envelope fluctuations, it results in an improved signal/noise ratio. Unfortunately, its implementation is often too complex and expensive for the majority of civil land mobile radio users, while certain practical difficulties are encountered in the aircraft situation.

This paper is concerned with the use of a fast acting form of AGC that can be simply added onto the output of non-diversity receivers or used to improve the performance of

diversity receivers. It has the ability to greatly reduce the envelope fading and its complexity and expense can be reduced to that of a single integrated circuit. The technique, called feedforward AGC (FFAGC), allows the use of very high orders of filtering to separate fading information from the required signal without introducing distortion or encountering any time-delay-induced stability problems. Although the basic operation has been described elsewhere [6–8], a brief description is given below.
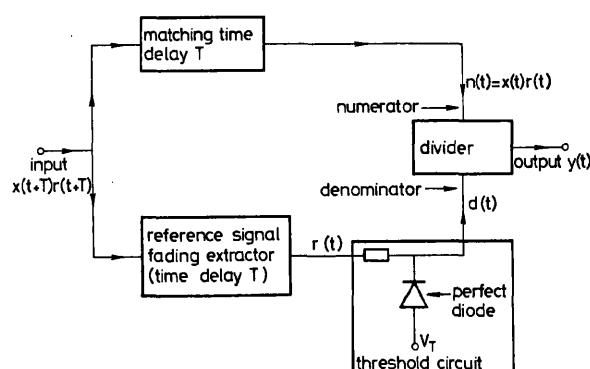

Fig. 1   Block diagram of a general FFAGC circuit

The operation principles of FFAGC are best understood by reference to the block schematic diagram of Fig. 1. For the purpose of mathematical convenience, the time reference is taken to be after the time delay unit. The required signal $x(t)$ is considered to be composed of the wanted modulation $m(t)$ added to or impressed on a carrier or pilot reference signal $c(t)$. The unwanted envelope modulation caused by fast fading is represented by $r(t)$. In the ideal case, the lower path extracts the fading from the carrier reference, and, if $r(t) > V_T$ such that $d(t) = r(t)$, then the desired output $y(t) = x(t)$ is obtained by dividing $r(t)$ into the top path signal. The processing time of the reference signal extractor is matched exactly by the signal path delay. If at some instant $r(t) < V_T$, the denominator is clamped at V_T, resulting in an output $y(t) = x(t)r(t)/V_T$. The threshold voltage is therefore a lower limit to the depth of fade below which the circuit will not divide.

It is the intention of this paper to analyse theoretically the performance limitations of FFAGC in the presence of deterministic signals. It will be shown that the use of a bandpass filter to extract the carrier reference doubles the fade suppression bandwidth and greatly increases the circuit's slew rate over conventional lowpass-filter-derived FFAGC. Particular attention is paid to the effect of carrier reference filtering operations on the circuit's performance and to the need for good correlation between the carrier and signal fades. In this

respect, the effects of decorrelation due to time delay spread and receiver prefiltering operations are discussed and evaluated. Finally, the analytic and subjective effects of noise on the circuit's performance are discussed together with the results obtained from its application to a 457 MHz SSB land mobile radio system.

2 Theory of feedforward automatic gain control

2.1 Conventional lowpass filter limited dynamics

This is the form of FFAGC originally proposed by Hopper [6] and is shown in Fig. 2. Since there is no selectivity before the envelope detector, an enhanced carrier reference is required for correct operation and it is most applicable to full carrier AM systems. The separation of the fading information from the required modulation is achieved by a high-order linear phase lowpass filter. It is assumed that the circuit is preceded by slow acting feedback AGC to suppress large mean level signal variations. The circuit's performance above threshold is now analysed, and all circuit elements are assumed to be perfect except for the lowpass filter.
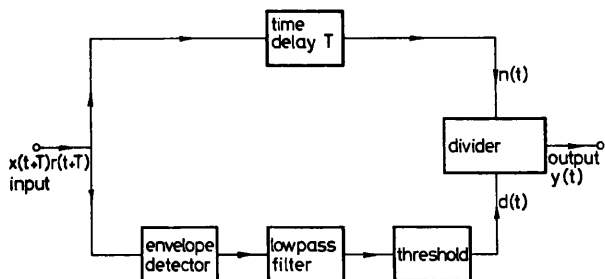

Fig. 2 *Conventional lowpass filter limited dynamics FFAGC circuit for full carrier AM systems*

For the purpose of this analysis, let the unwanted envelope fading component of the received signal be of the form

$$r(t) = 1 + D \sin \{\omega_f(t + T)\} \tag{1}$$

Thus the signal appearing at the numerator of the divider is

$$n(t) = (1 + D \sin \omega_f t)x(t) \tag{2}$$

If the lowpass filter has an amplitude response L and a group delay $(T - \tau)$ at ω_f, then the signal appearing at the denominator is

$$d(t) = 1 + LD \sin \omega_f(t + \tau) \tag{3}$$

The output of the feedforward circuit can be written as

$$y(t) = \frac{(1 + D \sin \omega_f t)x(t)}{1 + LD \sin \omega_f(t + \tau)} \tag{4}$$

The required output $x(t)$ is therefore subject to a residual modulation J, where

$$J = \frac{1 + D \sin \omega_f t}{1 + LD \sin \omega_f(t + \tau)} \tag{5}$$

The ratio of the maximum to minimum value of J, i.e. the output ripple, has been solved by the authors in an earlier paper concerning feedback AGC [3]. If this is defined by k, then

$$k = \frac{1 - LD^2 \cos \omega\tau + D\sqrt{L^2 D^2 \cos^2 \omega\tau + L^2 + 1 - 2L \cos \omega\tau - L^2 D^2}}{1 - LD^2 \cos \omega\tau - D\sqrt{L^2 D^2 \cos^2 \omega\tau + L^2 + 1 - 2L \cos \omega\tau - L^2 D^2}} \tag{6}$$

If the upper and lower signal paths are perfectly matched in time so that $\tau = 0$, then k simplifies to k', where

$$k' = \frac{1 - LD^2 + D|(L - 1)|}{1 - LD^2 - D|(L - 1)|} \tag{7}$$

When considering the unwanted input modulation in decibel form, the peak rate of change in decibels per second is given by

$$\text{peak rate} = \frac{20 \omega_f D \cos (\sin^{-1} D)}{\ln (10)(1 - D^2)} \tag{8}$$

where ω_f is in radians per second.

As a design example, consider the suppression of a 30 dB sinusoidal fade ($D = 0.9387$) to within ± 3 dB of output ripple with perfect time delay matching. Eqn. 7 indicates that L must be less than 1.0187 (+ 0.16 dB) for the + 3 dB variation and greater than 0.9742 (− 0.23 dB) for the − 3 dB variation, as shown in Fig. 3. The input and worst-case output waveforms in this case are shown by Fig. 4.
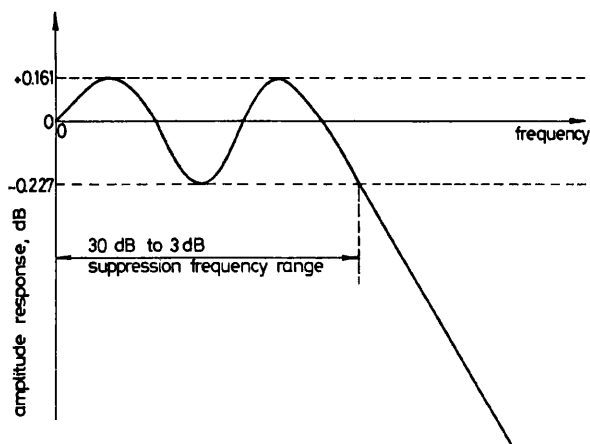

Fig. 3 *Amplitude/frequency response of lowpass filter for suppressing 30 dB sinusoidal fading to within 3 dB*
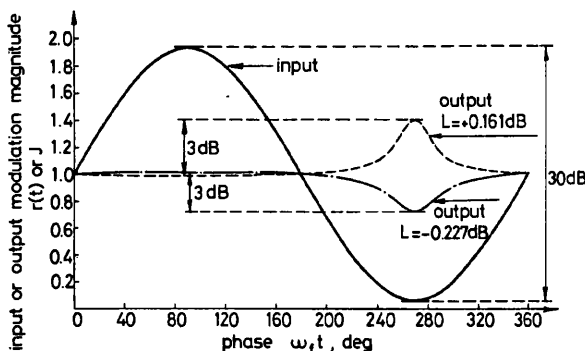

Fig. 4 *Input and worst-case output waveforms of an FFAGC circuit incorporating the lowpass filter described by Fig. 3 for 30 dB input modulation*

$r(t) = 1 + D \sin \omega_f t$

$J = \dfrac{1 + D \sin \omega_f t}{1 + LD \sin \omega_f t}$

where $D = 0.9387$ and $L = 1.0187$ (+ 0.161 dB) or $L = 0.9742$ (− 0.227 dB)

The fade suppression frequency limitations of this particular form of FFAGC are made most apparent by considering the spectrum of the received signal after the lower path envelope detector. The envelope detector is assumed to be of the precision rectifier type or, alternatively, a coherent (product) type capable of tracking the random FM of the received signal.

Fig. 5 shows the output of the envelope detector used in a full carrier AM system with the lowest frequency speech component represented by a tone of frequency f_L. Evidently, the use of a perfect (i.e. brickwall) lowpass filter will only allow fading with significant energy up to $f_L/2$ to be suppressed. Jakes [1]

shows that envelope fading in the land mobile radio multipath environment has a fundamental spectral density existing up to twice Doppler (although there is still 1.8% of the power above this frequency). Thus, if twice Doppler exceeds $f_L/2$, the spectra shown in Fig. 5 will overlap, making adequate suppression of even the fundamental component of the received signal's envelope fading impossible. However, a consideration of the RF or IF spectra prior to envelope detection indicates a method whereby the fade suppression bandwidth of FFAGC may be doubled. Fig. 6 depicts a typical spectrum prior to the envelope detector for the land mobile case. The signal is assumed to have no direct component and obeys Rayleigh statistics. It can be seen that, unlike the output of the envelope detector, the fading spectra of the input signals are
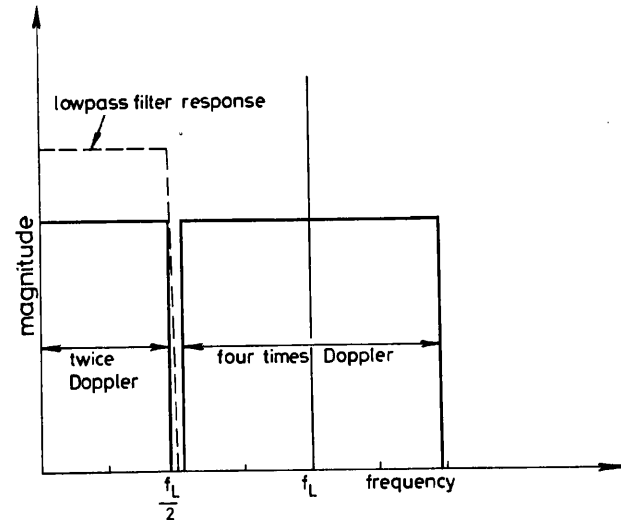

Fig. 5 *Illustration of the maximum frequency of operation of conventional lowpass filter FFAGC*
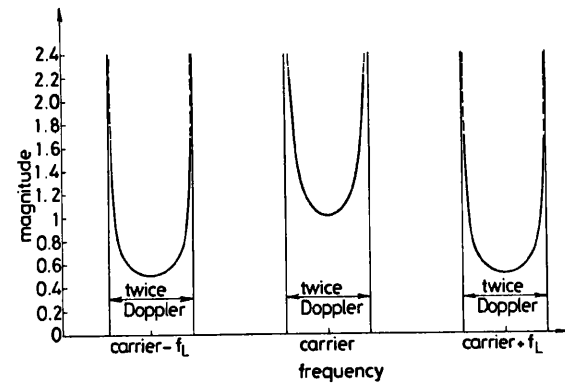

Fig. 6 *Input signal to the envelope detector that generated the output spectrum shown in Fig. 5*

still well separated. Indeed, the Doppler spread can be doubled before the carrier spectra and modulation spectra overlap. If therefore a bandpass filter is used to extract the carrier and its associated fading spectra prior to wideband envelope detection, FFAGC will be able to suppress fading at rates up to f_L instead of $f_L/2$. This arrangement is referred to as bandpass filter limited dynamics. It can be used with full carrier AM systems as well as with any other AM-type modulation system that has a pilot reference (such as DSBDC or pilot reference SSB).

2.2 Bandpass filter limited dynamics

In the following analysis, the performance of a FFAGC circuit employing a bandpass filter to extract the reference signal, as shown in Fig. 7, is investigated above threshold. In practice, as shown by Fig. 6, the required signal $x(t)$ has its spectrum 'smeared' to the familiar 'U' shape by multipath propagation effects, and, in land mobile radio, the components of greatest

magnitude occur at $\pm$ Doppler. For this reason, and in an attempt to use a worst-case test signal for analysing bandpass filter imperfections, the input to the circuit is assumed to be operated on by M, where

$$M\{x(t)\} = x(t)\Big|_{\omega \to (\omega - \omega_1)} + Rx(t)\Big|_{\omega \to (\omega + \omega_2)} \quad (9)$$

The resulting signal envelope is similar to that encountered in the field, and the equation, coincidentally, accurately describes the 'lobe modulation' encountered in UHF air-to-air communications (see Chap. 10 of Reference 9). If the received carrier reference in the absence of fading is given by

$$c(t) = E \cos \omega_c(t + T) \quad (10)$$

then, under the influence of the test signal defined in eqn. 9, the carrier reference is modified to

$$M\{c(t)\} = E \cos \{\omega_c(t + T) - \omega_1(t + T)\}$$
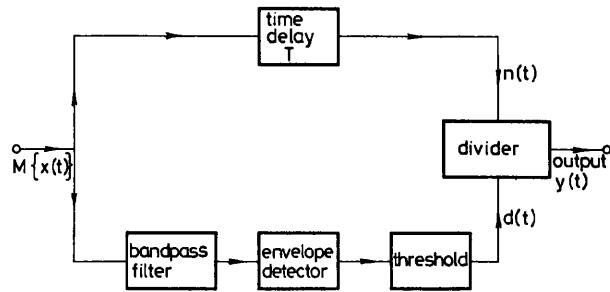$$+ RE \cos \{\omega_c(t + T) + \omega_2(t + T)\} \quad (11)$$

Fig. 7 *Bandpass filter limited dynamics FFAGC circuit*

It is convenient to express this equation as an amplitude and phase modulated carrier as follows:

$$M\{c(t)\} = E\{1 + R^2 + 2R \cos \omega_f(t + T)\}^{1/2} \cos \left[\omega_c(t + T) \right.$$

$$\left. + \tan^{-1} \left\{ \frac{R \sin \omega_2(t + T) - \sin \omega_1(t + T)}{R \cos \omega_2(t + T) + \cos \omega_1(t + T)} \right\} \right] \quad (12)$$

where

$$\omega_f = \omega_1 + \omega_2 \quad (13)$$

The action of the bandpass filter on the envelope of $M\{c(t)\}$ is now analysed with the aid of Fig. 8. The filtered version of the carrier reference at the output of the bandpass filter is $F(M\{c(t)\})$, where

$$F(M\{c(t)\}) = EB_1 \cos \{\omega_c(t + \tau_1) - \omega_1(t + \tau_1)\}$$
$$+ REB_2 \cos \{\omega_c(t + \tau_2) + \omega_2(t + \tau_2)\} \quad (14)$$

and its envelope function $d(t)$ is given by

$$d(t) = E\{B_1^2 + B_2^2 R^2 + 2B_1 B_2 R \cos(\omega_f t + \omega_1 \tau_1$$
$$+ \omega_2 \tau_2 + \omega_c(\tau_2 - \tau_1)\}^{1/2} \quad (15)$$

By letting $P = B_2/B_1$, eqn. 15 becomes

$$d(t) = B_1 E[1 + P^2 R^2 + 2PR \cos \{\omega_f t + \omega_1 \tau_1 + \omega_2 \tau_2$$
$$+ \omega_c(\tau_2 - \tau_1)\}]^{1/2} \quad (16)$$

The resulting residual modulation on the output of $y(t)$, J, is

given by

$$J = \frac{1}{B_1}\left[\frac{1 + R^2 + 2R\cos\omega_f t}{1 + P^2 R^2 + 2PR\cos\{\omega_f t + \omega_1\tau_1 + \omega_2\tau_2 + \omega_c(\tau_2 - \tau_1)\}}\right]^{1/2} \qquad (17)$$

The similarity between this expression and that for the lowpass filter case can be seen if eqn. 17 is rewritten in the form

$$J = \left(\frac{1 + R^2}{1 + P^2 R^2}\right)^{1/2}\frac{1}{B_1}\left[\frac{1 + \left(\dfrac{2R}{1 + R^2}\right)\cos\omega_f t}{1 + \left(\dfrac{2PR}{1 + P^2 R^2}\right)\cos\{\omega_f t + \omega_1\tau_1 + \omega_2\tau_2 + \omega_c(\tau_2 - \tau_1)\}}\right]^{1/2} \qquad (18)$$

Furthermore, eqn. 6 may be used to predict the peak/trough ratio of the residual modulation, provided that, after the substitutions

$$L = \frac{P(1 + R^2)}{1 + P^2 R^2} \qquad (19)$$

$$D = \frac{2R}{1 + R^2} \qquad (20)$$

$$\omega\tau = \omega_1\tau_1 + \omega_2\tau_2 + \omega_c(\tau_2 - \tau_1) \qquad (21)$$

are made, the square root of k is taken. However, the similarity between the two cases becomes even more apparent when the perfectly matched time delay case is considered. For

this situation,

$$J = \frac{1}{B_1}\left(\frac{1 + R^2 + 2R\cos\omega_f t}{1 + P^2 R^2 + 2PR\cos\omega_f t}\right)^{1/2} \qquad (22)$$

$$J_{max} = \frac{1}{B_1}\left(\frac{1 + R^2 \mp 2R}{1 + P^2 R^2 \mp 2PR}\right)^{1/2} = \frac{1}{B_1}\left(\frac{1 \mp R}{1 \mp PR}\right) \qquad (23)$$

$$J_{min} = \frac{1}{B_1}\left(\frac{1 + R^2 \pm 2R}{1 + P^2 R^2 \pm 2PR}\right)^{1/2} = \frac{1}{B_1}\left(\frac{1 \pm R}{1 \pm PR}\right) \qquad (24)$$

with the sign used (plus or minus) depending on whether P is greater or less than unity. Thus k'', the ratio of J_{max} to J_{min}, is

$$k'' = \left(\frac{1 \mp R}{1 \mp PR}\right)\left(\frac{1 \pm PR}{1 \pm R}\right) \qquad (25)$$

The sign ambiguity of eqn. 25 can be resolved by expanding eqn. 25 and reformulating such that

$$k'' = \frac{1 - PR^2 + R|(P - 1)|}{1 - PR^2 - R|(P - 1)|} \qquad (26)$$

Examination of eqn. 7 for the single-tone lowpass filter case and eqn. 26 shows that k' and k'' are identical expressions if $L = P$ and $D = R$. The peak rate of change of the unwanted modulation for this two-tone test signal in decibels per second is given by

$$\text{peak rate} = \frac{20\,\omega_f R\sin\left\{\cos^{-1}\left(\dfrac{-2R}{1 + R^2}\right)\right\}}{\ln(10)\left\{1 + R^2 - \dfrac{4R^2}{(1 + R^2)}\right\}} \qquad (27)$$

where ω_f is in radians per second.

Depending on the relative position of the two tones inside the bandpass filter, P can take on one of two values: one slightly greater than unity and one slightly less than unity. The circuit will therefore tend to overestimate or underestimate the depth of fade. Consequently, the passband ripple of the bandpass filter is only allowed to be, at most, half of the passband ripple of the lowpass filter case in order to achieve the same worst-case degree of fade suppression. For example, consider, as for the lowpass filter case, the suppression of a 30 dB two-tone fade to within ± 3 dB of output ripple with perfect time delay matching. The most stringent requirement placed on the bandpass filter's specification is set in meeting the $+3$ dB output variation, and this in turn results (from
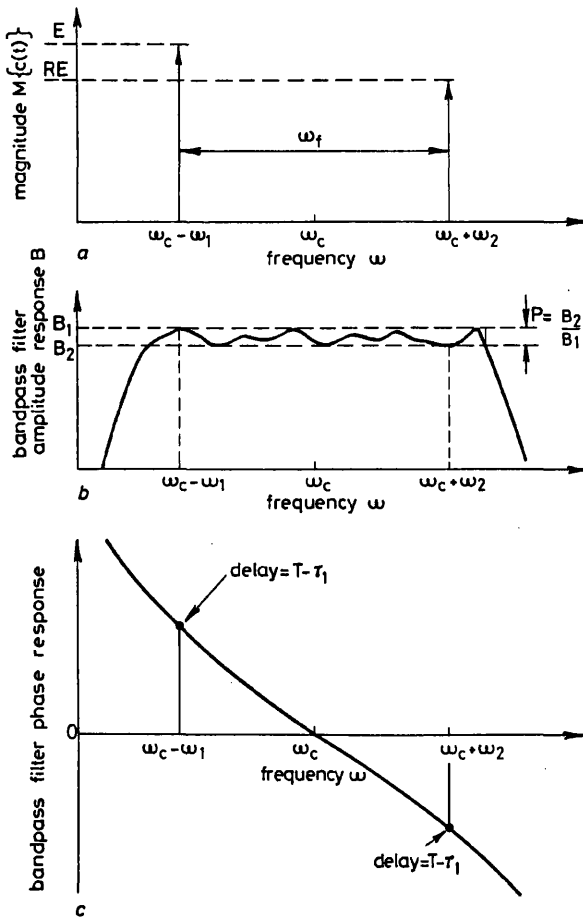

Fig. 8 *Effect of the FFAGC bandpass filter on $M\{c(t)\}$*

a Amplitude/frequency spectrum of input test signal
b Bandpass filter amplitude/frequency response
c Bandpass filter phase/frequency response

eqn. 26) in a maximum allowable passband ripple of 0.16 dB. This value is the same as the maximum positive ripple allowed in the equivalent lowpass filter case. Eqn. 26 predicts that the maximum negative output variation will be 2.2 dB. The computed input/output waveforms for this example are shown in Fig. 9.
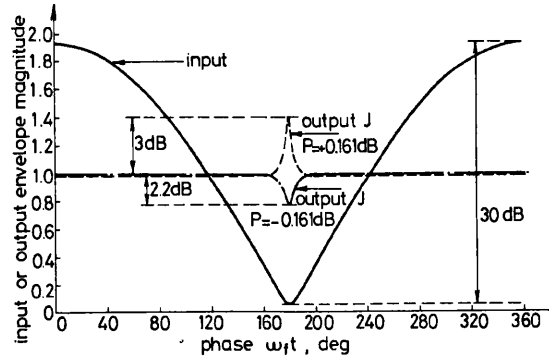

Fig. 9 *Input and worst-case output waveforms of an FFAGC circuit incorporating a bandpass filter with 0.16 dB passband ripple for 30 dB input variation*

Input envelope $= (1 + R^2 + 2R \cos \omega_f t)^{1/2}$

$$J = \left(\frac{1 + R + 2R \cos \omega_f t}{1 + P^2 R^2 + 2PR \cos \omega_f t} \right)^{1/2}$$

where $R = 0.9387$ and $P = 1.019$ $(+0.161 \text{ dB})$ or $P = 0.9817$ (-0.161 dB)

It is interesting to compare the lowpass and bandpass input waveform envelope slew rates when the FFAGC circuit is suppressing the same 30 dB fade. For the lowpass case, eqn. 8 gives the peak slew rate for the sinusoidal fade as

peak 30 dB sinusoidal slew rate $= 148.6 \times f_f \text{ dB/s}$

(where f_f is the input fade frequency in hertz), whereas, for the bandpass case, eqn. 27 gives the peak slew rate for the two tone test signal as

peak 30 dB two-tone slew rate $= 431.02 \times f_f \text{ dB/s}$

Thus, for the same frequency of fading and depth of fade, the bandpass filter limited dynamics FFAGC circuit slews much faster than the lowpass filter case. Furthermore, since the bandpass configuration can operate at twice the fading frequency of the lowpass case, the performance improvement is even more dramatic.

2.3 Filter stopband requirements

In general, the stopband requirements of the lowpass or bandpass filters used depend on the ratio of the carrier reference to peak modulation signal, and, for each modulation system (full carrier AM, DSBSC, pilot reference SSB), this ratio will be different. However, the following general comments apply to any system.

It is assumed that the magnitude of the detected carrier reference is unity and that the wanted modulation signal $\sigma(t)$, of peak value σ, lies as close to the carrier reference as possible. If the stopband response of the inserted lowpass or bandpass filter at the frequency of $\sigma(t)$ is S, then the peak-to-peak variation of $\sigma(t)$ is reduced to $2S\sigma$. Thus the FFAGC circuit suffers from an unwanted modulation of $1/\{1 + S\sigma(t)\}$, with a modulation index $S\sigma$. In general, only a modest stopband attenuation is required. For example, a -20 dB stopband attenuation in a full carrier AM system using lowpass filters results in 10% of unwanted output gain modulation for 100% input modulation. Further details of the harmonic distortion caused by this effect may be found elsewhere [3].

2.4 Information-reference carrier decorrelation effects

2.4.1 Time delay spread:
In the land mobile radio environment, nearly all the energy reaching the input of the receiver comes via line-of-sight signals or signals that have been scattered or refracted in the immediate vicinity of the vehicle. Occasionally, a significant proportion of the received signals' energy arrives via a large reflector some distance from the mobile. In such circumstances, it is possible that the fading induced on the received signal is no longer 'frequency flat'; i.e., at any one instant in time, the depth of fade at different RF frequencies is dissimilar. This decorrelation between fades of the carrier reference and fades of the required modulation results in residual audio modulation at the output of an otherwise perfect FFAGC circuit. In this context, Gans and Yeh [10] have shown that, if a very high correlation coefficient (such as 0.9999) is required between the carrier and the audio in the presence of time delay spread (e.g. 1 μs), then the signals have to be spaced very close in frequency (e.g. less than 2.25 kHz). Based on this quite arbitrarily high degree of correlation, Gans and Yeh state that 'for microwave mobile radio and deep fading, AM and SSB voice communication channels cannot provide telephone quality signals, even with fast-acting AGC of any type'. The authors consider that the assumptions made in reaching this conclusion were overly pessimistic. Even assuming the analysis to be reasonable, Gans and Yeh [10] show that FM communications also suffer from severe multipath distortion effects. This FM distortion also occurs in the air-to-air communication environment and Reed and Russel in Chap. 11 of Reference 9 have shown that simply converting aircraft communication systems from AM to FM will not provide as great a lobe modulation interference reduction as might be hoped.

To estimate the worst-case ripple at the output of a FFAGC circuit under conditions of time delay spread, consider the simple frequency-selective fade model shown in Fig. 10. For
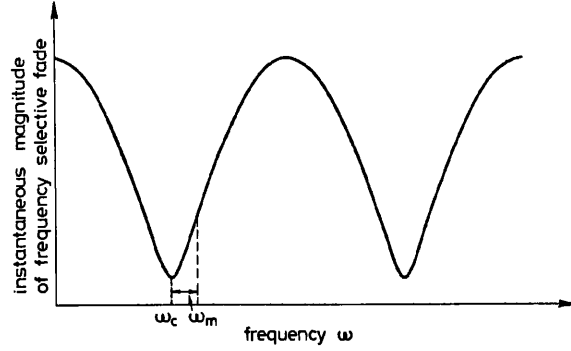

Fig. 10 *Relative positions of the carrier reference and modulation during a frequency-selective fade*

a given instant in time, the diagram shows the amplitude/frequency curve of a deep fade generated by two received signals with a differential time delay T_D between them. The equation of this curve is identical to that of the envelope of a two-tone signal as given in Section 2.2:

$$A = E(1 + R^2 + 2R \cos \omega T_D)^{1/2} \qquad (28)$$

where R is the relative difference between the amplitude of the two signal paths. For the worst case, the carrier reference ω_c is assumed to be positioned at the deepest part of the fade for the instant of time chosen. The FFAGC circuit will therefore overestimate the gain of the signal at ω_m by an amount G where

$$G = \left(\frac{1 + R^2 - 2R \cos \omega_m T_D}{1 + R^2 - 2R} \right)^{1/2} \qquad (29)$$

which gives

$$\omega_m = \frac{1}{T_D} \cos^{-1}\left\{\frac{G^2(2R-1-R^2)+1+R^2}{2R}\right\} \quad (30)$$

For example, consider the maximum carrier modulation frequency offset allowable when suppressing a 30 dB fade, $R = 0.9387$ (caused by two received signals with a 1 μs time delay spread) so that the peak of the residual modulation ripple at the output of an otherwise perfect FFAGC circuit is less than 3 dB ($G = 1.413$). Eqn. 30 gives ω_m as 6.3×10^4 rad/s, i.e. a maximum allowable frequency offset between carrier and signal of 10 kHz. One point of interest here is that the authors are currently investigating an in-band pilot tone form of SSB where the furthest frequency component of the modulating signal is never more than 1.4 kHz from the pilot reference [11]. This satisfies even the most stringent requirements for good correlation in the presence of time delay spread. It should be noted that restricting the maximum attainable circuit gain by means of the threshold places a limit on the peak modulation ripple appearing at the output. This simple twin-path model result has been confirmed for the more general multipath case by Leland and Sollenberger [12]. In a theoretical investigation, these authors have used a Monte Carlo simulation technique to show that the distortion introduced by time delay spread will be relatively modest and quite limited in occurrence for a particular coverage area.

2.4.2 Prefiltering decorrelation in the receiver: A far more serious problem in relation to decorrelation is the effect of filtering operations performed by the receiver prior to FFAGC processing. In the following treatment, perfect suppression of reference carrier fading is assumed by the FFAGC circuit as before and the residual fading of the wanted modulation caused by receiver prefiltering operations is analysed.
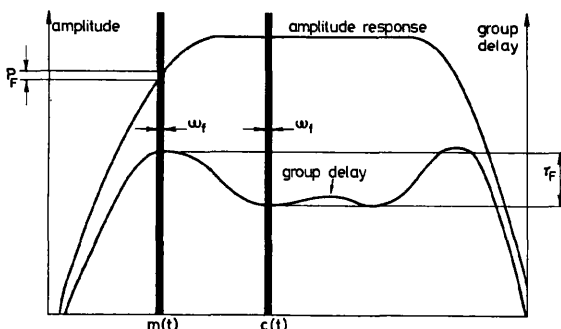

Fig. 11 *Amplitude and group delay response of a general prefilter*

Fig. 11 shows the amplitude and group delay response curves of a typical receiver's prefiltering stage, together with the relative positions of the carrier reference $c(t)$ and the modulation $m(t)$. If the group delay is assumed to be relatively flat across the twice Doppler spread ω_f but not necessarily the same for $m(t)$ and $c(t)$, then, following the approach used in deriving eqns. 15 and 16, the modulation suffers from a residual fading term at the output of the FFAGC circuit of

$$J_F = \left[\frac{1 + P_F R^2 + 2P_F R \cos\{\omega_f(t-\tau_F)\}}{1 + R^2 + 2R \cos\omega_f t}\right]^{1/2} \quad (31)$$

where P_F is the change in the prefilters amplitude response over the range ω_f at the frequency of $m(t)$. This expression is similar to the inverse of eqn. 17. The problem is particularly acute for signals positioned at the edge of a prefilter's bandwidth characteristic since, for such positioning, the group delay suffered by the signal can be typically twice as much as that experienced by a signal at the band centre. Thus the

upper frequency components of double sideband signals and both the lower and upper frequency components of SSB signals are affected after passing through a typical IF filter. Furthermore, if the carrier is positioned at one edge of the prefilter, as in pilot carrier and above-band pilot tone SSB systems [13, 14], then the decorrelation effect will be particularly enhanced. The situation deteriorates further if there is a significant change in the group delay of any prefilter over the range twice Doppler at any point on its characteristic. Any signal at this point, whether it is required modulation or the carrier reference, can have its envelope characteristics greatly changed with respect to the other signals present. However, unlike the time delay spread due to multipath fading, the decorrelation due to prefiltering can be compensated for by the incorporation of suitable filters prior to the FFAGC circuit. Note that eqn. 31 also applies to any filter which is incorporated in the top path of the FFAGC circuit. Again, the deployment of a threshold circuit places a limit on the peak value of the circuit's output ripple.

2.5 FFAGC operation in noise

2.5.1 Random gain modulation: Noise has two undesirable effects on the performance of FFAGC. First, the presence of noise on the bottom path of the circuit causes random modulation of the output signal. If the carrier reference is assumed to be a sinusoid with a noise signal added to it, then Rice [15] has shown that, providing the carrier/noise ratio is reasonably large ($\geqslant$ 15 dB say), then, to a good approximation, the output of the envelope detector may be considered to be a Gaussian-distributed signal with an average value equal to that of the detected carrier and a standard deviation equal to the RMS noise level. The noise bandwidth of the bottom path of a FFAGC circuit is usually much less than the modulation signal's bandwidth, and the above approximation of a Gaussian-distributed denominator variation applies. Extreme variations of the denominator from the mean are unlikely. For example, with a bottom path carrier/noise ratio of 20 dB, the denominator will be within $\pm$ 3 dB of the mean 99.8% of the time. The probability distribution of the denominator for lower signal/noise ratios is also given by Rice [15].

2.5.2 Fading into noise: The second effect of receiver noise occurs for relatively weak signals in the multipath fading environment. With the threshold voltage set to zero, a signal which fades into the noise remains constant in amplitude at the FFAGC output (apart from random gain modulation). Thus, as the signal fades into the noise at the circuit input, the noise appears to rise to the signal at the output of the circuit. Hence, in a manner similar to an FM receiver, fading into noise causes noise 'chuffs' at the output. However, unlike an FM receiver, the process is linear with no rapid degradation of quality. The incorporation of the threshold limit in the FFAGC circuit's denominator prevents the circuit from tracking out fades below a certain level in a noisy environment. By coupling the threshold control voltage to the receiver's feedback AGC circuitry, it is possible to vary the threshold voltage so that it is always set at a fixed level above the noise. During a deep fade into the noise, as shown in Fig. 12, the deepest part of the fade passes through the circuit with a reduction in the noise burst. The subjective effect of doing this is discussed later in this paper.

3 Circuit implementation and experimental results

3.1 Practical implementation of the circuit

There are two basic methods of implementing FFAGC circuits. In the first form of realisation, each of the elements shown in Figs. 2 and 7 is constructed using standard 'op. amp.'

techniques with filters and delay lines constructed using charge-transfer device technology. This particular approach has been discussed elsewhere [16] and will not be discussed further other than to say that it is important to synthesise all filter and delay line clocks from a master oscillator to minimise the effect of any differential time delay drift between the two signal paths.

With the second method of implementation, all operations are performed in software and executed in a digital signal processing system such as an 'analogue microprocessor'. The technology of this type of processor is the centre of considerable research and development and will offer a serious challenge in the near future to the hardware approach. It should be noted that, for the case of SSB, the use of a pilot carrier requires the processing to be performed at some IF prior to final demodulation, whereas, for in-band tone or above-band tone SSB systems, the processing can be directly applied to the demodulated audio signal.

Fig. 12 *Input and output signal and noise levels illustrating the effect of threshold*

a Input signal and noise levels to FFAGC circuit
b Output signal and noise levels of FFAGC circuit without threshold
c Output signal and noise levels of FFAGC circuit with threshold

3.2 Experimental results

Several hardware forms of FFAGC have been investigated by the authors. The earlier work used circuits with lowpass filter limited dynamics which were fitted to full carrier AM UHF radios. More recent work has employed FFAGC circuits with bandpass filter limited dynamics fitted to a 457 MHz 'in-band tone' SSB mobile radio system. Without FFAGC, UHF SSB sounds distorted, having a distinctive 'gravelly' characteristic due to the effects of multipath propagation. Incorporation of FFAGC into the system caused a marked subjective improvement in speech quality. Investigation showed that there was little subjective gain in having the threshold voltage more than

− 20 dB below the mean input level. In this context, it should be noted that, for a Rayleigh fading environment, the received signal spends 99% of the time above this level. As stated earlier, the noise bursts associated with fading in weak signal areas could be controlled by varying the threshold voltage in conjunction with the receiver's feedback AGC. Raising the threshold as the received signal/noise ratio deteriorates and allowing the deepest parts of fades to pass through the circuit was found to be preferable to completely tracking out all the fades with the resulting FM-receiver-type noise bursts. However, although the present FFAGC configuration removes envelope fluctuations, it obviously has no effect on the random frequency fluctuations of the incoming signal. In an FM receiver, these frequency fluctuations are demodulated, causing an additional source of click-type interference. With SSB, the fluctuations are not demodulated but simply superimposed on the audio signal. This results in the SSB audio sounding at times as if it were suffering from 'wow and flutter'. The effect is most noticeable on single tones and less noticeable on voice communications. As a consequence of further work in this area, several techniques for eliminating these frequency fluctuations have been developed for the SSB situation and will be the subject of an early publication. It is noteworthy that full carrier AM communications are not affected by this effect after demodulation and these frequency fluctuations were clearly not observed during the UHF AM field trials.

Fig. 13 shows the input and output waveforms of the feedforward circuit incorporated in a 457 MHz SSB mobile travelling in a suburban area of Bath at 65 km/h (40 miles/h). The two upper traces are those of the input and output waveforms of the 1.67 kHz pilot reference signal. The two lower traces are the input and output traces of the FFAGC circuit for a 3 kHz tone transmitted simultaneously with the 1.67 kHz reference. The maximum fade rate of twice Doppler is about 54 Hz, and the run segment lasts for 205 ms. The threshold, set − 20 dB below the input signal's mean level, can be seen coming into operation at the points marked i and ii. At point iii, a slight decorrelation effect attributed to the group delay change across the IF filter in the receiver is noticeable. The received signal strength's mean was approximately 10 μV EMF. In interpreting these results, it should be noted that the waveforms have already passed through the receiver's 11 Hz bandwidth feedback AGC circuitry, and this has obviously had little effect in suppressing the fading.
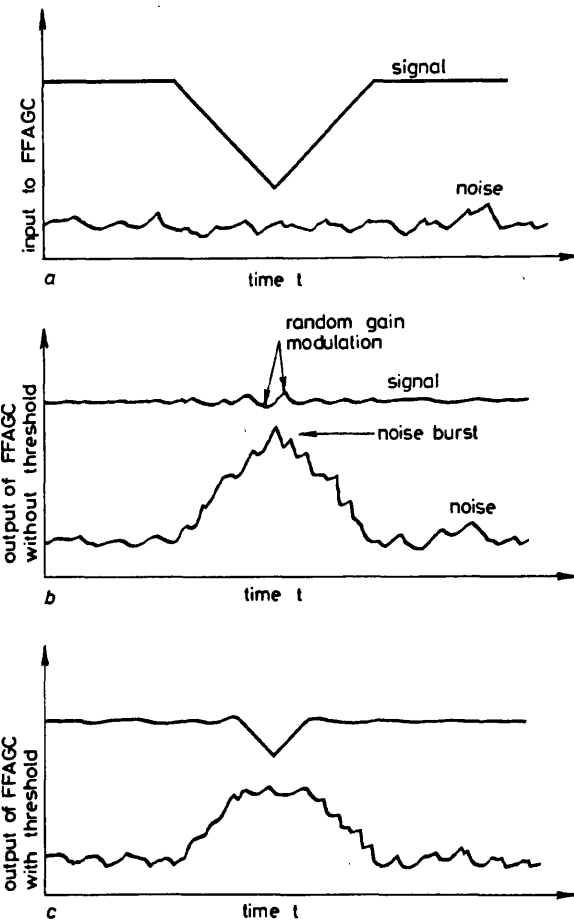
4 Conclusions

A feedforward AGC system has been described for suppressing unwanted multipath propagation envelope fluctuations in land and air mobile radio communication systems. The performance limits of FFAGC using lowpass filter limited dynamics have been investigated, and a modified technique using bandpass filters has been shown to be able to double the fade suppression bandwidth of FFAGC and greatly increase its slew rate. The limitations of signal carrier reference decorrelation effects have been analysed using a simple two-path model. The effect of time delay spread on the received signal in this case has been shown to be unimportant for narrowband signals in typical mobile radio systems. However, the effect of prefiltering the signal in the receiver can cause severe performance degradation unless compensation techniques are employed. A simple analysis of the effects of noise has been performed showing that the circuit is relatively immune to gain modulation for moderate signal/noise ratios. Nevertheless, a major performance limitation in poor signal/noise reception areas occurs when the received signal fades into the noise. In all the above

cases, the threshold circuit improves performance by limiting the maximum value of the positive-going output ripple errors.

An extensive set of field trials have been conducted using FFAGC in conjunction with a 457 MHz SSB land mobile radio system. FFAGC has been shown to operate successfully, reducing multipath-induced envelope fading to an arbitrary degree limited only by noise and decorrelation effects. The revelation that there is little subjective improvement in tracking out fades more than -20 dB below the signal's mean suggests a relaxation of the filters and dynamic range requirements of FFAGC. FFAGC can improve the quality and intelligibility of both land and air mobile communications and should seriously be considered for incorporation in any new system which is likely to suffer from multipath-induced envelope fading.
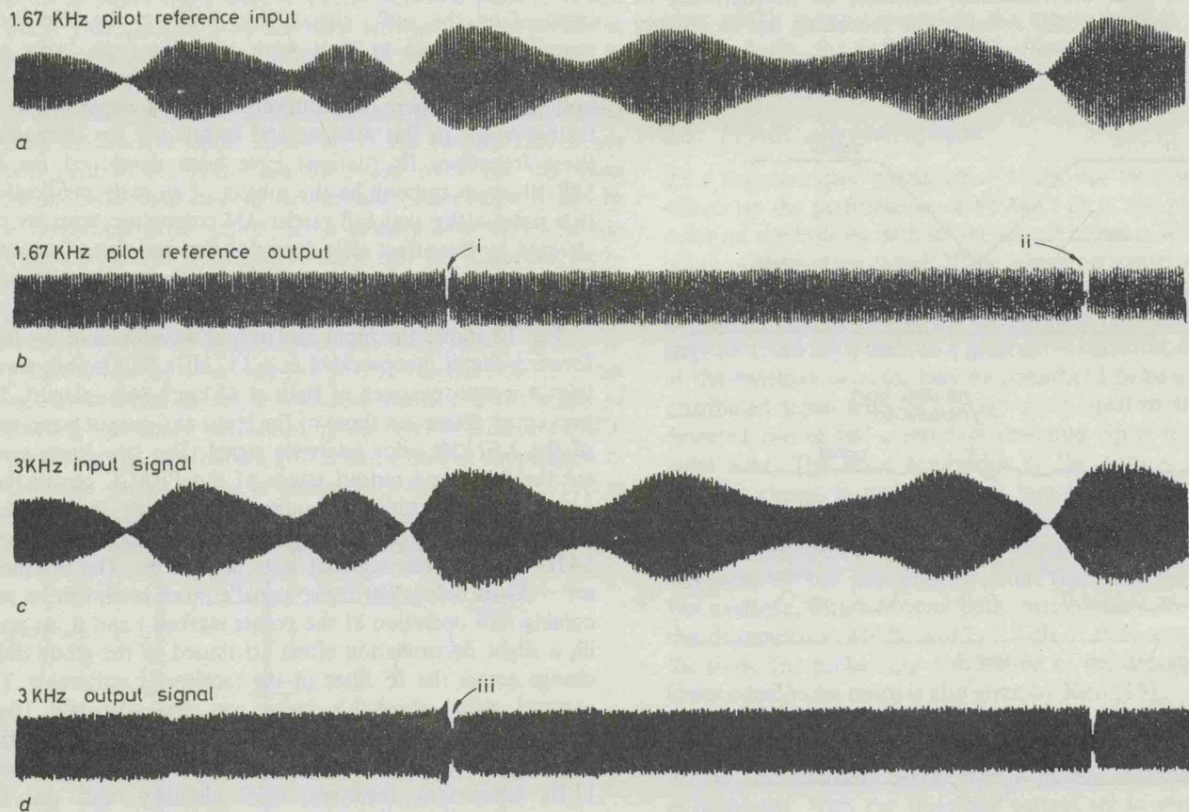
1.67 KHz pilot reference input

1.67 KHz pilot reference output

3KHz input signal

3 KHz output signal

Fig. 13 *Input and output waveforms of a bandpass filter FFAGC circuit measured under field trial conditions at Combe Down, Bath*

a 1.67 kHz pilot reference input to FFAGC circuit
b 1.67 kHz pilot reference output of FFAGC circuit
c 3 kHz signal input to FFAGC circuit
d 3 kHz signal output of FFAGC circuit

5 Acknowledgments

6 References

1 JAKES, W.C.: 'Microwave mobile communications' (Wiley-Interscience, New York, 1974), pp. 11–78

2 HARRIS, R.M.: 'Characterisation of the dynamical response of receivers to fading'. Clerk Maxwell commemorative conference on radio receivers and associated systems, IERE, July 1981, pp. 325–334

3 McGEEHAN, J.P., and BURROWS, D.F.: 'Large signal performance of feedback automatic gain control systems', *IEE Proc. F, Commun., Radar & Signal Process.*, 1981, **128**, (2), pp. 110–117

4 BURROWS, D.F., and McGEEHAN, J.P.: 'Time delay in receiver AGC systems', Clerk Maxwell commemorative conference on radio receivers and associated systems, IERE, July 1981, pp. 73–88

5 PARSONS, J.D., HENZE, M., RATLIFF, P.A., and WITHERS, M.J.: 'Diversity techniques for mobile radio reception', *Radio & Electron. Eng.*, 1975, **45**, pp. 357–367

6 HOPPER, A.L.: 'An experimental fast acting AGC circuit'. IRE convention record-vehicular communications, 1962, pp. 13–20

7 RAWLING, A.J., McGEEHAN, J.P., and GOSLING, W.: 'Forward feeding AGC with extended signal delays'. Proceedings of Conference on radio receivers and associated systems, IERE, London, 1978, pp. 85–92

8 BURROWS, D.F., and McGEEHAN, J.P.: 'The use of feedforward automatic gain control for reducing fast fading in single sideband mobile radio systems'. Proceedings of International Conference on radio spectrum conservation techniques, IEE, London, 1980, pp. 22–25

9 REED, H.R., and RUSSELL, C.M.: 'Ultra high frequency propagation' (Chapman and Hall, 1966)

10 JAKES, W.C.: 'Microwave mobile communications' (Wiley-Interscience, 1974), pp. 161–307

11 McGEEHAN, J.P., RICHARDSON, J.H., and GOSLING, W.: 'The Wolfson SSB mobile radio system'. 3rd world telecommunication forum, part 2, Geneva, 1979, pp. 2.3.4.1–2.3.4.5.

12 LELAND, K.W., and SOLLENBERGER, N.R.: 'Impairment mechanisms for SSB mobile communications at UHF with pilot-based Doppler/fading correction', *Bell Syst. Tech. J.*, 1980, **59**, pp. 1923–1942

13 WELLS, R.: 'SSB for VHF mobile radio at 5 kHz channel spacing'. Proceedings of conference on radio receivers and associated systems, IERE, London, 1978, pp. 29–36

14 WILMOTTE, R.M., and LUSIGNAN, B.B.: 'UHF Task Force Report – spectrum efficient technology for voice communications' Federal Communications Commission, Washington, 1978

15 RICE, S.O.: 'Mathematical analysis of random noise'. *Bell Syst. Tech. J.*, 1945, **24**, pp. 98–107

16 McGEEHAN, J.P., and BURROWS, D.F.: 'The impact of CCD technology on feedforward automatic gain control systems for mobile radio communications', 4th European conference on electrotechnics, EUROCON '80, Stuttgart, March 1980, pp. 184–188